ISTANBUL TECHNICAL UNIVERSITY ★ GRADUATE SCHOOL

ELECTROSPUN COMPOSITE NANOFIBERS WITH METAL/METAL OXIDE NANOPARTICLES

Ph.D. THESIS

Havva BAŞKAN

Department of Textile Engineering

Textile Engineering Programme

APRIL 2021

ISTANBUL TECHNICAL UNIVERSITY ★ GRADUATE SCHOOL

ELECTROSPUN COMPOSITE NANOFIBERS WITH METAL/METAL OXIDE NANOPARTICLES

Ph.D. THESIS

Havva BAŞKAN
(503142809)

Department of Textile Engineering

Textile Engineering Programme

Thesis Advisor: Prof. Dr. Hale KARAKAŞ

APRIL 2021

İSTANBUL TEKNİK ÜNİVERSİTESİ ★ LİSANSÜSTÜ EĞİTİM ENSTİTÜSÜ

METAL/METAL OKSİT NANOPARTİKÜL İÇERİKLİ ELEKTROEĞRİLMİŞ NANOLİF ÜRETİMİ

DOKTORA TEZİ

Havva BAŞKAN
(503142809)

Tekstil Mühendisliği Anabilim Dalı

Tekstil Mühendisliği Programı

Tez Danışmanı: Prof. Dr. Hale KARAKAŞ

NİSAN 2021

Havva BAŞKAN, a Ph.D. student of ITU Graduate School student ID 503142809, successfully defended the thesis entitled "ELECTROSPUN COMPOSITE NANOFIBERS WITH METAL/METAL OXIDE NANOPARTICLES", which she prepared after fulfilling the requirements specified in the associated legislations, before the jury whose signatures are below.

Thesis Advisor :	**Prof. Dr. Hale KARAKAŞ** Istanbul Technical University	.....
Jury Members :	**Prof. Dr. Ali DEMİR** Istanbul Technical University	.....
	Prof. Dr. Emine Dilara KOÇAK Marmara University	.....
	Prof. Dr. Fatma KALAOĞLU Istanbul Technical University	.....
	Prof. Dr. Aslı HOCKENBERGER Bursa Uludağ University	.....

Date of Submission : 23 March 2021
Date of Defense : 21 April 2021

To my family,

FOREWORD

First of all, I would like to express my sincere gratitude to my supervisor Prof. Dr. Hale KARAKAŞ for her professional guidance, continuos support, patience and kindness. She always motivated me for both academic and personal achievements. It is an honour for me to be a student of her. Secondly, I would like to thank to Prof. Dr. A. Sezai SARAÇ for his great contributions, useful suggestions, discussions and motivations.

The production of PHA-based nanofibers was performed as an additional workpackage under the EU project 'PolyBioSkin' (grant agreement number is 745839) in Ghent University. I am very thankful to Prof. Dr. Karen DE CLERCK for giving me an opportunity to make contributions on 'PolyBioSkin'. Also, I am very thankful to her to allow me to study on my thesis under her guidance in Ghent University. I would also like to thank to Timo MEIREMAN for his great effort on solubility studies of P(3HB) and P(3HO-3HD) and Dr. Serena DANTI for organizing and conducting biological evaluations of PHA-based nanofibers.

I am also grateful to my thesis jury members, Prof. Dr. Ali DEMİR and Prof. Dr. E. Dilara KOÇAK for their valuble discussions, suggestions, and support for completing this research.

I would like to thank to ITU Projects of Scientific Investigation for financially supporting this research (BAP; Project Number: MDK-2018-41127). Moreover, The Scientific and Technological Research Council of Turkey (TUBITAK)-2211-A programme supplied a scholarship (application number: 1649B031500306) during my PhD and thanks to TUBITAK 2214-A programme scholarship (application number: 1059B141800375) I was able to study in Ghent University, Belgium for 12 months. I am very grateful to TUBITAK.

I would also like to thank to my colleagues and friends for their support during this challenging term.

My special gratitude goes to my family for their eternal love, patience and understanding. I have accomplished everything with their encouragement.

April 2021

Havva BAŞKAN
(Textile Engineer, MSc)

TABLE OF CONTENTS

Page

ABBREVIATIONS

AA	: Acrylic Acid
AFM	: Atomic Force Microscopy
Ag	: Silver
Ag^+	: Silver Ion
$AgNO_3$	: Silver Nitrate
AgNPs	: Silver Nanoparticles
Ag@PPy	: Silver@Polypyrrole
Al_2O_3	: Aluminum Oxide
AMH	: 2-amino-3-methyl-1-hexanethiol
AN	: Acrylonitrile
ATCC	: American Type Culture Collection
C	: Carbon
Ca^{2+}	: Calsium Ion
$CHCl_3$	: Chlorofom
CO_2	: Carbondioxide
CTAB	: Cetyltrimethylammonium bromide
DI	: Deionized Water
DMAc	: Dimethylacetamide
DMC	: Dimethylcarbonate
DMEM	: Dulbecco's Modified Essential Medium
DMF	: Dimethylformamide
DMSO	: Dimethylsulfoxide
DSC	: Differential Scanning Calorimetry
DPBS	: Dulbecco's Phosphate Buffered Saline
E.coli	: Escherichia Coli
EDS	: Energy Dispersive Spectroscopy
EtOH	: Ethanol
Fe	: Iron
Fe_3O_4	: Iron (III) Oxide
FTIR-ATR	: Fourier Transform Infrared-Attenuated Total Reflectance
GO	: Graphene Oxide
H	: Hydrogen
HBD-2	: Beta Defensin-2
HBP	: Hyperbranched Polymers
IA	: Itaconic Acid
ICP	: Intrinsically Conducting Polymers
IL	: Interleukin
In_2O_3	: Indium (III) Oxide
KH_2PO_4	: Mono Potassium Phosphate
LCL	: Long Chain Length
$LiBr_2$	: Lithium Bromide
MA	: Methylacrylate
MCL	: Medium Chain Length

Mg^{2+} : Magnesium Ion
MgO : Magnesium Oxide
MHB : Mueller- Hinton Broth
MIC : Minimum Inhibitory Concentration
MMA : Methylmethacrylate
MS : Mass Spectroscopy
MWCNTs : Multi-walled Carbon Nanotubes
N : Nitrogen
$NaBH_4$: Sodium Borohydride
NaCl : Sodium chlorür
NaH_2PO_4 : Mono Sodium Phosphate
N_2H_5OH : Hydrazinium Hydroxide
NMPy : N-Methyl Pyrrole
NMR : Nuclear Magnetic Resonance
O : Oxygen
PAA : Poly (acrylic acid)
PAN : Polyacrylonitrile
PANI : Polyaniline
P (AN-co-AA) : Poly (acrylonitrile-co-acrylic acid)
P (AN-co-IA) : Poly (acrylonitrile-co-itaconic acid)
P (AN-VAc) : Poly (acrylonitrile-vinylacetate)
P. Aeruginosa : Pseudomonas Aeruginosa
PCL : Polycaprolactone
PDMPy : Poly (2,5 Dimethyl Pyrrole)
PEG : Poly (ethylene glycol)
PEMA : Poly (ethylmethacrylate)
PES : Poly (ethylenesuccinate)
PET : Poly (ethyleneterepthalate)
PEVA : Poly (ethylene-co-vinylacetate)
PHA : Polyhydroxyalkanoate
P(3HB) : Poly (3-hydroxybutyrate)
P (3HD) : Poly (3-hydroxydecanoate)
P (3HHx) : Poly (3-hydroxyhexanoate)
P (3HO) : Poly (3-hydroxyoctanoate)
P (3HO-3HD) : Poly (3-hydroxyoctanoate-3-hydroxydecanoate)
P (3HV) : Poly (3-hydroxyvalerate)
PGA : Polyglycolic Acid
PLA : Polylactic Acid
PMMA : Polymethylmethacrylate
PNMPy : Poly (N-Methylpyrrole)
PP : Polypropylene
PPy : Polypyrrole
Pt : Platinum
PTFE : Polytetrafluoroethylene
PVC : Polyvinylchlorür
PVP : Polyvinylpyrrolidone
Py : Pyrrole
RPMI : Roswell Park Memorial Institute
RT-PCR : Real Time Reverse Transcriptase Polymer Chain Reaction
S. Aureus : Staphylococcus Aureus

SCL	: Short Chain Length
SD	: Standart Deviation
SDBS	: Sodium Dodecyl Benzene Sulfonate
SDS	: Sodium Dodecyl Sulfate
SEM	: Scanning Electron Microscope
TEM	: Transmission Electron Microscope
TG	: Thermogravimetry
TGA	: Thermogravimetric Analysis
TGF-β	: Transforming Growth Factor Beta
TIsPy	: 1- Triisopropylsilyl Pyrrole
TiO_2	: Titanium Dioxide
TNF	: Tumor Necrosis Factor
TOS	: Thermal Oxidative Stabilization
TSA	: Tyriptic Soy Agar
TUBITAK	: The Scientific and Technological Research Council of Turkey
UV	: Ultra Violet
VAc	: Vinylacetate
XPS	: X-Ray Photoelectron Spectroscopy
XRD	: X-Ray Diffraction

SYMBOLS

α	: Alpha
β	: Beta
cfu	: Colony Forming Unit
cm	: Centimeter
cm^2	: Centimeter Square
°C	: Centigrade Degree
emu	: Electromagnetic Unit
γ	: Gamma
g	: Gram
h	: Hour
kDa	: Kilodaltons
kV	: Kilovolt
L	: Liter
m^2	**:** Meter Square
mg	: Miligram
ml	: Mililiter
nm	: Nanometer
M_r	: Remnant Magnetization
M_s	: Saturation Magnetization
v %	: Volume Percent
w %	: Weigth Percent
W	: Watt

LIST OF TABLES

Page

LIST OF FIGURES

Page

ELECTROSPUN COMPOSITE NANOFIBERS WITH METAL/METAL OXIDE NANOPARTICLES

SUMMARY

Functional materials have taken great interest due to their superior physical and chemical features which allow them to be succesfully used in a wide range of engineering applications. Nanomaterials, specifically nanofibers are regarded as functional materials due the their high surface area to volume ratio, high pore interconnectivity, small pore dimensions and superior chemical and mechanical features. Nanofibers are produced by mainly electrospinning which is a simple and inexpensive technique. Moreover, many types of polymers or polymer blends can be converted to nanofibers by electrospinning. Combination of two or more materials in a nanofibrous structure can result in functional materials.

In this thesis, the goal was obtaining functional nanofibrous materials by incorporating a noble metal (silver) and metal oxides (iron III oxide (Fe_3O_4) and aluminum oxide (Al_2O_3)) in novel polymeric nanofiber structures and evaluate the biological features of the samples for medical applications.

First of all, a novel Poly (acrylonitrile-co-itaconic acid) (P (AN-co-IA)) copolymer was synthesized by emulsion polymerization. In the literature, copolymerization of itaconic acid (IA) with acrylonitrile (AN) was performed for decreasing the cyclization temperature of polyacrylonitrile (PAN) homopolymer and consuming less energy for carbon fiber production. However, in the scope of the thesis, it was aimed to enhance the application areas of IA by integration of metals and metal oxides.

Since Fe_3O_4 nanoparticles and Al_2O_3 nanoparticles play an imperative role in many biomedical applications, they were utilized together with P (AN-co-IA) copolymer. It was very difficult to study with metal oxide nanoparticles due to their tendency to agglomeration. For that reason, the appropriate amount of metal oxide nanoparticles was determined first by using polyacrylonitrile /N,N Dimethylformamide (PAN/DMF) solutions. Afterwards, the optimized amout of Fe_3O_4/ Al_2O_3 nanoparticles were added into P (AN-co-IA)/DMF polymer solutions and the solutions were subjected to electrospinning to obtain a nanofibrous structure. In addition to conventional electrospinning, coaxial electrospinning was also performed for metal oxide nanoparticle incorporation. Detailed morphologic and spectroscopic characterizations of the obtained nanofibers were performed. Thermal features of the resultant nanofibers were also analyzed by Differential Scanning Calorimety (DSC) and Thermogravimetric Analysis (TGA). It was captured from the characterization results that addition of metal oxide nanoparticles to P (AN-co-IA) copolymer structure altered the features of the plain P (AN-co-IA) nanofibers. Even using very small amount (1 wt %) of Al_2O_3 caused improvements in thermal stability of the nanofibers.

On the other side, silver nanoparticles (AgNPs) formation and integration to polymer structures were achieved by different chemical and physical methods. By the assistance of P (AN-co-IA) polymer and DMF, AgNPs were formed in-situ in polymer

solution and then the polymer solution was electrospun for nanofiber production. The novelty of the method was related to the decreased reduction duration of silver nitrate ($AgNO_3$) by using P (AN-co-IA) polymer. The method was compared with the literature studies on the utilization of PAN polymer for reduction of $AgNO_3$. P (AN-co-IA) polymer allowed to obtain AgNPs from the precursor $AgNO_3$ two times faster than PAN. Moreover, it was understood that P(AN-co-IA)/Ag nanofibers had high electrical conductivity, enhanced thermal stability and satisfying nanofiber morphologies. Besides conventional electrospinning, AgNPs were introduced into P(AN-co-IA) polymer structure via coaxial electrospinning. In the process, $AgNO_3$/DMF solution was prepared to be used as a shell solution and P (AN-co-IA)/DMF solution was prepared as a core solution. Since the most important point in coaxial electrospinning is the feed-rate of core and shell solutions, a set of experimental study was performed for the optimization of flow-rate (0.2 ml/h) of shell solution. After coaxial electrospinning, P(AN-co-IA)(core)/ $AgNO_3$ (shell) nanofibers were subjected to UV-irradiation to generate AgNPs by the reduction of $AgNO_3$. UV-irradiation duration was optimized as 3 hours by using PAN(core)/ $AgNO_3$ (shell) nanofibers. In addition to P (AN-co-IA) and PAN polymers, biodegradable and biocompatible poly (3-hydroxybutyrate) P (3HB) and poly (3-hydroxyoctanoate-3 hydroxydecanoate)(P (3HO-3HD)) polymers were also utilized for the combination of AgNPs. To this end, nanofibers of P (3HB)/P (3HO-3HD) were collected via conventional electrospinning and by dip-coating they were coated with AgNPs. As in the nanofibers including metal oxide nanoparticles, detailed morphologic, spectroscopic and thermal characterizations of the resultant nanofibers were performed by Scanning Electron Microscope –Energy Dispersive Spectroscopy (SEM-EDS), Ultra Violet-Visible (UV-Visible) and Fourier Transform Infrared-Attenuated Total Reflectance (FTIR-ATR) spectroscopy, and DSC. Most importantly, antimicrobial activity studies of P(AN-co-IA)/Ag nanofibers (obtained via conventional electrospinning) against *S. aureus*, *E.coli*, *P. aeruginosa* and *C. albicans* and immunomodulatory properties of P (3HB)/P (3HO-HD)/Ag nanofibers against special cytokines (IL-1 (α and β), IL-6, IL-8, TNF-α, TGF-β and HBD-2) were evaluated. Related to the antimicrobial activity results of P (AN-co-IA)/Ag nanofibers, it was observed that the nanofibers produced inhibition zones against the studied microorganisms. That was also proved by susceptibility testing. According to time-kill analysis, without silver nanoparticles, either PAN or P (AN-co-IA) nanofibers did not show any antimicrobial activity against any microorganisms. However, bacteriostatic/fungistatic activity was observed for all nanofiber samples which include AgNPs at almost all time points. Bactericidal activity was started from 24-48 hours and lasted until 120 hours at 10x Minimum Inhibitory Concentration (MIC) whereas fungicidal activity was observed between 120 and 168 hours at 10xMIC. Based on the real-time reverse transcriptase polymer chain reaction (RT-PCR) tests of P (3HB)/P (3HO-3HD)/Ag nanofibers, it was understood that while plain P(3HB)/P(3HO-3HD) nanofibers did not show any difference in the basal production of these molecules by HaCaT cells in culture, AgNP-containing P(3HB)/P(3HO-3HD) nanofibers upregulated the studied proinflammatory cytokines which were IL-1(α and β), IL-6 and IL-8 after 6 hours to start the healing process. Those findings of AgNPs containing P (AN-co-IA) and P (3HB)/P (3HO-3HD) nanofibers revealed that they could be used in wound dressing or tissue engineering applications effectively.

Polypyrrole (PPy) is popular with its conductivity, but it can also be used in biological applications such as biosensors and drug delivery. However, due to the problems in processing with PPy, it is very difficult to obtain PPy nanofibers. In this thesis, it was

aimed to combine PPy with AgNPs to be used in biological applications and also converting it to a nanofibrous web structure by the help of P (AN-co-IA). Since it was difficult to electrospin P (AN-co-IA), PPy and AgNPs in a single step, AgPPy was synthesized via chemical oxidation polymerization first. Then AgPPy and P (AN-co-IA) was gathered in a nanofiber structure via coaxial electrospinning. AgPPy/DMF solution was prepared as shell solution and P (AN-co-IA) /DMF was prepared as core solution. It can be fairly said that the same protocol of the abovementioned coaxial electrospinning was performed for coaxial electrospinning of P (AN-co-IA) (core)/AgPPy (shell) nanofibers. Bead-free and continuous nanofiber morphologies with fine nanofiber diameters could be obtained.

As a conclusion, in the scope of this thesis, functional nanofibers were achieved by incorporating metal/metal oxide nanoparticles into polymeric nanofiber structures with various experimental procedures. The obtained nanofibers are good candidates for medical applications where conductivity and antimicrobial activity are desired.

METAL/METAL OKSİT NANOPARTİKÜL İÇERİKLİ ELEKTROEĞRİLMİŞ NANOLİF ÜRETİMİ

ÖZET

Fonksiyonel malzemeler, üstün fiziksel ve kimyasal özelliklerinden ve geniş uygulama alanlarından dolayı oldukça ilgi görmüştür. Nanomalzemeler, özellikle de nanolifler geniş yüzey alanı, yüksek gözeneklilik, küçük gözenek çapı ve üstün kimyasal ve fiziksel özelliklere sahip olmalarından dolayı fonksiyonel malzemeler olarak ifade edilmektedir. Nanoliflerin üretiminde değişik teknikler kullanılmakla birlikte bunlar içerisinde basit ve ekonomik olmasından dolayı en çok tercih edilen yöntem elektroeğirmedir. İki veya daha fazla malzemenin nanolif yapısı altında birleşmesi de fonksiyonel malzeme elde edilmesi ile sonuçlanır.

Bu tez kapsamında, metal (gümüş) ve metal oksit (demir (III) oksit (Fe_3O_4) ve alüminyum oksit (Al_2O_3)) nanopartikül içeren özgün polimerlerden elde edilen nanolif yüzeyinin oluşturulması ve medikal uygulamalarda kullanılmak üzere biyolojik özelliklerinin test edilmesi hedeflenmiştir.

Öncelikle, oldukça özgün olan poli (akrilonitril-ko-itakonik asit) (P (AN-ko-IA)) kopolimeri emülsiyon polimerizasyonu yöntemi ile sentezlenmiştir (Ayrıca sentez yöntemi US10781277B2 numaralı Amerikan patenti ile de tescillenmiştir).

Literatürde akrilonitril (AN) ve itakonik asidin (IA) kopolimerizasyonu çoğunlukla poliakrilonitril (PAN) homopolimerinin siklizasyon sıcaklığını düşürmek ve karbon lifi üretiminde daha az enerji tüketebilmek maksadıyla gerçekleştirilmiştir. Fakat bu tez kapsamında IA'nın metal ve metal oksit nanopartikülleri ile bir arada kullanılarak bilinen kullanım alanının dışına çıkılması hedeflenmiştir.

Fe_3O_4 ve Al_2O_3 nanopartiküllerinin biyolojik uygulamalarda etkin bir rol oynamalarından dolayı P (AN-ko-IA) ile bir arada kullanılmaları uygun görülmüştür. Metal oksitlerle çalışmak, bir araya toplanma eğilimlerinden dolayı oldukça zordur. Bu nedenle çözelti içerisinde kullanılması hedeflenen metal oksit miktarlarının optimize edilmesi gerekmiştir. Optimizasyon için gerçekleştirilen deneyler P (AN-ko-IA) yerine PAN polimerinin N,N dimetilformamid (DMF) içerisinde çözünmesi ile hazırlanan polimer solüsyonları kullanılarak yapılmıştır. Optimizasyon işleminin ardından ise metal oksitler P (AN-ko-IA) polimerinin DMF içerisinde çözünmesi ile hazırlanan polimer solüsyonlarına ilave edilmiş ve hazırlanan çözeltiler nanolif üretimi için elektroeğirme işlemine tabi tutulmuştur. Geleneksel elektroeğirme işlemine ilaveten, koaksiyel elektroeğirme ile de metal oksit nanopartikül içerikli nanolif üretimi sağlanmıştır. Üretilen nanoliflerin spektroskopik ve morfolojik özellikleri oldukça detaylı bir şekilde incelenmiştir. Bunlara ilaveten, nanoliflerin termal özellikleri de diferansiyel tarama kalorimetresi ve termogravimetrik analiz ile incelenmiştir. Karakterizasyon sonuçlarından nanolif içerisinde metal oksit nanopartiküllerinin varlığının sade P (AN-ko-IA) nanoliflerinin özelliklerinde özellikle de termal özelliklerde değişime sebep olduğu anlaşılmıştır. Oldukça küçük

bir oranda eklenen (kütlece % 1) Al_2O_3 nanopartiküllerinin bile termal stabiliteyi önemli derece iyileştirdiği ve termal bozunma sonucu kalan kütlenin oranını önemli derecede değiştirdiği görülmüştür.

Öte yandan, gümüş nanopartiküllerinin de değişik fiziksel ve kimyasal metodlarla polimer yapısı içerisine dahil edilmesi üzerinde çalışılmıştır. Gümüş nanopartikülleri P (AN-ko-IA) ve DMF yardımı ile P (AN-ko-IA) polimer çözeltisi içerisinde in-situ olarak sentezlenmiştir. Ardından da bu polimer çözeltilerinin elektroeğirme işlemine tabi tutulması ile nanolif eldesi gerçekleştirilmiştir. Bu çalışmanın özgün yanlarından biri, gümüş nitratın ($AgNO_3$) gümüş nanopartikülüne dönüşümünün P (AN-ko-IA) polimeri ile literatürde bilinen indirgenme süresinden daha kısa bir zaman diliminde gerçekleşmesidir. Literatürde yer alan verilerle kıyaslamak adına PAN/DMF çözeltisi içerisinde gümüş nanopartiküllerinin in-situ olarak da eldesi ayrıca gerçekleştirilmiştir ve elde edilen gözlemsel sonuçlara göre P (AN-ko-IA) polimeri varlığında gümüş nitratın gümüş nanopartiküllerine dönüşümü iki kat daha hızlı bir zamanda meydana gelmiştir. Elde edilen P (AN-ko-IA)/Gümüş nanoliflerin oldukça yüksek bir iletkenliğe, geliştirilmiş termal stabiliteye ve memnun edici nanolif morfolojisine sahip oldukları belirlenmiştir. Geleneksel elektroeğirme işleminin yanında koaksiyel elektroeğirme ile de gümüş nanopartiküllerinin P (AN-ko-IA) polimerine entegrasyonu sağlanmıştır. Bu amaçla, kabuk çözelti olarak gümüş nitrat /DMF çözeltisi, öz çözelti olarak da P (AN-ko-IA)/DMF çözeltisi hazırlanmıştır. Koaksiyel elektroeğirme işleminde en kritik nokta öz ve kabuk çözeltilerin beslenme oranıdır ve bu sebeple de kabuk çözeltinin beslenme oranının tespiti için bir seri optimizasyon çalışması yapılmıştır. Sonuç olarak kabuk çözeltinin 0.2 ml/saat oranında beslenmesinin uygun olacağı görülmüş ve hazırlanan öz ve kabuk çözetilere koaksiyel elektroğirme uygulanması ile P (AN-ko-IA) (öz)/ $AgNO_3$ (kabuk) nanolifleri elde edilmiştir. Koaksiyel elektroeğirmenin ardından UV ışığının uygulanması ile gümüş nitratın gümüş nanopartiküllerine indirgenmesi sağlanmıştır. UV ışığının uygulanma süresi ile ilgili de bir seri optimizasyon çalışması yapılmış ve yapılan çalışmaların ardından nanoliflere zarar vermeden indirgenmenin sağlanabileceği optimum süre, 3 saat olarak belirlenmiştir.

P (AN-ko-IA) ve PAN polimerlerine ilaveten biyouyumlu ve biyobozunur olan poli (3-hidroksibutirat) (P (3HB)) ve poli (3-hidroksioktanoat-3 hidroksidekanoat) (P (3HO-3HD)) polimerlerinin de gümüş nanopartikül ile nanolif formunda birleştirilmesi üzerine çalışılmıştır. Bu bağlamda öncelikle P (3HB)/P (3HO-HD) nanolifleri üretilmiş ve ardından daldırma-kaplama yöntemi ile nanolifler kolloidal gümüş çözeltisine batırılarak gümüş nanopartikülleri ile kaplanmıştır. Daldırıp-kaplama yönteminde üç farklı protokol denenmiştir. En yoğun ve homojen kaplanmanın sağlandığı üç defa ardarda daldırıp çıkarma ve ardından hemen yıkama yöntemi ile gümüş nanopartiküllerinin P (3HB)/P (3HO-HD) yüzeyine tutunması sağlanmıştır. Metal oksit içerikli nanolif çalışmasında olduğu gibi, gümüş nanopartikül içeren nanoliflere de oldukça detaylı spektroskopik, morfolojik ve termal karakterizasyon uygulanmıştır. Morfolojik karakterizasyonlar Taramalı Elektron Mikroskobu (SEM) ve Atomik Kuvvet Mikroskobu (AFM) ile, spektroskopik karakterizasyonlar Ultra-Viyole Görünür Spektroskopisi ve Fourier Dönüşüm Kızılötesi-Azaltılmış Toplam Yansıma Spektroskopisi (FTIR-ATR) ile termal özellikler de Diferansiyel Tarama Kalorimetrisi (DSC) ile analiz edilmiştir. Geleneksel elektroeğirme ile elde edilen P (AN-ko-IA)/Gümüş nanoliflerin antimikrobiyel aktivite performanslarının gram pozitif (*S. aureus*), gram negatif (*E.coli* ve *P. aeruginosa*) ve maya mantarına (*C. albicans*) karşı incelenmesi ve de P

(3HB)/P (3HO-HD)/Gümüş nanoliflerinin özel sitokinler olan IL-1 (α and β), IL-6, IL-8, TNF-α, TGF-β ve HBD-2 ye karşı immünömodülatör özelliklerinin araştırılması ve değerlendirilmesi idi.

P (AN-ko-IA)/Gümüş nanoliflerinin antimikrobiyel aktivite test sonuçlarına göre, çalışılan mikroorganizmalara karşı engelleme bölgelerinin oluştuğu görülmüş ve bu yanıtlar yapılan duyarlılık testleri ile de doğrulanmıştır. Zamana bağlı öldürme grafiklerinde ise gümüş nanopartikül içermeyen nanoliflerin herhangi bir mikroorganizmaya karşı aktivitesi olmazken, gümüş nanopartikül içerikli tüm nanoliflerin bakteriostatik ve fungistatik etkilerinin varlığından tüm zaman değerlerinde olduğu görülmüştür. Gümüş nanopartikül içerikli P (AN-ko-IA) nanoliflerinin bakteri öldürücü etkilerinin 24 ve 48 saat aralığında başladığı ve 10xMIC konsantrasyonla 120 saate kadar sürdüğü gözlenirken, mantar öldürücü etkilerinin 10xMIC konsantrasyonla 168 saate kadar devam ettiği anlaşılmıştır.

P (3HB)/P (3HO-HD) nanoliflerine uygulanan gerçek zamanlı ters transkriptaz polimer zincir reaksiyonu sonuçlarına göre ise gümüş nanopartikül içermeyen sade P (3HB)/P (3HO-HD) nanolifleri herhangi bir bazal üretim göstermezken, gümüş nanopartikül içerikli P (3HB)/P (3HO-HD) nanoliflerin oldukça önemli olan proinflamatuar sitokinleri 6 saat sonunda yukarı yönde regüle ettiği gözlenmiştir. Bu da doku iyileşmesinin başlaması için oldukça önem arz eden bir sonuçtur. Elde edilen bu sonuçlardan gümüş nanopartikül içerikli nanoliflerin doku mühendisliği ve yara örtüsü uygulamalarında oldukça etkin bir şekilde kullanılabileceklerini çıkarmak mümkündür. Ayrıca, akrilik, polipropilen, polietilen tabanlı klasik yara örtüleri geri dönüşüme uygun olmamalarından dolayı atık sorunu oluştururken, tez kapsamında üretilen ve yara örtüsü olarak kullanılması hedeflenen nanoliflerin biyo-tabanlı oluşlarından dolayı organik geri dönüşüme imkan tanımaları da büyük bir artıdır. Aynı zamanda, yapıları gereği yüksek polariteye sahip olan P (3HB)/P (3HO-HD) nanoliflerin herhangi bir ajanla deriye kolayca entegre edilip çıkarılabilmesi de tedavi edebilme özelliklerini önemli ölçüde etkilemekte ve literatürde var olan yara örtülerinden olan özgün farkını da ortaya koymaktadır.

Elektriksel iletkenlik özelliği ile popüler olan polipirol (PPy) ise aynı zamanda biyosensör, ilaç salınımı gibi alanlarda da tercih edilmesi sebebi ile bu tez kapsamında da biyolojik uygulamalara yönelik malzeme hazırlanmasında kullanılmak istenmiştir. Polipirol neme karşı duyarlı oluşu ve kırılgan oluşu sebebi ile işlem yapılması özellikle de tek başına nanolif üretimi pek mümkün olmayan bir malzemedir. Bu sebeple tez içerisindeki çalışmaların bütünlüğünü de koruyacağı düşünülerek polipirolün gümüş nanopartikülleri ile birleştirilmesi ve ardından da elektroeğirme ile nanolif üretimi hedeflenmiştir. Polipirol, gümüş nanopartiküller ve P (AN-ko-IA) polimerini tek bir adımla nanolife dönüştürmek mümkün olmayacağından öncelikle polipirol ve gümüş nanopartiküllerin birleştirilme işlemi gerçekleştirilmiştir. Kimyasal oksidasyon polimerizasyonu ile pirol ve gümüş nitrat sulu ortamda sentezlenmiştir. Ardından da, elde edilen çözelti etanol ile çöktürülmüş, kurutulmuş ve toz formunda elde edilmiştir. Geleneksel elektroeğirme yöntemi yerine koaksiyel elektroeğirme yöntemi ile AgPPy'ün nanolif yapısına katılması hedeflenmiştir. Bu amaçla da AgPPy/DMF çözeltisi kabuk çözelti olarak kullanılmak üzere hazırlanırken, P (AN-ko-IA)/DMF çözeltisi de öz çözelti olarak kullanılmak için hazırlanmıştır. Tez içerisindeki diğer koaksiyel elektroeğirme çalışmalarında kullanılan elektroeğirme parametrelerinin aynıları bu çalışma adımında da uygulanmıştır ve sonuç olarak boncuklu yapıya sahip olmayan, kontinü P (AN-ko-IA) (öz)/AgPPy (kabuk) nanolifleri elde edilmiştir.

Sonuç olarak, tez kapsamında yapılan deneysel çalışmaların sonucunda metal/metal oksit içerikli polimer tabanlı nanolifler elde edilebilmiştir. Detaylı karakterizasyon sonuçları da bu nanoliflerin fonksiyonel malzemeler olarak tıbbi alanda özellikle de doku mühendisliği ve yara örtüsü uygulamalarında kullanılabileceğini göstermiştir.

1. INTRODUCTION

Nanocomposite materials are of great interest due to their advantage of combining the properties of two or more different materials and their good mechanical, electrical and thermal properties. Polymers have been selected as proper materials for nanocomposites and nanocomposites can be generated by using nanometals, metal nanoparticles, conductive polymers etc. There has been an increasing interest in the deposition of the composite of nano-metal and conductive polymers onto polymer latexes since polymers are regarded as excellent binding materials for the formation of stable colloidal dispersion of metals [1–3].

Silver (Ag) is a nontoxic metal but also a toxic element for microorganisms. It generates bond to microbial DNA and sulfydryl groups of the metabolic enzymes, avoiding bacterial replication and bacterial electron transport. It can also be used as a conductive material for the applications requiring conductivity. Polyacrylonitrile (PAN) is an important engineering polymer that can be efficiently used in many applications due to its thermal stability, high mechanical properties and chemical resistance. Thus, by combining PAN and Ag, it is possible to generate functional materials with anti-electrostatic, fungicidial and UV-resisting effects. The modification of fibers with conducting polymer-silver composites enhances conductivity and further reduces microbial attack [4–6].

Moreover, obtaining fibers in the nano-scale gives so many benefits. Electrospun nanofibers have small pore size, high porosity and high surface area. The porous structure gives the advantage of higher fiber interconnectivity. The nanofiber composition can also be controlled or modified according to the required functionality of the nanofibers obtained by electrospinning. These outstanding properties make polymer nanofibers to be good candidates for many applications like filtration, tissue engineering, sensors, wound dressings, energy conversion and storage, catalysts and enzyme carriers, protective clothing, sensors, drug delivery, cosmetics, electronic and semi-conductive materials [7, 8].

The first aim of this thesis was the synthesis of P (AN-co-IA) copolymer and combination of it with Fe_3O_4 and Al_2O_3 nanoparticles in nanofibrous structure. Since the most crucial point was the dispersion of metal oxide nanoparticles in polymer solution, a great deal of optimization studies were conducted on finding the suitable amount of Fe_3O_4 and Al_2O_3 nanoparticles, by using PAN polymer solutions. Then electrospinning of the polymer solutions including metal oxide nanoparticles was performed via conventional electrospinning. In addition to conventional electrospinning, Al_2O_3 nanoparticles were also integrated into the polymer structure via coaxial electrospinning.

The second aim was introducing AgNPs into nanofiber structures. For this reason, in addition to P (AN-co-IA) and PAN polymers, P (3HB) and P (3HO-3HD) polymers were also utilized. Addition of AgNPs was achived via different chemical and physical methods. AgNPs were synthesized in-situ in the presence of P (AN-co-IA) and DMF without using any additional reductants. After their formation, nanofibers of P (AN-co-IA)/Ag was achieved via conventional electrospinning. Except in-situ reduction, UV-irradiation was applied to convert $AgNO_3$ to AgNPs. UV-irradiation was implemented on P (AN-co-IA) (core)/ $AgNO_3$ (shell) nanofibers which were obtained by coaxial electrospinning. Moreover, as a different study, colloidal AgNPs were deposited onto P (3HB) /P(3HO-3HD) nanofibers via dip-coating. For each mentioned studies, a detailed optimization was experimented not only for electrospinning parameters but also for preparation of the solutions and reduction processes.

As a final aim, AgNPs was obtained by the help of conducting polymer, pyrrole (Py). By using chemical oxidation reaction, AgPPy nanoparticles were synthesized and incorporated into P (AN-co-IA) via coaxial electrospinning.

For all the obtained nanofibers, detailed spectroscopic, morphologic and thermal characterizations were performed. Furthermore, antimicrobial activity studies and biological evaluations of P (AN-co-IA)/Ag nanofibers (obtained from conventional electrospinning) and P (3HB) /P(3HO-3HD)/Ag nanofibers were carried out.

Related to the characterization results, it could be fairly said that the properties of the host polymers were enhanced by the presence of silver, or metal oxide nanoparticles. Most importantly, the resultant nanofibers could be used in the applications where conductivity and antimicrobial activity are desired.

2. LITERATURE REVIEW

2.1 Information on Host Polymers Used in the Thesis

2.1.1 Polyacrylonitrile

Polyacrylonitrile (PAN) whose molecular formula is $[C_3H_3N]_n$, (Figure 2.1) has a high melting point and it is a relatively insoluble polymer [9].

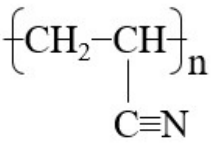

Figure 2.1 : Chemical formula of PAN.

PAN homopolymer was obtained via free radical polymerization process of acrylonitrile (AN) [10]. Although AN monomer was known from 1890s, PAN polymer was effectively used for fiber formation after 1925 due to the difficulties in dissolving it. In 1940, DuPont discovered an appropriate solvent for PAN and then PAN homopolymer was started to use for fiber production. PAN can be dissolved in polar solvents like N,N Dimethylformamide (DMF), dimethyl sulfoxide (DMSO), dimethylacetamide (DMAc), tetramethylsulfide, aqueous solutions of carbonate and some mineral salts. However, when crosslinked, PAN resists to swelling in common organic solvents [11]. The obtained PAN fibers are used in a wide range of applications in textile industry, but they are most widely utilized for carbon fiber production [9]. Compared to pitch and rayon, which are also carbon fiber precursors, PAN has been reported to be the most appropriate precursor for carbon fiber production due to higher carbon yield, melting point, high thermal stability and strength. The carbon yield of PAN is two times greater than rayon [9, 12, 13]. Carbon fibers produced from PAN precursor, have peculiar features such as light weight, excellent specific strength and stiffness, and low cost, which make them to be used as reinforcement materials for structural composites [14].

Intermolecular interaction between the polymer chains allows PAN to have a high melting point (~317 °C) and partial solubility in several solvents. In addition, highly polar nitrile groups of PAN hinder the alignment of molecular chains and cause difficulties in spinning. In order to ease the solubility and dyeability of PAN, PAN copolymers are formed by the addition of certain monomers like vinyl acetate (VAc), methylacrylate (MA), methylmethacrylate (MMA) during the polymerization process of PAN. The monomers can be included to the polymerization either single or one or more monomers can be used together [11, 15, 16].

A series of thermal treatments which are stabilization, carbonization and graphitization conducted in order to obtain carbon materials from PAN precursor. Among them, the most vital process is the thermal oxidative stabilization (TOS). The stabilization of PAN homopolymer is initated by a free radical cyclization reaction at a high temperature and sudden heat release can occur by causing faults in the resultant carbon fiber. It is aimed to decrease the initiation temperature of cyclization, occuring in the stabilization step, by the addition of comonomers into PAN structure [17–19]. Generally, PAN-based copolymers are consisted of at least 95 mol % AN and a maximum of 5 mol % comonomer [18]. Acrylate and methylacrylate are the monomers, specifically incorporated for enhancing solubility, drawability and spinnability, while acrylic acid (AA) and itaconic acid (IA) are preferred to initiate the cyclization reaction via ionic mechanism [17, 18]. The dye absorption of the fiber also increases when ketones, esters or alcohols are used since they are nonionizable comonomers [20, 21].

Miller and coworkers produced and examined PAN-MA copolymer to achieve melt spinning of economical precursor fibers for carbon fiber production. In the study, binary systems of polar additives were incorporated into PAN-MA copolmer structure as modifiers and the effect on melting temperature was observed. It was informed that PAN-MA copolymers which were either mixed with water or nitrile-containing melting point modifiers were good candidates for melt spinning [22].

Melt spinnable PAN-MA copolymer was also synthesized by Bhanu et al via redox and solution polymerization techniques, seperately. Each time, a parameter of the polymerization was changed and the copolymer structure was examined. It was mentioned that PAN-MA copolymers, which contain 15 mol % MA were the best to be carbon fiber precursors [20].

Solubility of PAN polymer was investigated after the copolymerization of PAN with VAc by Cetiner and coworkers. It was declared that in case of VAc presence, the solubility of PAN enhanced [23].

Rao et al. synthesized P (AN-VAc) copolymer and tried to improve the strength of PAN and reduce its brittleness. In order to use the copolymer in lithium-ion battery applications, it was activated by PMMA since PMMA had the compability with electrolyte and electrodes of lithium ion battery. It was captured that the polymer electrolyte produced from P (AN-VAc)/PMMA structure, had high ionic conductivity [24].

Ismar and Sarac studied on carbon nanofiber production from P (AN-co-AA) precursor. In the study it was aimed to reduce energy consumption during carbonization process by the use of AA. The addition of AA into PAN structure not only helped to decrease the energy comsumption during carbonization but also allowed to form ladder type structure during oxidation step. Due to the carboxyl group, existing in AA chemical stucture, cyclization process started at a lower temperature that was a great benefit for carbon fiber fabrication [25].

Beyond carbon fiber production, AA was utilized with PAN to obtain a nanofibrous membrane. Yang et al. fabricated PAN-AA/PAN nanofibrous composite membrane by double-layer electrospinning and crosslinked it with calsium (Ca^{2+}) and magnesium (Mg^{2+}) ions. The filtration performance of the produced composite membrane was tested and it was revealed that PAN-AA/PAN nanofibrous composite membrane could keep high permeate flux (> 170 L(m^2h)) after 12 test duration [26].

2.1.2 Poly (acrylonitrile-co-itaconic acid)

IA was discovered in 1837 by Baup after thermal decomposition of citric acid. It is defined as an α-substituted acrylic or methacrylic acid and also isomeric with citraconic and mesoconic acid. The chemical formula of IA is $C_5H_6O_4$ (Figure 2.2) and it is stable at acidic, neutral and middle basic conditions at moderate temperatures [27].

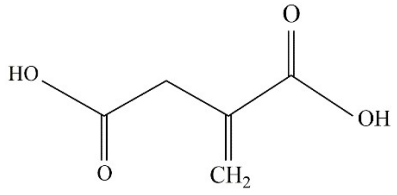

Figure 2.2 : Chemical formula of IA.

It can be simply integrated into polymers and effectively used in the production of synthetic fibers, in binders, coatings, adhesives and thickeners. When used together with PAN, deeper shades and better dying performance with improved dye absorption were observed [27].

IA is incorporated into PAN polymer in order to decrease the initiation temperature of cyclization step of carbon fiber production. Since IA has two carboxylic groups, it has been defined as one of the most efficient comonomers resulting in better adhesion and increased latex stability of polymers [17, 27, 28]. It causes ionic cyclization reaction during TOS by giving increased char yield due to having two carboxylic acid groups [17, 18].

Cho and Hong tried to determine the optimum composition of PAN copolymers for enhanced TOS temperature. In this regard, IA, MA and MMA were utilized as comonomers of PAN with similar amount (~3 mol %) of carbonyl groups. It was informed that by the use of MMA as comonomer, TOS reaction occurred quite similar to that of PAN. However, in the case of IA of MA use, efficient initiation reaction and a high ultimate degree of the TOS were observed [17].

Devasia et al. studied on the cyclization reaction of PAN-IA copolymer by differential scanning calorimetry (DSC) in the temperature range of 175-200 °C. The results showed that the cyclization reaction was initiated via an ionic mechanism. The initiation temperature was lowered to 180-200 ° C. Moreover, DSC exotherm curve turned to be broader and less intense [29].

The effect of IA on the structural evolution and thermal behaviour of PAN during TOS were examined by Ouyang et al. Fourier transform infrared (FTIR), DSC and thermogravimetry (TG) were used for the analysis. Just a small amount (1.5 mol %) of IA was copolymerized with AN. It was seen that the cyclization reaction initiated at a lower temperature. In addition, a new exothermic peak occurred at a lower temperature, which supported the ionic cyclization reaction. While a slight increase of weight loss was observed in the second step of TG curve, a decrease of weight loss was seen in the third step. It could be understood from the weight loss behaviours that both dehydrogenation and oxygen uptake reactions were promoted by IA. As a final conclusion, it was emphasized that even a small amount of IA contributed to save energy by initiating the cyclization reaction at a lower temperature [30].

Yu et al. aimed to distinguish the effect of air and IA on the enhancement of cyclization reaction. That why, via DSC, the thermal features of PAN-IA copolymer was analyzed in oxidative and nonoxidative atmospheres. Also by thermogravimetric analysis (TGA), the mechanism of oxygen effect on the stability of molecular chains was examined. It was noted that, in nonoxidative atmosphere, IA hardly had an influence on the initiation temperature of cyclization reaction. When the absence of IA, the oxidative atmosphere had a little effect on cyclization reaction. However, in case of both IA and oxidative atmosphere existence, the cyclization and oxidation reaction started at a lower temperature compared to PAN homopolymer. It was concluded that oxygen had a major impact on the molecular chain stability and carbon network formation as well [31].

Hao et al. produced atactic PAN-IA copolymers which had different IA amounts varying from 0 to 22 mol %. The goal was to determine the effect of IA on initiation mechanisms of the thermal stabilization reactions by using FTIR, DSC and nuclear magnetic resonance (NMR). It was obtained that incorporation of IA caused changes on AN segment length and ladder structure formation. PAN-IA copolymers decomposed at a higher temperature than PAN homopolymer. Moreover, using IA in high amounts blocked the cyclization initiated by IA itself [32]. Ismar et al also contributed that IA was crucial to improve the oxidation mechanism of the P(AN-co-IA) nanofiber webs. Oxygen uptake, dehydrogenation and cyclization processes were achieved more effectively for the P (AN-co-IA) nanofiber webs than the homopolymer PAN nanofiber webs [33].

While some researches [34–36] focused on examination of IA content of PAN-IA copolymers for the analysis of thermal behaviour, some of others determined the effect of polymerization factors [37–39]. The suitable IA content in PAN copolymers was investigated by Fu et al. P (AN-co-IA) copolymers were prepared by utilizing the IA in the amounts of 0.5 wt %, 0.5 mol %, 1.0 mol %, 2.0 mol %, and 3.0 mol % using one-step batch slurry polymerization. The structural change and thermal features of the copolymers were observed by DSC, FTIR and X-Ray diffraction (XRD). It was seen that copolymers containing 0.5 mol % and 1.0 mol % owned more conjugated carbonyl groups, cyclized structures, and faster evolution rate than the other IA containing copolymers. On the other side, it was understood that, P (AN-co-IA) copolymer with 3.0 mol % IA didn’t promote the cyclization reaction. Furthermore,

0.5 wt % and 1.0 mol % IA allowed to obtain higher carbon yield than the others. That's why, it was suggested to use IA amount from 0.5 mol % to 1.0 mol % in order to have carbon fibers with better performance [34]. Ghorpade et al. also concentrated on the effect of IA content to obtain high performance carbon fibers. By using free radical polymerization, P (AN-co-IA) copolymers were synthesized with different amounts of IA ranging from 1 to 6 mol %. The samples were subjected to carbonization at elevated temperatures (400 ~1200 °C). The yields of the samples were determined by TG. According to the results, the copolymers consisting IA in the content of 3 to 6 mol %, showed a large amount of weight loss at elevated temperatures. Subjected to carbonization at elevated temperatures, specifically at 1200 °C, P (AN-co-IA) copolymers which contained 1 mol % and 2 mol % resulted in better yield of the carbon and higher electrical conductivity compared to the other prepared copolymer samples. It was suggested from the authors to utilize the IA content between 1 and 2 mol % for the formation of high performance carbon fibers [35]. Zhang and coworkers also suggested to use IA content as 1.0 mol % in PAN-IA copolymers for reduced initiation temperature of cyclization process, a wider range of exothermic temperature in order to obtain carbon fibers of high performance [36].

Devasia and coworkers examined not only the kinetics of copolymerization at higher contents of IA but also the influence of water in DMF on the reactivity ratio. DMF was the most widely used solvent for the copolymerization of AN and IA. It was highly hygroscopic and when blended with water, the reactivity ratio of the copolymerization changed. While IA radicals had little reactivity towards its own monomer, AN radicals have a great reactivity to IA unit. In addition, if IA was fed to the polymerization at low concentrations, the copolymerization resulted in the enrichment of IA in the polymer. However, if the utilized amount of it was further increased, subsequent decrease of IA was observed in the polymer. It was emphasized that incorporation of IA more than 50 % was impossible. On the other hand, existence of water in the polymer medium decelerated the both reactivity of IA and the overall polymerization rate. Moreover, IA itself retarded the polymerization rate considerably [37]. Zhao et al. also made some contributions on the monomer reactivity ratios of AN and IA in case of aqueous deposited polymerization. It was commented that increasing the polymerization temperature gave an advantage to the aqueous deposited copolymerization process to be ideal copolymerization since the reactivity ratios of

AN and IA approached to unity. Additionaly, the reactivity ratio of AN increased and IA decreased when the polymerization conversion surpassed 5 % [38]. Fu et al. synthesized P (AN-co-IA) copolymer at different polymerization durations which were 30, 90 and 180 minutes and then evaluated the structural change of the copolymers by FTIR-ATR during TOS process. The analysis results demonstrated that by changing the polymerization time for each polymerization did not have a strong effect on the structural evolution of the copolymers during TOS [39].

Subri et al. prepared P (AN-co-IA) nonwoven fibers by electrospinning and then modified them chemically with thioamide. It was aimed to create active functional groups on the high surface area of the P (AN-co-IA) nonwoven fibers. The modification was examined via FTIR and scanning electron microscope (SEM). By using to the FTIR results, the prepation of P (AN-co-IA) nonwoven fibers was approved. Besides, SEM characterization showed that both the virgin P (AN-co-IA) and modified P (AN-co-IA) fibers were in micron range in diameter, which revealed high surface area of the fibers. It was thought that having micron size range allowed the fibers to be used in various applications such as for adsorption or extraction of analytes [40].

Abeykoon and coworkers developed a new way to fabricate electrode materials from P (AN-co-IA) nanofibers for high performance energy storage systems. Direct carbonization of carbon fibers by the incorporation of decomposable IA segments, behaving as an in-situ porogen, was achieved. Related to thermogravimetric analysis-mass spectrometry (TGA-MS), carbon dioxide (CO_2) gas evolution was observed from P (AN-co-IA) electrospun nanofiber web which were heated to nearly 220 °C in air. However, this was not the case for PAN nanofiber webs. That meant that carboxyl groups existing in P (AN-co-IA) structure acted as in-situ porogens and released CO_2 during carbonization process, which allowed to gain higher specific surface are of the carbon nanofibers. As a concluion, porous carbon nanofibers could be obtained by an easy and a simple step carbonization procedure [41].

2.1.3 Polyhydroxyalkanoates

Polyhydroxyalkanoates (PHAs) are a family member of nature polymers that are produced by microorganisms in the environment containing excessive carbon and limited nitrogen and phosphorus [42–45]. More than 90 types of gram-positive and

gram-negative bacterias producing PHAs under aerobic and anaerobic condition have been found. PHAs are defined as linear aliphatic polyesters, which are composed of R-hydroxyalkanoic acids (3-, 4-, 5- and 6-hydroxyalkanoic acids) [42].

2.1.3.1 Structure of polyhydroxyalkanoates

PHAs are linear aliphatic polyesters that are consisted of monomeric units of R-hydroxyalkanoic acids. Metabolic capability of microorganisms and the carbon sources determine the chemical structure of PHA (Figure 2.3). Related to the bacteria and metabolic capability of them, the molecular mass of PHAs change in the range of 200-300 kDa. In addition, pH and fermentation type are the other factors that have an impact on the molecular mass of PHAs [42].

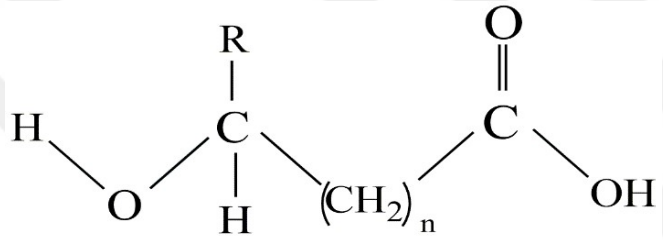

Figure 2.3 : Chemical structure of PHA.

The name of the polyhydroxyalkanoate-based polymers is given related to the R and n (number of the carbon atoms). If the R group is equal to CH_3 where n is 1, the polymer is named as poly(3-hydroxybutyrate) (P3HB) or polyhydroxybutyric acid. If the R group is C_3H_7, it is named as polyhydroxyoctanoate (PHO) [43]. Monomeric structure of different PHAs is shown in Figure 2.4.

2.1.3.2 Classification of polyhydroxyalkanoates

PHAs fall into three classes which are short-chain length (SCL) PHAs, medium-chain length (MCL) PHAs and long-chain length (LCL) PHAs. SCL-PHAs are consisted of 3 to 5 carbon atoms where MCL-PHAs and LCL-PHAs have 6 to 14 carbon atoms and more than 14 carbon atoms, respectively [42, 43, 46, 47]. The congeners of 3-hydroxyvalerate and 3-hydroxybutyrate are examples of SCL-PHAs, 3-hydroxydecanoate, 3-octanoate and 3-hydroxyhexanoate are the examples of MCL-PHAs, whereas LCL-PHAs are rarely studied.

Polymer	Monomer
Poly-3-hydroxybutyrate (P3HB)	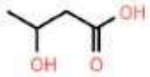
Poly-3-hydroxyvalerate (P3HV)	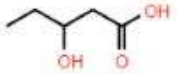
Poly-3-hydroxyhexanoate (P3HHx)	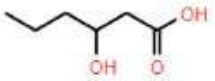
Poly-3-hydroxyoctanoate (P3HO)	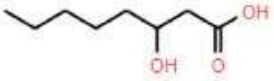
Poly-3-hydroxydecanoate (P3HD)	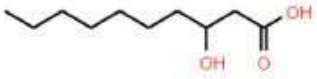

Figure 2.4 : Monomeric structures of different PHAs [42].

Structure of SCL and MCL-PHAs are given in Figure 2.5 [43]. Furthermore, a combination of SCL-PHA and MCL-PHA can also be produced [48]. The most widely utilized PHA is poly (3-hydroxybutyrate) (P (3HB)) [47].

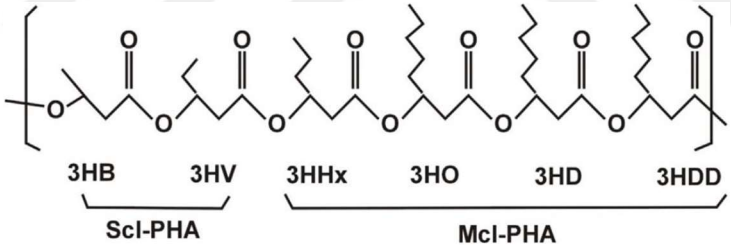

Figure 2.5 : Structure of PHAs with respect to classification, where 3HB = 3-hydroxybutyrate, 3HV = 3-hydroxyvalerate, 3HHx = 3-hydroxyhexanoate, 3HO = 3-hydroxyoctanoate, 3HD = 3-hydroxydecanoate and 3HDD = 3-hydroxydodecanoate [43].

2.1.3.3 Properties of polyhydroxyalkanoates

PHA is a bio-based, biodegradable and biocompatible material [45–47, 49, 50]. Monomer side chain length has a major effect on thermal and mechanical properties. Therefore, properties of PHAs change according to the chemical structure [43, 44]. Many PHAs demonstrate mechanical and thermal features resembling polypropylene (PP) which is a petroleum-based plastic. PHAs are insoluble in water but soluble in chloroform and other chlorinated solvents. Melting temperature and glass transition temperature of PHAs vary between 40-180 °C and -50-4 °C, respectively. However,

degradation temperature, Young's modulus, and tensile strength are all dependent on the type of the chemical composition [43].

SCL-PHAs are brittle, stiff and have a a high degree of crystallinity (60-80 %) [42, 46]. PHB which is a SCL-PHA, has an outstanding resistance to moisture, hydrolytic attack, and UV. In addition, it has a good barrier characteristic to gases [43]. Since SCL-PHAs are rigid and brittle, they are not appropriate for drug delivery, vascular and soft issue applications. Compared to the SCL-PHAs, MCL-PHAs has lower crystallinity and thus a lower glass transition temperature, tensile strength and a high elongation at break. The hydrolysis of ester-bonds occurs in amorph regions and since MCL-PHAs possess more amorphous regions, in-vitro and in-vivo degradation rate increases. Moreover, because of having a flexible structure, it is advantageous to use MCL-PHAs in tissue engineering applications. However, viscoelastic features of them at room temperature create limitations in electrospinning process of MCL-PHAs. Electrospun nanofibers of MCL-PHAs can not preserve their shape because of being sticky [46]. In order to enhance the use and flexibility of SCL-PHAs, they can be combined with MCL-PHAs [51].

Compared to the widely used synthetic biopolymers such as polylactic acid (PLA), polyglycolic acid (PGA), and polycaprolactone (PCL), PHAs are more advantageous materials. For instance; while the mechanical and physical features of PLA, PGA, and PCL can not be changed, those properties differ in PHAs according to the chemical composition of PHAs. Furthermore, degradation monomers of PHAs are less acidic than PLA, and PGA, which allows PHAs to be more biocompatible [46].

2.1.3.4 Applications of polyhydroxyalkanoates

Since PHAs are biocompatible and biodegradable polymers, they are mainly used in biomedical applications such as tissue engineering, drug delivery, protein microarray, bone regenaration, osteoblast attachment, proliferation and differentiation, anti-cancer activity, vascular grafts, memory enhancer, etc. applications [43, 48, 50]. Specifically, P (3HB) can be used for delivery of antibiotics [50], P (3HO-co-3HHx) copolymers can be utilized as drug delivery agents for ketoprofen and tamsulosin [50], 3-hydroxydecanoic acids conjugated to D-peptide can serve as anti-cancer agent [52], PHB-Hydroxyapatite composite can help the regeneration of bones [53], Poly-3-

hydroxybutyrate, Poly-4-hydroxybutyrate can be applied for inhibiting the inflammation and enhancing wound healing capacity [53].

Li et al. produced nanofibers of PHB, PHB/P (HB-HHx) and PHB/P (3HB-4HB) in order to integrate the advantages of biopolymers and nanofiber structures. It was mentioned that better cell support and cell viability were achieved via PHA-based nanofibers than solid PHA matrices. Additionally, mechanical and structural features of the obtained materials could be altered by changing the monomer ratios in the blends [54].

Xu et al. prepared films and nanofiber mats from three different PHA polymers and evaluated their possibility to be used on neural stem cells growth and differentiation. It was dictated that compared to the films, nanofiber webs exhibited better cellular adhesion and connection on neural stem cells. Furthermore, it was proposed that utilizing PHAs in copolymer form for the neural stem cells applications, especially for repairing spinal cord injury, more satisfying results could be obtained [55].

Lu and coworkers suggested to modify PHAs for competing with their hydrophicity and thus enhancing the nueral regeneration and cell adhesion. In this regard, functionalized PHBHHx films were produced in order to cure ischemic brain damage. It was revealed that when neural stem cells/neural progenitor cells cultured on PHBHHx films, a huge amount of them achieved to survive and had the ability to differentiate into neurons [56]. Various method for surface functionalization of SCL-PHAs was also reviewed by Vigneswari et al. [47].

Lee et al. also prepared PHA-based nanofibers for drug, which was paclitaxel, delivery applications. It was aimed to eliminate the side effects such as cardiotoxicity, neurotoxicity and nephrotoxicity of paclitaxel by releasing it via PHA-based nanofibers. Beyond the release studies, the influence of electrospinning parameters on the fabrication of PHA-based nanofibers was examined as well. It was said that the most crucial parameter was polymer molecular weight to achieve a favorable nanofiber mat for drug accommodation. In addition, it was seen that drug release pattern was more stable at low drug loading concentrations compared to the higher ones [57].

PHA based core-shell nanofibers for wound dressing applications were prepared by Li et al. As core layer dodecyltrimethylammoniumchloride (DTAC) and polyvinylpyrrolidone (PVP), where as shell layer PHA/ poly(ethylene succinate)

(PES) were selected. Due to the hydrophobic feature of PHA/PES shell layer, biocide was prevented from unsatisfactory release. Hydrolyzation of shell layer in the existence of bacterial lipase contributed to obtain requested antimicrobial impacts on the bacteria, which was a proof for the novel core-shell PHA-based nanofibers to be used for the curing of wound diseases [58].

2.2 Information on Additive Materials Used in the Thesis

2.2.1 Iron (II, III) oxide (Fe_3O_4)

Metal oxides are of great interest due to their peculiar chemical and electrical properties. They are generated by surrounding the metal ions by oxide ions. There are quite a number of metal oxides all having diferent physical, chemical, optical and magnetic properties which allow them to be successively used in various applications [59, 60].

Iron is the most current transition metal in Earth's crust, that's why it is regarded as the heart of the existing infrastructure. Iron oxides are generated by the chemical combination of iron and oxygen and up to now nearly 16 types of iron oxides have been detected. Visibly, iron oxides are identified in the form of rust. Since iron oxides are widespread and cheap materials, their existence is indispensable in many geological and biological processes [61].

Fe_3O_4 (ferroferric oxide /magnetite), γ- Fe_2O_3 (maghemite) and α- Fe_2O_3 (hematite) are the most commonly utilized iron oxide forms. Among these three iron oxide forms, Fe_3O_4 and γ- Fe_2O_3 nanoparticles have attracted more attention because of their superparamagnetic features, low toxicity and high surface area to volume ratio. They are popular in biomedical applications such as drug delivery, magnetic resonance imaging (MRI), thermal therapy and protein immobilization. Moreover, they can be used in coatings, concretes and paints [61].

Zhang et al produced nanocomposite fibers of PAN/ Fe_3O_4 via electrospinning by loading 4 wt %, 5 wt %, 6 wt %, 6.5 wt %, 7 wt % and 10 wt % amounts of Fe_3O_4 (nearly 13 nm in size) into the prepared PAN/DMF solutions. Prior to electrospinning, 40 minutes ultrasonication was applied to the Fe_3O_4 containing solutions to achieve well dispersion of nanoparticles in the solutions. Electrospinning parameters and morphologic, chemical, and magnetic properties of the prepared nanofibers were

examined in detail. It was observed that electrosinning parameters had a major impact to obtain bead-free and continuous nanofibers. Fe_3O_4 presence affected the crystallization structure of PAN nanofibers pointing out that Fe_3O_4 and PAN had an interaction. Most importantly, Fe_3O_4 nanoparticles evolved into magnetically harder materials compared to their dry powder form after the dispersion in PAN/DMF solutions [62].

Guo and coworkers combined Fe_3O_4 nanoparticles and poly (acrylonitrile-co-acrylic acid) P (AN-co-AA) polymer, which was synthesized by water phase precipitation polymerization, in order to obtain P (AN-co-AA)/ Fe_3O_4 composite nanofibers. 44 wt % and 60 wt % loadings of Fe_3O_4 nanoparticles were carried out. Prior to electrospinning, the solutions were subjected to ultrasonication for well dispersion of the nanoparticles. Then, by the application of electrospinning parameters as 14 kV voltage, 15 cm needle tip-to-collector distance and 1 ml/h feed-rate, electrospun nanofibers of P (AN-co-AA)/ Fe_3O_4 could be fabricated. It was pointed out that uniform distribution of Fe_3O_4 nanoparticles on the nanofiber webs could not be achieved even though the ultrasonication which was applied before electrospinning. The nanoparticles had the tendency to accumulate on the nanofiber surfaces, which was mostly the case for 66 wt % Fe_3O_4 loading. However, related to the characterization results conducted for the identification of magnetic properties of Fe_3O_4, it was understood that the produced nanofibers were good candidates to be used in enzyme immobilization [63].

Sabzroo and coworkers also studied on the production of P (AN-co-AA)/ Fe_3O_4 by focusing mainly on the investigation of electrospinning parameters and impact of the amount of Fe_3O_4 loadings on the prepared nanofiber morphologies. In the study, Fe_3O_4 nanoparticles were synthesized via solvothermal method and incorporated into the P (AN-co-AA) polymer solutions at 0 wt %, 10 wt %, 25 wt % and 40 wt %, seperately. It was seen that bead-free and continuous nanofiber structures were available when the electrospinning parameters were optimized as 12 wt % polymer solution concentration, 20 kV applied voltage, 20 cm needle tip-to-collector distance and 0.5 ml/h feed-rate. Related to the optimized electrospinning parameters, increase (from 0 wt % to 40 wt %) in the Fe_3O_4 nanoparticles amount resulted in decreased nanofiber diameters (from 359 nm to 74 nm). Moreover, magnetic features of the nanofiber samples were examined and the results were mentioned as 3.64 emu/g saturation

magnetization (Ms), 0.0918 emu/g remnant magnetization (Mr), 21.67 Oe coercivity (Hc) and 0.0252 Mr/Ms ratio. That's why, the nanofibers could be used in nanofiltration or adsorption applications [64].

Liu et al. prepared PAN/ Fe_3O_4 composite nanofibers in order to use them as an adsorption material for tetracycline, a frequently used antibiotic and a crucial contaminant in aquatic systems. Simultenaously, Fe_3O_4 nanoparticles and PAN nanofibers were produced and then via solvothermal treatment, the nanoparticles were coated onto PAN nanofiber surface. Deposition of Fe_3O_4 nanoparticles on nanofiber surface resulted in rougher nanofiber surface with average diameter of 458 ± 38.2 nm. For testing the maximum adsorption capacity of the nanofibers against tetracycline, pH impact study and X-ray photoelectron spectroscopy (XPS) characterization were performed. The maximum adsorption capacity of PAN/ Fe_3O_4 composite nanofibers was noted as 257.07 mg/g at equilibrium when pH was 6. Based on that result, it was suggested to use the prepared composite nanofibers for the elimination of several contaminants and antibiotics [65].

In addition to the studies conducted for the production of PAN/ Fe_3O_4 composite nanofibers via conventional electrospinning, Wang and coworkers prepared hollow PAN/ Fe_3O_4 composite nanofibers via coaxial electrospinning to use them as microwave absorption materials. In the study, by using chemical co-precipitation process, Fe_3O_4 nanoparticles were synthesized and added into the prepared PAN/DMF solution with the amount of 9.1 wt% to be utilized as shell fluid. Simultaneously, 30 wt % PVP/DMF solution was prepared as core solution. Then, after coaxial electrospinning process, the core component was withdrawn with a post-treatment and thus hollow PAN/ Fe_3O_4 composite nanofibers were collected. It was concluded that, the strong absorption frequency banwidth was expanded and the maximum reflection loss was enhanced when the composite nanofibers were in hollow form [66].

Moreover, scientists also tried to functionalize PAN/ Fe_3O_4 nanofibers for improving the final properties of the composite nanofibers. In this regard, Huang et al. incorporated polyaniline (PANI) into PAN/ Fe_3O_4 nanofiber structure for both facilitating the spinnabilty of PANI and enhancing the stability and electrical conductivity of the resultant product. Fe_3O_4 nanoparticles were mixed during the microemulsion in-situ polymerization of aniline. By the help of the surfactant, cetyltrimethylammonium bromide (CTAB), a satisfactory coating of Fe_3O_4

nanoparticles by PANI was achieved. By using the electrospinning method, PANI/ Fe_3O_4-PAN nanofibers were fabricated with the diameters of 168 nm-300 nm. The resultant nanofiber diameters had a direct relationship with the added Fe_3O_4 amount. Furthermore, the conductivity and magnetic features of the nanofibers strongly depended on the amount of doped Fe_3O_4 amount as well as the presence of PANI in the nanofibrous structure [67].

Ouyang and coworkers synthesized aluminum doped iron oxide nanoparticles via precipitation method since aluminum doped iron oxide nanoparticles had a superior thermal and chemical stability. The aim of the scientists was to examine the influence of the synthesized nanoparticles on magnetic properties of PAN-based composite nanofibers. It was indicated that the resultant nanofiber diameters were decreased in the presence of aluminum doped iron oxide nanoparticles due to viscosity and electric field change after the addition of them. It was summarized that when the incorporated nanoparticle content was 4 wt %, magnetic features of the nanofiber webs was enhanced greatly (nearly 10 times); however, when their amount was increased up to 8 wt %, the positive effect on increasing the magnetic features was hindered [68].

Ghapanvari et al. developed an electrochemical sensor consisted of Fe_3O_4@ multiwalled carbon nanotubes (MWCNTs) and PAN nanofibers nanocomposite film for the detection of imatinib anticancer drug. By the combination of Fe_3O_4 nanoparticles, MWCNTs and PAN nanofibers, it was desired to obtain an electrochemical sensor with high sensitivity and selectivity compared to the conventional ones. As desired, the modified electrochemical sensor containing Fe_3O_4 nanoparticles could be able to detect imatinib anticancer drug at lower concentrations due to the admirable electrocatalytic performance [69].

2.2.2 Aluminum oxide (Al_2O_3)

Aluminum oxide (Al_2O_3) nanoparticles which are also called as alumina are of great interest owing to their novel features such as small particle size, high specific surface area, high porosity and high thermal stability. Related to these essential properties, they find applications as semiconductors, polishing and packing materials, cosmetic fillers, high performance ceramics and so on. In addition, they are widely used in resins and composite materials [70].

Azad fabricated electrospun alumina nanofibers by electrospinning after preparation of a homogenous electrospinning solution consisted of blending aluminum 2, 4-pentanedionate precursor and polyvinyl pyrrolidone (PVP). It was desired to obtain a ceramic material from the prepared electrospun composite, that's why the as-spun fibers were subjected to calcination in an acceptable heating rate protocol between 1000°C and 1500 °C. Phase change of alumina nanofibers was observed in order to understand the possibility of convertion of fibrous structures to ceramic materials. It was noted that electrospun nanofiber mats of alumina could be changed to ceramic materials since they own superior structural character [71].

Shehata reported the impact of Al_2O_3 nanoparticles on the abrasive wear resistance of Al_2O_3 /copper matrix composites. For that purpose, Al_2O_3 nanoparticle reinforced copper matrix composites were produced by two different mechanochemical routes. In the composites, the amount of Al_2O_3 nanoparticles were determined to be 5, 10, and 15 wt %. Both of those simple and inexpensive chemical routes contributed to produce homogeneous distribution of Al_2O_3 nanoparticles in copper matrix. Furthermore, existence of Al_2O_3 nanoparticles enhanced the abrasive wear resistance of the composites and it was found that the enhancement had a direct relationship with the amount of utilized Al_2O_3 nanoparticle [72].

Since it was very difficult to obtain alumina samples with high surface area at elevated temperatures, Peng and coworkers focused on the examination of structural variations in fibrous crystallites of alumina materials which were obtained after the calcination of boehmite nanofibers at several temperatures. The observation results revealed that increase in calcination temperature resulted in coarser and shorter-shaped of Al_2O_3 nanofibers. Simultaneously, decrease in the specific surface area of them was determined. Most importantly, during the calcination, performed at different temperatures, Al_2O_3 nanofibers preserved their fibrous structure [73].

Dadvar et al fabricated magnesium oxide (MgO) and Al_2O_3 containing PAN-based carbon nanofibers and examined the change on pore characteristics of the resultant fibers in the presence of metal oxide nanoparticles. The content of MgO was 5, 10 and 15 wt % and it was 10, 15, 20 wt % for Al_2O_3. It was reported that the total pore volume and specific surface area of the samples increased by metal oxide nanoparticle addition. Additionally, those improvements enhanced the catalytic activity of samples.

Moreover, when the effect of MgO ve Al_2O_3 nanoparticles on the pore characteristics were compared, Al_2O_3 nanoparticles were found to be more effective [74].

Broujeni and Nilchi produced modified PAN/Al_2O_3 nanofibers by 2-amino-3-methyl-1-hexanethiol (AMH) in order to use the nanofiber mat as an adsorption material for thorium (IV) ion. First of all, Al_2O_3 nanoparticles were synthesized by hydrothermal process and then composite nanofibers of PAN/Al_2O_3/AMH were obtained by electrospinning. The adsorption performance of the resultant composite nanofibers was optimized by an experimental design, response surface methodology, and the results were explained with Langmuir and Freundlich models. Based on the adsorption results, it was fairly said that the elimination of thorium (IV) ion via the produced nanofiber web was much more effective than the ones existing in the literature with 67.8 minutes contact time at 5.7 pH [75].

Ke and Li aimed to give an insight on the changes of thermal properties of PAN-based composite nanofiber structure by loading different amounts of Al_2O_3 nanoparticles. Al_2O_3 nanoparticles were loaded in the amounts of 0, 5 and 10 wt % and regarded as heat transfer fillers in the PAN-based nanofibrous webs. While the melting enthalpies and melting peak of the composite nanofibrous membrane were 131–139 kJ/kg and 25°C, respectively; it was proved that by increasing the loaded Al_2O_3 amount, the values seriously shifted to higher numbers. In addition, the melting and freezing times of the samples were reduced. Related to the obtained results, the Al_2O_3 nanoparticle containing PAN-based nanofibrous webs had a high potential to act as temperature-regulating fibers [76].

Any other thermally stable nanofiber structure was fabricated by Fu et al. A blend of Al_2O_3 and titanium dioxide (TiO_2) was used to achieve 'particle-on-fiber' structure via electrospinning. The presence of Al_2O_3 nanoparticles gave the chance to control the grain size and phase transformation of TiO_2 nanofibers. The small grain size of Al_2O_3/ TiO_2 nanofibers assisted them to have a high adhesion energy to metals. In detail; it was seen that Al_2O_3/TiO_2 nanofibers had the ability to stabilize platinum (Pt) nanoparticles against sintering at high temperatures like 500 °C. Stabilizing the metal nanoparticles such as platinum (Pt) at 500 °C implied a new perspective for improving the thermal stability of ceramic nanofibers [77].

2.2.3 Silver nanoparticles (AgNPs)

Silver nanoparticles (AgNPs) have taken great attention due to their antibacterial [78–80], antiviral [81–84] and fungicidal [85–87] properties. These unique features allow them to be used in various applications in textile industry [88].

AgNPs can be synthesized by either chemical or physical methods. In chemical method, reducing agents are used in order to obtain AgNPs from silver precursors whereas in physical method laser impulse energy is applied to form AgNPs from silver ions. Although forming AgNPs from silver precursors is easier via physical method, chemical reduction is the most preferred technique [88].

In chemical reduction process, silver ions (Ag^{+}) are formed from silver precursors, converted to oligomeric clusters by reduction and further gathered in the form of AgNPs [88]. For the formation of AgNPs, the most widely used precursor is silver nitrate [89–92]. Silver acetate [93, 94], silver citrate [94–96] and silver chlorate [94, 95, 97] are also utilized as silver precursors for the formation of AgNPs. In addition, in order to achieve the reduction process successfully, several reducing chemicals such as borohydride, ascorbate, citrate, carbohydrates, alcohols, aldehydes etc are consumed [98–100]. Morphology and particle size of the synthesized AgNPs are incredibly affected by dispersion medium which also behaves as a stabilizer to prevent the particles from agglomeration [101, 102]. PVP [103], PAN [104], poly (ethylene glycol) (PEG) [105] etc are the most frequently used polymers as a stabilizer during the reduction process of silver ions.

Related to the applied process, AgNPs can be directly obtained from a polymer solution where the solvent is responsible to dissolve both the polymer and silver precursor or an additional step is required for the methods that do not include the common solvent for polymer and silver precursor [88].

In conventional method, AgNPs are formed and further doped in a polymer solution. However, by the application of conventional method, homogeneous dispersion of AgNPs can not be achieved since the AgNPs have the tendency to agglomerate. Therefore, more attention is given to in-situ synthesis of AgNPs [106].

It was explained that deposition of silver nanoparticles onto nanofibers were performed to improve their functions [107, 108].

Wang et al synthesized AgNPs in-situ to dispers them in PAN nanofiber mat. Formation of AgNPs was performed in-two steps. Within this context, 10 wt % PAN solution was prepared in N, N Dimethylformamide (DMF) and then loaded with silver nitrate ($AgNO_3$) whose molar ratio was equal to the molar ratio of repeat unit of PAN. After stirring for 24 hours at room temperature, the prepared solution was electrospun and PAN/$AgNO_3$ nanofiber mat was collected on a drum. Then, in order to reduce $AgNO_3$ to AgNPs, the prepared nanofiber mat was immersed into hydrazinium hydroxide (N_2H_5OH) aqueous solution. In 30 minutes of immersion, by the help of N_2H_5OH, $AgNO_3$ was transformed to AgNPs at room temperature and so AgNPs dispersed PAN nanofibrous structure could be obtained. Dispersion of AgNPs on a single PAN nanofiber was observed via Transmission Electron Microscopy (TEM) characterization and shown in Figure 2.6. In addition, the size of the silver nanoparticles was measured as 10 nm [109].

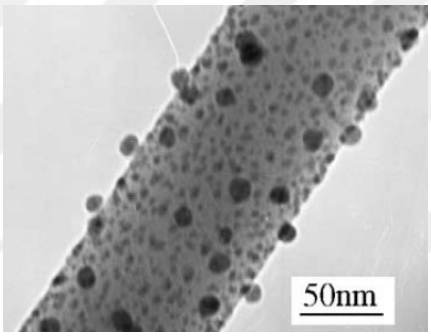

Figure 2.6 : TEM image of a single PAN nanofiber including dispersed AgNPs [109].

Selvam and Nallathambi produced AgNPs containing PAN nanofibers which were collected on PP spun-bonded nonwoven mat to be used as a filter membrane for bacterial filtration against *Staphylococcus Aureus* (*S. aureus*) and *Escherichia coli* (*E. coli*). $AgNO_3$ was first dissolved in DMF at various concentrations (5, 10 and 15 wt %) then mixed with 8 wt % PAN to form an approriate electrospinning solutions. Reduction of $AgNO_3$ to AgNPs was achieved in-situ by stirring the prepared polymer solution for 48 hours at room temperature. It was declared that nanofiber diameters and utilized $AgNO_3$ amount had an inverse proportion which meant that increasing the content of $AgNO_3$ resulted in decrease in PAN/Ag nanofiber diameters. Moreover, bacterial filtration efficiency of the prepared nanofibers was tested and reported that in order to obtain a bacterial efficiency of 99 % accuracy, the used amount of $AgNO_3$ had to be between 10 and 12.5 wt % [110].

Bortolassi et al. aimed to produce PAN/Ag nanofibers for not only filtration applications but also to gain bactericidal activity. In the study, different amounts (1, 10 and 50 wt %) of $AgNO_3$ were incorporated into the prepared PAN (9 wt %) solution and kept under stirring at room temperature for 48 hours in order to accomplish in-situ reduction of $AgNO_3$ to AgNPs. Afterwards, the polymer solution was electrospun and the nanofibers were collected on a rotating drum which was covered by a polyethylene terephthalate (PET) film. Filtration performance and bacterial activity tests of the resultant nanofibers were conducted and it was concluded that even 1 wt % $AgNO_3$ loading resulted in a superior filtration efficiency and perfect bacterial activity against *E coli*. Moreover, it was suggested to use the obtained nanofiber mats in medical masks, airline cabin, electronics and automotive industry since they were designed to be resistant and economic [111].

For the reduction of $AgNO_3$ to AgNPs, Ren and coworkers applied temperature in in-situ reduction method. First, 10 wt % PAN polymer solution was prepared in DMF. Since they aimed to functionalize neat PAN nanofibers, cellulose nanocrytals were added into the prepared PAN solution with the concentration of 0.2 wt %. Then, $AgNO_3$ (1.5 wt %) and silicon nanoparticles (0.15 wt %) were incorporated into the functionalized polymer solution which was heated to 90 °C for 15 minutes in a water bath. The heating application succeeded the reduction process of $AgNO_3$. In those chemical reactions, $AgNO_3$ acted also as an oxidant. Prior to electrospinning, the polymer solution was cooled to room temperature. After electrospinning via SEM characterization, the morphologies of AgNPs containing nanofibers were examined and it was seen that pores occured on the rough surface nanofibers. Those functionalized AgNPs containing nanofiber web was aimed to be used as a substrate for surface-enhanced raman scattering [112].

Wang et al. also applied temperature during in-situ reduction of $AgNO_3$ to AgNPs. 8 wt % PAN polymer solution was prepared in DMF and then $AgNO_3$ (molar ratio of $AgNO_3$ and repeat unit of PAN was 1/20) was mixed with the prepared PAN polymer solution in an ice-bath by stirring for 2 hours. Thereafter, only for 10 minutes the temperature of the solutions were increased to 90 °C in order to attain AgNPs. Furthermore, with the aim of improving antibacterial performance and achieving slow-release of AgNPs in nanofiber structure, β-cyclodextrin (2 wt %) was integrated into the PAN/Ag polymer solution before electrospinning. At the end, antibacterial

performance of the obtained PAN/Ag/ β-cyclodextrin nanofiber mat was evaluated and it was told that the resultant web could be favorably used against *S. aureus* and *E. coli* [113].

Karbownik et al. used ascorbic acid as a reducing agent for in-situ reduction of $AgNO_3$ to AgNPs. The reduction process of $AgNO_3$ occured by the existence of a PAN terpolymer, ascorbic acid and DMF solvent. Since PAN terpolymer molecules played a role as stabilizer for Ag^+ ions, no additional stabilizer was consumed in the method. Moreover, it was emphasized that the interaction of nitrile groups in PAN chain with silver ions prevented AgNPs from agglomeration. The representative mechanism of silver nanoparticles generated in PAN polymer was illustrated in Figure 2.7. After the reduction was completed, AgNPs containing polymer solution was wet-spun to fabricate PAN-based nanofibers [114].

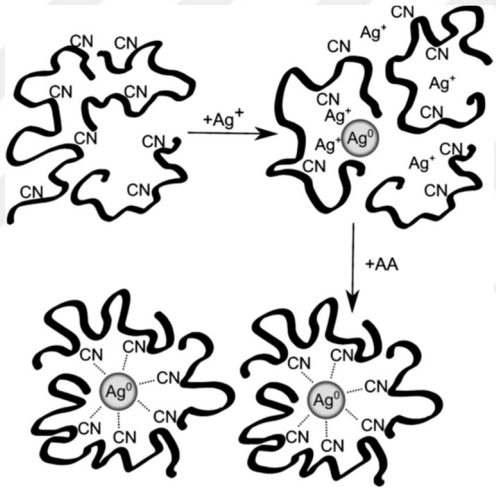

Figure 2.7 : Representative mechanism of silver nanoparticles generated in PAN polymer [114].

Another PAN/Ag nanofibers were collected by Siyanbola and coworkers. However, different from the studies mentioned above, AgNPs were not synthesized in polymer solution. First, PAN/$AgNO_3$ nanofiber web was prepared via electrospinning and then the electrospun mat was immersed into the solution containing N_2H_5OH. The reduction process of $AgNO_3$ to AgNPs took place in N_2H_5OH based solution for 30 minutes and then PAN/Ag nanofiber mat was washed with distilled water and alcohol followed by drying in a vacuum oven. The produced sample was aimed to be used to prevent bacterial growth against *E. coli* and based on the conducted antibacterial activity studies, the suitability of the nanofibers for bacterial growth inhibition was approved [115].

Huang et al. used a novel in-situ reduction process of $AgNO_3$ to AgNPs, in which formic acid vapor treatment was performed. 9 wt % PAN polymer solution was prepared in DMF and subsequently, with the same weigth ratio of $AgNO_3$ was added into the polymer solution and stirred for an appropriate duration. After that, by electrospinning PAN/ $AgNO_3$ nanofibers were fabricated. Reduction of $AgNO_3$ to AgNPs was achieved over nanofiber films by subjecting them to formic acid vapor treatment at several temperatures such as 50, 80, 120 and 160 °C. Two different experimental set-ups (Figure 2.8) were used for the chemical reduction [116].

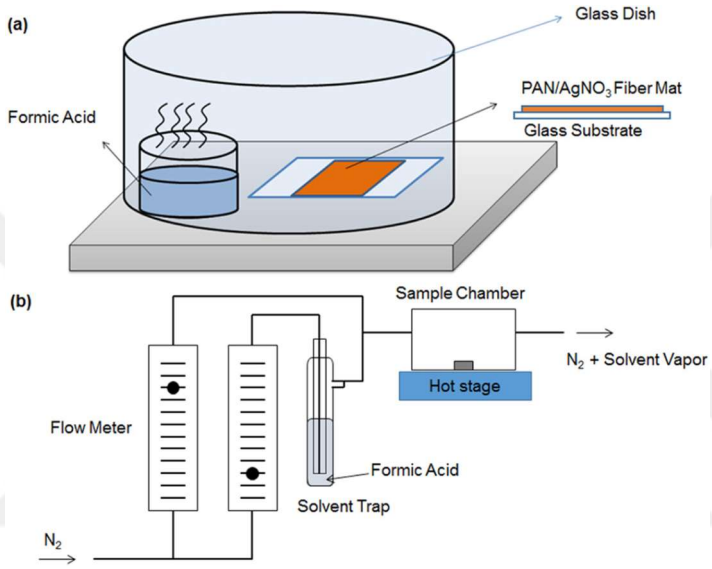

Figure 2.8 : Experimental set-ups for formic acid vapor treatment [116].

In the first set-up (shown with a), formic acid was placed in a small beaker in an enclosed petri dish, which was preheated to the requested temperature value. The reduction process was achieved by keeping PAN/$AgNO_3$ nanofibers into the set-up for 2 hours. The second system (shown with b) included two nitrogen lines, one of which went to formic solvent while the other one was responsible for supplying pure nitrogen. The concentration of the formic acid vapor could be controlled by tuning the flow-rates in the lines in that system. It was concluded that when the reduction of $AgNO_3$ was conducted at room temperature, homogeneously distributed AgNPs could be seen. When the temperature was increased the nanoparticles had the tendency to deposit mostly on the nanofiber surfaces. Moreover, it was found out that less formic acid vapor amounts allowed to obtain better particle size distribution on nanofiber webs at different temperatures [116].

Sichani and coworkers decreased the reduction duration of $AgNO_3$ to AgNPs by the help of Xenon arc lamp. In this regard, $AgNO_3$ of which the content was changed in the range of 0.05-0.5 wt % was added to the prepared 10 wt % PAN polymer solutions and stirred for 24 hours at room temperature. Then Xenon arc lamp was applied to PAN/ $AgNO_3$ polymer solutions for 4 hours until reaching an equilibrium in reduction which was observed spectroscopically. AgNPs formation was approved via TEM, SEM, FTIR and XRD characterizations. Moreover, satisfying results were obtained from the studies conducted on the observation of silver release from PAN/Ag nanofibers and evaluation of antibacterial properties against *E. coli*, *S. aureus* and *Pseudomonas Aeruginosa* (*P. aeruginosa*) [117]. Duy-Nam et al also used Ultra Violet (UV)-irradiation for the formation of AgNPs from $AgNO_3$. UV light was applied to the polymer solutions of aqueous $AgNO_3$ containing PAN nanofibers, which were previously fabricated via electrospinning, for 24 hours and at the end of 24 hours, antibacterial PAN/Ag nanofibers could be gained. It was noticed that by using that simple technique, antibacterial samples to be used in bacterial filtration, biomedical devices and water purification could be generated [118].

Kudryashov et al. used both a photoinitator, 2,2-dimethoxy-1,2-diphenylethanone, and a UV lamp to facilitate the reduction of $AgNO_3$ to AgNPs for the production of PAN/Ag nanofibers. In the process, PAN, $AgNO_3$ and the photoinitator were blended and put between two glasses where UV lamp was applied for the conversion of $AgNO_3$ to AgNPs. It was understood that if the amount of $AgNO_3$ and photoinitiator were changed, it could be possible to obtain PAN/Ag nanofibers with different morphologies. For instance; increasing the photoinitiator content allowed to generate more silver nanoparticles, which meant that the reduction process was fastened [119]. Another UV photoinitator named 2,2′dimethoxy-2-phenil acetophenone was consumed by Tyurin et al. to form AgNPs from $AgNO_3$ and polymerize AN. It was seen that initial amounts of $AgNO_3$ and 2,2′dimethoxy-2-phenil acetophenone had a great influence on the size and morphology of the obtained AgNPs, which also had an indirect relation between the optical, morphologic and electrical features of the final products [120].

Mahapatra and coworkers used three different reduction methods which were refluxing in DMF before electrospinning, heating the solution up to 160°C and application of sodium borohydride ($NaBH_4$) for the formation of AgNPs from $AgNO_3$. It was aimed

to produce antibacterial PAN/Ag nanofibers and compare the effects of reduction process on antibacterial properties of the resultant membranes. It was revealed that among those three reduction methods, $NaBH_4$ treatment caused to obtain coarser nanofibers. When the antibacterial activities of the nanofiber membranes were compared, it was observed that even though all the methods resulted in antibacterial nanofiber mats, the samples in which AgNPs were formed via refluxation were more resistant to the growth of *S.aureus*. It was commented that the result might depend mainly on the number of generated AgNPs [121].

Zhang and coworkers mentioned a novel way to deposit AgNPs onto functionalized PAN fibers in a hot steaming environment. Functionalization of PAN fibers were achieved by using amino hyperbranched polymers (HBP) which also acted as a complexing and reducing agent to hold Ag^+ ions. Thanks to the internal nanocavity and spherical form of amino HBP, AgNPs were prevented from agglomeration and could be uniformly deposited onto PAN fibers (Figure 2.9). Moreover, the presence of amino HBP eliminated the needs of any other auxiliaries. The resultant AgNPs containing functionalized PAN fiber membrane was reported to be washable and bactericidal as well [122].

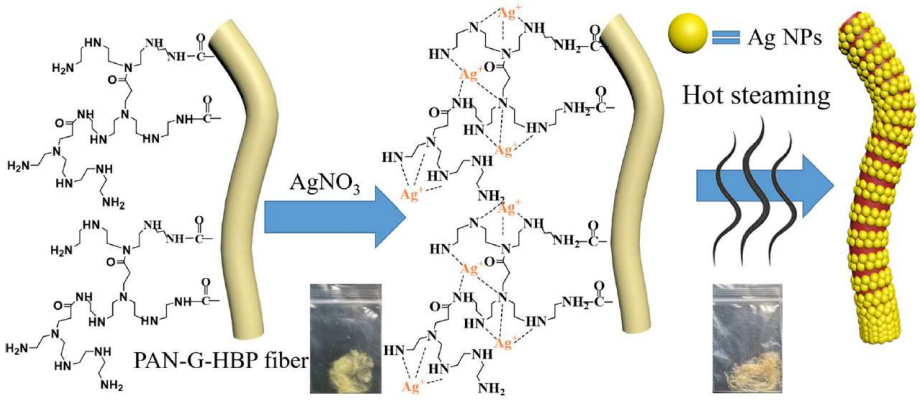

Figure 2.9 : Image of AgNPs coated functionalized PAN fiber [122].

2.2.4 Pyrrole and pyrrole derivatives

The discovery of intrinsically conductive polymers (ICP) was achieved by Shirakawa et al. in 1977 by doping polyacetylene and obtaining metal-like features [123]. ICP have taken great attention due to their good electrical conductivity and high chemical stability [124]. Owing to the metallic-like conductivity, environmental stability, low cost and suitability for film fabrication, polypyrrole (PPy) is very popular among the conducting polymers [125]. PPy can find applications in sensors, especially in gas

sensors [126, 127] and biosensors [128, 129], microactuators [130], electronic devices [131], antielectrostatic coatings [125] and so on. Moreover, PPy is the most widely preferred conducting polymer for drug loading and releasing [132, 133].

Conducting polymers are sensitive to humidity and cannot be dissolved in many solvents, thus, processibility of them is significantly restricted [134, 135]. In addition to these drawbacks, PPy is very brittle, which hinders the applicability of it [136]. In order to find a solution to these dilemmas, it is preferred to use pyrrole (Py) and Py derivatives in composite form with insulating polymers [137]. Poly (acrylic acid) (PAA)[138], Poly (ethylmethacrylate) (PEMA) [139], Poly (ethylene-co-vinylacetate) (PEVA) [140], PAN [141] and PAN-based polymers [142] are the main insulating materials that are used to form composite structures with Py.

To this end, Sarac et al fabricated PPy/ P (AN-co-VAc) composite films to investigate the impact of Py on the morphology and conductivity of the resultant composite. Chemical polymerization was performed to synthesize Py in P (AN-co-VAc) matrix. It was declared that, the existence of Py in the film structures caused rougher grains compared to neat P (AN-co-VAc) films. Moreover, as expected, the prepared films behaved like a semiconductor due to electrical features of PPy [143].

Cetiner et al. obtained electrospun nanofibers of PPy/ P (AN-co-VAc) by oxidative polymerization of different amounts of Py in polymer matrix followed by simple electrospinning. As demonstrated in Figure 2.10, higher amounts of Py in nanofiber structure created rougher and finer nanofibers as well as increased electrical conductivity. Moreover, it was commented that the reason for improved electrical conductivity might mainly depend on the generation of more active charge transport [142]. Arman and Sarac also proved that by increasing the Py amount in electrospinning solutions finer nanofiber diameters of PPy/ P (AN-co-VAc) could be achieved with enhanced electrical conductivity [144].

For the incorporation of Py into nanofiber structure, Li et al. served PPy as core and PAN as shell material in PAN/PPy nanofibers. By altering the PPy and PAN concentrations in the solutions, it could be possible to achieve core-shell nanofibers with different structures. Following that simple method, difficulty of processibility of PPy could be eliminated and design of core-shell nanofiber structures could be modified via changing the PAN and PPy amounts [141].

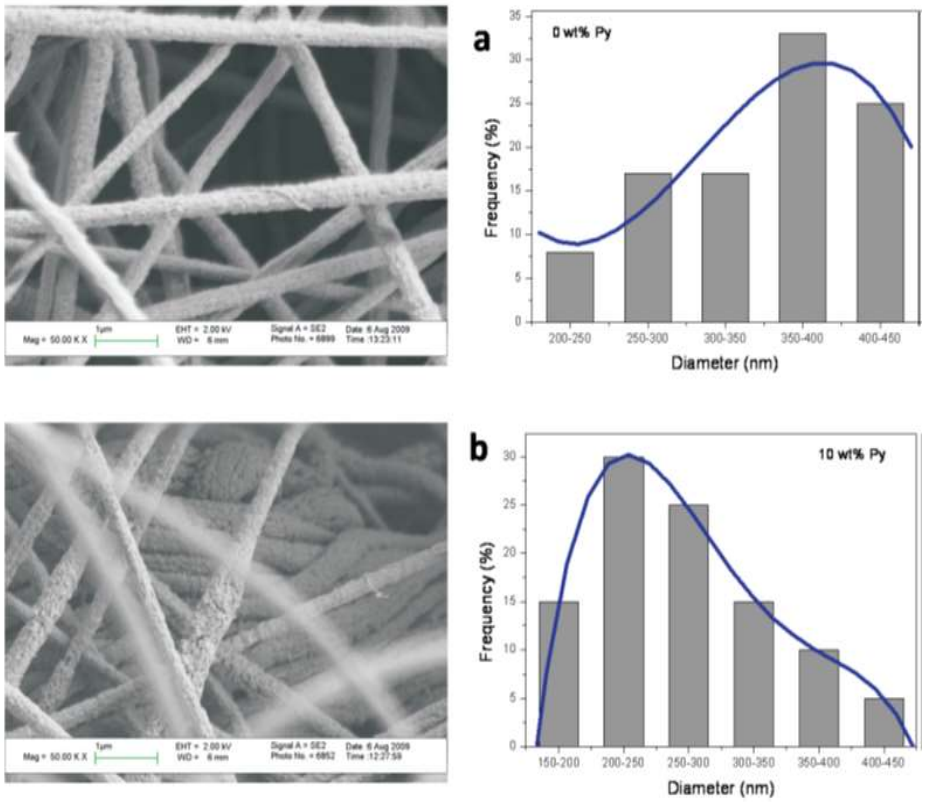

Figure 2.10 : SEM images and diameter distributions of nanofibers resulting from a solution with 7 wt % P(AN-co-VAc) at 50.00 kx magnification: (a) 0 wt % Py; (b) 10 wt% Py [142].

Beyond the conductivity of PPy, since it is non-toxic and can be used in biomedical applications, Ince-Yardımcı and coworkers fabricated both aligned and random PAN/PPy electrospun nanofibers for osteogenic differentiation of mesenchymal stem cells. In the study, previously synthesized PPy was used as a copolymer for PAN. Related to the biological tests, it was observed that cell proliferation and differentiation were enhanced in the presence of PPy. It was approved that PAN/PPy nanofibers could be good candidates for the regeneration of bone tissues [145].

The formation of PPy nanopowders and addition of them into PAN polymer solution and further electrospinning the obtained solution was carried out by Matysiak et al who said that the performed was rare in literature. The existence of nanopowders in the resultant nanofiber structure was certified by several characterization techniques and finally it was suggested to use PPy nanopowder containing PAN nanofibers for the preparation of new generation dye-sensitized solar cells [146].

N-substituted Py, called as N-methylpyrrole (NMPy), is advantageous than Py since it creates hydrophobic effect, has higher anode activity, better mechanical strength and

lower production costs [147]. Tüken et al. used NMPy to obtain enhanced protection of PPy films against corrosion. In this regard, a set of PPy and PNMPy copolymers was synthesized electrochemically with different Py and NMPy concentrations. It was captured that PNMPy coating contributed to improve the protection while decreasing the water permeability [148].

Sarac et al electropolymerized PNMPy on carbon fiber microelectrode and examined the morphology and electrical features of PNMPy samples. It was declared that PNMPy had porous structure and sufficient conductivity to be used in supercapacitors and batteries [149]. In another study of Sarac and coworkers, morphology change related to Py derivatives was also emphasized [150]. Ursache et al explored dielectric properties of PAN/PNMPy composites. Different amounts of NMPy monomer was added into the prepared PAN/DMF solution to polymerize NMPy. It was revealed that NMPy content had a major impact on not only dielectric properties but also electromagnetic features [151].

Ozkazanc et al. synthesized PNMPy via chemical oxidative polymerization. Simultenously, PNMPy copolymers including indium (III) oxide (In_2O_3) and tungsten(VI) oxide (WO_3) nanoparticles were prepared, as well. As consistent with other studies, it was seen that combination of nanoparticles and PNMPy could alter the electrical properties of the resultant samples. Differently from the other studies, it was shown that utilized nanoparticles improved the antimicrobial activity of PNMPy polymer by generating electrostatic interaction between nanoparticles and bacteria cell walls [152].

In literature, a number of studies about the nanocomposites, especially polymers of Py and NMPy, have appeared, but no detailed studies on polymers of poly (2,5 dimethylpyrrole)(PDMPy) and poly (1-(Triisopropylsilyl)pyrrole)(PTIsPy) were published. Patil et al. examined anticonvulsant activities of small N-substıtuted 2, 5-Dimethyl Pyrrole [153] while Chirico and Kazakov investigated thermodynamics of 2, 5-Dimethyl Pyrrole [154].

2.3 Emulsion Polymerization

Emulsion polymerization which is a type of free radical polymerization is initiated by either a water soluble or oil soluble initiator of the emulsified hydrophobic/relatively hydrophobic monomer in water [155].

Emulsion polymerization was discovered during World War II due to the requirement of replacing of the natural latex by a synthetic rubber. That synthetic rubber was produced by 1,3-butadiene and styrene. After this major development, synthetic rubber industry boosted up in the United States. Both scientists and industry expanded the fabrication of synthetic rubber in many homo and copolymer forms. AN, acrylic esters, styrene, butadiene and VAc were the main monomers used in emulsion polymerization for that years. In the mid 1940s, a great deal of books and papers were written on the mechanism, kinetics and applications of emulsion polymerization [156–158].

It has some advantages over other polymerization systems. Since water is used as dispersion medium, the polymerization method is cheap, nontoxic and nonflammable. The possibility of incorporation of the ingredients at any stage allows to obtain the molecular weigth of the final latex as required. The molecular weight of the final latex can be also tuned by changing the polymerization duration or applied temperature. Unfortunately, there are two disadvantages which are the unavoidable contamination in the system because of the existence of emulsifiers and requirement of additional operations to collect the polymer particles from dispersion medium [156, 157].

Today, beyond being used as synthetic rubber, the materials obtained by emulsion polymerization can be used in many applications such as paper coatings, adhesives, floor polishes, concrete adhesives, biomaterials, high-tech products etc [156, 159].

2.3.1 Ingredients of emulsion polymerization

Emulsion polymerization has four main ingredients which are monomer, dispersion medium, emulsifier and initiator [159]. Additionally, related to the needs, some auxiliaries which can be buffers, acids, bases, transfer agents are utilized during polymerization [156].

2.3.1.1 Monomer

Vinylacetate, acrylic acid, methacrylic acid, acrylonitrile, styrene, butadiene, acrylate ester, methacrylate ester, vinyl chloride are expressed as the most commonly utilized monomers in emulsion polymerization [156]. Although having different structural, chemical and physical features, they are all free-radical polymerizable monomers [159].

If styrene copolymers are changed by acrylonitrile, solvent resistant and elastic copolymers can be obtained. Morphological designs, hydrophilicity and film forming temperatures of styrene can also be tuned by copolymerization with esters. Polyvinylchloride (PVC) latexes, synthesized by emulsion polymerization, are widely used in food packaging applications. Furthermore, the copolymers of vinyl acetate are generally used in coating and adhesive [156].

According to the solubility degrees in water, the monomers can be classified into 3 categories. For instance; with a 8 % solubility in water, acrylonitrile is referred as having good soluility in water. the monomers like methyl methacrylate and other acrylates with solubility of water 1-3 % have a moderate solubility degree and the monomers like butadiene, sytrene, vinyl chloride etc with solubility of water below than 1 % are defined as insoluble in water [156].

2.3.1.2 Dispersion medium

In emulsion polymerization, water is the most preferred dispersion medium among the other dispersing liquids due to being cheap, inert and environment friendly. It is also effectively used to dissolve the emulsifier, initiator and other ingredients. Moreover, it supplies a superior heat transfer which allows the polymerization process to have a stable temperature during the polymerization duration [156].

2.3.1.3 Emulsifier

Emulsifiers are surface-active agents and named as soap, surfactant, dispersing agent or detergents [160].

Emulsifiers reduce the interfacial tension between the monomer and water, thus contribute to the generation of micelles. Micelles have two edges which are oil-soluble and water soluble. While water-soluble edge orients towards the water, oil-soluble

edge orients towards the center of the cluster. Therein, emulsifier stabilizes the monomer droplets and acts as a chain transfer agent [161, 162].

Emulsifiers are classified as anionic, cationic, zwitterionic or non-ionic according to the nature of their water-soluble edge. Among these four groups, anionic emulsifiers are the most widely used ones in emulsion polymerization due to their property of being strong particle generator and stabilizing the latex particles. Sodium lauryl (dodecyl) sulfate, sodium doceyl benzene sulfonate, sodium dioctyl sulfosuccinate are some of the examples of anionic emulsifiers [155, 156].

2.3.1.4 Initiator

The role of initiator in emulsion polymerization is activating free-radicals and then forming the polymer molecules. Initiators can be water-soluble and oil-soluble. Since water is the dispersion medium in emulsion polymerization, water-soluble initiators are widely preferred to initiate the polymerization. Peroxodisulfates (potassium-, sodium- and ammonium-persulfate) are the most popular water soluble initiators. Persulfate ion decomposes in dispersion medium, which is water, and gives two sulfate radical anions that start the polymerization. Besides water or oil-soluble initiators, thermal decomposition type and redox initiators exist for the production of free radicals at relatively low temperatures [156, 163].

2.3.2 Mechanism of emulsion polymerization

Emulsion polymerization has three main steps which are initiation, propagation and termination.

At the initiation step; dispersion medium, surfactant, monomer and initiator are gathered together. At this step, interfacial tension between the monomer surface and dispersion medium is reduced by emulsifier and after the decomposition of free-radicals, they interact with the monomer. As a result, spontaneous latex particles begin to occur. Exact polymer molecules are generated by the decrease of the number of monomer molecules and increase of the number of polymer molecules at the propagation stage. Finally, the growing polymer chain is terminated at the termination stage and the final product named as a milky fluid or latex is obtained [164]. Figure 2.11 shows the representative image of emulsion polymerization step by step.

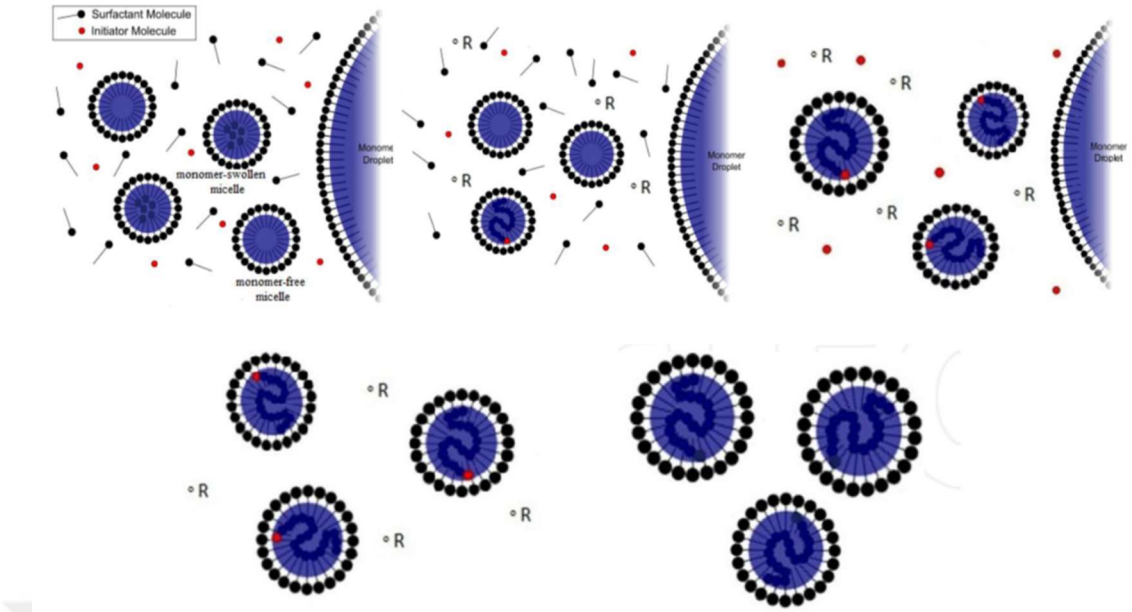

Figure 2.11 : Respresentative image of emulsion polymerization step by step [156].

2.4 Nanofiber Production Methods

The term 'nanofiber' can be defined as a fiber having a diameter in the nanometer scale [165]. Sub-micron ranged nanofibers have some peculiar features such as having large surface area to volume ratio, porous structure with high pore interconnectivity, small pore dimensions and superior mechanical properties [8, 166, 167]. Due to their outstanding properties, nanofibers can be used in a wide range of applications as tissue engineering scaffolds [7, 168–171], wound dressing [7, 170], drug delivery carrier [7, 170, 172], cosmetic skin mask [7], artificial organs [170], filtration membranes [168], nanosensors [7, 168], protective clothing [169], photovoltaic devices [7] and so on. There are several methods in order to obtain nanofiber structure and some of the mostly used ones can be mentioned as drawing, template synthesis, phase seperation, self-assembly and electrospinning [8].

Drawing: The method, shown in Figure 2.12, is based on drawing a polymer solution with a sharp and then subjecting the drawn fiber to solidification by evaporation of the solvent rapidly [173].

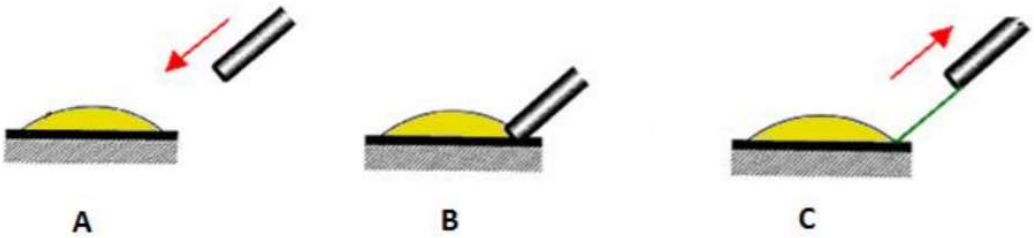

Figure 2.12 : Representative image of drawing fiber [173].

The process has some drawbacks, for instance; droplet viscosity increases with time solvent evaporation. Thats why, the fibers has to be pulled in a very short time. In addition, the fiber diameter is affected by continual shrinkage of the volume of the polymer solution droplet, which hinder to obtain a continous drawing process [173].

Template Synthesis*:* In this method, a nanoporous membrane is used to achieve nanofiber structure. The fiber diameter is directly related to the diameter of the pores [8]. Figure 2.13 depicts the template synthesis process.

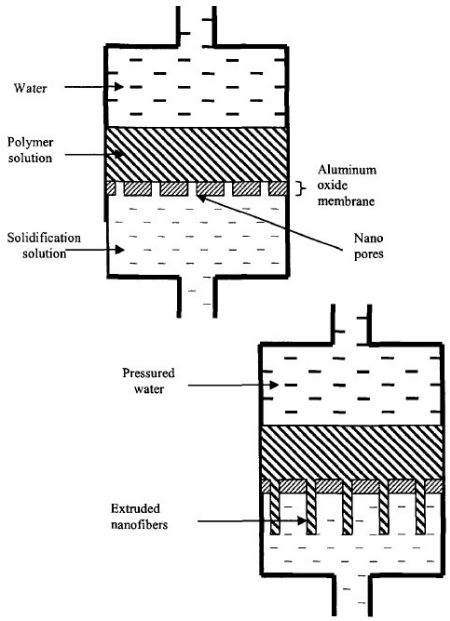

Figure 2.13 : Template synthesis for the production of nanofibers [8].

Polymer solution is forced through the solidfying solution by water pressure which lets the nanofiber production from the pores [8]. However, the process is not suitable for continuous nanofiber production [174].

Phase Seperation*:* Phase seperation process (Figure 2.14) is based on five basic steps which are preparation of polymer solution, phase seperation and gelation, extraction of solvent from the gel via water, freezing and finally freeze-drying under vacuum [8].

Gelation temperature is mainly determines the nanofiber structure. Fibers in nanoscale are obtained by low gelation temperature while high gelation temperature causes platelet-like morphology. Moreover, uniform nanofibers can be produced by increasing the cooling rate [175].

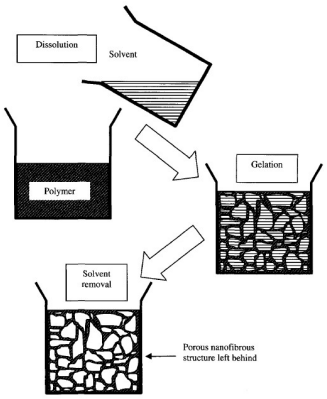

Figure 2.14 : Phase seperation process for nanofiber production [166].

Self-Assembly*:* Small molecules and atoms assemble by noncovalent forces like hydrogen bonding and generate stable structure. Several structures such as membranes, nanoparticles, films, micelles etc. can be achieved by this method. The disadvantage of the process is it takes a long period of time [175].

2.4.1 Conventional electrospinning

The term electrospinning originates from 'electrostatic spinning' and dates back to 1897. The process was gained great interest at the beginning of 2000s related to the improvements in nanoscience and nanotechnology [8].

Electrospinning is a simple, versatile and efficient technique that used to produce continous nanofibers with diameters in the scale of nano and micrometers [176]. The method is based on using electrostatic forces in order to produce nanofibers from several solutions. Various materials like natural and synthetic polymers, composites, ceramics can be utilized for the preparation of electrospinning solutions and nanofibers with several diameters can be obtained [8]. Basically, electrospinning set-up (Figure 2.15) is composed of three main parts which are a high voltage power supply, a syringe with a metal spinneret and a collector. In addition, the set-up can be vertical or horizontal [7].

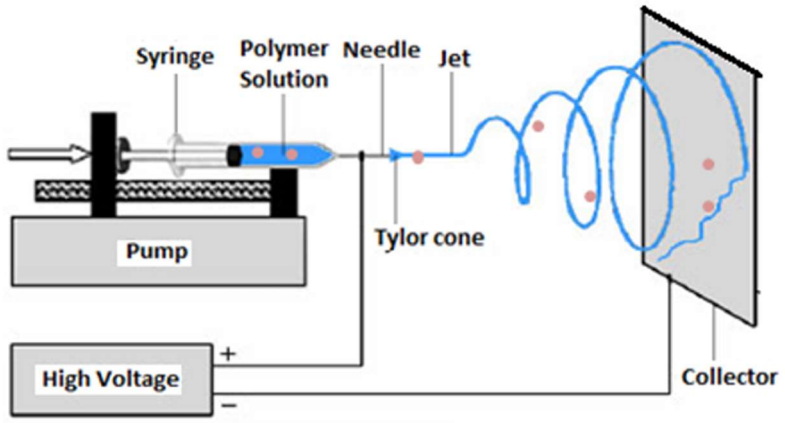

Figure 2.15 : Electrospinning set-up.

In the process, prepared electrospinning solution is subjected to high voltage in order to charge the polymer solution and obtain a charged jet in conical shape at the tip of the needle. This conical shape is called as Taylor cone. When the electrical force overcomes the surface tension of the solution, the charged jet is ejected from the tip of the needle and randomly deposited on the collector as a result of solvent evaporation [7, 8, 177–180].

Electrospinning Parameters

The obtained nanofiber morphology and diameter are the critical outcomes of electrospinning process. It is desired to obtain consistent and controllable diameters with defect-free nanofiber surface. It is easy to produce nanofibers with required features by tuning the electrospinning parameters. Eletrospinning parameters can be classified under three main headings which are solution parameters, process parameters and ambient parameters [8]. The classification of electrospinning parameters are shown in Figure 2.16.

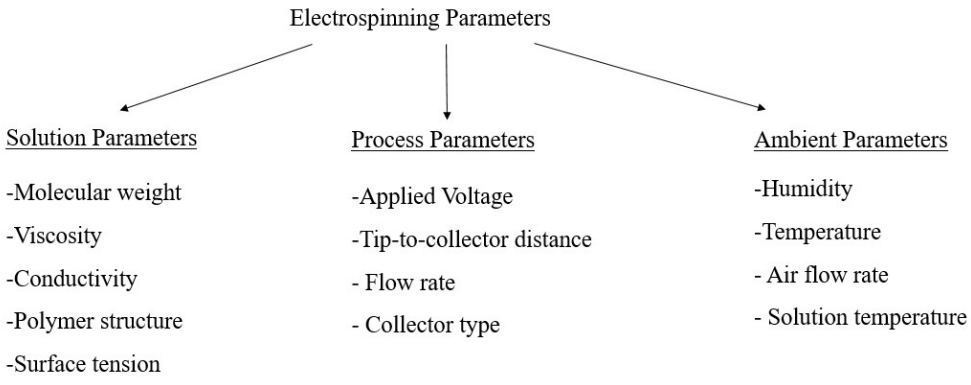

Figure 2.16 : Classification of electrospinning parameters.

***Solution Concentration**:* Both concentration and viscosity of the prepared electrospinning solution are directly related to the molecular weight of the polymer. Very low solution concentrations generate electrospraying rather than electrospinning because of the low viscosity and high surface tension of the electrospinning solution [181]. Low solution concentrations are able to produce nanofibers with beaded structure. When the solution concentration is increased, the form of the beads become spindle-like and at the optimum solution concentration, nanofibers with uniform diameters and smooth surface can be obtained [8]. Moreover, production of nanofibers is hindered at very high solution concentrations due to the high viscosity [182].

Molecular Weight: Molecular weight represents polymer chain entanglement in electrospinning solution and affects the solution concentration, viscosity, surface tension that's why it can be said that it is the most crucial electrospinning parameter. At a fixed solution concentration, using a polymer with too low molecular weight results in beads rather than nanofibers. Increasing the molecular weight of the polymer leads to obtain nanofibers whereas too high molecular weight fabricates fibers with very coarse diameters [8, 183, 184].

Viscosity: Solution viscosity, molecular weight and concentration are all dependent to each other. Too low solution viscosity fails to produce nanofibers. Increasing solution viscosity can result in smooth and bead-free nanofibers. Optimal viscosity can be obtained by adjusting the polymer concentration. Furthermore, desired nanofiber diameter can be achieved by changing the solution viscosity [8, 166, 184].

Conductivity: Polymer and solvent type, addition of salts to the solution all affect the conductivity of the electrospinning solution. Nanofibers with finer diameters can be obtained by using the solutions with high conductivity [8, 168]. Sometimes, in order to increase the conductivity, various salts such as mono potassium phosphate (KH_2PO_4), mono sodium phosphate (NaH_2PO_4) and sodium chlorür (NaCl) are incorporated into the electrospinning solution and hence finer nanofiber diameters can be produced [185].

Surface Tension: Surface tension is directly related to the used solvent type. In general, it is suggested to use lower surface tension for the fabrication of uniform nanofibers without beads. However, using too low surface tension don't enable the electrospinning. Therefore, optimum surface tension should be achieved for the production of nanofibers with desired features [186].

Applied Voltage: For the generation of Taylor Cone and formation of nanofibers, threshold voltage must be exceeded for the charged jet, thus, the value of applied voltage is critical [8, 187].There are different arguments between the researchers about the effect of the applied voltage on nanofiber diameter. Reneker et al. mentioned that applied voltage does not have a significant influence on the nanofiber diameter [188] whereas Zhang et al informed that more polymer ejection could be observed in case of using higher voltages [189]. Demir et al and Beachley et al declared that increasing the applied voltage resulted in finer fiber diameters due to the increase in electrostatic repulsive force on the charged jet [168, 190].

Tip-to-Collector Distance: The effect of tip-to-collector distance on the produced nanofiber morphology is less significant compared to the other electrospinning parameters. Optimum distance must be decided in order to enable the evaporation of the solvent from the solution [191].

Flow rate: Flow rate means the material transfer rate and directly affects the velocity of the charged jet. Higher flow rate leads nanofibers with coarser diameters. It is recommended to work with the slower flow rate in order to give enough time to the solvent for evaporation [8].

Collector Type: A plain metal surface, conductive paper, cloth, rotating drum, wire mesh, parallel or grided bar are some of the examples used as a collector for the deposition of fabricated nanofibers [187]. Selection of the collector type is mainly dependent the application area of the obtained nanofibers. For instance; producing aligned nanofibers is much more important for tissue engineering applications than randomly collected nanofibers [171].

Temperature and Humidity: Lower humidity is required for the solvent to be completely evaporated. In addition, high humidity levels cause pores on the nanofiber surface. High temperature facilitates to achieve nanofibers with finer diameters [192].

2.4.2 Coaxial electrospinning

Recently, in order to enhance performance of nanofiber webs, some modifications have been invented in conventional electrospinning set-up. To this end, co-axial electrospinning (Figure 2.17) which produces core-shell nanofibers is one of the most popular modification. For coaxial electrospinning process, a specially designed needle is used and core and shell solutions are fed to this special needle independently [193].

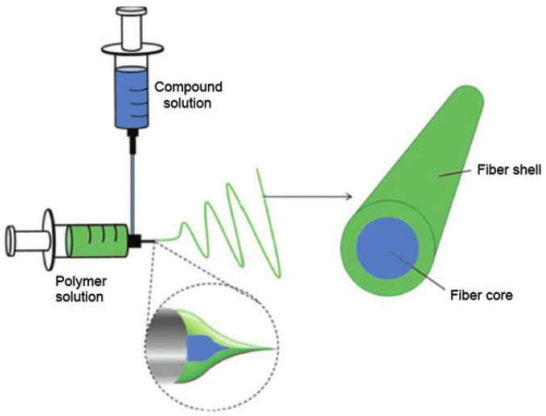

Figure 2.17 : Co-axial electrospinning set-up [193].

In coaxial electrospinning, also called as 'two-fluid electrospinning' two syringe pumps were used in order to fed the core and shell solutions, seperately. The same voltage source is used for these two syringe pumps. When the applied voltage surpasses the critical value for the formation of a stable Taylor Cone, the polymer solution creates a jet which is ejected from the tip of the needle and after the evaporation of the solvent, nanofibers are collected on a collector. The type of the collector can vary according to the needs [194].

The resultant nanofiber properties are significanly affected by not only the electrospinning parameters but also flow rates of core and shell solutions significantly [195]. If it is desired to cover the core solution totally with shell solution, feed-rate of the shell solution must be kept higher than the feed-rate of core solution. If the thickness of the core and shell solutions in the resultant nanofibers are required to be nearly the same, flow-rate of the both solutions had to be adjusted as nearly equal related to the viscosity of the solutions [193].

Yu et al. used coaxial electrospinning for the preparation of PVA (core)/NaCI (shell) nanofibers. NaCI aqueous solution was used as sheat solution and the impact of it on the resultant nanofibers was examined. It was informed that finer nanofibers could be obtained by altering the concentration NaCI aqueous solution [196].

Fallahiarezoudar and coworkers performed coaxial electrospinning in order to integrate magnetic nanoparticles in PVA easily and produce core-shell nanofibers. It was declared that via coaxial electrospinning, core-shell nanofibers including magnetic nanofibers could be achieved with desired structure [197].

Komur et al. covered starch around PCL nanofibers by using coaxial electrospinning. It was observed that if the amount of starch was increased, strengther nanofibers could be obtained. Moreover, the amount of starch increase could lead to enhance cell viability of the resultant nanofibers, which allowed them to be used in wound dressing applications [198]. In order to encapsulate two different drugs into a nanofiber structure, Mao and coworkers prepared PLA/grapheneoxide (GO) core-shell nanofibers via electrospinning. It was seen that the presence of GO promoted the drug release performance [199].

Kaewsaenee et al. desired to produce flexible nanofibers of titania. For this purpose, titanium tetraisopropoxide-PVP and PAN were served as shell and core materials, respectively [200]. Baykara and Taylan covered PVA nanofibers with Nigella seed oil via co-axial electrospinning for wound dressing applications [201].

3. EXPERIMENTAL STUDY

3.1 Materials

Acrylonitrile (AN (>99.5%)) was provided by Aksa Acrylic Chemistry Company. Itaconic acid (IA (>99.5%)), sodium dodecylbenzene sulphonate (SDBS), silver nitrate ($AgNO_3$), polyacrylonitrile (PAN (Mw = 150,000)), pyrrole (Py (>98%)), N-methylpyrrole (NMPy (>99%)), 2,5-dimethylpyrrole ((DMPy (>98%)), 1-(Triisopropylsilyl) pyrrole (TIsPy (>95%)), iron (III) oxide nanoparticles (Fe_3O_4 (ferroferric oxide) nanopowder (<50 nm particle size)) and aluminum oxide nanoparticles (Al_2O_3 (alumina) nanopowder (<50 nm particle size)) were purchased from Sigma-Aldrich. Ammonium per sulphate (APS), N, N dimethylformamide (DMF) and ethanol were all Merck reagents. Deionized (DI) water was produced in both ITU Textile Engineering laboratories and Ghent University, Centre for Textile Science and Engineering laboratories.

Staphylococcus aureus (S. aureus) ATCC 29213, *Escherichia coli (E. coli)* ATCC 25922, *Pseudomonas aeruginosa (P. aeruginosa)* ATCC 27853, and *Candida albicans* (*C. albicans*) were provided by American Type Culture Collection (ATCC® CLL-163TM, Manassas, VA, USA). Mueller-Hinton Broth (MHB) and Tyriptic Soyagar (TSA) medium were obtained from Difco, Roswell Park Memorial Institute (RPMI)-1640 medium; levofloxacin and fluconazole were supplied from Sigma-Aldrich.

Poly-3hydroxybutyrate (P(3HB)) and poly (3-hydroxyoctanoate-co-3-hydroxydecanoate) (P (3HO-3HD)) were synthesized by the Roy's lab University of Westminster (London, UK). Aqueous colloidal silver solution (4000 ppm, size of the silver nanoparticles in the solution was between 10-80 nm) was purchased from Argenol Laboratories. Chloroform ($CHCl_3$), 2-butanol, lithium bromide ($LiBr_2$), ethanol (EtOH), and Dulbecco's phosphate-buffered saline (DPBS) were provided by Sigma-Aldrich (Milan, Italy). Immortalized human keratinocytes, HaCaT cell line, were obtained from ATCC-LGC Standards (Milan, Italy). $MgCl_2$, Dulbecco's Modified Essential Medium (DMEM), L-glutamine, penicillin, streptomycin

(penstrep) and fetal calf serum were purchased from Invitrogen, (Carlsbad, CA, USA). Alamar Blue was bought from Thermo Fisher Scientific (Waltham, MA, USA). LC Fast Start DNA Master SYBR Green kit was obtained from Roche Applied Science (Euroclone S.p.A., Pero, Italy).

All these reagents were used without further purification.

3.2 Synthesis of P (AN-co-IA) Copolymer

P (AN-co-IA) copolymer was synthesized by emulsion polymerization utilizing water, SDBS and APS as dispersion medium, surfactant and initiator, respectively. 0.1 mol monomer mixture in total was utilized and feed ratio of AN to IA was selected as 99 mol%. The ratio of surfactant to total monomer was determined to be 20 wt %. 200 ml of polymerization medium was copolymerized in a three-necked flask. In the first stage, the surfactant SDBS was dissolved in 150 ml distilled water and stirred for 15 min. The monomers IA and AN were incorporated into the solution and stirred for approximately 30 min. Until this process, 5.3831 g monomer was consumed. After that, the polymerization temperature was set at 70˚C and the polymerization medium was heated to this temperature in the flask, while being stirred with reflux. When the temperature reached to 70˚C, the initiator APS, which had been dissolved in 10 ml distilled water and the feed ratio of it to monomers was 15 wt %, was fed into the system. The polymerization was lasted for 3 hours at 70°C and then stopped by using ethanol and cooled to room temperature. The obtained emulsion latex was precipitated and washed with ethanol and water for 5 times. Eventually, P (AN-co-IA) powders could be obtained after drying. In Figure 3.2 reaction sheme of AN and IA, and in Figure 3.2 polymerization steps of P (AN-co-IA) emulsion latex are shown [202].

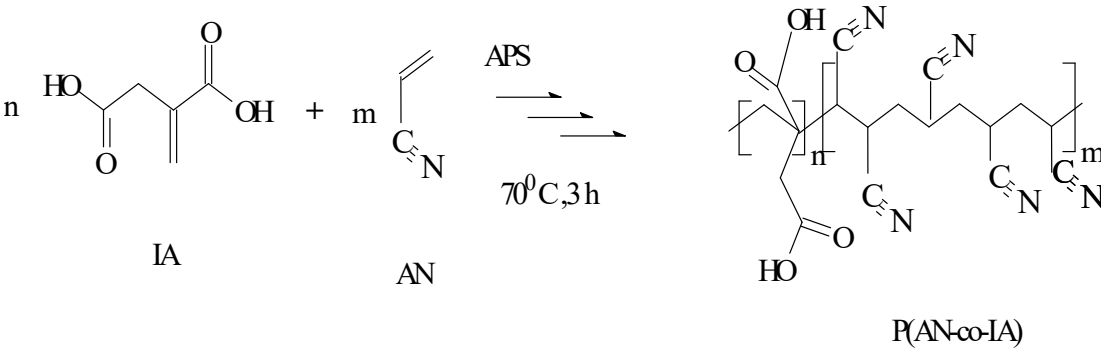

Figure 3.1 : Reaction sheme of AN and IA.

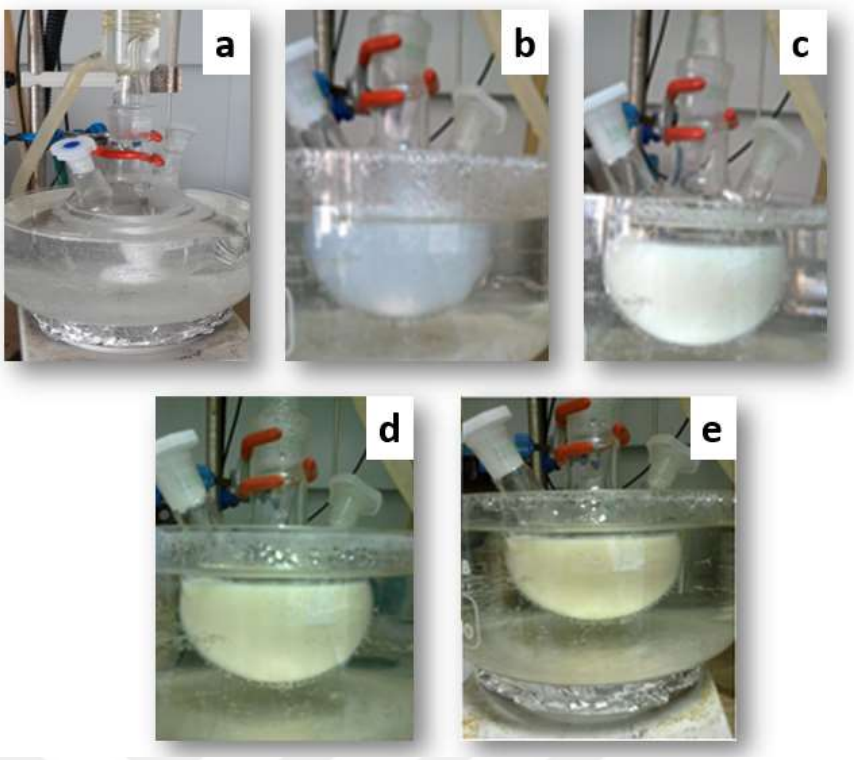

Figure 3.2 : Emulsion latex of P (AN-co-IA) a) at the beginning of the copolymerization; b) just after initiator addtion; c) 1 h after the copolymerization; d) 2 h after the copolymerization and (e) 3 h after the copolymerization.

PAN homopolymer also was synthesized by emulsion polymerization by using the same protocol of P (AN-co-IA) copolymer. The only difference was the absence of IA monomer in the polymerization. After precipitation, washing and drying, PAN powders could be collected. Figure 3.3 shows emulsion latex of PAN homopolymer and P (AN-co-IA) copolymer at the end of the polymerization, respectively.

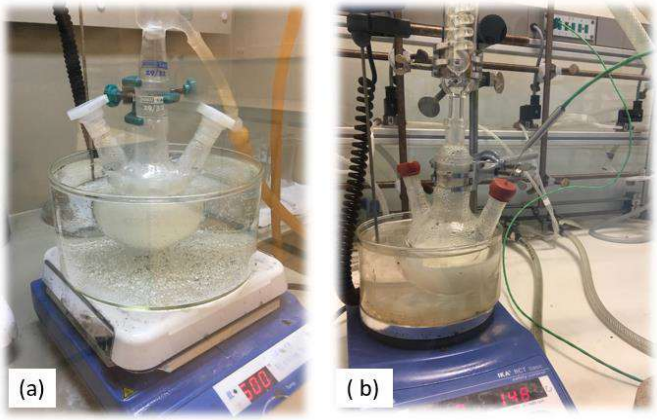

Figure 3.3 : Emulsion latex of a) PAN homopolymer and b) P (AN-co-IA) copolymer at the end of the emulsion polymerization.

3.3 Production of Metal Oxide Nanoparticle Containing Nanofibers

3.3.1 Preparation of PAN/Fe_3O_4 and P (AN-co-IA)/ Fe_3O_4 solutions

10 wt % PAN (Mw 150,000) polymer was prepared in DMF by stirring at room temperature for 24 hours. After that 1, 3, 5 and 10 wt % Fe_3O_4 nanoparticles (the weight of Fe_3O_4 nanoparticles were calculated on the basis of PAN weight) were loaded into the prepared PAN solutions in different beakers. Just after the addition of metal oxide nanoparticles to PAN solutions, the solutions were subjected to ultrasonic bath (1510 Branson) for 4 hours to achieve a well dispersion of nanoparticles in PAN polymer solutions. PAN/ Fe_3O_4 polymer solutions were prepared in order to optimize the Fe_3O_4 nanoparticle content.

Based on the optimization results of PAN/ Fe_3O_4 polymer solutions, P (AN-co-IA)/ Fe_3O_4 polymer solutions were prepared. 10 wt % P (AN-co-IA) polymer was dissolved in DMF and stirred for 24 hours at room temperature. Simultaneously, 10 wt % PAN (Mw 150,000) polymer solution was prepared in DMF by stirring for 24 hours at room temperature. Then these two polymer solutions were mixed at equal volume ratio (1:1 v:v %) and stirred for 2 hours at room temperature to obtain a homogenous blend. Afterwards, 5 wt % Fe_3O_4 nanoparticles (the weight of Fe_3O_4 nanoparticles were calculated on the basis of polymer weight) were incorporated into prepared polymer solution and the metal oxide nanoparticle containing P(AN-co-IA)-PAN polymer solution was treated with ultrasonic bath (1510 Branson) for well-dispersion of nanoparticles in the polymer solution for 4 hours.

These protocols were performed for conventional electrospinning of polymer solution.

3.3.2 Electrospinning of PAN/Fe_3O_4 and P (AN-co-IA)/Fe_3O_4 solutions

The prepared PAN/ Fe_3O_4 polymer solutions were electrospun by the application of optimized electrospinning parameters as 15 kV applied voltage (Glassman High Voltage Series), 15 cm distance between the needle tip-to-collector and 1 ml/h flow-rate (KD Scientific Pump Series 100). During the electrospinning process, the relative humidity was around 40 % and the temperature was nearly 22 °C.

P (AN-co-IA)-PAN / Fe_3O_4 (5 wt %) polymer solution was also electrospun with the same electrospinning parameters, which were 15 kV applied voltage (Glassman High Voltage Series), 15 cm tip-to-collector distance and 1 ml/h feed-rate (KD Scientific

Pump Series 100). During the electrospinning process, the relative humidity was measured as 41 % where the temperature was 22°C.

3.3.3 Preparation of PAN/Al_2O_3 and P (AN-co-IA)/Al_2O_3 solutions

For the production of Al_2O_3 nanoparticle containing P (AN-co-IA) based nanofibers, as in the study of preparation of PAN/Fe_3O_4 and P (AN-co-IA)/ Fe_3O_4 solutions, 10 wt % P (AN-co-IA) and 10 wt % PAN polymer solutions were prepared seperately. For the optimization of appropriate amount of Al_2O_3 nanoparticles, studies were conducted on the utilization of 10 wt % PAN polymer solution. Related to optimization results of electrospinning of PAN/Al_2O_3, attention was given to produce P (AN-co-IA) based Al_2O_3 containing electrospun nanofibers. The lowest amount of Al_2O_3 nanoparticles was determined to be 1 wt % (the weight of Al_2O_3 nanoparticles were calculated on the basis of polymer weight in the solution) during the experiments. It can be fairly said that the same protocol of P (AN-co-IA)/ Fe_3O_4 was applied for both optimization and production of P (AN-co-IA)/Al_2O_3 nanofibers. The only difference was the changing the value of applied voltage (from 15 kV to 20 kV) to observe a stable Taylor Cone during the production.

In this regard, 10 wt % PAN (Mw 150,000) polymer solution was prepared in DMF and stirred for 24 hours at room temperature. Then, 1 wt % Al_2O_3 nanoparticles were incorporated into the prepared solution and the obtained solution was subjected to ultrasonic bath (1510 Branson) for 4 hours. On the other hand, 10 wt % P (AN-co-IA) polymer solution was prepared in DMF and blended with 10 wt % PAN polymer solution at equal volume ratio (1:1 v:v %) in order to tune the total solution viscosity. Afterwards, 1 wt % Al_2O_3 nanoparticles (the weight of Al_2O_3 nanoparticles were calculated on the basis of polymer weight in the solution) were loaded into the prepared solution and the resultant solution was subjected to ultrasonic bath (1510 Branson) for 4 hours.

The abovementioned experiments on the preparation of Al_2O_3 containing polymer solutution were performed for conventional electrospinning process.

For coaxial electrospinning; 10 wt % P (AN-co-IA) polymer solution was prepared in DMF. Simultaneously, 10 wt % PAN (Mw 150,000) polymer solution was prepared in DMF. These two polymer solutions were blended at equal volume ratio (1:1 v: v %) and stirred for 2 hours at room temperature to be used as core solution. As shell fluid,

1 wt % Al_2O_3 nanoparticles were dispersed in DMF by the help of ultrasonication for 2 hours.

3.3.4 Electrospinning of PAN/Al_2O_3 and P (AN-co-IA)/Al_2O_3 solutions

Conventional electrospinning of PAN/Al_2O_3 (1 wt %) and P (AN-co-IA)-PAN/ Al_2O_3 (1 wt %) polymer solutions were performed with the following electrospinning parameters: 20 kV applied voltage (Glassman High Voltage Series), 15 cm needle tip-to-collector distance and 1 ml/h feed-rate (KD Scientific Pump Series 100). The relative humidity was approximately 38 % and the temperature was nearly 20°C during the electrospinning process.

3.3.5 Coaxial electrospinning of PAN, P (AN-co-IA)/-PAN and Al_2O_3 solutions

In order to perform coaxial electrospinning, a special needle system (Raméhart Custom Needle, 100-10-COAXIAL-2016, outer needle diameter: 1,7 mm and inner needle diameter: 0,9 mm), two syringe pumps (KD Scientific Pump Series 100) and a power supply (Glassman High Voltage Series) were used. The coaxial needle is shown in Figure 3.4.

Figure 3.4 : The coaxial needle (Raméhart Custom Needle, 100-10-COAXIAL-2016).

Core solution (PAN and P (AN-co-IA)-PAN in sequence) was directly connected to needle and shell solution (Al_2O_3/DMF) was fed to the coaxial needle via polytetrafluoroethylene (PTFE) tubings of which outer diameter was 1,6 mm. Feed-rate of the core solutions were kept as 1 ml/h and shell solution was fed to the coaxial needle via PTFE tubings with 0.2 ml/h feed-rate while the other electrospinning parameters were used as 20 kV applied voltage, 15 cm needle tip-to-collector distance. The coxial electrospinning set-up is given in Figure 3.5, as well. The relative humidity and temperature values were recorded as 38 % and 20 °C, respectively during the co-axial electrospinning.

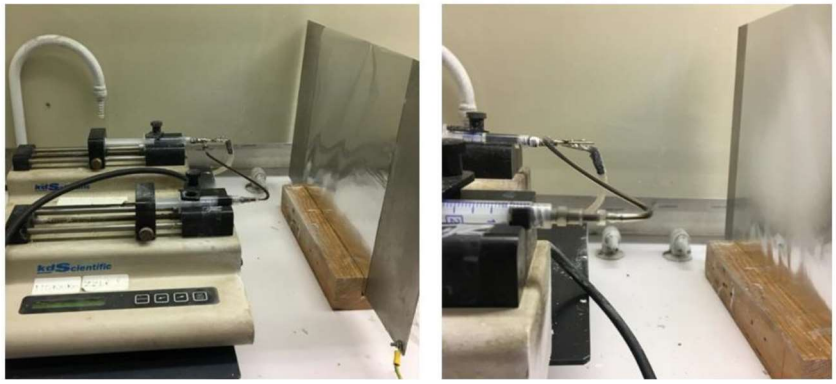

Figure 3.5 : The coaxial electrospinning set-up.

3.4 Production of Silver Nanoparticle Containing Nanofibers

3.4.1 Production of P (3HB)/P (3HO-3HD)/Ag nanofibers

3.4.1.1 Synthesis of P (3HB) and P (3HO-3HD) polymers

Short chain lenght PHA (P (3HB), 796 ±40 kDa) and medium chain length PHA (P (3HO-3HD), 377±24 kDa) were produced at a large scale by means of a bioreactor using liquid bacterial culture. A standard purification protocol was applied to obtain ultra-pure PHAs.

The synthesis of P (3HB) and P (3HO-3HD) were carried out in Roy's Lab at the University of Westminster, London, UK.

3.4.1.2 Solubility studies of P (3HB) and P (3HO-3HD) polymers

Solubility tests of both P (3HB) and P (3HO-3HD) polymers were performed in order to find a human and environment friendly solvent for dissolving them.

P (3HB) was dissolved in a variety of solvents which were benzyl alcohol, anisole, cyclohexanone, acetone, methyl ethyl ketone, dimethyl carbonate, ethylacetate, ethanol/anisole (70:30 v:v %), 2-butanol/anisole (70:30 v:v %), ethylacetate /anisole (70:30 v:v %), acetone / anisole (70:30 v:v %), ethylacetate / benzyl alcohol (70:30 v:v %), anisole/ propylene carbonate (20:80 v:v %), butylacetate /2-butanol (70:30 v:v %), ethylacetate /2-butanol (70:30 v:v %), acetone/water (90:10 v:v %), 2-butanol/water (80:20 v:v %), acetone /DMSO (80:20 v:v %), anisole /DMSO (60:40 v:v %), dimethyl carbonate /DMSO (80:20 v:v %) and propylene carbonate / dimethyl carbonate (20:80 v:v %). Solubility studies of P (3HB) were summarized in Table 3.1. The studies were conducted at 20 °C, 50 °C, 70 °C, 80 °C and 100°C.

Table 3.1 : Solubility studies of P (3HB).

		(v:v %)	20 °C	50 °C	70 °C	80 °C	100 °C
Benzlyalcohol		100				X	
Anisole		100				X	
Cyclohexanone		100				X	
Acetone		100				X	X
Methyl ethyl ketone		100				X	X
Dimethyl carbonate		100				X	
Ethylacetate		100				X	X
Ethanol	Anisole	70:30				X	
2-Butanol	Anisole	70:30				X	
Ethylacetate	Anisole	70:30				X	
Acetone	Anisole	70:30				X	X
Ethylacetate	Benzly alcohol	70:30				X	
Anisole	Dimethyl carbonate	20:80					
Anisole	Propylene carbonate	80:20					
Butylacetate	2-Butanol	70:30				X	
Ethylacetate	2-Butanol	70:30				X	X
Acetone	Water	90:10				X	X
2-Butanol	Water	80:20				X	
Acetone	DMSO	80:20				X	
Anisole	DMSO	60:40					
Dimethyl carbonate	DMSO	80:20					
Propylene carbonate	Dimehtyl carbonate	20:80					

Solubility studies of P (3HO-3HD) were conducted, as well. For the trials, anisole, acetone, dimethyl carbonate, butylacetate, ethylacetate, methyl ethyl ketone, DMSO, iso-propanol, 2-butanol, acetone/ anisole (80:20 v:v %), dimethyl carbonate/ anisole

(80:20 v:v %), butylacetate/ anisole (80:20 v:v %), acetone/DMSO (80:20 v:v %), butylacetate /2-butanol (80:20 v:v %), butylacetate /2-butanol (60:40 v:v %), iso-propanol/ water (80:20 v:v %) and iso-propanol/ water (60:40 v:v %) were used to dissolve P (3HO-3HD) polymer. Table 3.2 summarizes solubility studies of P (3HO-3HD).

Table 3.2 : Solubility studies of P (3HO-3HD).

		(v:v %)	20°C	40°C	50°C	70°C	80°C	100°C
Anisole		100				X	X	
Acetone		100				X	X	
Dimethyl carbonate		100				X	X	
Butylacetate		100				X	X	
Ethylacetate		100	X	X	X	X	X	
Methyl ethyl ketone		100	X	X	X	X	X	
DMSO		100						
Iso-propanol		100					X	X
2-Butanol		100		X				
Acetone	Anisole	80:20			X	X	X	X
Dimethyl carbonate	Anisole	80:20			X	X	X	X
Butylacetate	Anisole	80:20			X	X	X	X
Acetone	DMSO	80:20				X	X	X
Butylacetate	2-Butanol	80:20			X	X	X	X
Butylacetate	2-Butanol	60:40			X	X	X	X
Iso-propanol	Water	80:20						
Iso-propanol	Water	60:40						

3.4.1.3 Preparation of P (3HB) /P (3HO-3HD) solution

5 wt % of P (3HB)/P (3HO-3HD) (1:3, w:w) was prepared in chloroform/2-butanol (7:3, v:v). In order to increase the conductivity of the solution and facilitate

electrospinning 0.002 g/ml $LiBr_2$ was added into the prepared solution. The prepared solution was stirred for 24 hours at room temperature.

3.4.1.4 Electrospinning of P (3HB) /P (3HO-3HD) solution

The prepared P (3HB)/P (3HO-3HD) solution was electrospun with an applied voltage of 20 kV (Glassman High Voltage Series), a tip-to-collector distance of 15 cm and a flow rate of 1 ml/h (KD Scientific Pump Series 100).

3.4.1.5 Silver deposition on P (3HB) /P (3HO-3HD) nanofibers

The P (3HB)/P (3HO-3HD) nanofibers were dipped into a colloidal silver solution in water (4000 ppm, 10-80 nm particle size), and taken out with a speed of 170 mm/min. Figure 3.6 presents the representative and real image of dip-coating.

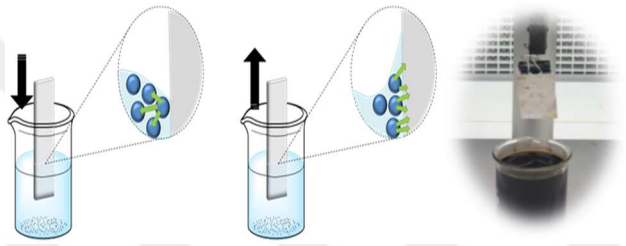

Figure 3.6 : The representative (left) and real (right) image of dip-coating.

Three different protocols were tried in order to achieve the best silver deposition on P (3HB)/P (3HO-3HD) nanofibers. In the first trial, the nanofibers were dipped in a beaker containing the colloidal silver solution and taken out immediately, followed by washing with distilled water and drying.

In the second trial, the nanofibers were immersed into the aqueous silver solution and kept in the solution for 1 min. Afterwards, the samples were taken out, washed with distilled water and left to dry.

In the last protocol, the nanofibers were dipped into the aqueous silver solution and taken out immediately for three successive times, followed by washing and drying.

3.4.2 Production of PAN/Ag and P (AN-co-IA)/Ag nanofibers

3.4.2.1 Preparation of PAN/Ag and P (AN-co-IA)/Ag solutions

The synthesized PAN (10 wt %) homopolymer was dissolved in DMF and stirred for 24 hours at room temperature for complete dissolution. Then, 10 wt % and 20 wt %

$AgNO_3$ (the weight percentage of $AgNO_3$ in the solution was calculated on the basis of PAN weight) were added to the prepared PAN solutions seperately and stirred at room temperature for 10 days in order to reduce Ag^+ ions to AgNPs. During stirring, all samples were kept in the same conditions and protected from sunlight in order to avoid decomposition of $AgNO_3$.

P (AN-co-IA) (5 wt %) was dissolved in DMF and stirred for 24 h at room temperature. Then, as in the case of PAN/Ag solution, 10 wt % and 20 wt % $AgNO_3$ (the weight percentage of $AgNO_3$ in the solution was calculated on the basis of P (AN-co-IA) weight) were added to the prepared P (AN-co-IA) solutions separately and began stirring at room temperature. During stirring, all samples were kept in the same conditions and protected from sunlight in order to inhibit decomposition of $AgNO_3$. It was observed that five days of stirring were sufficient for the conversion of Ag^+ ions to AgNPs. Moreover, it was seen that addition of $AgNO_3$ into P (AN-co-IA) solution immediately caused the solution to become a gel.

3.4.2.2 Electrospinning of PAN/Ag and P (AN-co-IA)/Ag solutions

To produce PAN/Ag nanofibers, electrospinning was applied to the prepared PAN/Ag solutions. For this reason, prepared solutions were loaded into a syringe having 0.8 mm needle diameter and 15 kV voltage, 1 ml/h feed rate, and 10 cm distance between needle tip and collector were used as optimized electrospinning parameters.

For the production of P (AN-co-IA)/Ag nanofibers, due to the gel form of P (AN-co-IA)/Ag solutions, they were blended with homopolymer of PAN (10 wt %) solution in volume ratios of P(AN-co-IA)/Ag/PAN 80:20 (v:v %) in order to obtain a spinnable electrospinning solution. The prepared solutions were loaded into a syringe having 0.8mm needle diameter. Then, the same electrospinning parameters which were 15 kV voltage, 1 ml/h feed rate, and 10 cm distance between needle tip and collector were applied to P (AN-co-IA)/Ag polymer solution.

3.4.3 Production of coaxial PAN/Ag and P (AN-co-IA)/Ag nanofibers

3.4.3.1 Preparation of core (PAN, P (AN-co-IA)) and shell ($AgNO_3$) solutions

Before the production of P (AN-co-IA)/Ag nanofibers, studies were conducted on coaxial electrospinning of PAN/Ag nanofibers. Because after the electrospinning, the obtained nanofibers must be subjected to UV irradiation to obtain Ag nanoparticles (as

a result of the reduction of $AgNO_3$ to AgNPs) and it was desired to optimize the duration of UV-light treatment by using prepared coaxial PAN/$AgNO_3$ nanofibers. For this reason, 10 wt % PAN (Mw 150,000) solution was prepared in DMF as core solution. Simultaneously, 10 w:v % $AgNO_3$ was dissolved in DMF and used as shell solution. Both solutions were stirred overnight at room temperature.

On the other hand, 10 wt % P (AN-co-IA) polymer solution was dissolved in DMF and blended with the previously prepared 10 wt % PAN (Mw 150,000) polymer solution at equal volume ratio (1:1) to be used as core solution. Blending was performed to obtain a core solution with high viscosity. For shell solution, 10 w:v % $AgNO_3$ was dissolved in DMF. Both prepared solutions were stirred overnight at room temperature.

3.4.3.2 Optimization study for feed-rate of the shell ($AgNO_3$) solution

The most critical point for coaxial electrospinning was feed-rate of the shell solution due to the low viscosity of the solution and it was desired to achieve a stable Taylor Cone during the spinning process. The experimented parameters for the optimization of feed-rate of shell solution for PAN/Ag nanofibers were given in Table 3.3.

Table 3.3 : Parameters for the optimization of feed-rate of the shell solution.

Applied Voltage (kV)	Needle tip-to-collector distance (cm)	Feed rate of the core solution (ml/h)	Feed rate of the shell solution (ml/h)
15	15	1	0.1
15	15	1	0.2
15	15	1	0.3
15	15	1	0.4

During the optimization studies, feed-rate of the core solution was kept constant as 1 ml/h while feed-rate of the shell solution was altered in the range of 0.1 ml/h-0.4 ml/h.

3.4.3.3 Coaxial electrospinning of core (PAN, P (AN-co-IA)) and shell ($AgNO_3$) solutions

For processing coaxial electrospinning, a special needle system (Raméhart Custom Needle, 100-10-COAXIAL-2016, outer needle diameter: 1,7 mm and inner needle diameter: 0,9 mm) was used.

For coaxial electrospinning of PAN (core)/$AgNO_3$ (shell) solutions, PAN solution was directly connected to needle while shell solution was fed to the coaxial needle via PTFE tubing. As mentioned in the section 3.4.3.2, the same voltage, 15 kV (Glassman High Voltage Series), was applied to the polymer solutions. Feed-rate of PAN solution was kept constant as 1 ml/h (KD Scientific Pump Series 100) and feed-rate of $AgNO_3$ solution was tried to be between 0.1 ml/h and 0.4 ml/h. The relative humidity was approximately 42 % and the temperature was nearly 23°C during the experiments.

For coaxial electrospinning of P (AN-co-IA)-PAN (core)/$AgNO_3$ (shell) solutions, the same electrospinning parameters were used which were 15 kV (Glassman High Voltage Series) applied voltage, 15 cm distance between the needle tip to collector and 1 ml/h (KD Scientific Pump Series 100) flow-rate of core solution. However, the feed-rate of the shell solution was adjusted to be 0.2 ml/h related to the optimization studies performed with PAN (core)/$AgNO_3$ (shell) solutions. The relative humidity and the temperature were 42 % and 23°C, respectively.

3.4.3.4 Reduction of $AgNO_3$ to AgNPs by UV-irradiation on coaxial electrospun nanofibers

After electrospinning, PAN/ $AgNO_3$ coaxial nanofibers were subjected to 300 W UV light (Osram Ultra Vitalux) for 30 minutes, 1 hour, 1,5 hours, 2 hours, 3 hours, 5 hours and 7 hours seperately and it was tried to optimize the appropriate duration for reduction of $AgNO_3$ to Ag nanoparticles. Representative image of UV treatment to the nanofibers is shown in Figure 3.7.

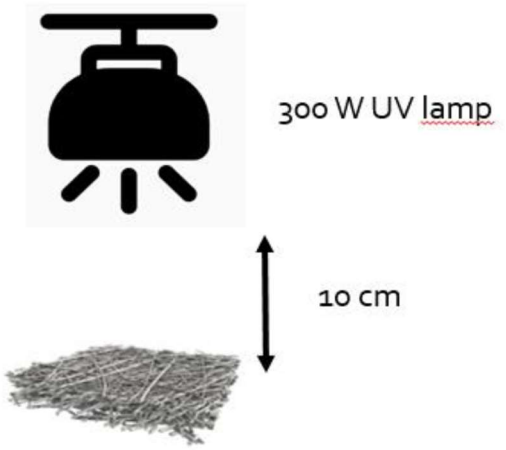

Figure 3.7 : Representative image of UV treatment to the nanofibers.

3.5 Production of Silver and Polypyrrole Containing Nanofibers

3.5.1 In-situ polymerization of pyrrole and pyrrole derivatives on P (AN-co-IA) matrix

P (AN-co-IA) nanocomposite was synthesized by emulsion polymerization as described in the section 3.2. After matrix polymer which was P (AN-co-IA) was obtained, it was divided into containers all having 10 ml. Then, without any surfactant and initiator addition of 40 µl of Py, NMPy, DMPy, and TIsPy were added dropwise into the matrix polymer seperately and in situ polymerization was lasted for 3 hours. At the end of this process, P (AN-co-IA)/PPy, P (AN-co-IA)/PNMPy, P (AN-co-IA)/PDMPy, and P (AN-co-IA)/PTIsPy nanoparticles were obtained in different solution colors. Then, produced nanoparticles were precipitated by ethanol and washed with water and ethanol for five times, respectively. They were then dried and finally nanocomposites were obtained in the powder form. Figure 3.8 depicts the synthesizing scheme of P (AN-co-IA)/PPy nanocomposite.

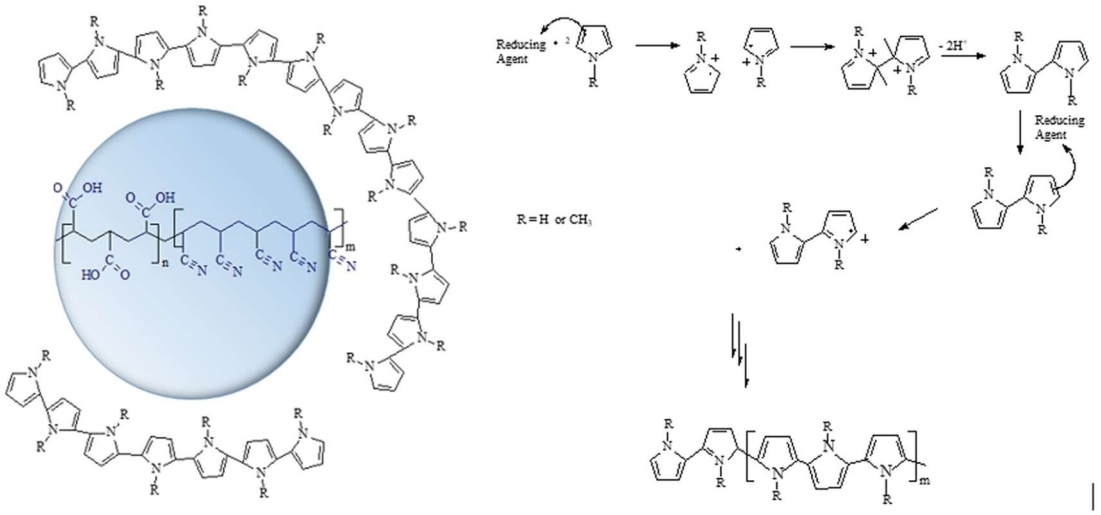

Figure 3.8 : Synthesizing scheme of P (AN-co-IA)/PPy nanocomposite.

3.5.2 Synthesis of AgPPy

Since it was not possible to synthesize and electrospun the structure P (AN-co-IA)/AgPPy in a single step, synthesis of AgPPy was performed first.

1 gram $AgNO_3$ and 0.1 gram SodiumDodecylSulfonate (SDS) were incorporated into 50 ml DI water and stirred for 30 minutes. Then 50 µl Py monomer was added to the prepared solution dropwise and stirred for 8 hours. At the end of 8 hours, APS (0.6 gram of which was dissolved in 3 ml dionized water) was added to the solution and polymerization started. Polymerization was lasted for 24 hours at room temperature and then polymerization medium was precipitated by using ethanol, washed with ethanol and water for 5 times and finally dried at ambient atmosphere. At the end of those processes, AgPPy (silver @PPy) polymer was obtained in powder form.

Polymerization of pyrrole derivates (NMPy, DMPy, TIsPy) with $AgNO_3$ was also tried but at the 10^{th} minute of the polymerization, silver mirror reaction was observed, for this reason, Ag-PNMPy, Ag-PDMPy and Ag-PTIsPy structures could not be obtained. Figure 3.9 shows the image of silver-mirror reaction of Ag-PDMPy.

Figure 3.9 : Image of silver-mirror reaction of Ag-PDMPy.

3.5.3 Preparation of core (PAN, P (AN-co-IA)) and shell ($AgNO_3$) solutions

For the formation of PAN (core)/AgPPy (shell) nanofibers; 10 wt % PAN (Mw 150,000) and 10 wt % AgPPy was dissolved in DMF seperately by stirring the polymer solutions for 24 hours at room temperature. PAN and AgPPy solutions were desired to be used as core and shell solutions, respectively.

On the other side, for the generation of P (AN-co-IA) (core)/AgPPy (shell) nanofibers; both, P (AN-co-IA) and AgPPy polymers were dissolved in DMF, separately at the polymer solution concentration of 10 wt %. Simultaneously, 10 wt % PAN (Mw 150,000) polymer solution was prepared in order to make a blend with P (AN-co-IA) polymer solution. Equal volume ratios of P (AN-co-IA) polymer solution and PAN solution was blended. The reason for blending was adjusting the viscosity of the final core solution. P (AN-co-IA)-PAN polymer solution was used as core solution and AgPPy solution was used as shell solution.

3.5.4 Coaxial electrospinning of core (PAN, P (AN-co-IA)) and shell ($AgNO_3$) solutions

For the electrospinning of PAN (core)/ AgPPy (shell) and P (AN-co-IA)-PAN (core)/ AgPPy (shell) solutions; core solutions were directly connected to needle and shell solution was fed to the coaxial needle via PTFE tubings, seperately.

Flow-rates of the core and shell solutions, which were the most critical point in coaxial electrospinning, were determined as 1 ml/h and 0.2 ml/h, respectively for both coaxial electrospinning systems. The spinning process was performed with the parameters of 15 kV applied voltage and 15 cm distance between the needle-tip to collector. In

addition, the relative humidity was recorded as approximately 42 % and the temperature was recorded as nearly 23 °C during the electrospinning process.

3.6 Characterization

The obtained nanofibers were characterized morphologically by Scanning Electron Microscope (SEM) (FEI Quanta FEC 250, MAIA3 TESCAN, Jeol Quanta 200F and Phenom ProX), spectroscopically by Ultra-Violet Visible (UV-Vis) Spectroscopy (Perkin Elmer Lambda 900, Perkin Elmer Lambda 45) and Fourier Transform Infrared-Attenuated Total Reflection (FTIR-ATR) (Perkin Elmer Spectrum One, Perkin Elmer Spectrum Two, Nicolet iS50). PAN/Ag, P (AN-co-IA)/Ag nanoparticles and conducting polymer containing nanoparticles were characterized by Atomic Force Microscopy (AFM) (Nanosurf Easy Scan 2, in non-contact mode using aluminum (Al) coated high resonance frequency silicon tips which were Nanosensors NCRL tips) morphologically, as well.

The existence of AgNPs and Fe amount in the samples was certified by Energy Dispersive Spectroscopy (EDS) (MAIA3 TESCAN, Jeol Quanta 200F).

Raman spectroscopy (DXR Raman Spectrophotometer, Thermo Scientific) was also used for the analysis of conducting polymer containing P (AN-co-IA) nanoparticles to evaluate the suitability of the samples for the conversion to carbon fibers.

The conductivity values of the PAN/Ag, P (AN-co-IA)/Ag, which were obtained via conventional electrospinning, were measured by four-point probe (ENTEK, FPP-460).

Moreover, thermal characterizations of the obtained nanofibers were made by Differential Scanning Calorimetry (DSC) (Perkin Elmer, DSC 4000). For the nanofibers including Al_2O_3 nanoparticles, in addition to DSC, Thermogravimetric analysis (TGA) (TA Instruments, TGA Q50) was also performed.

Antimicrobial activity studies of P (AN-co-IA)/Ag and PAN/Ag nanofibers, prepared via conventional electrospinning, against *S. aureus, E. coli, P. aeruginosa*, and *C. albicans* were analyzed by disc diffusion method, microdilution susceptibility testing and time–kill analysis.

Biological evaluation of P (3HB)/P (3HO-3HD)/Ag nanofibers were performed against interleukins IL-1α, IL-1β, IL-6 and IL-8, as well as TNF-α, TGF-β and HBD-2 via real-time reverse transcriptase polymer chain reaction (RT-PCR).

4. RESULTS AND DISCUSSION

4.1 Results of P (AN-co-IA)/Fe_3O_4 Nanofibers

4.1.1 Morphology of P (AN-co-IA)/Fe_3O_4 nanofibers (SEM-EDS)

Morphologic analysis of Fe_3O_4 nanoparticles containing nanofibers was achieved by SEM. Since the appropriate amount of Fe_3O_4 nanoparticles addition was decided from the optimization studies of electrospinning of PAN/Fe_3O_4, attention was given first to examine SEM images of PAN/ Fe_3O_4 nanofibers. SEM images of 1 wt %, 3 wt %, 5 wt % and 10 wt % Fe_3O_4 nanoparticles containing PAN/ Fe_3O_4 nanofibers are given in Figure 4.1, Figure 4.2, Figure 4.3 and Figure 4.4, respectively.

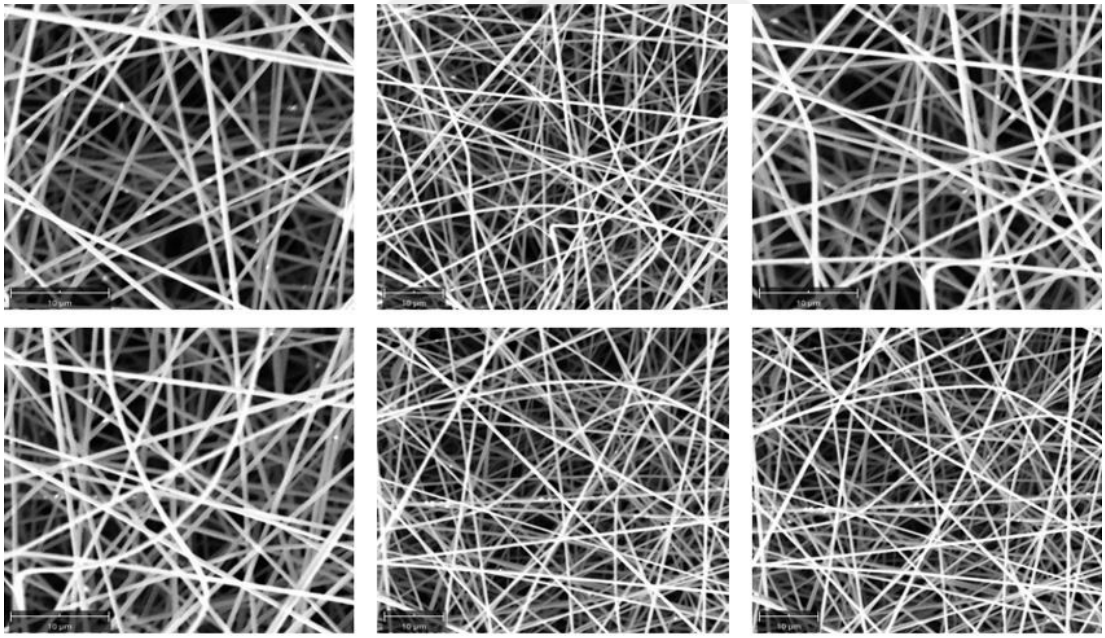

Figure 4.1 : SEM images of 1 wt % Fe_3O_4 nanoparticles containing PAN/ Fe_3O_4 nanofibers.

1 wt % Fe_3O_4 nanoparticles containing PAN/ Fe_3O_4 nanofibers were continuous and smooth. Fe_3O_4 nanoparticles could also be seen in discrete regions in the nanofiber structures.

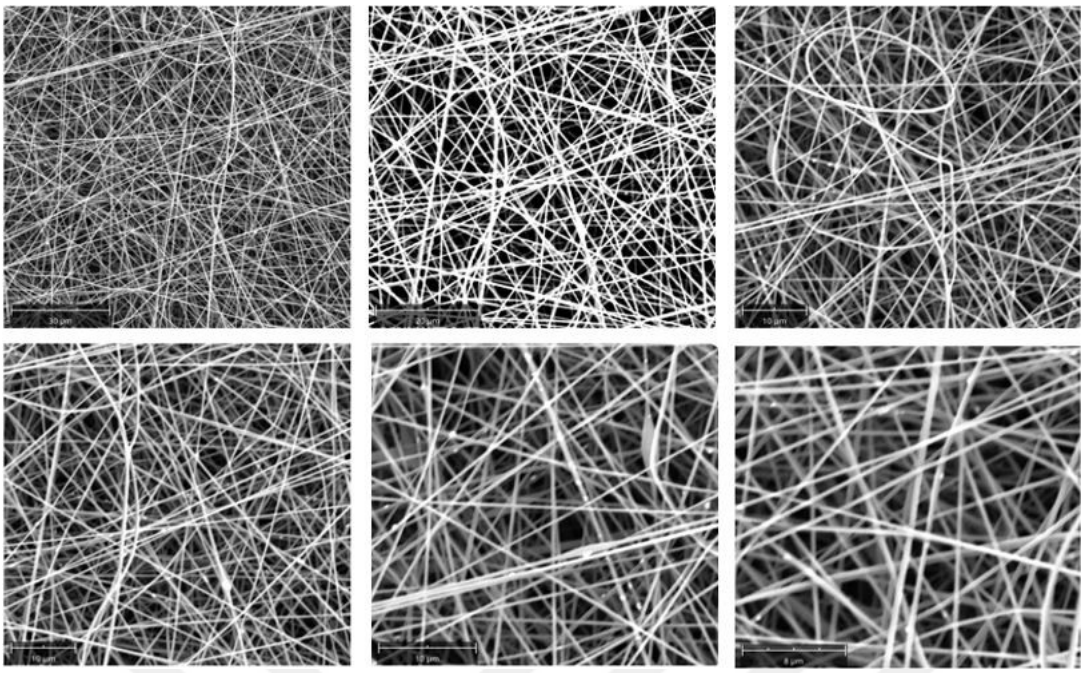

Figure 4.2 : SEM images of 3 wt % Fe_3O_4 nanoparticles containing PAN/ Fe_3O_4 nanofibers.

3 wt % Fe_3O_4 nanoparticles containing PAN/ Fe_3O_4 nanofibers were also continuous and smooth as 1 wt % Fe_3O_4 nanoparticles containing PAN/ Fe_3O_4 nanofibers. Fe_3O_4 nanoparticles distributed on the nanofiber structures.

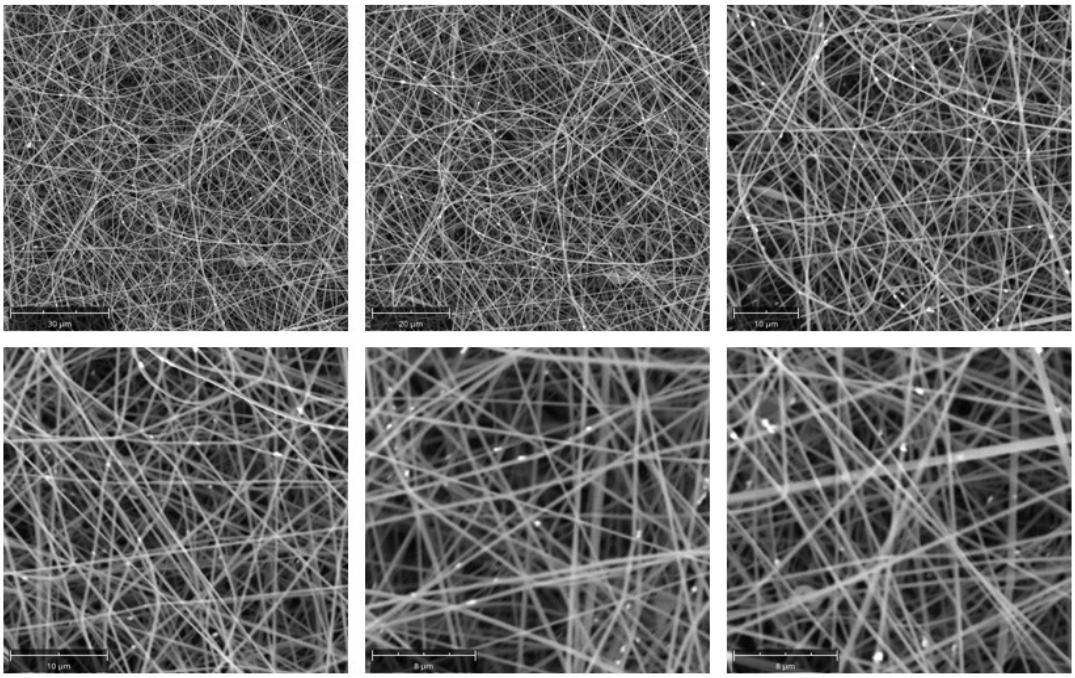

Figure 4.3 : SEM images of 5 wt % Fe_3O_4 nanoparticles containing PAN/ Fe_3O_4 nanofibers.

Smooth and continuous surface morphology were seen in 5 wt % Fe_3O_4 nanoparticles containing PAN/ Fe_3O_4 nanofibers. Compared to the 1 wt % and 3 wt % Fe_3O_4

nanoparticles containing PAN/ Fe_3O_4 nanofibers, Fe_3O_4 nanoparticles were more visible and dense in 5 wt % Fe_3O_4 nanoparticles containing PAN/ Fe_3O_4 nanofibers.

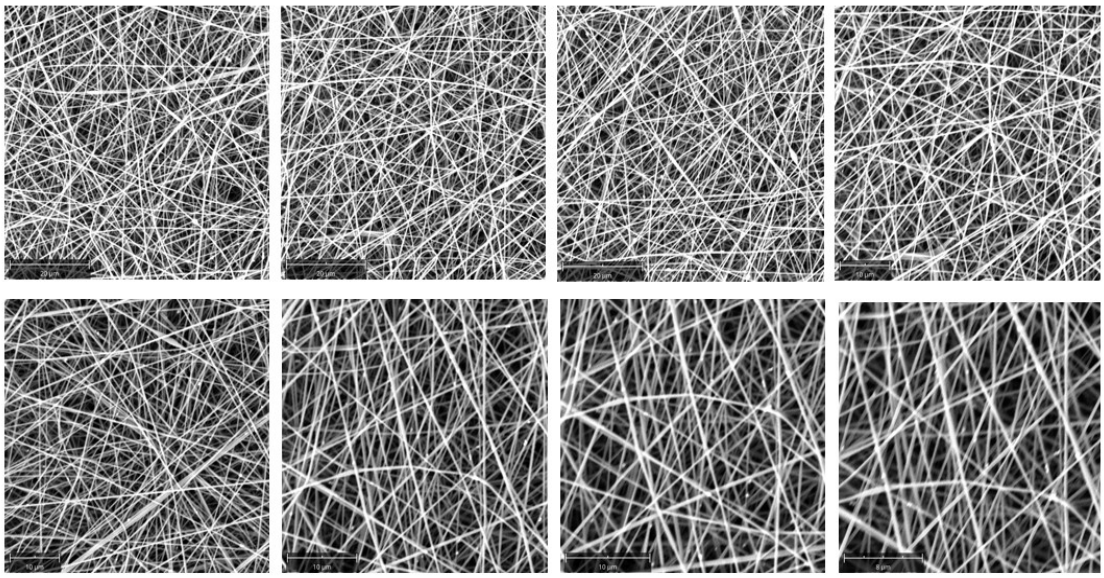

Figure 4.4 : SEM images of 10 wt % Fe_3O_4 nanoparticles containing PAN/ Fe_3O_4 nanofibers.

When SEM images of 5 wt % and 10 wt % Fe_3O_4 nanoparticles containing PAN/ Fe_3O_4 nanofibers were compared, no considerable difference was observed on the morphologies of the nanofibers. 10 wt % Fe_3O_4 nanoparticles containing PAN/ Fe_3O_4 nanofibers were also continuous, smooth and the nanoparticles were distributed over the nanofibers uniformly. The density of the nanoparticles was not higher than PAN/ Fe_3O_4 nanofibers (with 5 wt % Fe_3O_4 nanoparticles) in PAN/Fe_3O_4 nanofibers with 10 wt % Fe_3O_4 nanoparticles.

Moreover, it was tried to add Triton X-100, surfactant, to see its influence on the dispersion of Fe_3O_4 nanoparticles. SEM images of the resultant nanofibers (10 wt % Fe_3O_4) obtained in the presence of Triton X-100 are presented in Figure 4.5.

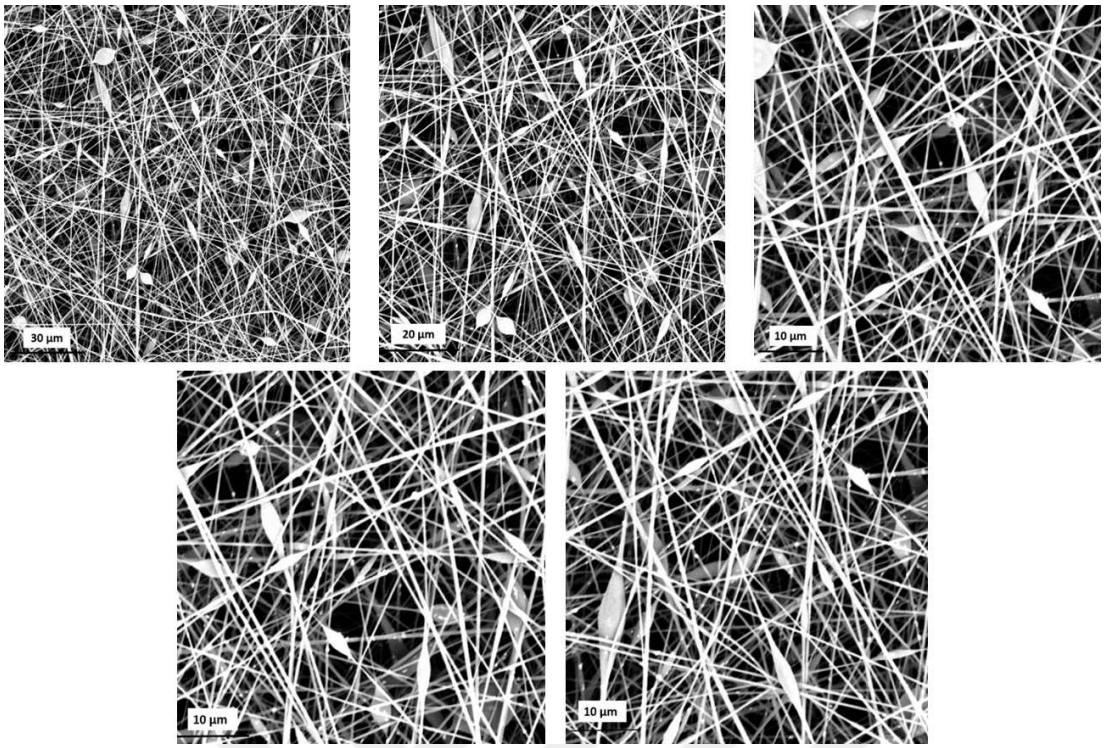

Figure 4.5 : SEM images of the PAN/ Fe_3O_4 (10 wt %) nanofibers obtained in the presence of Triton X-100.

Since beaded structures were observed in the existence of Triton X-100, it was decided not to add Triton X-100 to the polymer solutions for nanofiber production.

SEM images of PAN nanofibers including different amounts of Fe_3O_4 nanoparticles revealed that the obtained nanofibers were smooth, bead-free and continuous. Moreover, Fe_3O_4 nanoparticles could be seen over the nanofiber surfaces. Related to the studies conducted on the production of PAN/ Fe_3O_4 nanofibers, it was tried to obtain P(AN-co-IA)-PAN/ Fe_3O_4 nanofibers containing 10 wt % Fe_3O_4 nanoparticles. However, during electrospinning, inhomogeneous parts were observed on the resultant nanofiber mat, which was not the case for 5 wt % Fe_3O_4 nanoparticles containing P(AN-co-IA)-PAN/ Fe_3O_4 nanofibers. For this reason, attention was given on the production of P(AN-co-IA)-PAN/ Fe_3O_4 nanofibers including 5 wt % Fe_3O_4 nanoparticles.

SEM images of the produced P (AN-co-IA)-PAN/ Fe_3O_4 (5 wt %) nanofibers can be seen in Figure 4.6.

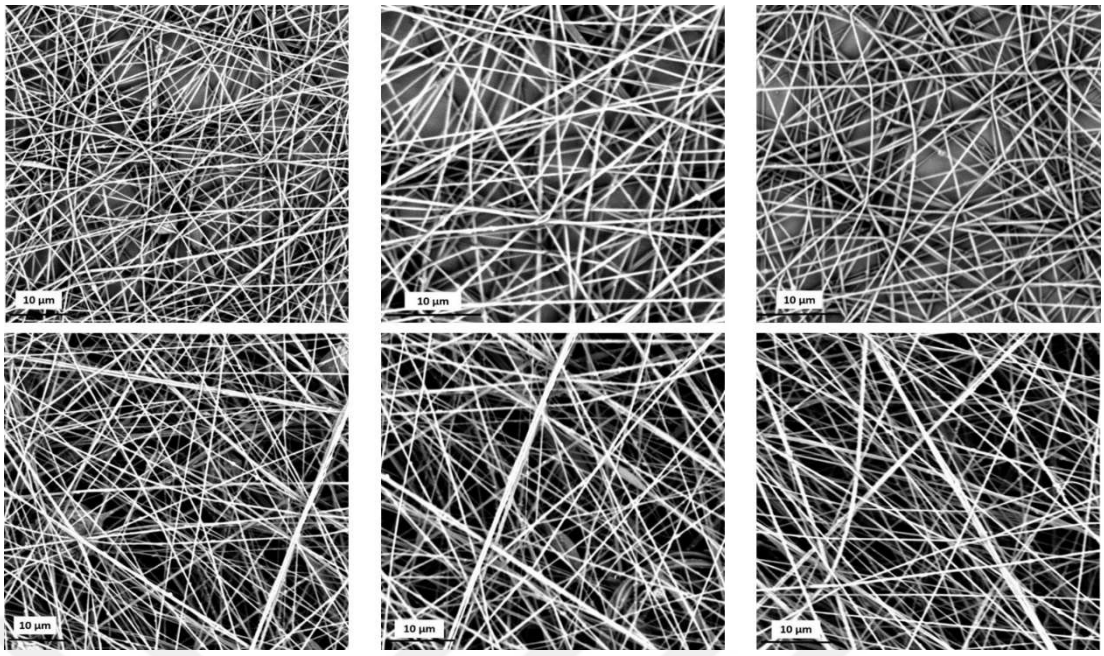

Figure 4.6 : SEM images of P(AN-co-IA)-PAN/ Fe_3O_4 nanofibers containing 5 wt % Fe_3O_4 nanoparticles.

It could be observed from Figure 4.6 that bead-free, smooth, continuous nanofibers could be achieved in the presence of Fe_3O_4 (5 wt %) nanoparticles, which were detected as dots on nanofiber surfaces.

Additionally, average nanofiber diameters of both PAN and P (AN-co-IA) based Fe_3O_4 nanoparticles (5 wt %) containing nanofibers were calculated via Image J software by selecting at 50 random nanofibers and the results were mentioned as 330±71 nm for PAN/ Fe_3O_4 nanofibers and 293±74 nm for P (AN-co-IA)-PAN/ Fe_3O_4 nanofibers. Figure 4.7 (a) and Figure 4.7 (b) depict nanofiber diameter distribution graphs of PAN/ Fe_3O_4 and P (AN-co-IA)-PAN/ Fe_3O_4 nanofibers, respectively.

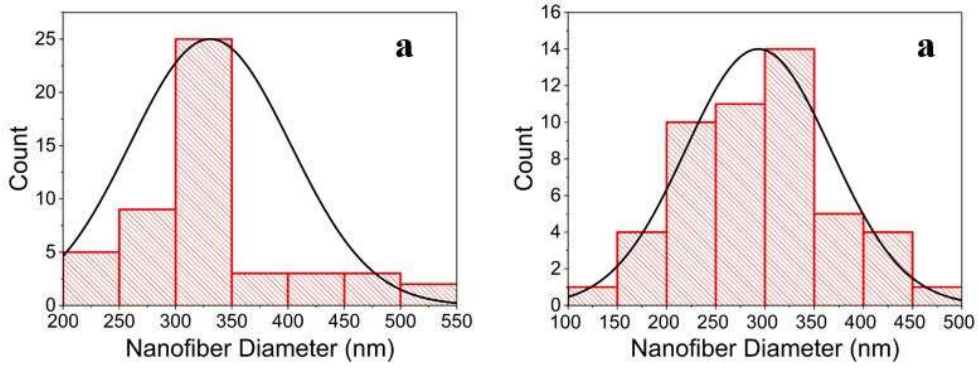

Figure 4.7 : Nanofiber diameter distribution graph of (a) PAN/ Fe_3O_4 (5 wt %) and (b) P (AN-co-IA)-PAN/ Fe_3O_4 (5 wt %) nanofibers.

Moreover, the existence of Fe_3O_4 nanoparticles was proved by EDS characterization and declared as wt % and at % amounts. For PAN/ Fe_3O_4 (5 wt %) nanofibers, the amount of Fe was found to be 10.28 wt % and 5.24 at %, while for P (AN-co-IA)-PAN/ Fe_3O_4 (5 wt %) nanofibers it was 14.32 wt % and 7.49 at %.

4.1.2 UV-Visible spectroscopy

UV-Visible spectroscopy characterizations of PAN/ Fe_3O_4 (5 wt %) and P (AN-co-IA)-PAN/ Fe_3O_4 (5 wt %) nanofibers were performed in the range of 200-800 nm. Figure 4.8 belongs to UV-Visible spectroscopy PAN/ Fe_3O_4 (5 wt %) and Figure 4.9 shows UV-Visible spectroscopy P (AN-co-IA)-PAN/ Fe_3O_4 (5 wt %) nanofibers.

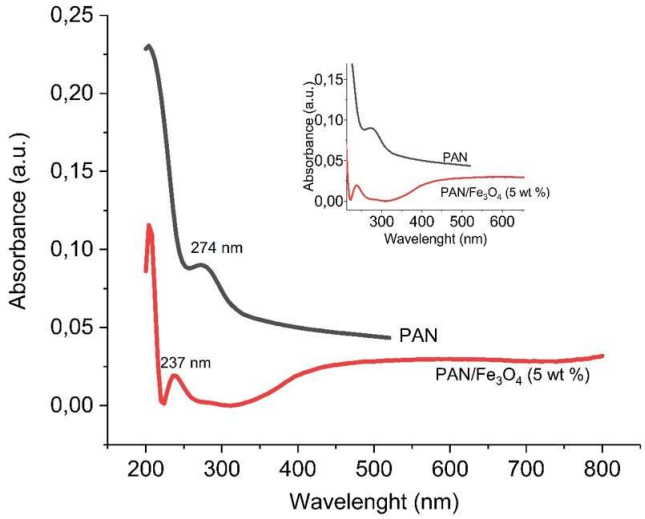

Figure 4.8 : UV-Visible spectroscopy PAN/ Fe_3O_4 (5 wt %) nanofibers.

It could be commented on that the presence of Fe_3O_4 nnaoparticles was observed in the region of 350-700 nm with a maxima at nearly 525 nm in PAN/ Fe_3O_4 (5 wt %) nanofibers while neat PAN nanofibers did not show any absorbance peak in that region.

In Figure 4.9, it was seen that while neat P (AN-co-IA) nanofibers did not show any maxima between 300 nm and 600 nm, Fe_3O_4 nanoparticles containing P (AN-co-IA)-PAN/ Fe_3O_4 nanofibers had an absorbance band between 300 and 600 nm with a peak approximately at 470 nm.

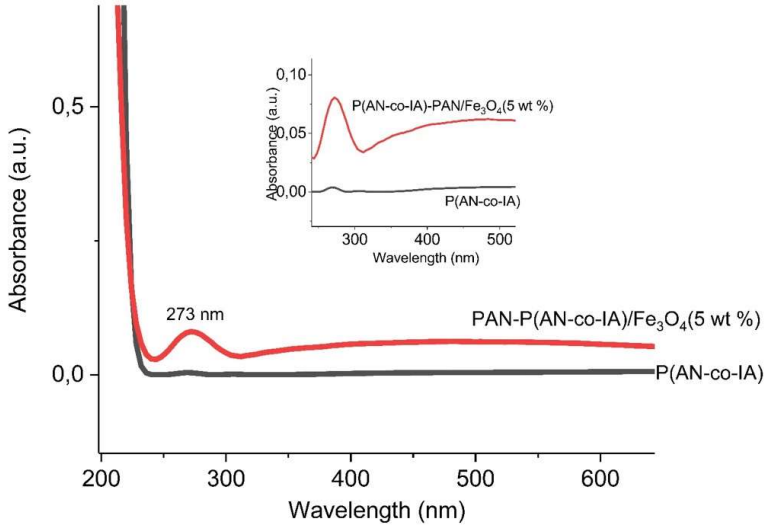

Figure 4.9 : UV-Visible spectroscopy P (AN-co-IA)-PAN/ Fe_3O_4 (5 wt %) nanofibers.

The peaks showing the presence of Fe_3O_4 nanoparticles varied according to the synthesis method and the polymer which they were blended. In a study, the generation of Fe_3O_4 nanoparticles was observed with an absorption peak at 290-450 nm [203]. In another study, the absorbance curve of Fe_3O_4 nanofibers was between 600 and 700 nm indicating the existence of Fe_3O_4 nanoparticles [204]. Absorbance curve of 5 wt % Fe_3O_4 nanoparticles containing nanofiber mat was detected at 470-620 nm in a different study [205]. Moreover, the absorbance peak of Fe_3O_4 nanoparticles could be shifted to 700-900 nm when the nanoparticles were synthesized via sol-gel process [206].

4.1.3 FTIR-ATR spectroscopy

FTIR-ATR spectroscopy characterizations of the neat PAN and P (AN-co-IA) nanofibers and Fe_3O_4 (5 wt %) nanoparticles containing PAN and P (AN-co-IA) nanofibers were performed in the range of 400 cm^{-1} and 4000 cm^{-1} with the signal resolution of 4 cm^{-1}. FTIR-ATR spectrums of PAN and PAN / Fe_3O_4 (5 wt %) nanofibers and P (AN-co-IA) and P (AN-co-IA)-PAN/ Fe_3O_4 (5 wt %) nanofibers are given in Figure 4.10 and Figure 4.11, respectively.

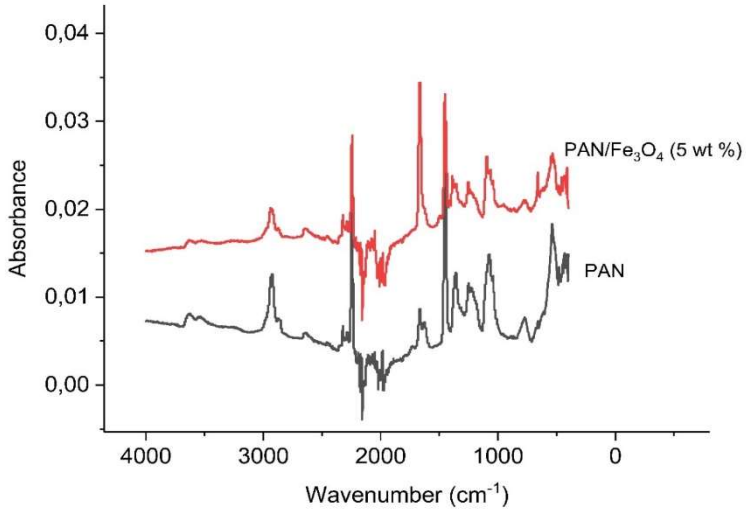

Figure 4.10 : FTIR-ATR spectrum of PAN and PAN/ Fe_3O_4 (5 wt %) nanofibers.

The wavenumbers 2931 cm^{-1} and 1372 cm^{-1} were attributed to stretching and bending vibrations of -CH_2-, respectively. 673 cm^{-1} was assigned to specific band of magnetite for PAN/ Fe_3O_4 (5 wt %) nanofibers. The peak at 1072 cm^{-1} shifted to 1102 cm^{-1} as an effect of Fe_3O_4 nanoparticles. In addition, the peak at 1625 cm^{-1} disappeared in PAN/ Fe_3O_4 (5 wt %) nanofibers [62, 207].

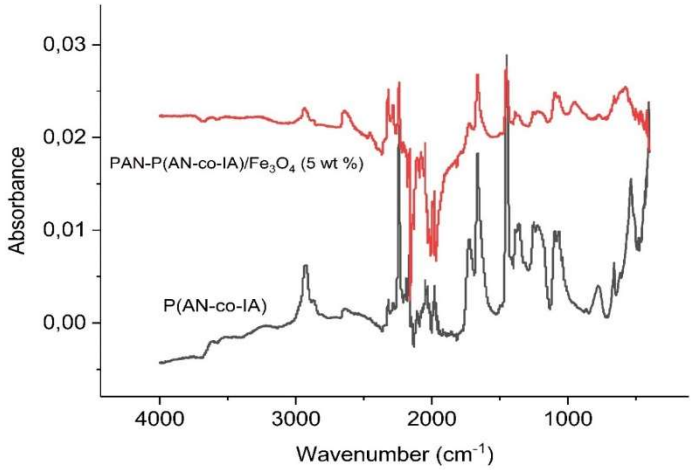

Figure 4.11 : FTIR-ATR spectrum of P (AN-co-IA) and P (AN-co-IA)-PAN/ Fe_3O_4 (5 wt %) nanofibers.

It was understood from Figure 4.11 that a shoulder arised between 1958 cm^{-1} and 1800 cm^{-1} as a result of Fe_3O_4 addition as well as a new peak at 948 cm^{-1}. Absorbance of the peak at 779 cm^{-1} reduced and shifted to 768 cm^{-1} as well. To make a general evaluation, it can be clearly said that the spectrum changed considerably in the range of 711 cm^{-1} and 400 cm^{-1} due to the presence of Fe_3O_4 nanoparticles.

4.1.4 DSC

DSC characterizations of the nanofiber samples of PAN, P (AN-co-IA), PAN/ Fe_3O_4 (5 wt %) and P (AN-co-IA)-PAN/ Fe_3O_4 (5 wt %) were performed in order to examine the thermal behaviour of them. In the measurements, the samples were heated from 0°C to 400°C at a heating rate of 10°C/min in the presence of N_2 atmosphere. Figure 4.12 depicts DSC thermograms of PAN and PAN/ Fe_3O_4 (5 wt %) nanofibers while Figure 4.13 and Figure 4.14 depict DSC thermograms of neat P (AN-co-IA) and P (AN-co-IA)-PAN/ Fe_3O_4 (5 wt %) nanofibers and PAN/ Fe_3O_4 and P (AN-co-IA)-PAN/ Fe_3O_4 (5 wt %) nanofibers, respectively.

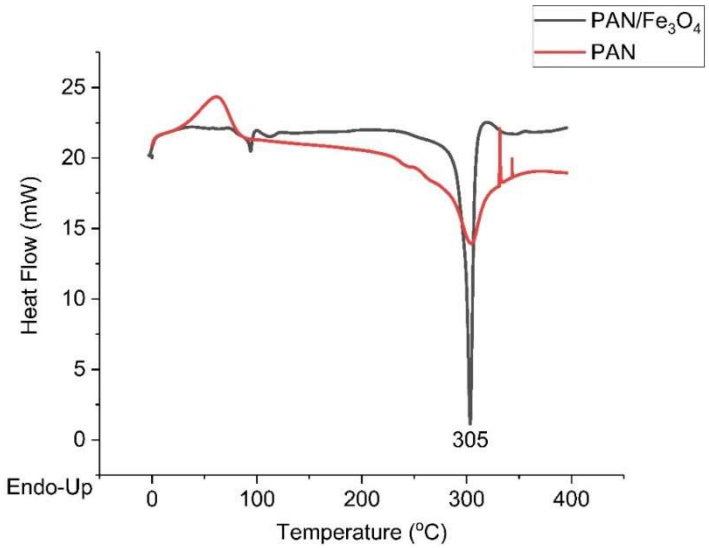

Figure 4.12 : DSC thermograms of PAN and PAN/ Fe_3O_4 (5 wt %) nanofibers.

In DSC thermograms, the characteristic exothermic peak which is determined as cyclization temperature (T_c) is seen approximately at 300°C, Cyclization reaction takes place during the conversion of C≡N groups to C=C and C=N groups [29]. By the addition of comonomers or nanoparticles in PAN structure, T_c value changes.

From Figure 4.12, it was captured that addition of Fe_3O_4 did not change T_c considerably where both of the neat PAN and PAN/ Fe_3O_4 (5 wt %) nanofibers nearly had the same T_c at 305°C.

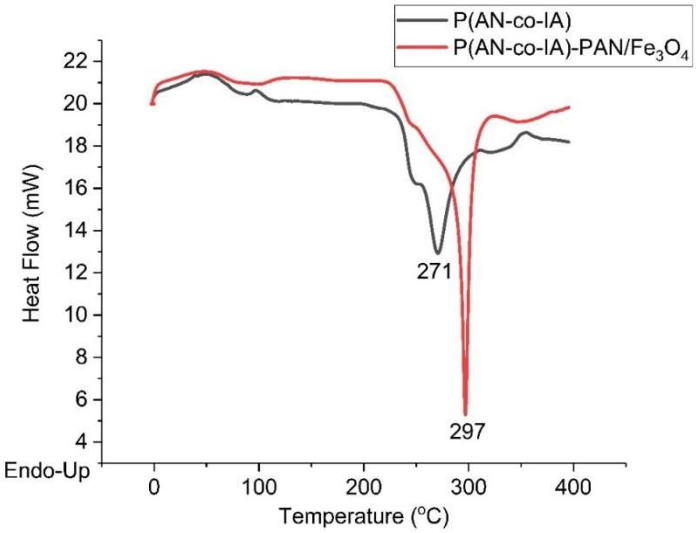

Figure 4.13 : DSC thermograms of neat P (AN-co-IA) and P (AN-co-IA)-PAN/ Fe_3O_4 (5 wt %) nanofibers.

Cyclization reactions of P (AN-co-IA) takes place through an ionic mechanism rather than a free radical mechanism [29], that's why T_c value of P (AN-co-IA) is lower than PAN. The addition of Fe_3O_4 nanoparticles into P (AN-co-IA) nanofibers increased the T_c from 271°C to 297°C. Addition of Fe_3O_4 nanoparticles into different polymer stuctures like polimide and acrylic-based nanocomposites contributed to increase glass transition temperature [208, 209]. From these results, it could be thought that addition of magnetic nanoparticles enhances the thermal stability of the polymers.

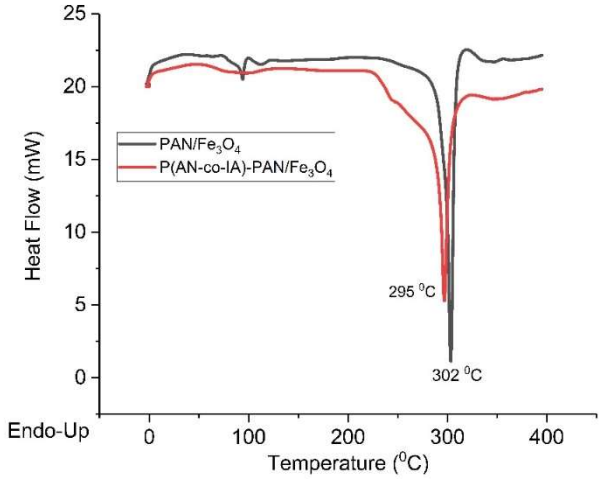

Figure 4.14 : DSC thermograms of neat PAN/ Fe_3O_4 (5 wt %) and P (AN-co-IA)-PAN/ Fe_3O_4 (5 wt %) nanofibers.

When DSC thermograms of PAN/ Fe_3O_4 (5 wt %) and P (AN-co-IA)-PAN/ Fe_3O_4 (5 wt %) nanofibers were compared, it was observed that T_c value was lower in P (AN-

co-IA)-PAN/ Fe_3O_4 (5wt %) nanofibers. T_c of PAN/ Fe_3O_4 nanofibers decreased from 302 °C to 295°C due to the presence of IA in nanofiber structure. Instead of two exothermic peaks, a distinct exothermic peak at 295°C and a shoulder were observed when P (AN-co-IA)-PAN/ Fe_3O_4 nanofibers was examined in detail.

4.2 Results of P (AN-co-IA)/Al_2O_3 Nanofibers

4.2.1 Morphology of P (AN-co-IA)/ Al_2O_3 nanofibers (SEM-EDS)

Morphologic analysis of both conventionally electrospun PAN/ Al_2O_3 (1 wt %) and co-axially electrospun P (AN-co-IA)-PAN/ Al_2O_3 (1 wt %) nanofibers were performed by SEM. Figure 4.15 presents SEM images of Al_2O_3 (1 wt %) containing PAN nanofibers.

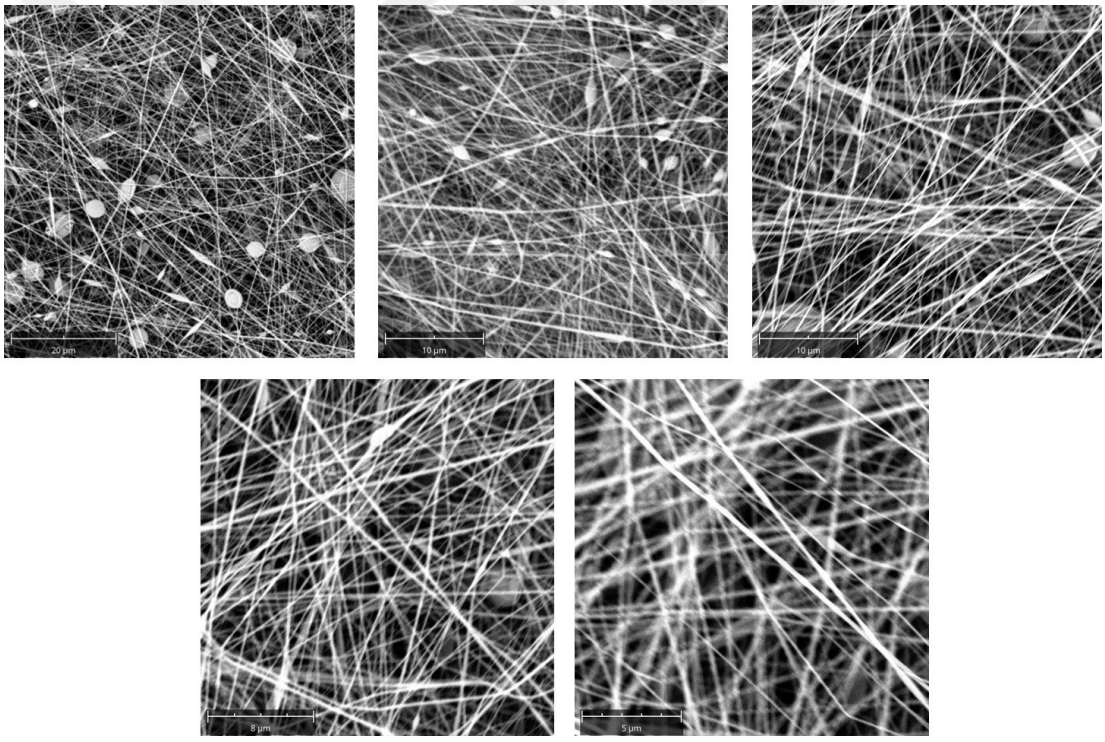

Figure 4.15 : SEM images of Al_2O_3 (1 wt %) containing PAN nanofibers.

Figure 4.15 showed that PAN/ Al_2O_3 (1 wt %) nanofibers had many beads in the nanofiber structure. Since stable electrospinning process could not be achieved with 1 wt % Al_2O_3, increasing the amount of Al_2O_3 loading was not experimented.

On the other hand, Figure 4.16 reveals SEM images of P (AN-co-IA)-PAN/Al_2O_3 (1 wt %) nanofibers. When SEM images of PAN/Al_2O_3 nanofibers and P (AN-co-IA)-PAN/Al_2O_3 nanofibers were compared, it could be mentioned that P (AN-co-IA) based nanofibers had less beads with more homogeneous nanofiber distribution.

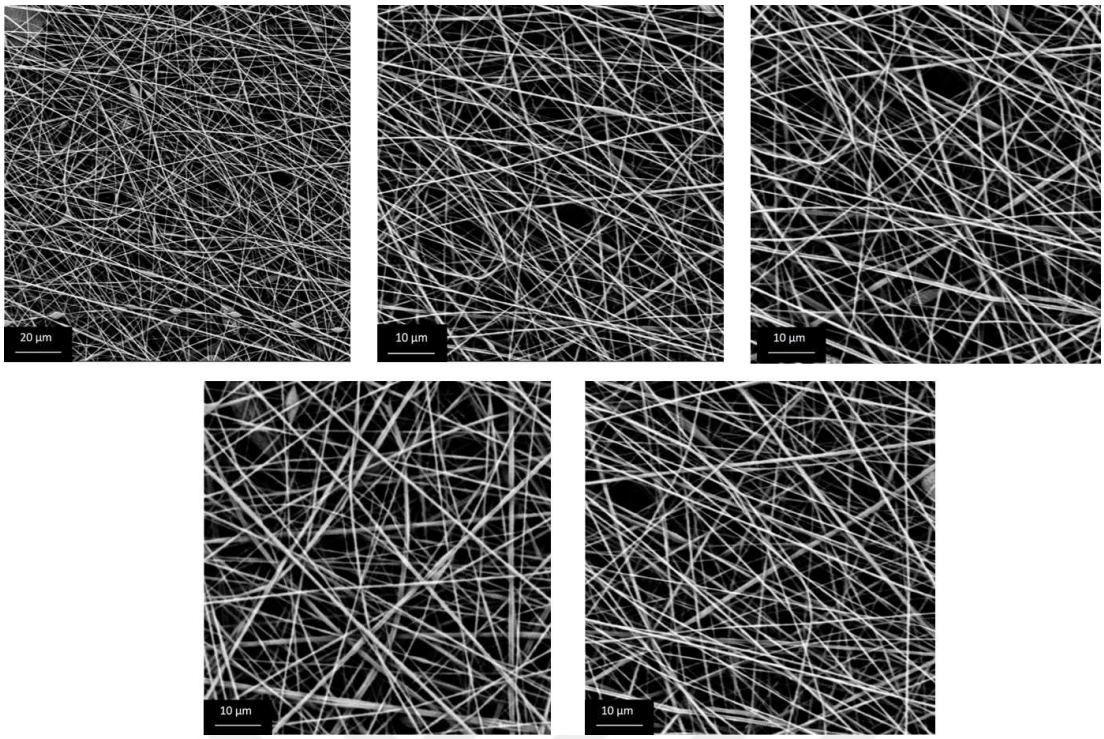

Figure 4.16 : SEM images of P (AN-co-IA)-PAN/ Al_2O_3 (1 wt %) nanofibers.

Moreover, the average nanofiber diameters of all the nanofiber samples were calculated via Image J program and nanofiber diameter distribution graphs of Al_2O_3 (1 wt %) containing PAN and P (AN-co-IA) based nanofibers were demonstrated in Figure 4.17 (a) and (b).

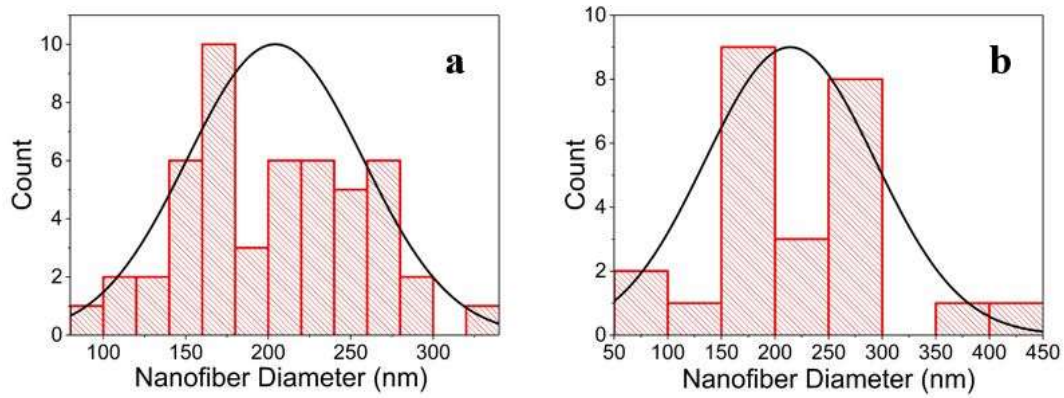

Figure 4.17 : Nanofiber diameter distribution graphs of a) PAN/ Al_2O_3 (1 wt %) and b) P (AN-co-IA)-PAN/ Al_2O_3 (1 wt %) nanofibers.

PAN/Al_2O_3 (1 wt %) nanofibers were fine, whose average nanofiber diameter was calculated as 204 ± 53 nm. Average nanofiber diameter of P (AN-co-IA)-PAN/ Al_2O_3 nanofibers was very close to the average nanofiber diameter of PAN/Al_2O_3 (1 wt %) nanofibers with the value of 214±79 nm.

Since beaded structure was observed for PAN/Al_2O_3 (1 wt %) nanofibers, coaxial electrospinning was performed by using two different feed-rates, 0.2 ml/h and 0.5 ml/h, of shell solution. Figure 4.18 and Figure 4.19 demonstrate SEM images of PAN (core)/ Al_2O_3 (shell) nanofibers obtained by the application of feed-rate as 0.2 ml/h and 0.5 ml/h for shell solution, respectively.

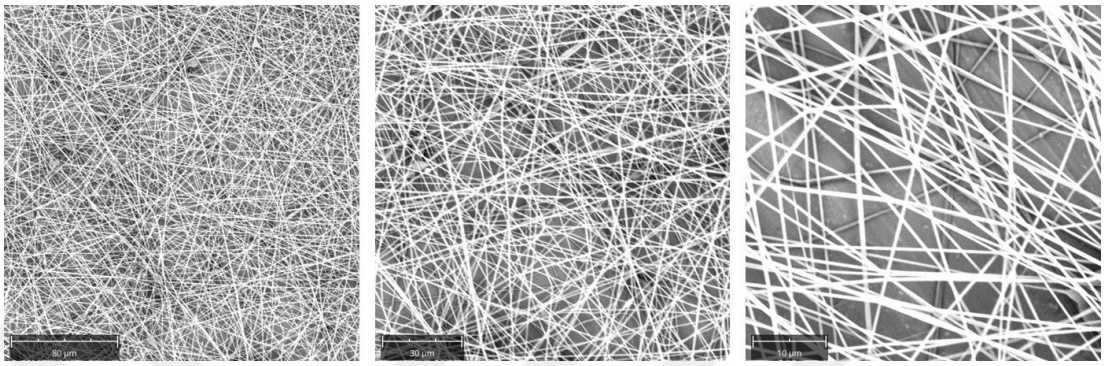

Figure 4.18 : SEM images of PAN (core)/ Al_2O_3 (shell) (0.2 ml/h) nanofibers.

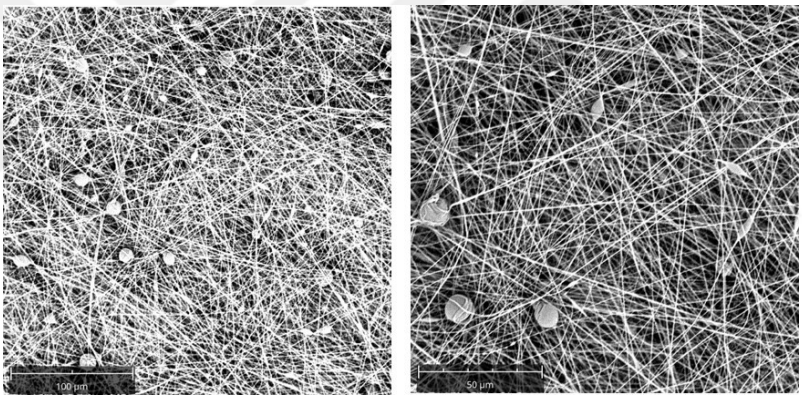

Figure 4.19 : SEM images of PAN (core)/ Al_2O_3 (shell) (0.5 ml/h) nanofibers.

Beaded nanofiber structure was not observed when feed-rate of the shell solution was applied as 0.2 ml/h; however, many beads were seen when feed-rate of shell solution was increased up to 0.5 ml/h. Therefore; for the fabrication of P (AN-co-IA)-PAN (core)/ Al_2O_3 (shell) nanofibers, feed-rate of shell solution was kept constant as 0.2 ml/h.

Figure 4.20 shows to SEM images of P (AN-co-IA)-PAN (core)/ Al_2O_3 (shell) nanofibers produced by the application of feed-rate as 0.2 ml/h for shell solution.

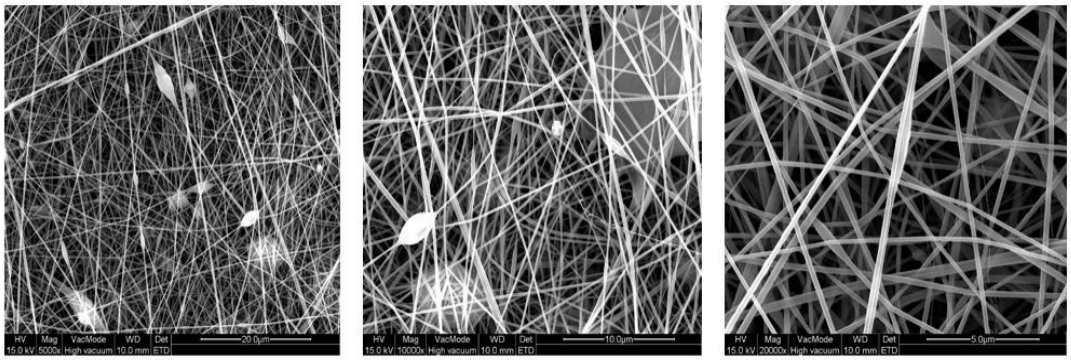

Figure 4.20 : SEM images of P (AN-co-IA)-PAN (core)/ Al_2O_3 (shell) (0.2 ml/h) nanofibers.

Unfortunately, even though feed-rate of the shell solution was applied as 0.2 ml/h, beads were observed in P(AN-co-IA)- PAN(core)/ Al_2O_3 (shell) nanofibers. Furthermore, average nanofiber diameters were assessed as 536 ± 120 nm for PAN(core)/ Al_2O_3 (shell) (0.2 ml/h) nanofibers and 244 ± 81 nm for P(AN-co-IA)-PAN(core)/ Al_2O_3 (shell) (0.2 ml/h) nanofibers. Figure 4.21 (a) and (b) display nanofiber diameter distribution graphs of PAN(core)/ Al_2O_3 (shell) (0.2 ml/h) and nanofibers and P(AN-co-IA)-PAN(core)/ Al_2O_3 (shell) (0.2 ml/h) nanofibers, in sequence.

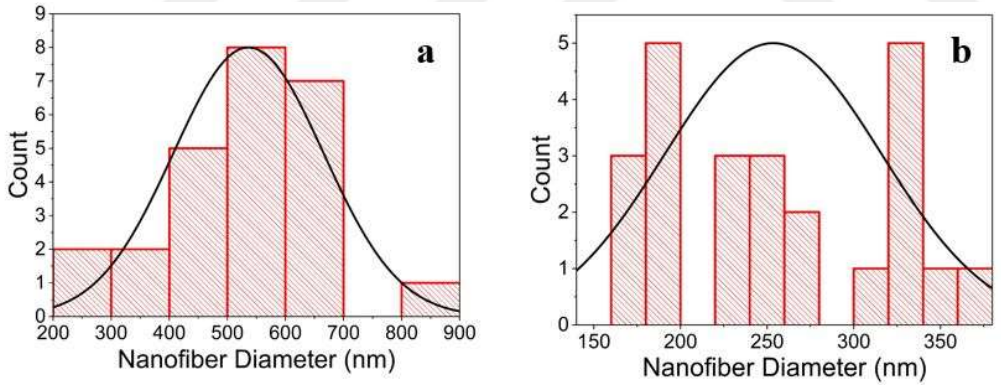

Figure 4.21 : Nanofiber diameter distribution graphs of (a) PAN(core)/ Al_2O_3 (shell) (0.2 ml/h) and P(AN-co-IA)-PAN(core)/ Al_2O_3 (shell) (0.2 ml/h) nanofibers.

4.2.2 UV-Visible spectroscopy

UV-Visible spectroscopies of neat PAN, PAN/ Al_2O_3 (1 wt %), PAN(core)/ Al_2O_3 (shell) (0.2 ml/h) and PAN(core)/ Al_2O_3 (shell) (0.5 ml/h) nanofibers were carried out in the range of 200-500 nm and the corresponding results are introduced in Figure 4.22.

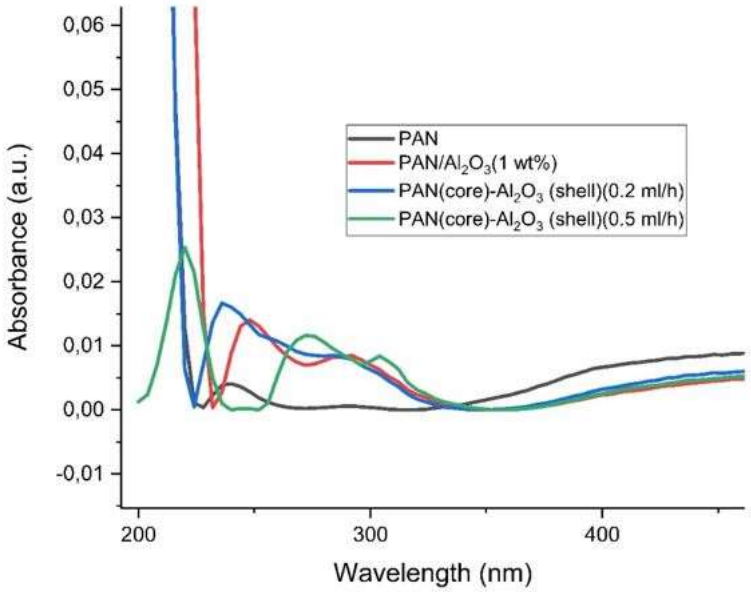

Figure 4.22 : UV-Vis. spectroscopy of PAN, PAN/ Al_2O_3 (1 wt %), PAN (core)/ Al_2O_3 (shell) (0.2 ml/h) and PAN (core)/ Al_2O_3 (shell) (0.5 ml/h) nanofibers.

The characteristic absorption peak of PAN nanofibers was seen at 240 nm [202]. In case of Al_2O_3 presence, the peak shifted to 247 nm and a new peak occurred at 289 nm. When Al_2O_3 nanoparticles were incorporated to nanofiber structure as shell, three distinct peaks were seen at 236 nm, 258 nm and 290 nm. When they were fed with a higher flow-rate, the placement of those three peaks changed to 219 nm, 274 nm and 304 nm.

UV-Vis. spectroscopy of the pure P (AN-co-IA), P (AN-co-IA)-PAN/ Al_2O_3 (1 wt %) and P (AN-co-IA)-PAN (core)/ Al_2O_3 (shell) (0.2 ml/h) nanofibers are displayed in Figure 4.23. It was understood from the Figure 4.23 that pure P (AN-co-IA) nanofibers showed the characteristic peak at 269 nm, which shifted to a lower value, 237 nm for P (AN-co-IA)-PAN/ Al_2O_3 (1 wt %) nanofibers. Instead of three distinct peaks, seen for PAN (core)/ Al_2O_3 (shell) nanofibers, two distinct peaks at 236 nm and 290 nm occurred.

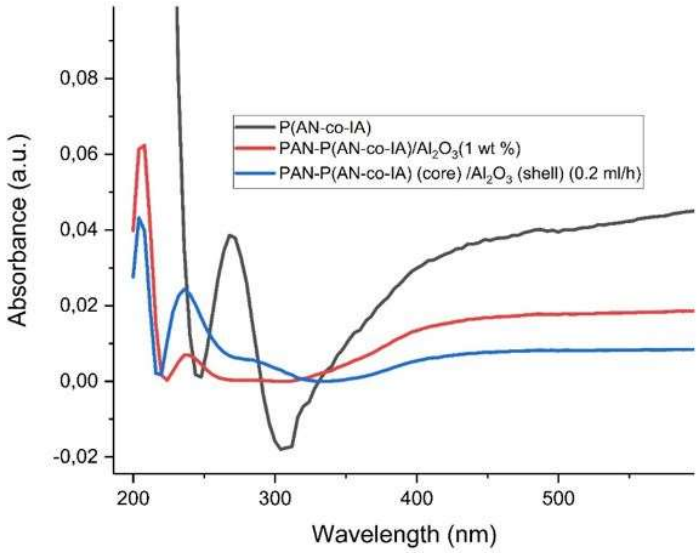

Figure 4.23 : UV-Vis. spectroscopy of the pure P (AN-co-IA), P (AN-co-IA)-PAN/ Al_2O_3 (1 wt %) and P (AN-co-IA)-PAN (core)/ Al_2O_3 (shell) (0.2 ml/h) nanofibers.

4.2.3 FTIR-ATR spectroscopy

FTIR-ATR spectroscopy tests of all nanofiber samples were made in the range of 400 cm^{-1} and 4000 cm^{-1} with the signal resolution of 4 cm^{-1}. The characterization results of PAN, PAN/ Al_2O_3 (1 wt %), PAN (core)/ Al_2O_3 (shell) (0.2 ml/h) and PAN (core)/ Al_2O_3 (shell) (0.5 ml/h) nanofibers are shown in Figure 4.24 while the results of P (AN-co-IA), P (AN-co-IA)-PAN/ Al_2O_3 (1 wt %) and P (AN-co-IA)-PAN (core)/ Al_2O_3 (shell) (0.2 ml/h) nanofibers are demonstrated in Figure 25.

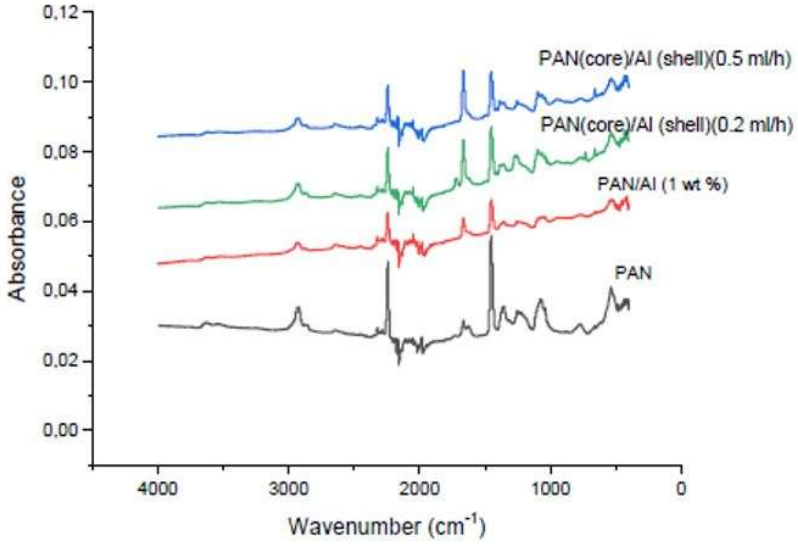

Figure 4.24 : FTIR-ATR spectroscopy of PAN, PAN/ Al_2O_3 (1 wt %), PAN (core)/ Al_2O_3 (shell) (0.2 ml/h) and PAN (core)/ Al_2O_3 (shell) (0.5 ml/h) nanofibers.

The band between 3300-3400 cm^{-1} and the peak at 1628 cm^{-1} indicated the stretching and bending vibration of hydroxylgroups, respectively. In addition, the absorption band between 3000 cm^{-1} and 3500 cm^{-1} was related to stretching vibration of NH_2. The peaks at 842 cm^{-1} and 520 cm^{-1} were attributed to CH bending and amide bonds stretching vibrations. Characteristic absorption peak of Al_2O_3 was seen in the band of 400-1000 cm^{-1}. Moreover, absorption of the peak at 1671 cm^{-1} increased for Al_2O_3 nanoparticles containing nanofibers, which confirmed the interaction between PAN and Al_2O_3. Finaly, Al-O group was detected at 557 cm^{-1} [75]. In addition to the mentioned results, for P (AN-co-IA) based Al_2O_3 nanoparticles containing nanofibers, a shoulder occurred at 1874 cm^{-1} caused by the presence of IA.

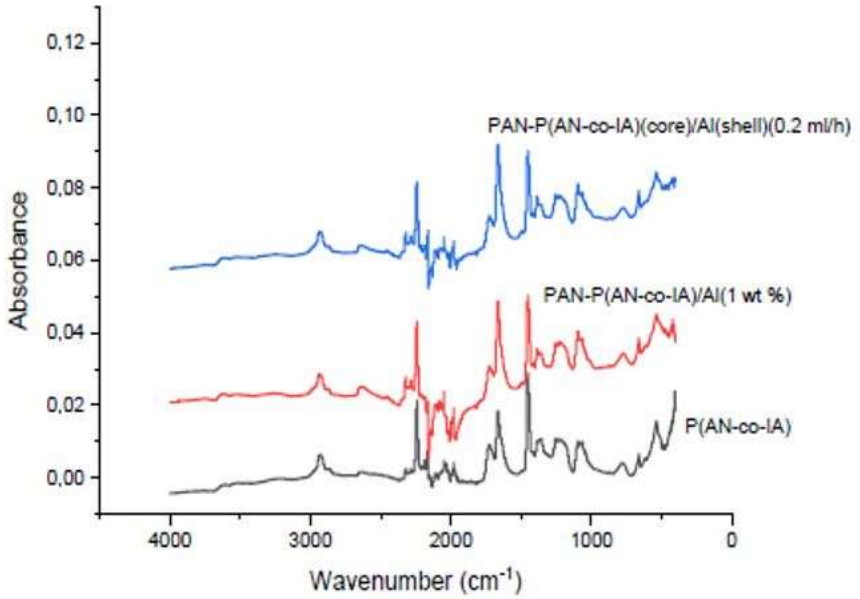

Figure 4.25 : FTIR-ATR spectroscopy of P (AN-co-IA), P (AN-co-IA)-PAN/ Al_2O_3 (1 wt %), P (AN-co-IA)-PAN (core)/ Al_2O_3 (shell) (0.2 ml/h) and PAN (core)/ Al_2O_3 (shell) (0.5 ml/h) nanofibers.

4.2.4 DSC

DSC measurements of the samples were conducted between 0°C and 400°C at a heating rate of 10°C/min in the presence of N_2 atmosphere. DSC thermograms of PAN/ Al_2O_3 (1 wt %), P (AN-co-IA)-PAN/ Al_2O_3 (1 wt %), PAN (core)/ Al_2O_3 (shell) (0.2 ml/h) and P (AN-co-IA)-PAN (core)/ Al_2O_3 (shell) (0.2 ml/h) nanofibers are given in Figure 4.26.

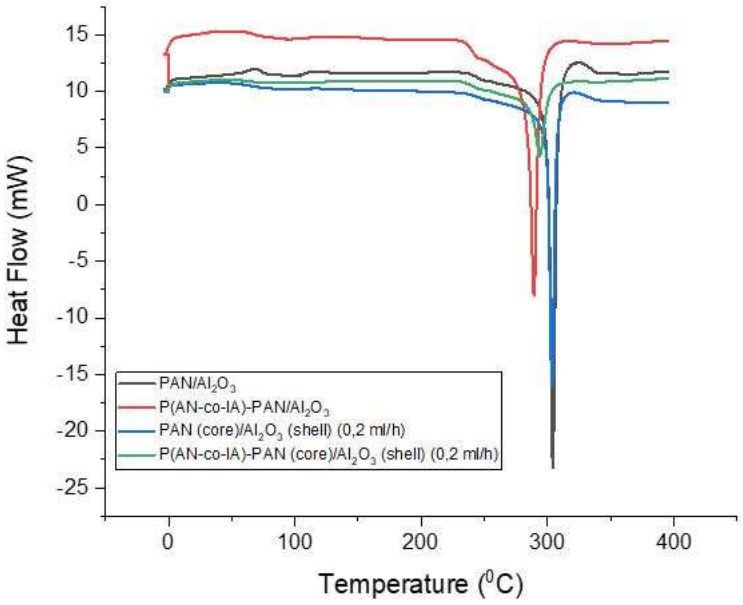

Figure 4.26 : DSC thermograms of PAN/ Al_2O_3 (1 wt %), P (AN-co-IA)-PAN/ Al_2O_3 (1 wt %), PAN (core)/ Al_2O_3 (shell) (0.2 ml/h) and P (AN-co-IA)-PAN (core)/ Al_2O_3 (shell) (0.2 ml/h) nanofibers.

According to Figure 4.26, it was understood cyclization temperature decreased from 303°C to 288°C for PAN based Al_2O_3 nanoparticle containing nanofibers and 299°C to 293°C for P (AN-co-IA) based Al_2O_3 nanoparticle containing nanofibers. Furthermore, P (AN-co-IA) shows two exothermic peaks in its neat form [30], however; it showed only a strong exothermic peak when it was combined with Al_2O_3. When the nanoparticles were incorporated to the nanofiber structure by coaxial electrospinning, a slight increase in cyclization temperature was observed for P (AN-co-IA) nanofibers. However, cyclization temperature of PAN nanofibers did not differ when Al_2O_3 nanoparticles were integrated to the nanofibers via coaxial electrospinning. As a summary, it could be summarized that Al_2O_3 nanoparticles had a considerable impact on the thermal features of P (AN-co-IA) based nanofibers.

4.2.5 TGA

In order to explore thermal decomposition behavours of the nanofibers, TGA characterization was performed by heating from 0°C to 750°C with a heating rate of 10°C/min. Figure 4.27 depicts TGA curves of PAN, PAN/Al_2O_3 (1 wt %) and PAN (core)/ Al_2O_3 (shell) (0.2 ml/h) nanofibers.

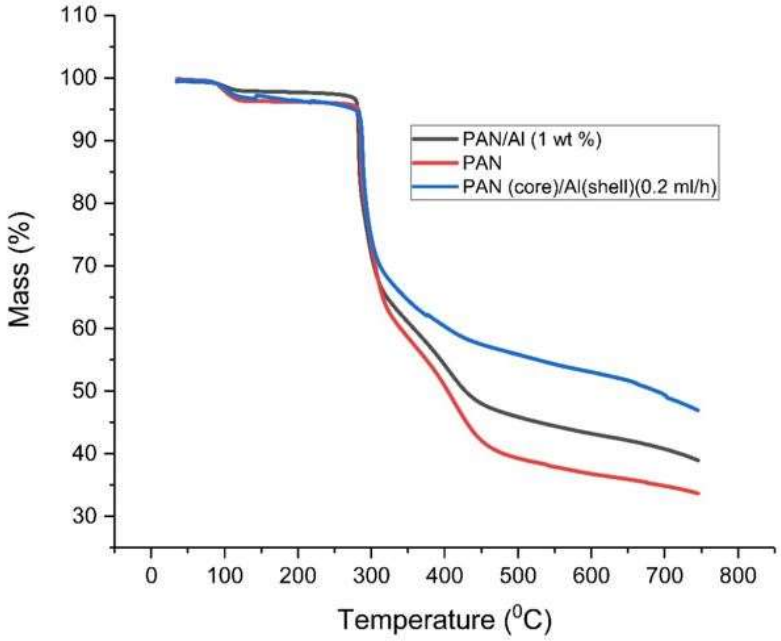

Figure 4.27 : TGA curves of PAN, PAN/ Al_2O_3 (1 wt %) and PAN (core)/ Al_2O_3 (shell) (0.2 ml/h) nanofibers.

The mass loss up, which was 4 %, up to 120°C was the evaporation of moisture or trapped solvent in the samples [210]. The first dramatic mass loss was observed between 300°C and 450°C. In that region, oligomers or short polymer chains started to degrage and then main polymer backbone started to decompose [211]. At the end of that, neat PAN nanofibers lost their mass nearly 54 %, where the value was approximately 46 % for PAN/Al_2O_3 (1 wt %) nanofibers and 36 % for PAN (core)/Al_2O_3 (shell) (0.2 ml/h) nanofibers. After 450°C, degradation of the final residue continued with a slower decomposition rate and at 750 °C, it was seen that PAN (core)/ Al_2O_3 (shell) (0.2 ml/h) nanofibers kept 47 % of their mass. Compared to resultant mass loss of PAN/Al_2O_3 (1 wt %) nanofibers (62 %) and PAN (core)/Al_2O_3 (shell) (0.2 ml/h) (53 %) nanofibers, it could be concluded that addition of Al_2O_3 nanoparticles in PAN nanofiber structure enhanced the thermal stability of PAN nanofibers. Besides, addition of Al_2O_3 nanoparticles via coaxial electrospinning caused higher thermal stability in the nanofibers.

In addition, Figure 4.28 displays TGA curves of P (AN-co-IA), P (AN-co-IA)-PAN/Al_2O_3 (1 wt %) and P (AN-co-IA)-PAN (core)/ Al_2O_3 (shell) (0.2 ml/h) nanofibers.

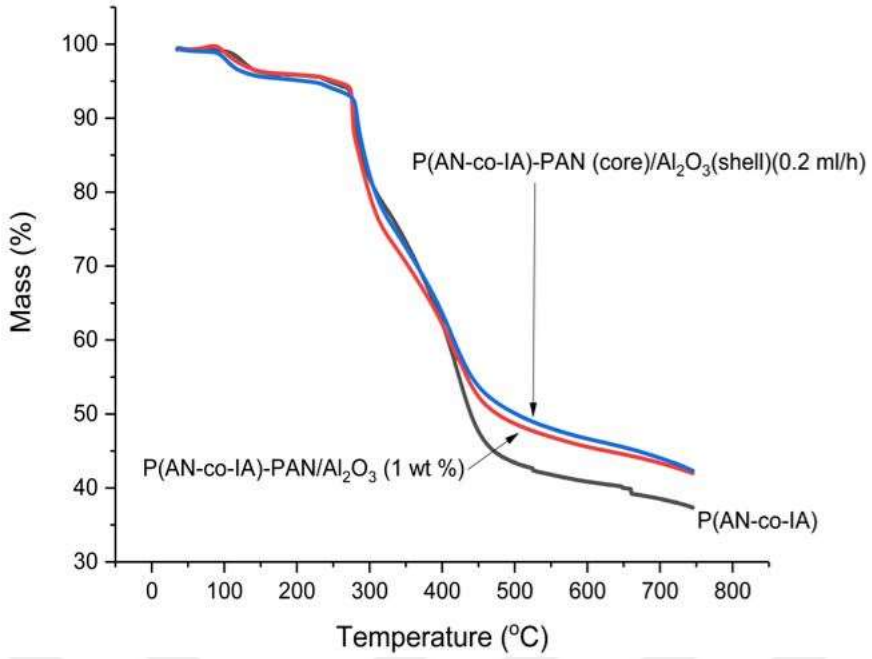

Figure 4.28 : TGA curves of P (AN-co-IA), P (AN-co-IA)-PAN/ Al_2O_3 (1 wt %) and P (AN-co-IA)-PAN (core)/ Al_2O_3 (shell) (0.2 ml/h) nanofibers.

Based on the TGA curves in Figure 4.28, the first mass loss was observed for all samples between 100-155 °C in which volatilization of water molecules [212] happened as in Figure 4.27. Then, a slight decrease in mass loss occured from 155°C to 276°C due to the degradation of oligomers existing in the backbone of the polymer [211]. Up to that point, total mass loss (%) for those three nanofibers samples was calculated as 7 %. The major mass loss took place between 276°C and 460°C. At 460°C, the mass loss for P (AN-co-IA) nanofibers was 55 %, while it was 50 % and 48 % for P (AN-co-IA)-PAN/Al_2O_3 (1 wt %) and P (AN-co-IA)-PAN (core)/ Al_2O_3 (shell) (0.2 ml/h) nanofibers. That mass loss was due to the decomposition and burning of host polymers [210]. Up to 750°C, it could be said that mass loss proceeded with a slower decomposition rate. At the end of the heat treatment, P (AN-co-IA) nanofibers preserved their mass in the ratio of 37 %. Moreover, the value was higher for Al_2O_3 nanoparticles containing nanofibers, which were very close to each other and recorded as 41 % and 40 % for P (AN-co-IA)-PAN/Al_2O_3 (1 wt %) and P (AN-co-IA)-PAN (core)/ Al_2O_3 (shell) (0.2 ml/h) nanofibers, in sequence.

4.3 Results of P (3HB)/P (3HO-3HD)/Ag Nanofibers

4.3.1 Results of solubility studies of P (3HB) and P (3HO-3HD)

As explained in the section 3.4.1.2, before electrospinning, solubility studies were performed for P (3HB) and P (3HO-3HD). In order to facilitate electrospinning, the evaporation rate of the solvents needs to be sufficiently high [213]. This was taken into account for solubility studies. Figure 4.29 summarizes the solubility study results of P (3HB).

		v:v %	20 °C	50 °C	70 °C	80 °C	100 °C
Benzlyalcohol		100	Not Dissolved				Partially Solved
Anisole		100					
Cyclohexanone		100					
Acetone		100					
Methyl ethyl ketone		100					
Dimethyl carbonate		100					Dissolved
Ethylacetate		100					
Ethanol	Anisole	70:30					Dissolved
2-Butanol	Anisole	70:30					Partially Solved
Ethylacetate	Anisole	70:30					
Acetone	Anisole	70:30					
Ethylacetate	Benzylalcohol	70:30					
Anisole	Dimethylcarbonate	20:80					
Anisole	Propylene carbonate	80:20	Partially Solved				
Butylacetate	2-Butanol	70:30	Not Dissolved				Not Dissolved
Ethylacetate	2-Butanol	70:30					
Acetone	Water	90:10					
2-Butanol	Water	80:20					Partially Solved
Acetone	DMSO	80:20	Not Dissolved		Partially Solved		
Anisole	DMSO	60:40	Not Dissolved				Dissolved
Dimethyl carbonate	DMSO	80:20					
Propylene Carbonate	Dimethylcarbonate	20:80					Partially Solved

Figure 4.29 : Solubility study results of P (3HB).

It was observed from Figure 4.29 that the polymer could be dissolved in dimethyl carbonate, ethanol/anisole (70/30), anisole/DMSO (60/40), dimethyl carbonate/DMSO (80/20) at 100°C. But, the most crucial point was the temperature. In order to dissolve the polymer in those solvents, high temperature such as 100°C was needed. If it is desired to solve the polymer at lower temperatures, moleculer weight of the polymer can be decreased.

In literature, for solubility studies 'Hildebrand radius' is commonly used. Hildebrand radius (Figure 4.30) is a parameter to estimate how likely it is for a polymer to dissolve in a solvent. If the Hildebrand radius between a polymer and a solvent is low, the polymer is more likely to be dissolved in that solvent [214].

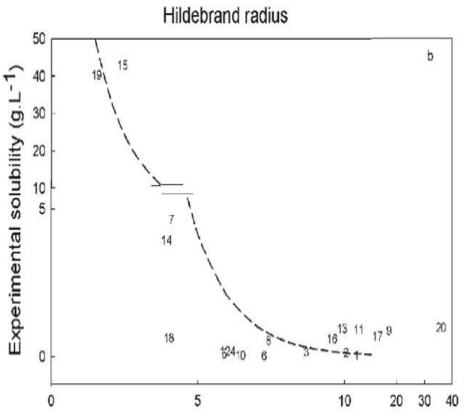

	Hydrocarbons		Ketones		
1	*n*-Hexane	8	Acetone		
2	*n*-Octane		Alcohols		
3	Cyclohexane	9	Methanol		
	Aromatic compounds	17	Ethanol		
4	Benzene	16	1-Butanol		
5	Toluene		Acids		
	Halogenated compounds	11	Acetic acid		
7	1,2-Dichloroethane		Nitrogen compounds		
15	Chloroform	13	*N,N* dimethylformamide		
19	Dichloromethane	14	Aniline		
	Ethers	18	Pyridine		
6	Diethyl ether	20	Water		
	Esters				
10	Ethylacetate				
12	*n*-Butylacetate				

Figure 4.30 : Graph of Hildebrand radius for P (3HB) [214].

Besides, dichloromethane and chloroform, it was very hard to dissolve P (3HB) lower than the temperature of 100°C. Suitability of dichloromethane and chloroform for dissolving the polymer was also proved by Hildebrand radius [214].

On the other hand, Figure 4.31 summarizes the solubility study results of P (3HO-3HD).

		v:v %	20 °C	40 °C	20 °C	50 °C	70 °C	80 °C	100 °C	
			2%	2%	4%	2%	2%	2%	2%	10%
Anisole		100	Dissolved							Dissolved
Acetone		100								
Dimethylcarbonate		100								
Butylacetate		100								
Ethylacetate		100								
Methyl ethyl ketone		100								
DMSO		100	Not Dissolved				Partially Solved			
iso-propanol		100					Dissolved			
2-Butanol		100				Dissolved				
Acetone	Anisole	80:20	Dissolved							
Dimethylcarbonate	Anisole	80:20								
Butylacetate	Anisole	80:20								
Acetone	DMSO	80:20	Partially Solved							
Butylacetate	2-Butanol	80:20	Dissolved							
Butylacetate	2-Butanol	60:40								
iso-propanol	Water	80:20	Not Dissolved				Partially Solved			
iso-propanol	Water	60:40								

Figure 4.31 : Solubility study results of P (3HO-3HD).

Since the polymer is more amorphous than P (3HB), it could be dissolved in a wide range of solvents, specifically in green solvents such as anisole, acetone, ether, dimethylcarbonate (DMC), butylacetate, ethylacetate, methylethylketone and blends of those solvents at low temperatures (20°C and 40°C). However, the polymer was not soluble in alcohols, DMSO and water at room temperature.

4.3.2 Morphology of P (3HB)/P (3HO-3HD)/Ag nanofibers (SEM-EDS)

Before electrospinning of P (3HB)-P (3HO-3HD) blend, electrospinning of P (3HB) and P (3HO-3HD) were studied, seperately.

As solubility tests revealed that P (3HB) can be dissolved in chloroform or dichloromethane at room temperature, a solvent system of chloroform-2 butanol in the ratio of 70:30 (v:v %) was used for electrospinning of P (3HB). In the solvent system, 2-butanol helped the stabilization of the electrospinning process and increased the conductivity of the solutions since chloroform was highly volatile. SEM image of the neat P (3HB) nanofibers electrospun from 2 wt % P (3HB) polymer solution of chlorofom/2-butanol solvent system is given in Figure 4.32.

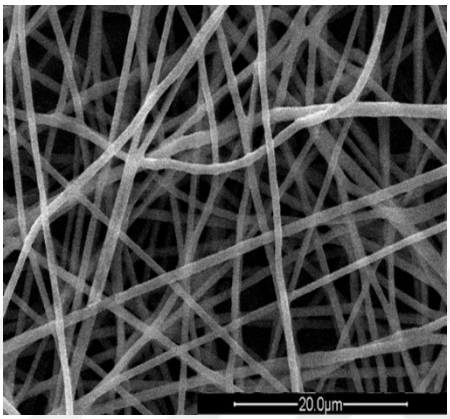

Figure 4.32 : SEM image of electrospun P (3HB) (2 wt %) nanofibers.

Electrospun P (3HB) nanofibers were continuous with with an average diameter of 775 ± 106nm.

Electrospinning of P (3HO-3HD) polymer was tried by using different solvents since the rubber like P (3HO-3HD) retains the solvent very well and causes fused fibers. Due to its high evaporation rate, acetone was selected as an appropriate and electrospinning of 6 wt % and 8 wt % P (3HO-3HD) were tried. The morphologies after electrospinning of 6 wt % P (3HO-3HD) polymer by applying 40 kV voltage, 0.5 ml/h feed-rate, 20 cm needle tip-to-collector distance for 10 minutes are introduced in Figure 4.33.

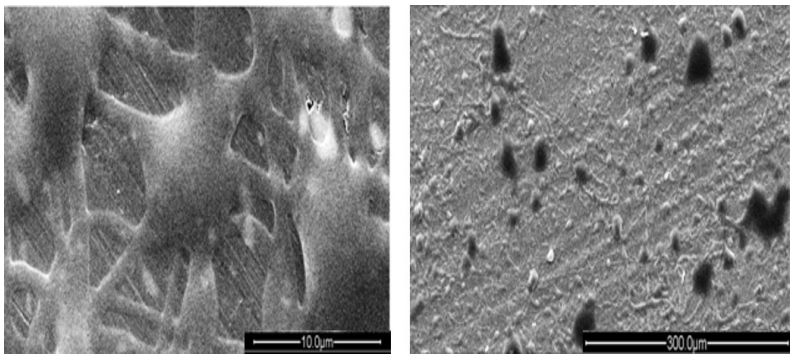

Figure 4.33 : SEM images of 6 wt % P (3HO-3HD) fibers after electrospinning.

It was seen that rather than a satisfying nanofiber structure, a fused structure was obtained. The reason might be mainy due to the low polymer concentration (6 wt %) of P (3HO-3HD).

Additionaly, 8 wt % polymer concentration of P (3HO-3HD) was electrospun with the electrosinning parameters as 40 kV applied voltage, 0.5 ml/h flow-rate, 30 cm distance between the needle tip and collector, 30 min electrospinning duration and the resultant morphologies are displayed in Figure 4.34.

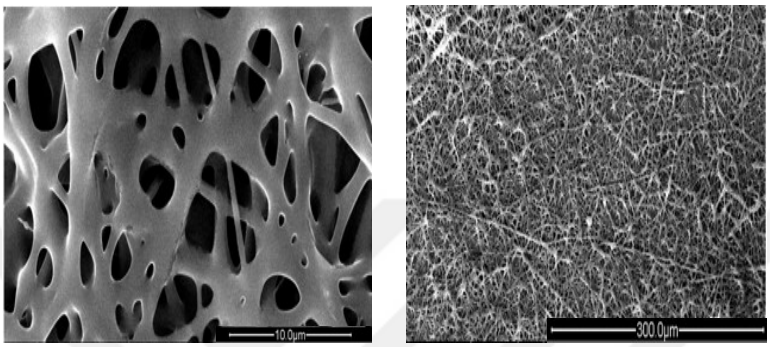

Figure 4.34 : SEM images of 8 wt % P (3HO-3HD) fibers after electrospinning.

Compared to Figure 4.33, more satisfying fiber structures were obtained when the polymer concentration of P (3HO-3HD) was increased from 6 wt % to 8 wt %.

Pure P (3HO-3HD) nanofibers could be obtained from a more eco-friendly solvent mixture which contained anisole, acetone and ether. The slow evaporating anisole was balanced with fast-evaporating acetone and ether because for an efficient electrospinnning process. The electrospinning parameters for P (3HO-3HD) nanofibers were investigated in terms of concentration, relative humidity, temperature and solvent composition. Solutions of 6 wt % and 10 wt % of P (3HO-3HD) were prepared in 30% An-35% Ac-35% ether and electrospun at 25°C and a relative humidity (RH) of 10%. Two different relative humidities (10 % and 40 %) were tested for 10 wt %P (3HO-3HD) containing nanofibers in 30% An-35% Ac-35% ether solvent mixture at 25°C. The impact of solvent composition was evaluated using 10 wt % P(3HO-3HD) solution in two different solvent compositions (40% An-30% Ac-30% ether; ether; 10% An-45% Ac-45 % ether) at 25 °C with a RH of 40 %. Finally, the effect of temperature was evaluated at 25 °C and 40 °C for 10 wt % P (3HO-3HD) when the solvent mixture was 30% An-35% Ac-35% ether at 40 % RH. For the electrospinning, 40 kV voltage, 40 cm needle tip-to-collector distance, 0.5 ml/h feed-

rate was kept constant for each experiment. SEM images of the resultant nanofibers from various electrospinning parameters can be observed from Figure 4.35.

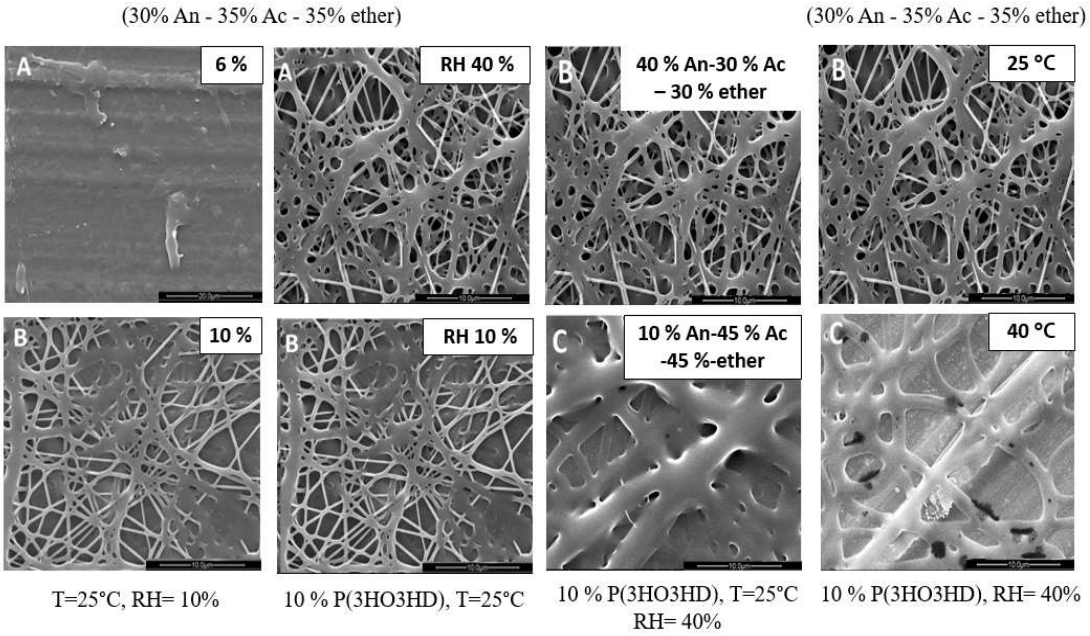

Figure 4.35 : SEM images of P (3HO-3HD) nanofibers obtained by the application of different electrospinning parameters.

It was concluded from Figure 4.35 that when the temperature and relative humidity were constant, at low polymer concentrations a film structure occurred rather than a fiber morphology. The polymer concentration has to be sufficiently high to avoid the formation of droplets and fused fibers and 10 wt % concentration resulted in a more fibrous structure although some fibers were fused. When keeping all the parameters constant except relative humidity, nearly the same fiber morphologies were obtained for both 10 % and 10 % RH. When the solvent composition changed, which meant the amount of anisole and acetone and ether increased, thicker fibers were obtained. Since thicker fibers have low specific surface area, it should be preferred to use higher amounts of anisole in the solvent composition. Furthermore, thicker fibers occur at higher temperatures due to the high evaporation rate of the solvent.

In addition to those optimization studies, electrospinning of P (3HO-3HD) polymer with fast evaporating solvents like ethylacetate, diethylether and chloroform was experimented, as well. The obtained fiber structures are shown in Figure 4.36. Electrospinning parameters for the production of nanofibers from fast evaporating solvent was operated as 40 kV voltage, 40 cm distance between the needle tip and the collector and 0.5 ml/h feed-rate.

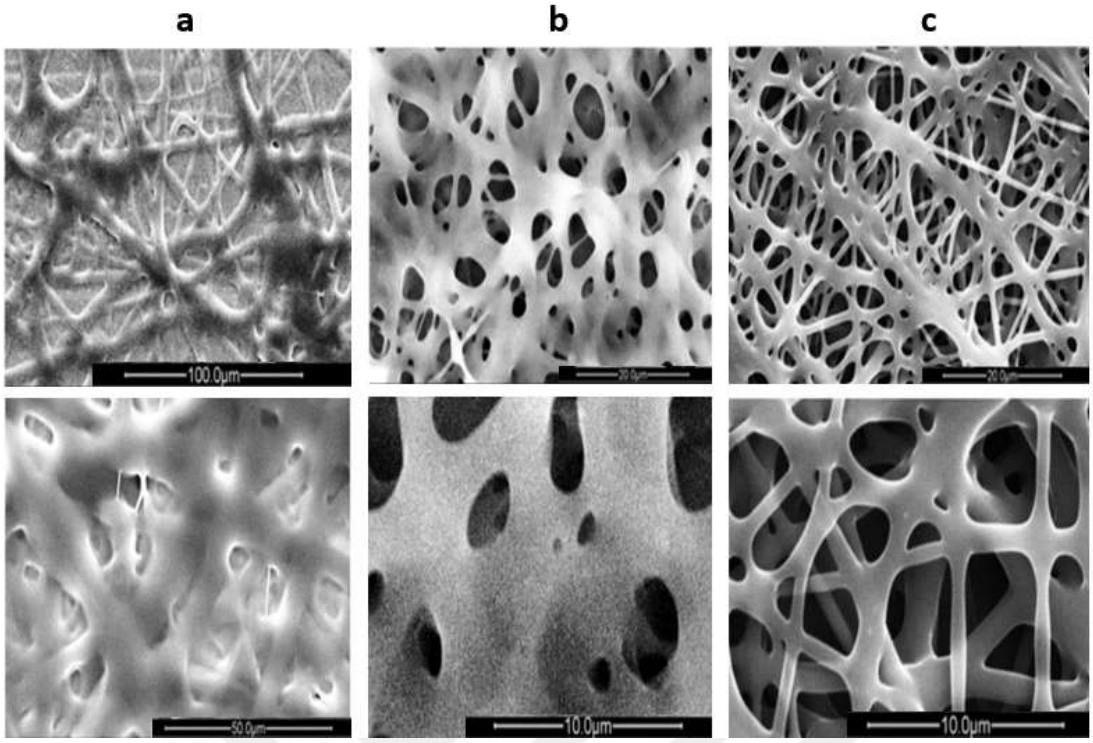

Figure 4.36 : SEM images of electrospun P (3HO-3HD) fibers from fast evaporating solvents a) ethylacetate; b) diethylether and c) chloroform.

When SEM images of the resultant P (3HO-3HD) fibers were evaluated from Figure 4.36, it was captured that the best surface morphology was achieved as a result of electrospinning with chloroform.

Since it was understood that chloforom was a common solvent for both P (3HB) and P (3HO-3HD) and resulted in desired fibrous structure, electrospinning of P (3HB) / P (3HO-3HD) blend was performed via chloroform:2-butanol (7:3 v:v) solvet system. P (3HB) / P (3HO-3HD) nanofibers were obtained electrospinning of 5 wt % of P (3HB)/P (3HO-3HD) (1/3, w/w) polymer solution, prepared in chloroform/2-butanol (7:3 v:v) by the application of 20 kV voltage, 15 cm distance of the needle tip-to-collector and 1 ml/h flow rate. During the preparation of electrospinning solution, 0.002 g/ml $LiBr_2$ was added to the solution in order to increase the conductivity of the solution. The average diameter of the neat P (3HB)/ P (3HO-3HD) nanofibers was 411±175 nm with bead-free and homogenous morphology (Figure 4.37) and they were further used for AgNPs immobilization.

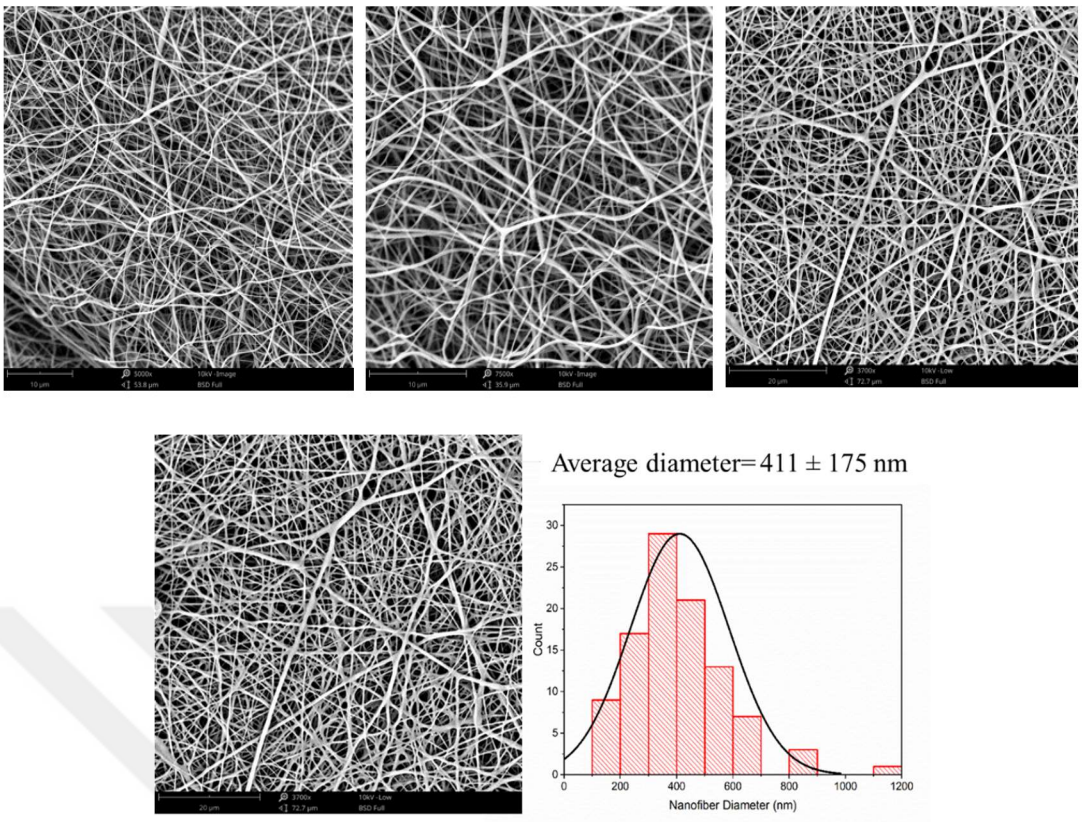

Figure 4.37 : SEM images and diameter distribution graph of P (3HB)/P (3HO-3HD) nanofibers.

As explained in the section 3.4.1.5 in detail, The P (3HB)/P (3HO-3HD) nanofibers were modified with silver nanoparticles (AgNPs) via dip-coating technique, in order to supply anti-microbial property to the nanofiber webs. Three different protocols were examined in order to achieve the best silver deposition. In the first trial, P (3HB)/P (3HO-3HD) nanofibers were dipped in a beaker containing the colloidal silver solution and taken out immediately, followed by washing with distilled water and drying. That protocol allowed the immobilization of the AgNPs, however the distribution of the nanopaticles were not homogenous and dense. The second protocol did not also contribute to achieve an intense and uniform dispersion of AgNPs over the P (3HB)/P (3HO-3HD) nanofibers. Moreover, the nanoparticles had the tendency to agglomerate due to the increased immersion time. Figure 4.38 demonstrates corresponding SEM images.

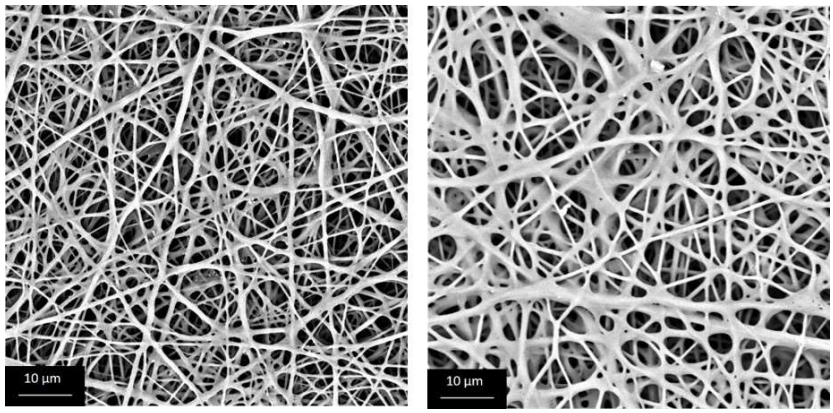

Figure 4.38 : SEM images of nanofibers obtained from a) protocol 1 and b) protocol 2.

The most homogenous and intense immobilization of the AgNPs was achieved by using the third protocol. Although some agglomerations were observed, homogenous dispersion of the silver nanoparticles over P (3HB)/P (3HO-3HD) nanofibers could be clearly seen in Figure 4.39.

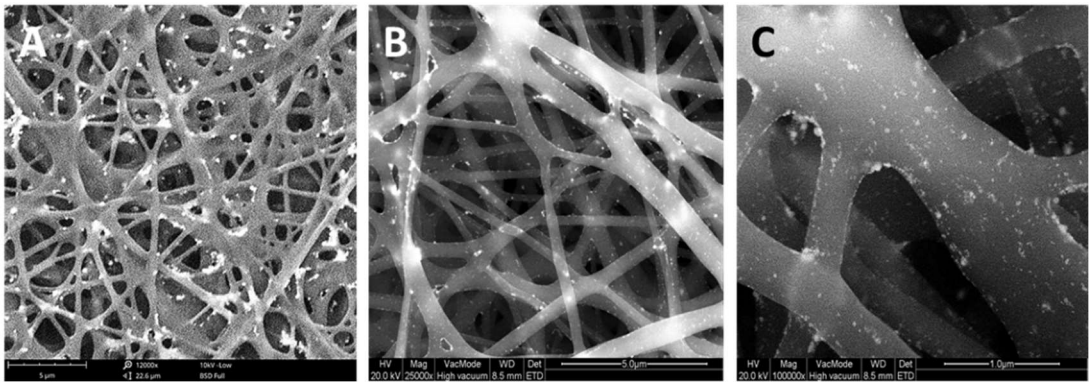

Figure 4.39 : SEM images of AgNP-containing P (3HB)/P (3HO-3HD) nanofibers obtained by protocol 3 with magnifications a) x12000 b) x25000 c) x100000.

Furthermore, the amount of the silver nanoparticles on the P (3HB)/P (3HO-3HD) nanofibers, obtained from third protocol, was determined by EDS characterization and expressed in terms of wt % and at % as 18.05 and 5.29, respectively.

4.3.3 FTIR-ATR Spectroscopy

FTIR-ATR spectroscopy characterization of neat and AgNPs containing P (3HB)/P nanofiber samples was carried out in the range of 400 cm^{-1} and 4000 cm^{-1} with the signal resolution of 4 cm^{-1}. FTIR-ATR spectrum of neat P (3HB)/P (3HO-3HD) nanofibers and AgNPS containing P (3HB)/P (3HO-3HD) nanofibers are presented in Figure 4.40.

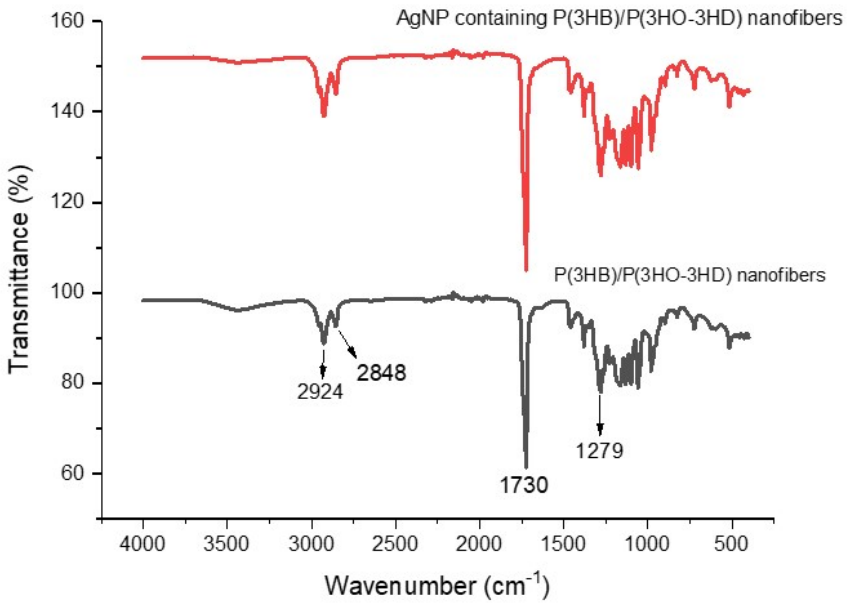

Figure 4.40 : FTIR-ATR spectrum of neat P (3HB)/P (3HO-3HD) nanofibers and AgNPS containing P (3HB)/P (3HO-3HD) nanofibers.

There was no considerable shift of the peaks in the presence of silver nanoparticles. The spectrum between 3600 cm^{-1} and 3250 cm^{-1} represented stretching band of amine groups. The peaks at 2924 cm^{-1} and 2848 cm^{-1} was attributed to asymmetric CH_3 and symmetric CH_2 vibrations, respectively. The peak at 1730 cm^{-1} was assigned to the ester carbonyl C=O stretching mode. In addition, the peak 1279 cm^{-1} occured as a result of CN stretching and NH bending. Moreover, as consistent with the literature, nearly the same spectrum was observed for AgNP containing P (3HB)/P (3HO-3HD) nanofibers [215–217].

4.3.4 UV-Visible spectroscopy

The AgNPs deposition on the P (3HB)/P (3HO-3HD) nanofibers was also characterized by UV-Vis spectroscopy in the range of 200-800 nm. Since nanofiber webs are not homogenous materials, Kubelka-Munk model was taken into account. Kubelka-Munk is a scattering coefficient that considers the geometric eccentricities in a single parameter. That coefficient is proportional to the concentration of the utilized media [218]. It is known from the literature that characteristic silver surface plasmon resonance band is attributed to the maximas between 400-420 nm, depending on the size of the particle, stabilizing molecules, and dielectric constant of the medium [109, 117, 216, 217]. While AgNP containing P (3HB)/ P (3HO-3HD) nanofibers showed a strong absorbance peak at 417 nm, neat P (3HB)/P (3HO-3HD) nanofibers did not

show any peaks between 250-600 nm which confirmed the deposition of AgNPs on the nanofibers (Figure 4.41). The peak at 221 nm was associated with the presence of ester group in the polymer structure [219].

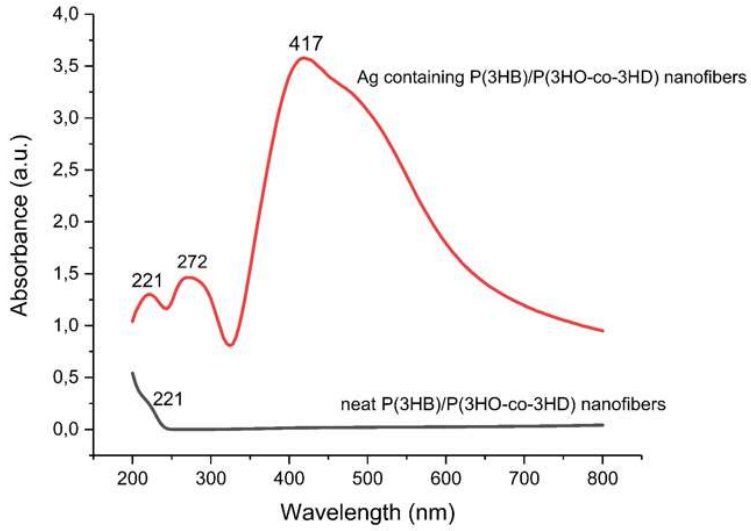

Figure 4.41 : UV-Visible spectroscopy of neat P (3HB)/P (3HO-3HD) nanofibers and AgNPs containing P (3HB)/P(3HO-3HD) nanofibers.

4.3.5 DSC

Thermal properties of the functionalized P (3HB)/P (3HO-3HD) nanofibers and the neat P (3HB)/P (3HO-3HD) nanofibers were studied by DSC by heating the nanofiber samples from 0°C and 400°C at a heating rate of 10°C/min in the presence of N_2 atmosphere. DSC thermograms of neat and functionalized P (3HB)/P (3HO-3HD) nanofibers are shown in Figure 4.42.

Figure 4.42 informed that both the neat and functionalized P(3HB)/P(3HO-3HD) nanofibers showed two melting endotherms, of which the second ones were sharp. It is known that PHB shows a single peak nearly at 170 °C [220], while comonomers of PHB such as P(HB-co-Hxx) where Hxx=2.5, 3,4 and 12 mol % resulted in double peaks [220, 221]. According to the Figure 4.42, it could be understood that two melting endotherms observed since P(3HB)/P(3HO-HD) nanofibers were composed of two seperate polymers (P(3HB) and P(3HO-3HD)). DSC thermograms of the neat P(3HB)/P(3HO-3HD) nanofibers had two-step melting behaviour at 162°C and 255°C, respectively. That two-step melting behaviour was not altered significantly for silver nanoparticle containing P(3HB)/P(3HO-3HD) nanofibers, which was consistent with the literature [219, 222–224]. The melting endotherms shifted slightly to higher temperatures (160°C and 276°C) in case of silver nanoparticle deposition onto

P(3HB)/P(3HO-3HD) nanofibers [222]. In the literature, the first melting peak was associated with defective crystals that could recrystallize by generating more perfect crystals which had a melting endotherm at higher temperatures [225]. However, based on the other author comments, double melting endotherms were corresponded to different crystalline phases which were HB-rich and HV-rich domains [226]. It could be concluded that functionalization of P(3HB)/P(3HO-HD) nanofibers with silver nanoparticles contributed to increase the melting temperatures slightly.

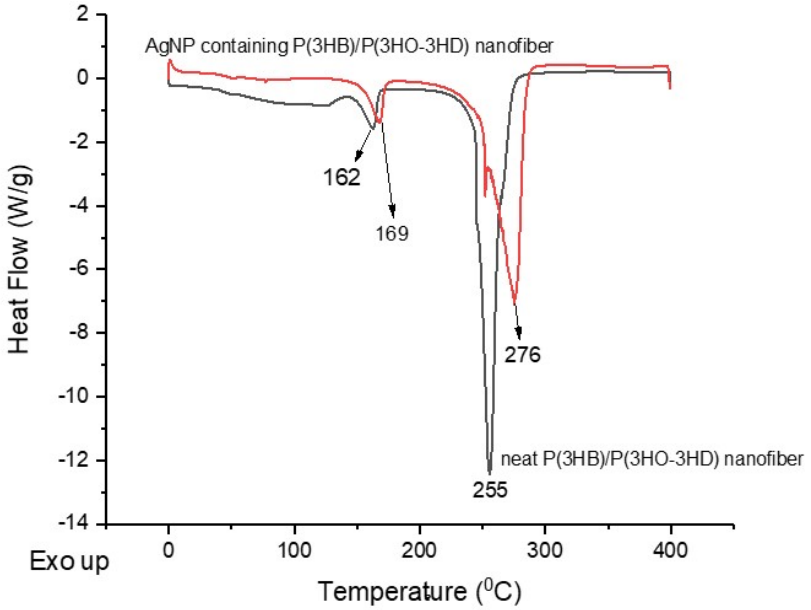

Figure 4.42 : DSC thermograms of AgNP-containing P(3HB)/P(3HO-3HD) and neat P(3HB)/P(3HO-3HD) nanofibers.

4.3.6 Biological evaluation of P (3HB)/P (3HO-3HD)/Ag nanofibers

The neat and AgNPs-containing P (3HB)/P (3HO-3HD) nanofibers were sterilized overnight in ethanol then rinsed three times with Phosphate-Buffered Saline (1x). Immortalized human keratinocyte HaCat cell line were cultured in Dulbecco's Modified Eagle Medium (DMEM) supplemented with 1% Penstrep, 1% glutamine and 10% fetal calf serum (Invitrogen, Carlsbad, CA) at 37°C in air and 5% CO_2. The cells were seeded in plates for 6 and 24 hours. After seeding, total RNA was isolated with TRizol and 1 µm of RNA was reverse-transcribed into complementary DNA (cDNA) using random hexamer primers, at 42 °C for 45 min, according to the manufacturer's instructions. Real time polymer chain reaction (PCR) was carried out with the LC Fast Start DNA Master SYBR Green kit by using cDNA, $MgCl_2$ antisense primers (Table 4.1). Real-time reverse transcriptase polymer chain reaction (qRT-PCR) was used to

evaluate the expression of interleukins IL-1α, IL-1β, IL-6 and IL-8, as well as TNF-α, TGF-β and HBD-2.

For Alamar Blue Assay, the HaCat cells, were used at 80% of confluence, incubated for 24 hours with the samples. At the end of this time, resazurine was added and incubated for 4 hours.

The absorbance (λ) of supernatants was recorded with a spectrophotometer (Victor 3; PerkinElmer, Waltham, MA, USA) using a double wavelength reading (570 nm and 600 nm). Lastly, $\%AB_{RED}$ was determined which considered the relation between the absorbance values and the molar extinction coefficients of the dye at the studied wavelengths, following the protocol provided by the manufacturer. The corresponding equation is shown in (5.1), in which: λ = absorbance, s = sample, and c = control:

$$\%AB_{red} = 100 \cdot \frac{\left(117{,}216 \cdot \lambda_{s(570\ nm)} - 80{,}586 \cdot \lambda_{s(600\ nm)}\right)}{\left(155{,}677 \cdot \lambda_{c(600\ nm)} - 14{,}652 \cdot \lambda_{c(570\ nm)}\right)} \quad (5.1)$$

The results obtained were expressed as percentage of dye resuction ($\%AB_{RED}$), which was related to metabolically active cells.

Alamar Blue test results showed that both the neat and the AgNPs-containing P(3HB)/P(3HO-HD) nanofibers did not show significant cytotoxic activity by indicating percentages of dye reduction of 100% and 105%, respectively.

Keratinocytes, which completely cover the outmost layer of human body, led the immune response and inflammation in the skin by the production of pro-inflammatory, anti-inflammatory and antimicrobial molecules in response to injury and external excitement. The complexity of immune reactions occurs via the production of both pro- and anti-inflammatory cytokines and antibacterial molecules with different time scale.

The obtained immunomodulatory property results showed that, while the neat P (3HB)/P (3HO-3HD) nanofibers that did not show any difference in the basal production of these molecules by HaCaT cells in culture, P (3HB)/P (3HO-3HD)/Ag nanofibers were able to upregulate the most important proinflammatory cytokines after 6 h, namely, IL-1 (α and β), IL-6 and IL-8, in order to trigger the healing process.

Table 4.1 : Real-time reverse transcriptase polymer chain reaction (RT-PCR) details, including gene, primer sequences, operational conditions, and product size.

Molecule	Primer Sequence (forward/reverse)	Conditions	Size (bp)
IL-1 α	5′CATGTCAAATTTCACTGCTTCATCC-3′5′-GTCTCTGAATCAGAAATCCTTCTATC-3′	5 s at 95 °C, 8 s at 55 °C, 17 s at 72 °C for 45 cycles	421
IL-1 β	5′-GCATCCAGCTACGAATCTCC-3′ 5′-CCACATTCAGCACAGGACTC-3′	5 s at 95 °C, 14 s at 58 °C, 28 s at 72 °C for 40 cycles	708
IL-6	5′-ATGAACTCCTTCTCCACAAGCGC-3′5′-GAAGAGCCCTCAGGCTGGACTG-3′	5 s at 95 °C, 13 s at 56 °C, 25′ s at 72 °C for 40 cycles	628
IL-8	5-ATGACTTCCAAGCTGGCCGTG-3′ 5TGAATTCTCAGCCCTCTTCAAAAACTTCTC-3′	5 s at 94 °C, 6 s at 55 °C, 12 s at 72 °C for 40 cycles	297
TNF-α	5′-CAGAGGGAAGAGTTCCCCAG-3′ 5′-CCTTGGTCTGGTAGGAGACG-3′	5 s at 95 °C, 6 s at 57 °C, 13 s at 72 °C for 40 cycles	324
TGF-β	5′CCGACTACTACGCCAAGGAGGTCAC-3′5′-AGGCCGGTTCATGCCATGAATGGTG-3′	5 s at 94 °C, 9 s at 60 °C, 18 s at 72 °C for 40 cycles	439
HBD-2	5′GGATCCATGGGTATAGGCGATCCTGTTA-3′5′-AAGCTTCTCTGATGAGGGAGCCCTTTCT-3′	5 s at 94 °C, 6 s at 63 °C, 10 s at 72 °C for 50 cycles	198

The immunomodulatory properties of the studied cytokines, namely IL-1(α and β), IL-6 and IL-8, are shown in Figure 4.43, Figure 4.44, Figure 4.45 and Figure 4.46, respectively.

Data are reported as mean ± SD and are expressed as percentage of increment relative to untreated HaCaT cells. Later on, 24 h after being in contact with the cells, all the abovementioned ILs were reduced.

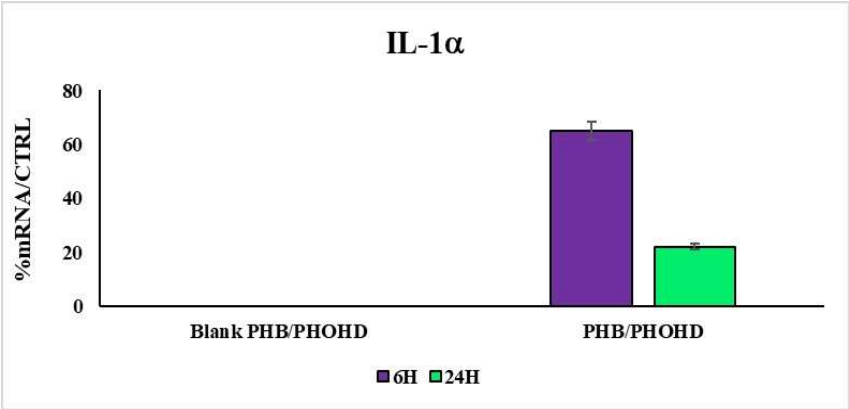

Figure 4.43 : Relative gene expression of IL-1α.

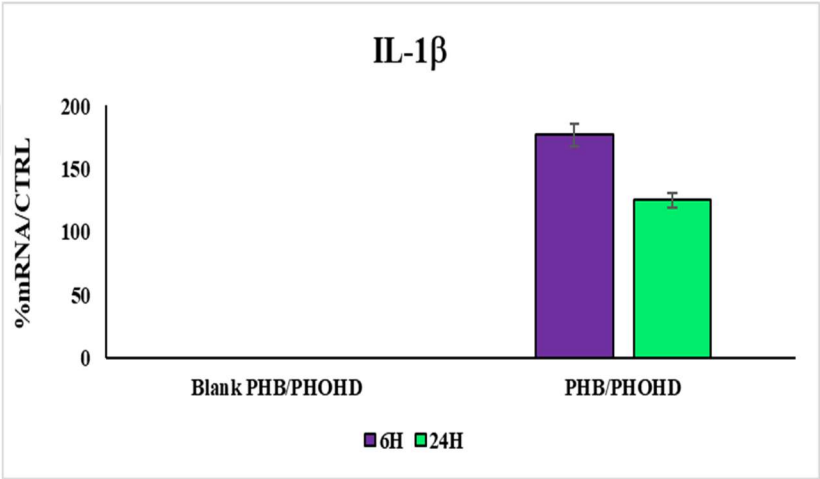

Figure 4.44 : Relative gene expression of IL-1β.

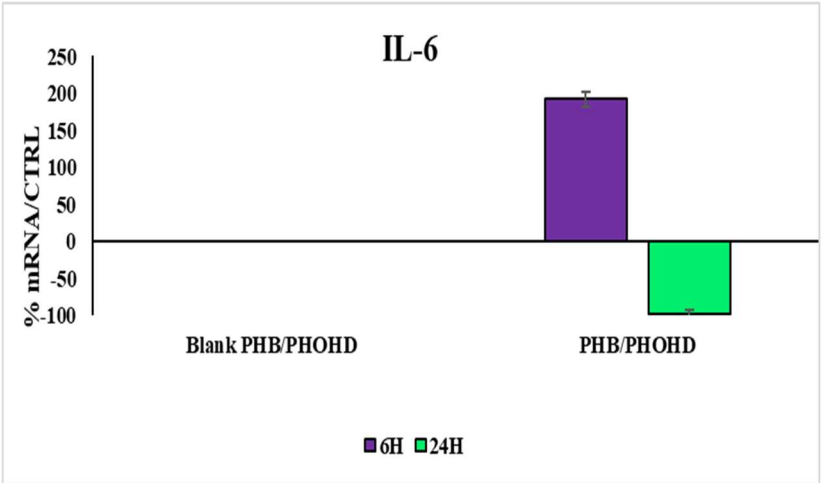

Figure 4.45 : Relative gene expression of IL-6.

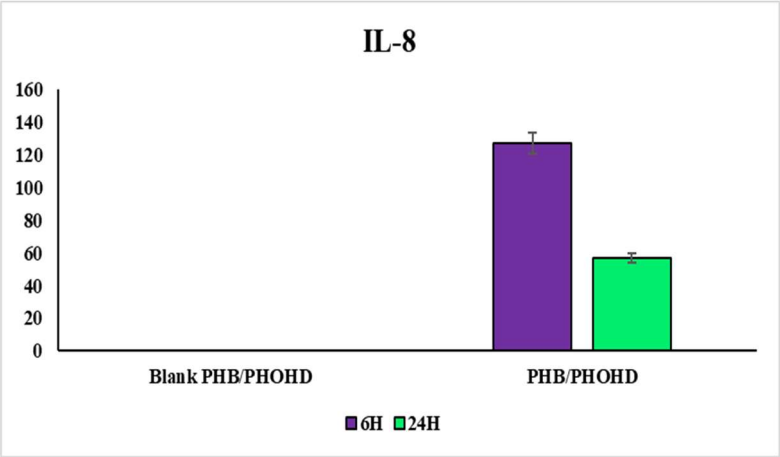

Figure 4.46 : Relative gene expression of IL-8.

Differently, TNF-α (Figure 4.47) showed up only at 24 h. TNF-α is an essential mediator in inflammation by recruiting inflammatory cells [227]. TNF-α also acts on platelet adhesiveness, favoring the formation of thrombus to reduce bacterial invasion and infection processes.

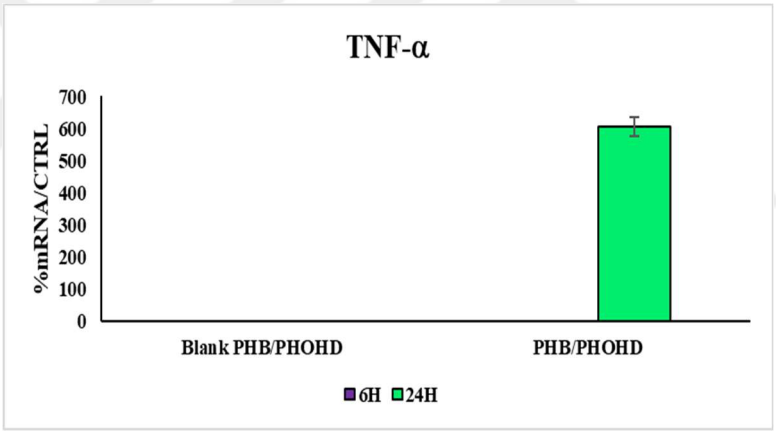

Figure 4.47 : Relative gene expression of TNF-α.

Most importantly, the AgNPs-containing P (3HB)/P (3HO-3HD) nanofibers were able to induce the mRNA production of HBD-2 (Figure 4.48), thus stimulating the innate defense capability of skin from harmful entities, which affect the wound repair processes. Such an indirect antimicrobial activity is desirable as the need for antibiotic drug is reduced.

The TGF-β (Figure 4.49) expression was very slightly downregulated.

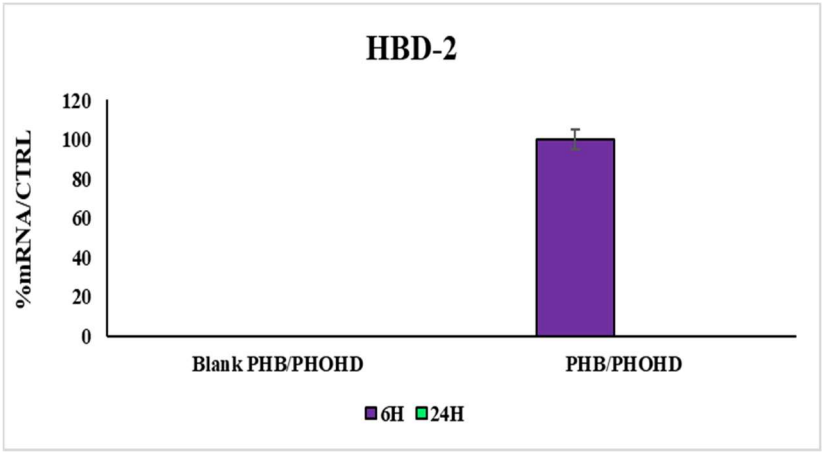

Figure 4.48 : Relative gene expression of HBD-2.

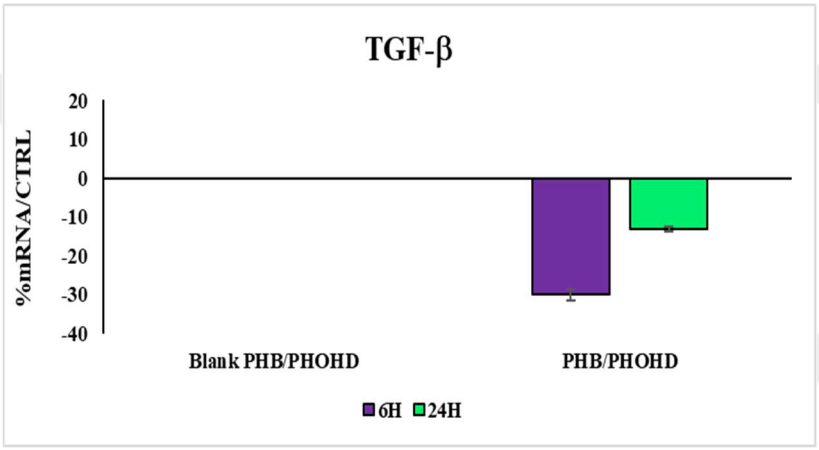

Figure 4.49 : Relative gene expression of TGF-β.

4.4 Results of P (AN-co-IA)/Ag Nanofibers

4.4.1 UV-Visible spectroscopy

UV-visible spectroscopy characterization was performed using PAN and P(AN-co-IA) nanofibers prepared with and without $AgNO_3$. Reduction of $AgNO_3$ to AgNPs could be observed from UV-Vis. characterization as well as visual observation of color change of the solutions [117].

Reduction of Ag^+ ions to AgNPs occur in several steps such as primary nucleation, secondary nucleation, crystal growth, and agglomeration of some adjacent particles into aggregated clusters [228]. Reduction of Ag^+ ions to AgNPs in the presence of DMF starts with the oxidation reaction of DMF at room temperature according to following mechanism:

$$HCONMe_2+2Ag^+ + H_2O \longrightarrow 2Ag^0 + Me_2NCOOH + 2H^+$$ [228, 229]

As the reaction continues, the color of the solutions changes from transparent to light yellow, dark yellow, brown, and finally black. Therefore, without any spectroscopic characterization, color change of the solution can be regarded as visual confirmation of Ag nanoparticles formation [28–30].

In the experiments, color change of the solutions for both $AgNO_3$ containing PAN and P(AN-co-IA) solutions was clearly observed. The color of the $AgNO_3$ containing PAN solutions changed from transparent to light yellow after five days of stirring and became dark yellow after 10 days of stirring.

Figure 4.50 depicts the color of PAN/Ag solutions after 10 days of stirring. However, the color of the $AgNO_3$ containing P(AN-co-IA) solutions became light brown, brown, and dark brown just after half an hour, 2 hours, and five days of stirring, respectively, as shown in Figure 4.51.

Figure 4.50 : PAN/Ag polymer solutions prepared from 10 wt % $AgNO_3$ (left) and 20 wt % $AgNO_3$ (right) after stirring of 10 days.

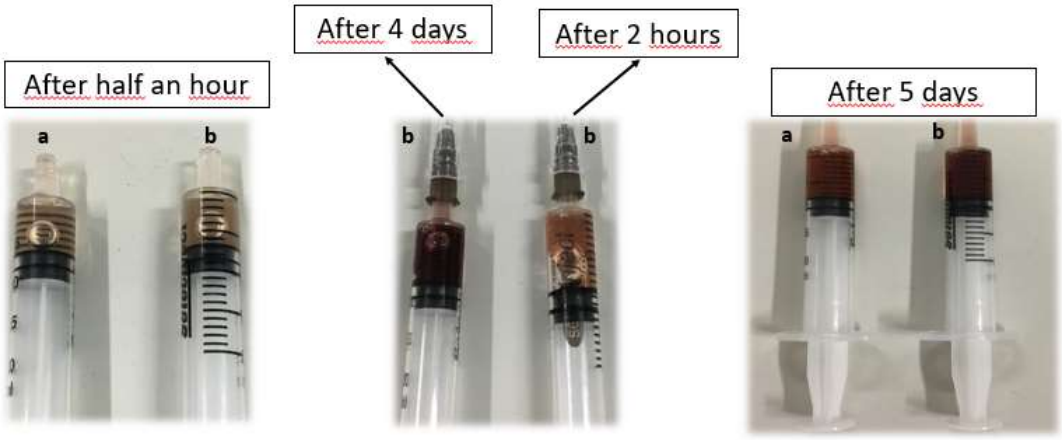

Figure 4.51 : P(AN-co-IA)/Ag polymer solutions prepared from a) 10 wt % $AgNO_3$ and b) 20 wt % $AgNO_3$.

UV-Vis. spectrum of PAN and PAN/Ag nanofibers were investigated in the range of 200-1100 nm and was shown in Figure 4.52.

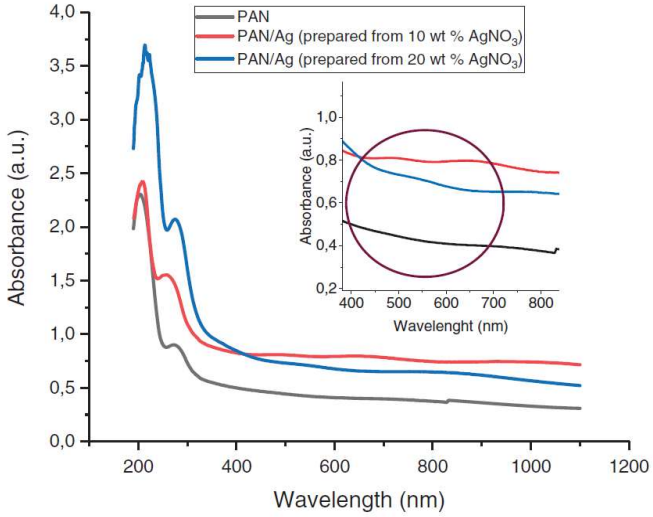

Figure 4.52 : UV-Vis. spectrums of PAN/Ag nanofibers.

It is known that existence of silver nanoparticles in the samples could be verified by the examination of absorbance band between 300-600 nm [109, 114, 117, 229]. However, the exact position of the absorption maxima depends on the used concentrations of $AgNO_3$, the amount of deposited metal, the form of the sample and the size of the nanoparticles [117, 229]. If silver nanoparticles have diameters smaller than 5 nm, they show a high absorbance band with a peak nearly at 400 nm. If they have diameters of ~10 nm, they exhibit absorption band between 410-450 nm. Moreover, when the absorption band shifts to higher wavelengths, it means that the produced silver nanoparticles have diameters bigger than 10 nm [109]. In Figure 4.51, it can be clearly seen that Ag containing PAN nanofibers showed an absorbance band between 400-500 nm without a sharp peak while no absorbance was seen for pure PAN nanofibers in that range. With the light of these informations, it can be interpreted that the produced PAN/Ag nanofibers contain Ag nanoparticles with coarser diameters than 10 nm.

UV-Vis. spectrum of P(AN-co-IA) and P(AN-co-IA)/Ag nanofibers were also examined between 200-1100 nm and was demonstrated in Figure 4.53. For the verification of Ag nanoparticle formation, 300-600 nm wavelength was examined deeply.

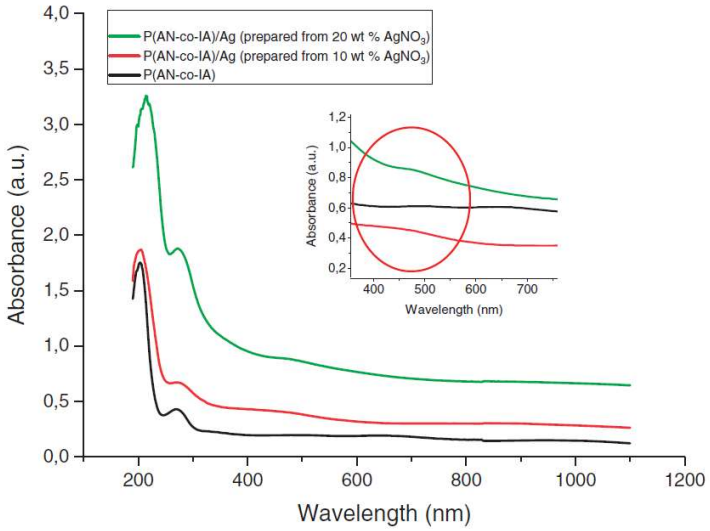

Figure 4.53 : UV-Vis. spectrums of P(AN-co-IA)/Ag nanofibers.

It was seen from Figure 4.53, while pure P (AN-co-IA) nanofibers did not show any peak in that range, Ag containing P (AN-co-IA) nanofibers reflected absorbance between 400-500 nm with maximas approximately at 450 and 470 nm for the samples prepared from 10 wt % and 20 wt % $AgNO_3$, respectively. Sichani et al also mentioned that both dielectric constant and range of the nanoparticles affect the absorption maximum of UV-Vis. spectra [117]. Since UV-Vis. spectrum give preliminary information about the size and distribution of the produced silver particles, according to literature [109, 117] it can be said that the produced nanoparticles in this study both have higher diameters than 10 nm and size distribution. In addition, increase in the intensity was related to the increase in the amount of reduced silver [117]. From Figure 4.53, it can be monitored that P (AN-co-IA)/Ag nanofibers prepared from 20 wt % $AgNO_3$ had higher intensity than the P (AN-co-IA)/Ag nanofibers prepared from 10 wt % $AgNO_3$, thus P (AN-co-IA)/Ag nanofibers prepared from 20 wt % $AgNO_3$ have higher amounts of reduced silver than the other sample. Moreover, the intensies of P (AN-co-IA)/Ag nanofibers were higher than the intensities of PAN/Ag nanofibers (Figure 4.52) which was also a proof that P (AN-co-IA) reduced more amount of $AgNO_3$ to Ag nanoparticles than PAN.

4.4.2 FTIR-ATR spectroscopy

In order to examine the effect of existence of Ag nanoparticles in both PAN and P(AN-co-IA) nanofibers, FTIR-ATR spectroscopy was carried out in the range of 400 cm^{-1}

and 4000 cm^{-1} with the signal resolution of 4 cm^{-1} and FTIR-ATR spectrums are demonstrated in Figure 4.54 and Figure 4.55, respectively.

The positions of all peaks of for PAN and PAN/Ag nanofibers were almost the same as seen in Figure 4.54. Presence of Ag nanoparticles in the samples did not make any considerable shift in the C≡N triple bond (at 2244 cm^{-1}) [117, 230]. However, the intensity of the peaks of PAN/Ag nanofibers decreased compared to PAN nanofibers and even according to the increase in $AgNO_3$ amount from 10 wt % to 20 wt %. Thus, it can be said that nitrile groups in PAN chains polymerized by the existence of Ag^+ ions [117]. The only shift was seen at 1303 cm^{-1} that the sharp peak disappeared and just turn to be a shoulder with the presence of Ag nanoparticles. In addition, the peak at 1453 cm^{-1} corresponded to bending vibration of –CH [202].

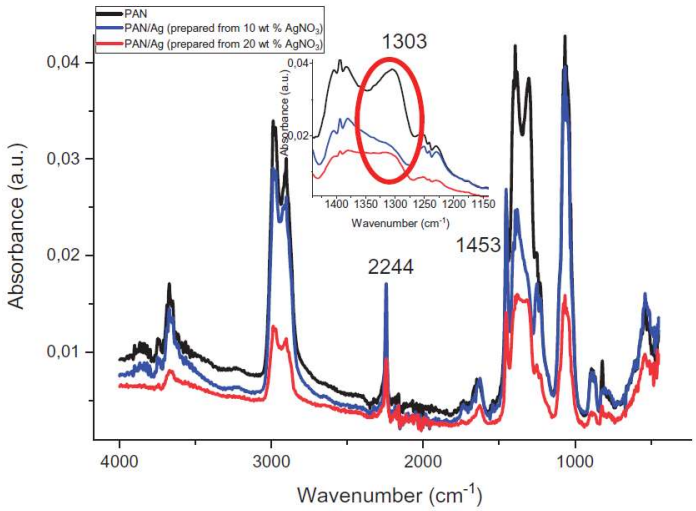

Figure 4.54 : FTIR-ATR spectrums of PAN and PAN/Ag nanofibers.

FTIR-ATR spectrums of P (AN-co-IA) and P (AN-co-IA)/Ag nanofibers (shown in Figure 4.54) also mentioned that the positions of the peaks were nearly the same for P (AN-co-IA)/Ag nanofibers. The peak at 2244 cm^{-1} was related to the C≡N triple bond and there was no noticeable shift on the position of it with the presence of silver nanoparticles. However, the intensity of this peak increased due to presence of silver nanoparticles but decreased with the increase in as the amount of used silver salt (from 10 wt % to 20 wt %) as in case of PAN and PAN/Ag nanofibers [117]. New peaks occured at 3657 cm^{-1} and 1663 cm^{-1} and a shift from 1731 cm^{-1} to 1721 cm^{-1} was seen for silver containing P (AN-co-IA) nanofibers which could be taken as a proof for the ionization of carboxyl groups and interaction of Ag^+ ions between P (AN-co-IA) copolymer [230–232]. The interaction of Ag^+ ion with P (AN-co-IA) was also shown

in Figure 4.56. Related to the interaction of Ag^+ ion with P (AN-co-IA), a new shoulder at 1314 cm^{-1} occured and the peak at 1235 cm^{-1} shifted to 1237 cm^{-1} by giving three broad peaks.

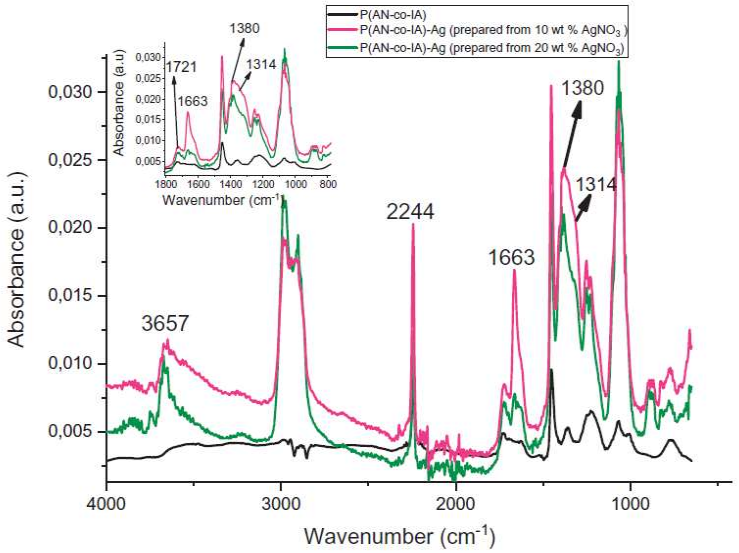

Figure 4.55 : FTIR-ATR spectrums of P (AN-co-IA)/Ag nanofibers.

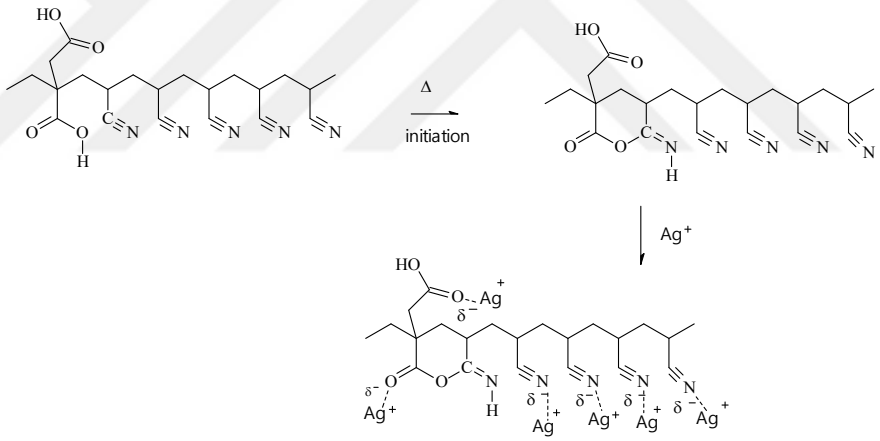

Figure 4.56 : Interaction of silver ion with P (AN-co-IA).

4.4.3 Morphology of PAN/Ag and P (AN-co-IA)/Ag nanofibers (SEM-EDS)

To observe the surface morphology of the produced nanofibers, SEM analysis was performed. Average diameter of the nanofibers was also determined using a special program, Image J. Figure 4.57 [202] shows SEM images of PAN and P(AN-co-IA) nanofibers along with their diameter distribution graphics. Figure 4.57 [202] showed that PAN and P(AN-co-IA) nanofibers were continuous, smooth, and fine with the average diameters of 120 and 132 nm, respectively.

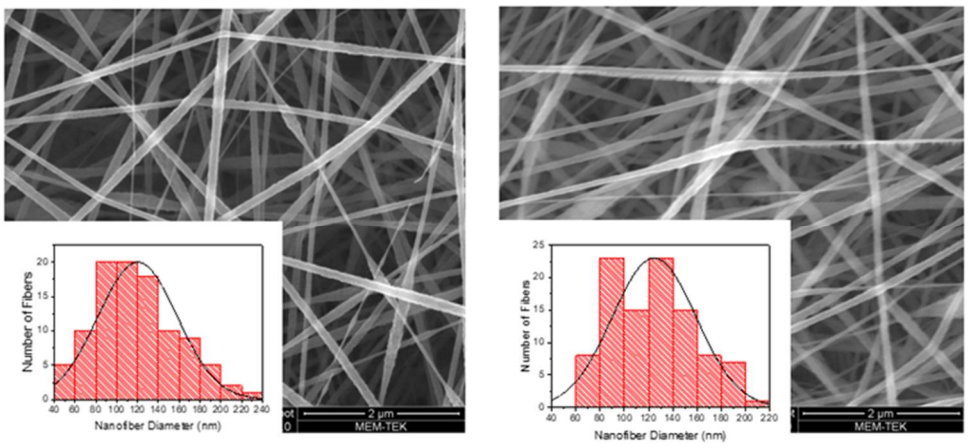

Figure 4.57 : SEM images of PAN (left) and P(AN-co-IA) (right) nanofibers [202].

Figure 4.58 is related to the SEM images of PAN/Ag and P(AN-co-IA)/Ag nanofibers, prepared by using 10 wt % AgNO3, with different magnification ratios and Figure 4.59 shows SEM images of PAN/Ag and P(AN-co-IA)/Ag nanofibers, prepared by using 20 wt % AgNO3, with different magnification ratios. Also, the nanofiber diameter distribution graphics were added onto the SEM images.

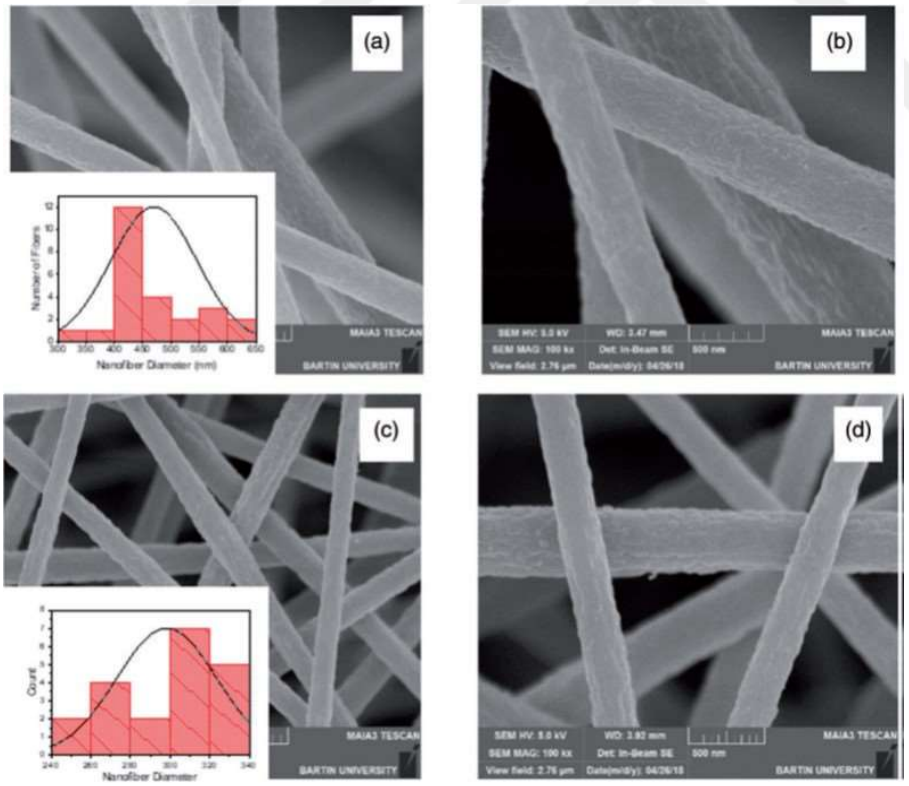

Figure 4.58 : SEM images of a and b: PAN/Ag nanofibers (prepared from 10 wt % $AgNO_3$) with 50 kx and 100 kx magnification ratios, respectively; c and d: P(AN-co-IA)/Ag nanofibers (prepared from 10 wt % $AgNO_3$) with 50 kx and 100 kx magnification ratios, respectively.

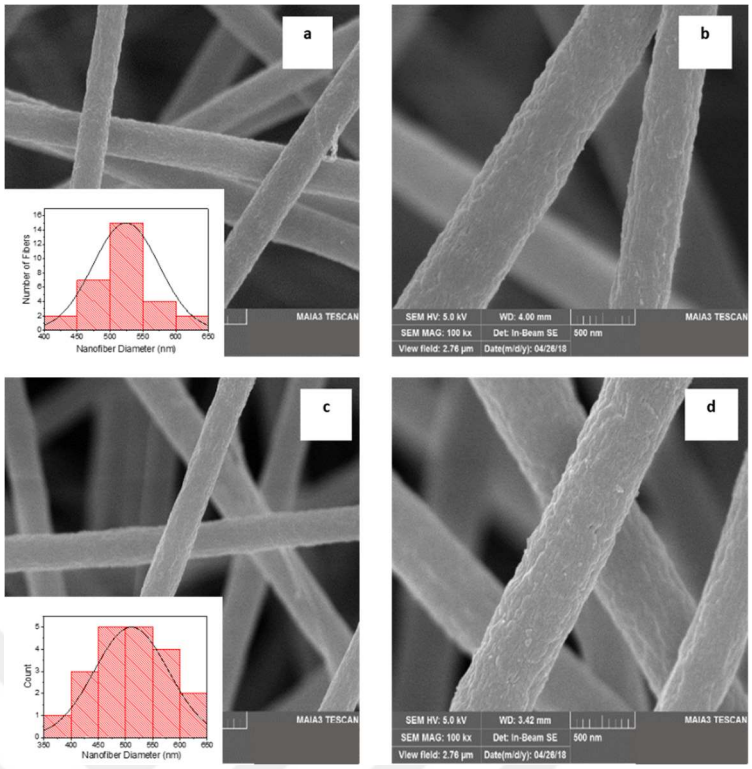

Figure 4.59 : SEM images of a and b: PAN/Ag nanofibers (prepared from 20 wt % $AgNO_3$) with 50 kx and 100 kx magnification ratios, respectively; c and d: P(AN-co-IA)/Ag nanofibers (prepared from 20 wt % $AgNO_3$) with 50 kx and 100 kx magnification ratios, respectively.

It can be accurately observed from Figure 4.58 and Figure 4.59 that AgNPs containing nanofibers were continuous and had rougher surface compared to pure PAN and P(AN-co-IA) nanofibers. No beads were seen related to the electrospinning parameters and especially due to the strong elongation forces applied on the jet during electrospinning [117]. Rough surface morhology of nanofibers which include AgNPs was also observed in the studies conducted by Chaudhary et al. [104] and Ucar et al. [233].

The diameters of the obtained nanofibers increased with AgNP inclusion from 120 nm to ~520 nm for PAN nanofibers and from 132 nm to ~510 nm for P(AN-co-IA) nanofibers. Nanofiber diameters of the produced samples can be seen in Table 4.2 in detail.

According to the reduction method, stabilizer and initial concentration of $AgNO_3$, nanofiber diameters can increase in the presence of silver nanoparticles [233].

From Table 4.2, it can be evaluated that increasing the amount of $AgNO_3$ caused to produce coarser nanofibers. This could be due to silver salt, changing in conductivity cause to fiber diameter increase.

Table 4.2: Nanofiber samples and their average nanofiber diameters (nm).

Nanofiber Samples	**Average Nanofiber Diameter (nm)**
PAN	120 ± 38
P(AN-co-IA)	132 ± 36
PAN/Ag (prepared from 10 wt % $AgNO_3$)	469 ± 75
P(AN-co-IA)/Ag (prepared from 10 wt % $AgNO_3$)	300 ± 25
PAN/Ag (prepared from 20 wt % $AgNO_3$)	520 ± 50
P(AN-co-IA)/Ag (prepared from 20 wt % $AgNO_3$)	510 ± 65

When the salt is added to solution the diameter decrease but if the additive amount increased the fiber diameter tends to increased too. In addition, either the amount of deposited silver nanoparticles on the surface [6] or agglomeration of silver nanoparticles occured in the syringe tip during electrospinning might be another reason for that increase [104]. Similarly, Chaudhary et al. observed that in case of silver nanoparticles existence in PAN nanofibers, surface morpholoy of the nanofibers changed from smooth to rough and nanofibers had diameters between 600-900 nm [104]. In addition, Huang et al. produced PAN/Ag nanofibers in the range of 500-800 nm [116].

Table 4.2 also informed that in the presence of silver nanoparticles, P(AN-co-IA) matrix allowed to obtain finer nanofibers than PAN matrix, which might depend on the increased charge density during electrospinning process [234].

Presence of silver nanoparticles and atomic % of them was observed by using EDS analysis. Table 4.3 demonstrates the atomic % of Ag nanoparticles present in the samples. As expected, neat PAN and P(AN-co-IA) nanofibers did not contain any silver nanoparticles but the other samples contained silver nanoparticles. Final atomic % of silver nanoparticles in the samples had a direct relation with the amount of $AgNO_3$. Furthermore, for the same amount of $AgNO_3$, it was observed that P(AN-co-IA) nanofibers had much more AgNPs than PAN, which can be taken as an evidence for the enhanced reduction of $AgNO_3$ to AgNPs by P(AN-co-IA) polymer.

Table 4.3 : EDS analysis results of atomic % of Ag nanoparticles present in the produced samples.

Nanofiber Samples	Ag (Atomic %)
PAN	0
P(AN-co-IA)	0
PAN/Ag (prepared from 10 wt % $AgNO_3$)	0.1
PAN/Ag (prepared from 20 wt % $AgNO_3$)	0.3
P(AN-co-IA)/Ag (prepared from 10 wt % $AgNO_3$)	1.1
P(AN-co-IA)/Ag (prepared from 20 wt % $AgNO_3$)	2.9

4.4.4 AFM

Surface morphology of both produced nanoparticles and nanofibers of PAN, P (AN-co-IA), PAN/Ag and P (AN-co-IA)/Ag was also analyzed by using AFM which uses a tip to evaluate the surface features by scanning the sample.

For nanoparticle observation, thin films were prepared via spin-coating process by using prepared electrospinning solutions of PAN, P (AN-co-IA), PAN/Ag and P (AN-co-IA)/Ag compositions. Figure 4.60 displays AFM images of PAN nanoparticles with different magnification ratios.

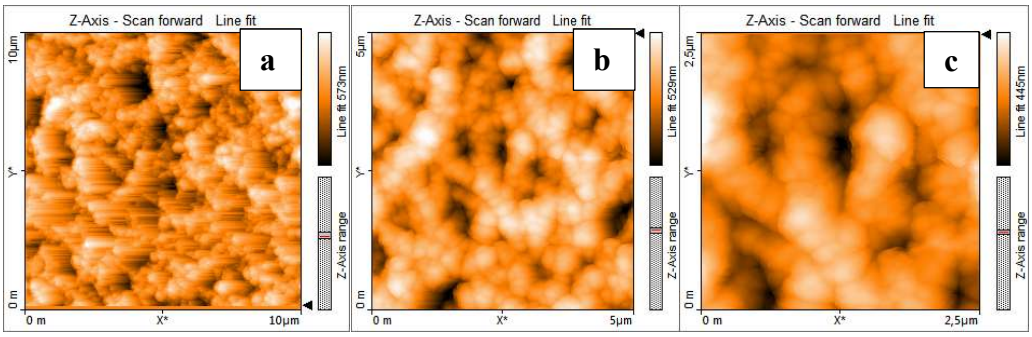

Figure 4.60 : AFM images of PAN nanoparticles with magnification ratios of a:10 µm, b:5 µm and c: 2,5 µm.

Although some agglomerates were seen in the images, it can be said that produced PAN nanoparticles were almost distributed homogeneously. Moreover, surface roughness values of PAN nanoparticles varied as 72 nm, 61 nm and 55 nm related to the magnification ratios of 10 µm, 5 µm and 2.5 µm, respectively.

Figure 4.61 shows AFM images of P (AN-co-IA) [202] and P(AN-co-IA)/Ag nanoparticles with different magnification ratios.

Similar to AFM images of PAN nanoparticles, it can be said that nanoparticle distribution of P (AN-co-IA) and P (AN-co-IA)/Ag samples were homogeneous even though presence of some agglomerates. Surface roughness values of the nanoparticles were calculated as 16 nm, 111 nm and 86 nm for P (AN-co-IA), P (AN-co-IA)/Ag (magnification ratio of 10 µm) and P (AN-co-IA)/Ag (magnification ratio of 5µm), respectively. It can be accurately declared that AgNPs containing P (AN-co-IA) samples had rougher surfaces than the pure P (AN-co-IA) sample.

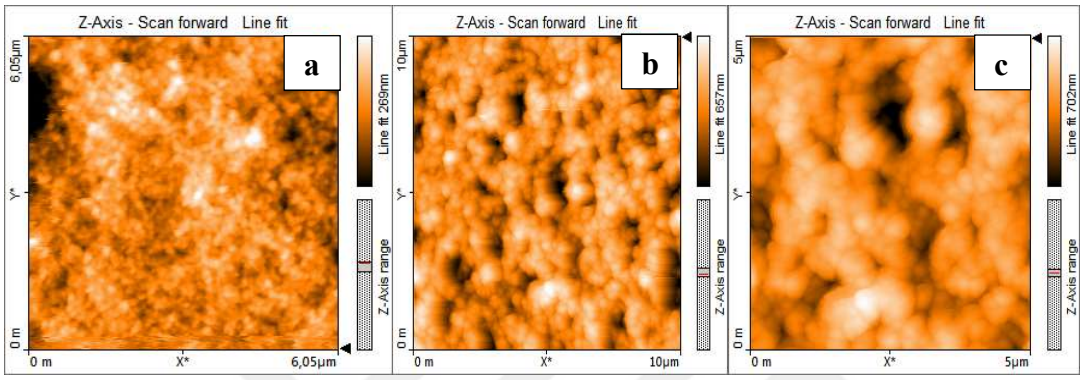

Figure 4.61 : AFM images of a: P(AN-co-IA) nanoparticles [202], b: P(AN-co-IA)/Ag nanoparticles with 10 µm magnification ratio and c: P(AN-co-IA)/Ag nanoparticles with 5 µm magnification ratio.

Furthermore, AFM image of P(AN-co-IA)/Ag nanofibers was demonstrated in Figure 4.62.

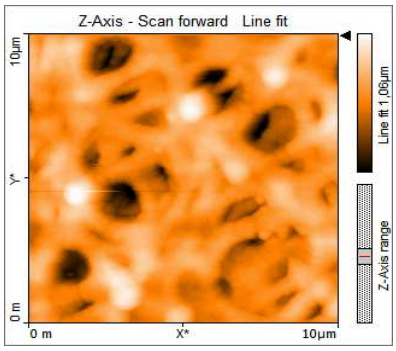

Figure 4.62 : AFM image of P (AN-co-IA)/Ag nanofibers.

Deposition of AgNPs over the surface of nanofibers could be observed from Figure 4.62 and it was clear that brighter regions existing in nanofiber mats were related to the silver nanoparticles. Surface roughness value of P(AN-co-IA)/Ag nanofibers was measured as 129 nm which was higher than the surface roughness values of both PAN and P(AN-co-IA)/Ag nanoparticles. That might be mainly because of the either deep inclusion of Ag nanoparticles in the polymer chain during the reduction process or deposition of the produced nanoparticles over the nanofiber surface [104].

4.4.5 Electrical conductivity

Electrical conductivity of the produced nanofiber samples was measured by four-point probe. Four-point probe method has four tips as shown in Figure 4.63.

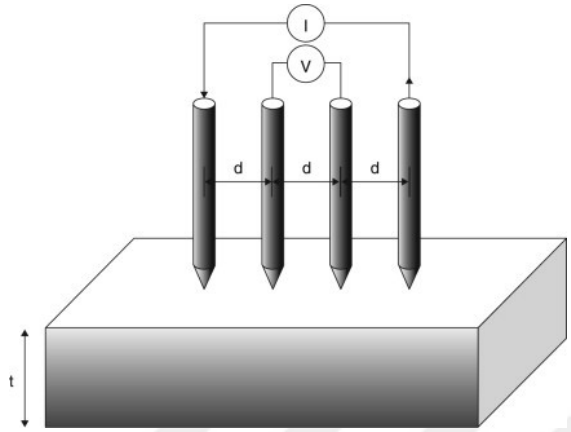

Figure 4.63 : Representative image of four-point probe system (URL-1) [235].

The outer tips touch the sample surface and a voltage is applied which results in a current through the sample. No current flows through the inner part of contacts, that means no voltage drops at the probe contacts form [236].

The electrical conductivity (σ) is calculated by using the equation as follows:

$$\sigma\ (S/cm)=(1/(R\ (\Omega))).((L(cm))/(T(cm).W(cm))) \quad (4.2)$$ [237].

where R is electrical resistance, L is distance between two electrodes, T is thickness of the sample and W is width of the sample [237].

Electrical conductivity results of the produced nanofiber samples are explained in Table 4.4.

It is well-known from the literature that neat PAN has 10^{-12} S/cm electrical conductivity and when the value reaches to 10^{-7} S/cm, it becomes a semi-conductive material [238]. It is also possible to increase the electrical conductivity of PAN by incorporation of metal nanoparticles like silver into the structure [233]. Table 4.4 shows that while neat PAN nanofibers were really insulators with 3.24 E^{-13} S/cm electrical conductivity value, presence of AgNPs made them to become conductive materials and gain ~ 2.70 E^{-5} S/cm electrical conductivity. P (AN-co-IA) nanofibers also showed nearly the same behaviour. Existence of AgNPs in P(AN-co-IA) nanofibers considerably contributed to the electrical conductivity values. They were increased from 2.64 E^{-12} to ~2.80 E^{-4}. In addition, a slight increase was seen in the

conductivity values related to the used $AgNO_3$ amount. It was mentioned that using even a small silver salt amount [117] and changing the initial concentration of $AgNO_3$ [228] can influence the electrical conductivity dramatically.

Table 4.4 : Electrical conductivity values (S/cm) of the obtained nanofiber samples.

Nanofiber Samples	Conductivity (S/cm)
PAN	$3.24\ E^{-13}$
P(AN-co-IA)	$2.64\ E^{-12}$
PAN/Ag (prepared from 10 wt % $AgNO_3$)	$2.60\ E^{-5}$
PAN/Ag (prepared from 20 wt % $AgNO_3$)	$2.71\ E^{-5}$
P(AN-co-IA)/Ag (prepared from 10 wt % $AgNO_3$)	$2.63\ E^{-4}$
P"(AN-co-IA)/Ag (prepared from 20 wt % $AgNO_3$)	$2.80\ E^{-4}$

The relation between electrical conductivities and atomic % Ag values of the obtained nanofibers was revealed in Figure 4.64.

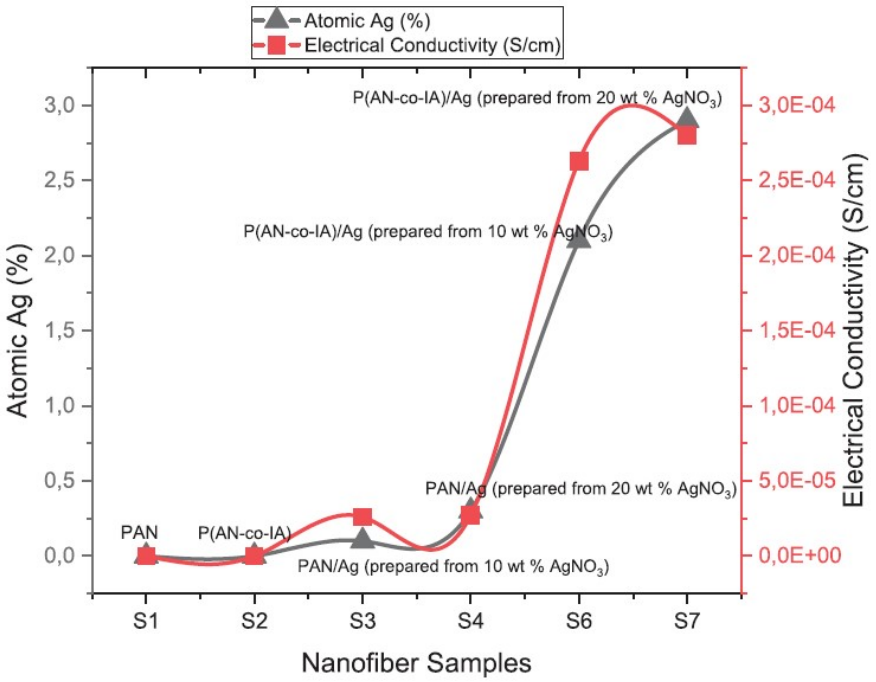

Figure 4.64 : Relation between electrical conductivities and atomic % Ag values of the obtained nanofibers.

Figure 4.64 informed that electrical conductivity of the produced nanofibers was directly affected by atomic % of silver nanoparticles present in the samples. Thus, in order to increase the electrical conductivity, the amount of the reduced silver

nanoparticles should be increased and initial concentration of silver salt should be optimized.

4.4.6 DSC

DSC was applied in order to examine the thermal behaviour of the produced nanofiber samples. DSC thermograms of PAN, PAN/Ag (prepared from 20 wt % $AgNO_3$) and P (AN-co-IA)/Ag (prepared from 20 wt % $AgNO_3$) nanofibers are shown in Figure 4.65.

During the transformation of C≡N groups into C=C and C=N groups, some chemical reactions which are cyclization, dehydrogenation and oxidation occur. These chemical reactions allow PAN fibers to have ladder-like molecular structure and become heat-resistant [233].

Cyclization reactions of PAN takes place through a free radical mechanism and can only be initated at high temperatures. PAN displays an exothermic peak with a maxima nearly at 300°C and this maxima is defined as Tc. However, it is possible to decrease this cyclization temperature up to 250 °C by the incorporation of itaconic acid monomer into PAN structure [29, 30].

Figure 4.65 informed that while cyclization temperature of PAN nanofibers was 315 °C, it was 304 °C and 300 °C for PAN/Ag and P (AN-co-IA)/Ag nanofibers which were prepared from 20 wt % $AgNO_3$, respectively. It was understood that both silver nanoparticles and itaconic acid contributed to decrease the cyclization temperature of PAN by generating sharp exothermic peaks. In case of IA existence in PAN structure, cyclization reactions initiates with an ionic mechanism rather than a radical mechanism and shows doublet exothermic peak with maximum points approximately at 180°C and 310 °C, respectively [30]. However, only a single and sharp exothermic peak of P (AN-co-IA)/Ag nanofibers was seen in Figure 4.65. It can be said that incorporation of silver nanoparticles into P (AN-co-IA) copolymer resulted in a new material which exhibits different thermal features than neat P (AN-co-IA).

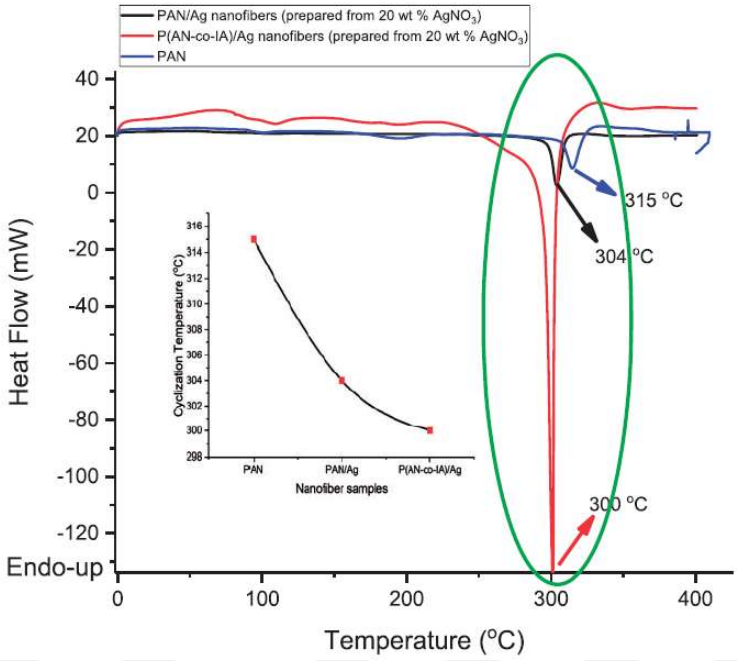

Figure 4.65 : DSC thermograms of PAN, PAN/Ag (prepared from 20 wt % $AgNO_3$) and P (AN-co-IA)/Ag (prepared from 20 wt % $AgNO_3$) nanofibers.

In addition, cyclization of C≡N groups can be calculated from the area of exothermic peak and called as delta H (ΔH) [233]. Considering this, ΔH values of the nanofiber samples were calculated and given in Table 4.5 as well as cyclization temperatures of the nanofiber samples.

Table 4.5 : Cyclization temperatures and enthaply values of produced PAN, PAN/Ag and P(AN-co-IA)/Ag nanofibers.

Nanofiber Samples	T_c (°C)	ΔH (J/g)
PAN	315	264
PAN/Ag (prepared from 20 wt % $AgNO_3$)	304	400
P(AN-co-IA)/Ag (prepared from 20 wt % $AgNO_3$)	300	3065

It was seen that silver nanoparticles increased ΔH values of the nanofibers when compared to pure PAN nanofibers. Ucar and coworkers also studied on the thermal behaviour of Ag nanoparticle containing PAN nanofibers and observed that the enthaply of the nanofibers increased due to the silver nanoparticles. Moreover, it was mentioned that reduction method of $AgNO_3$ to silver nanoparticles had effect on not only the enthalpy values but also cyclization temperature [233]. Considering this, it can be concluded that reduction of $AgNO_3$ to silver nanoparticles in the presence of P (AN-co-IA) rather than PAN had a great influence on ΔH values.

4.4.7 Antimicrobial activity studies

4.4.7.1 Disk diffusion method

In order to determine in vitro antimicrobial activities of the produced nanofibers of PAN, P (AN-co-IA), PAN/Ag (prepared from 20 wt % $AgNO_3$) and P (AN-co-IA)/Ag (prepared from 20 wt % $AgNO_3$) and the powders of PAN and P (AN-co-IA) polymers and $AgNO_3$, disk diffusion method based on the Clinical and Laboratory Standards Institute (CLSI) criteria was used as a pre-screening test against various microorganisms [239]. For this purpose, S. aureus ATCC 29213 as a Gram-positive bacteria, E. coli ATCC 25922 and P. aeruginosa ATCC 27853 as Gram-negative bacteria and C. albicans ATCC 10231 as a yeast fungus were used.

Briefly, the cell suspensions (equivalent to 0.5 McFarland) were inoculated over plates containing solidified agar medium onto sterile petri-plates by spread plate method. The nanofiber samples with and without silver nanoparticles were cut in the area of approximately 1 cm^2 and the powder solutions in DMSO were immersed on empty sterile disks (in diameters of 6 mm). Then, the samples were placed over the solidified agar gel under aseptic conditions. The plates were placed into an incubator at 37 °C for bacteria and at 25 °C for yeasts. After 24 hours, the zone inhibitions were observed.

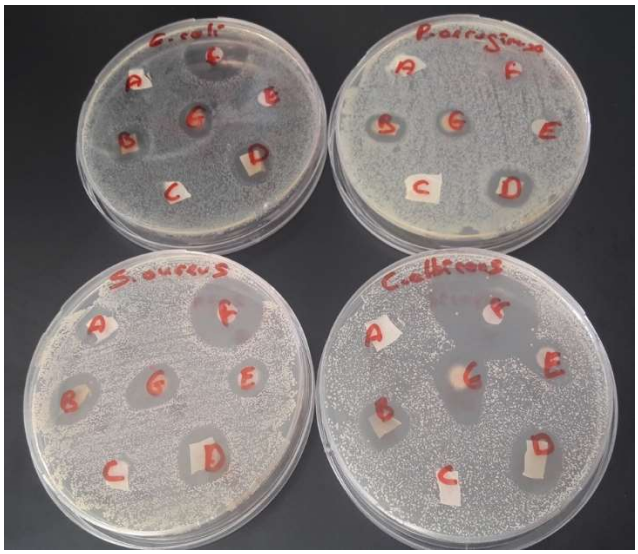

Figure 4.66 : Observed inhibition zones of A: PAN nanofiber, B: PAN/Ag nanofiber (prepared from 20 wt % $AgNO_3$), C: P (AN-co-IA) nanofiber, D: P (AN-co-IA)/Ag nanofiber (prepared from 20 wt % $AgNO_3$), E: PAN powder, F: P (AN-co-IA) powder and G: $AgNO_3$ powder against four different microbial culture in plates.

Ag nanoparticles are broad spectrum antimicrobials exhibiting very strong bactericidal activity against both gram-positive and gram-negative bacteria and antifungal activity against Candida species [87, 240]. As a result of disk diffusion method for pre-screening the antimicrobial activity, it was observed that the powder of $AgNO_3$ and the nanofibers of PAN/Ag and P (AN-co-IA)/Ag nanofibers produced inhibition zones against the studied microorganisms. Obtained inhibition zones against E. coli ATCC 25922, P. aeruginosa ATCC 27853, S. aureus ATCC 29213 and C. albicans ATCC 10231 cultures in plates are shown in Figure 4.66.

4.4.7.2 Microdilution susceptibility testing

In vitro antimicrobial activities of the nanofiber samples with and without silver nanoparticles against S. aureus ATCC 29213, E. coli ATCC 25922, P. aeruginosa ATCC 27853 and C. albicans ATCC 10231 strains were investigated. Minimum inhibitory concentrations (MICs) of the nanofibers were determined by microbroth dilution method based on the CLSI criteria [241]. For comparison, the antimicrobial activities of the powders of PAN and P (AN-co-IA) polymers and $AgNO_3$ were also assessed.

The samples used in the study were dissolved in DMSO and then diluted in Mueller-Hinton Broth medium (MHB, Difco, Detroid, USA). While the inoculums of the bacteria were prepared using 4-6 h cultures in MHB medium at the final concentration of 5×10^5 cfu/ml (colony forming unit), the inoculum of the yeast strain was prepared using 24 h culture in RPMI-1640 medium (Sigma, St. Louis, MO, USA) at the concentration of $0.5\text{-}2.5 \times 10^3$ cfu/ml in the test tray. The trays were covered and placed in plastic bags to prevent evaporation and incubated at 37°C during 18-24 h for the bacteria and at 25°C during 48 h for the yeasts. The MICs were defined as the lowest concentration of compound giving no visible growth. The activity of DMSO, which is used as solvent in the study, was also tested as negative control and the results were taken into account when calculating the results. Levofloxacin was used as reference antibacterial for bacteria and fluconazole was used as reference antifungal for yeasts. The MIC values of levofloxacin and fluconazole were within the accuracy range in CLSI [242] throughout the study.

According to the results, which were shown in Table 4.6, the MIC values of $AgNO_3$ powder against S. aureus, E. coli, P. aeruginosa and C. albicans were 20 μg/mL, 5

μg/mL, 5 μg/mL and 40 μg/mL, respectively. The powders of PAN and P (AN-co-IA) polymers and their electrospun nanofibers (PAN nanofiber and P (AN-co-IA) nanofiber) did not show any antimicrobial activity. In literature, it was also stated that neat PAN nanofibers did not exhibit any antimicrobial activity [3, 228, 243, 244]. However, when silver nanoparticles containing composite nanofibers were produced, resulting nanofibers (PAN/Ag (prepared from 20 wt % $AgNO_3$) and P (AN-co-IA)/Ag (prepared from 20 wt % $AgNO_3$)) both gained antimicrobial activities. Especially PAN/Ag nanofiber was highly active against Gram positive S. aureus and yeast C. albicans, at lower concentrations than $AgNO_3$. Additionally, PAN/Ag nanofiber showed antibacterial activity against gram negative E. coli and P. aeruginosa strains, similar to $AgNO_3$. These results were compatible with the literature [6, 228, 243, 244]. Itaconic acid is a natural non-amino and non-toxic organic acid that is exhibiting good antimicrobial activity [245]. To date, there is not any study published that is evaluating the antimicrobial activity of P (AN-co-IA) nanofibers containing silver nanoparticles. According to our results, while P (AN-co-IA)/Ag nanofiber was active against S. aureus, E. coli and P. aeruginosa at higher concentrations than $AgNO_3$, it was more active against C. albicans at lower concentrations than $AgNO_3$. It can be said that silver nanoparticles containing P (AN-co-IA) nanofibers were highly good antibacterial and antifungal membranes and copolymerization with itaconic acid contributed to especially their antifungal activity.

Table 4.6 : Minimum inhibitory concentration (MIC) values determined for the nanofiber samples with and without silver nanoparticles and powders.

Samples	**MIC values (μg/ml)**			
	S. aureus	***E. coli***	***P. aeruginosa***	***C. albicans***
PAN nanofiber	-	-	-	-
PAN/Ag nanofiber (prepared from 20 wt % $AgNO_3$)	8	8	4	16
P(AN-co-IA) nanofiber	-	-	-	-
P(AN-co-IA)/Ag nanofiber (prepared from 20 wt % $AgNO_3$)	62,5	16	32	32
PAN powder	-	-	-	-
P(AN-co-IA) powder	-	-	-	-
$AgNO_3$ powder	20	5	5	40

4.4.7.3 Time-kill analysis

Time kill analysis were performed to investigate the antimicrobial activities of the nanofiber samples with and without silver nanoparticles against various microorganisms over time according to the time killing curve method which was reported by NCCLS [246]. S. aureus ATCC 29213, E. coli ATCC 25922, P. aeruginosa ATCC 27853 and C. albicans ATCC 10231 strains were used in the study. The rate of killing of the microorganisms was determined by incubating the test organisms with different concentrations of nanofiber samples or powders in MHB or RPMI-1640 medium for bacteria and yeast, respectively.

PAN/Ag (prepared from 20 wt % $AgNO_3$) and P (AN-co-IA)/Ag (prepared from 20 wt % $AgNO_3$) nanofibers and $AgNO_3$ powder were prepared at the final concentrations equivalent to 1 x MIC and 10 x MIC. The polymers of PAN and P (AN-co-IA) were also weighted in the same amounts and all of the samples were added into test tubes containing 5 ml of MHB or RPMI-1640 medium. Then, bacterial or fungal suspensions were added to each tubes to give a final concentrations of 1-5 x 10^5 cfu/ml. One tube containing only bacterial or fungal inoculum of 1-5 x 10^5 cfu/ml was prepared as control. The tubes were incubated on a shaker water bath at 37˚C for bacteria and at 25˚C for yeast at an agitation speed of 70 rpm. At predetermined time points (0, 2, 4, 6, 24, 48, 120 and 168 hours), samples were removed and diluted in saline, if necessary. 100 µl aliquots were spreaded onto TSA agar plates and incubated overnight after drying. Then, surviving colonies were counted (cfu/ml) after incubation. The time-kill curves were constructed by plotting the log10 colony counts (cfu/ml) against time in different concentrations.

According to the results, which are shown in Figure 4.67, nanofibers without silver nanoparticles (PAN and P (AN-co-IA)) did not show any antimicrobial activity against any microorganism during the studied 168 hour-time period as expected. However, bacteriostatic/fungistatic activity was observed with all nanofiber samples containing silver nanoparticles (PAN/Ag and P (AN-co-IA/Ag)) against S. aureus, P. aeruginosa and C. albicans at almost all time points, bactericidal activity was started from 24-48 hours until 120 hours at 10xMIC. Especially against E. coli, it starts from 6 hours at 10xMIC and 24 hours at 1xMIC. In addition, fungucidal activity was observed in 120 and 168 hours at 10xMIC.

Nanofibers with silver nanoparticles and $AgNO_3$ powder samples showed their most effective bactericidal activities against Gram negative bacteria E. coli and P. euruginosa started from 6 hours and 24 hours at 10xMIC and 1xMIC, respectively. Additionally, they showed bactericidal or fungicidal activities at their 10xMIC started after 24-48 hours against S. aureus and C. albicans.

In conclusion, bactericidal/fungicidal activities were obtained with nanofibers incorporating silver nanoparticles especially at 10 x MIC concentration and $AgNO_3$ powder at 1 x MIC and 10 x MIC concentrations. Moreover, these activities started at 6-24th hours and continued for up to 168 hours.

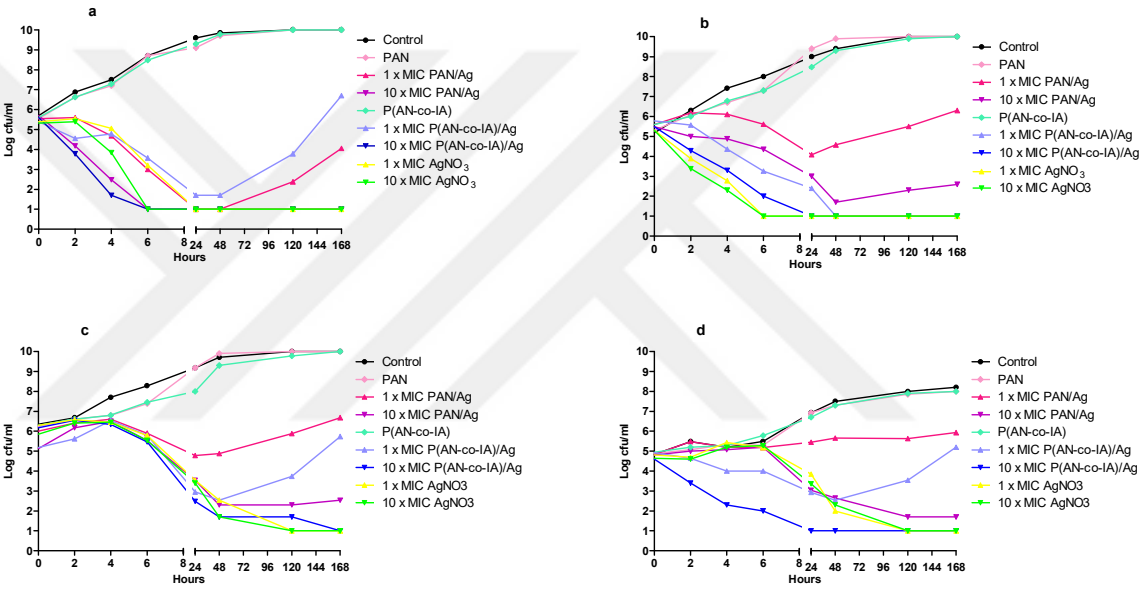

Figure 4.67 : Time-kill curves of nanofibers of PAN, P (AN-co-IA), PAN/Ag (prepared from 20 wt % $AgNO_3$) and P (AN-co-IA)/Ag (prepared from 20 wt % $AgNO_3$) and $AgNO_3$ powder at 1 x MIC and 10 x MIC concentrations against a: Escherichia coli b: Pseudomonas aeruginosa c: Staphylococcus aureus and d: Candida albicans strains after 0, 2, 4, 6, 24, 48, 120 and 168 hours. The x-axis represents the killing time (hours), and the y-axis represents the logarithmic counts of survival microorganisms.

4.5 Results of Coaxial PAN/Ag and P (AN-co-IA) /Ag Nanofibers

4.5.1 Morphology of coaxial PAN/Ag and P (AN-co-IA)/Ag nanofibers (SEM-EDS)

As mentioned in Table 3.3, different feed-rates of shell solution were tried to determine the most appropriate flow-rate for the formation of a stable Taylor cone at the tip of

the needle [246]. Spinnability observations related to the different feed-rates of shell solution are indicated in Table 4.7.

Table 4.7 : Comments on the spinnability related to the feed-rates of the shell solution.

Feed rate of the shell solution (ml/h)	Spinnability (observation)
0.1	Spinnable
0.2	Spinnable
0.3	After a while, droplet did not turn into Taylor cone.
0.4	Just droplet occured at the tip of the needle

Based on the spinnability observations of different feed-rate trials, the optimum feed-rate of shell solution was decided to be 0.2 ml/h while it was kept constant (1.0 ml/h) for core solution.

SEM characterization was performed to investigate the surface morphology of coaxial PAN/Ag and P (AN-co-IA)/Ag nanofibers.

SEM images of PAN (core)-$AgNO_3$ (shell)(0.1 ml/h) and PAN (core)-$AgNO_3$ (shell) (0.2 ml/h) nanofibers are demonstrated in Figure 4.68 and Figure 4.69, respectively.

PAN (core)- $AgNO_3$ (shell) (0.1 ml/h) and P (AN-co-IA)-PAN (core)- $AgNO_3$ (shell)(0.1 ml/h) nanofibers were continous and bead-free.

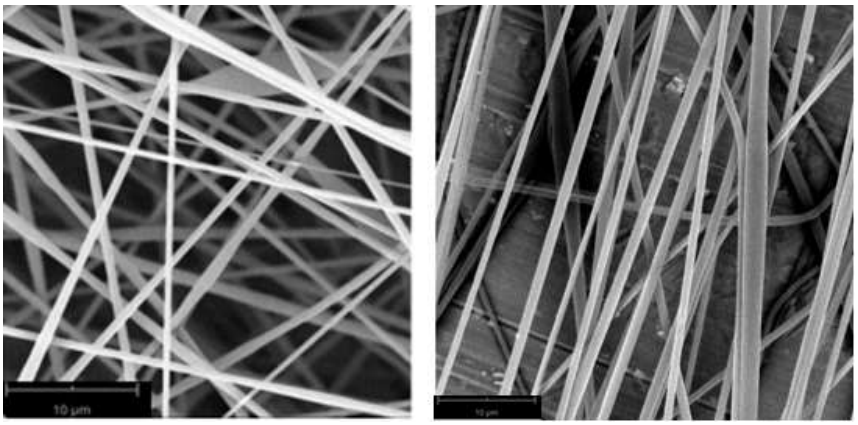

Figure 4.68 : SEM images of the PAN(core)- $AgNO_3$ (shell) (0.1 ml/h) nanofibers.

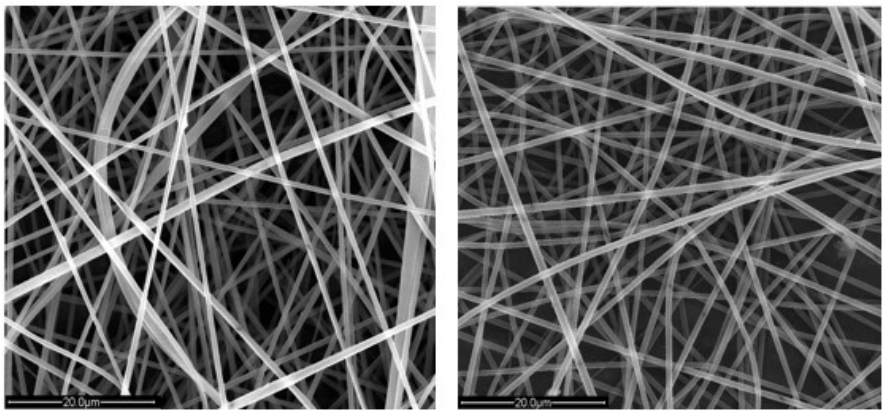

Figure 4.69 : SEM images of the PAN (core)- $AgNO_3$ (shell) (0.2 ml/h) nanofibers.

As mentioned in the section 3.4.3.4, in order to obtain Ag nanoparticles, the obtained PAN(core)- $AgNO_3$ (shell) (0.2 ml/h) nanofibers were subjected to UV-irradiation for different time periods. SEM images of the obtained nanofibers after 30 minutes, 1 hour and 1.5 hours UV-irradiation are given in Figure 4.70. SEM images of the obtained nanofibers after 2 hours and 3 hours UV-irradiation are shown in Figure 4.71 whereas Figure 4.72 belongs to SEM images of the nanofibers after 5 hours and 7 hours UV-light treatment.

SEM images of PAN (core) - $AgNO_3$ (shell) (0.2 ml/h) nanofibers after UV-light treatment for different time periods revealed that 30 minutes, 1 hour and 1.5 hours did not make any considerable change on the nanofiber surfaces while 2 hour-UV irradiation made a slight change (unevenness on nanofiber surface) and 3 hour-UV irradiation caused a considerable change on the smoothness of the nanofiber surfaces. 3 hour-UV light treatment caused more unevennes on the nanofiber surfaces compared to lower UV- irradiation durations. However, 5 hour-UV light treatment began to broke the nanofibers and 7 hour-UV light treatment broke them dramatically. Based on the SEM images, for the reduction process of $AgNO_3$ to Ag nanoparticles, 3 hour-UV- irradiation was selected to be sufficient for keeping the nanofibers either unbroken or unwrinkled.

Figure 4.73 corresponds to SEM images of PAN (core)- $AgNO_3$ (shell)(0.2 ml/h) nanofibers after 3 hours UV-irradiation.

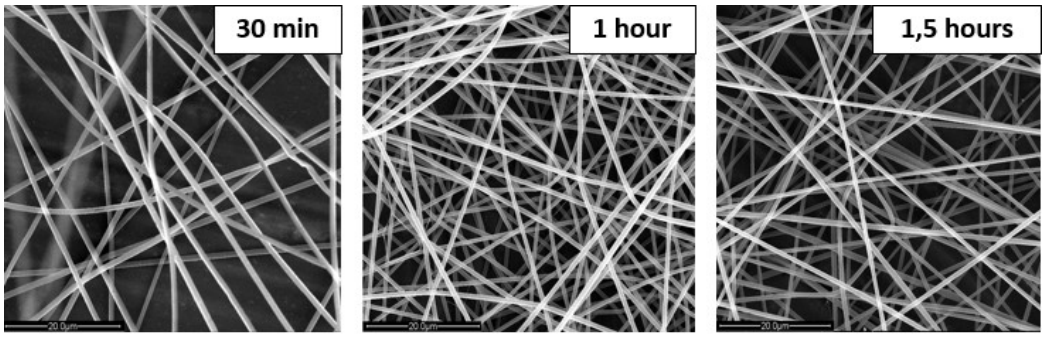

Figure 4.70 : SEM images of PAN (core)- $AgNO_3$ (shell)(0.2 ml/h) nanofibers after 30 minutes, 1 hour and 1.5 hours UV-irradiation.

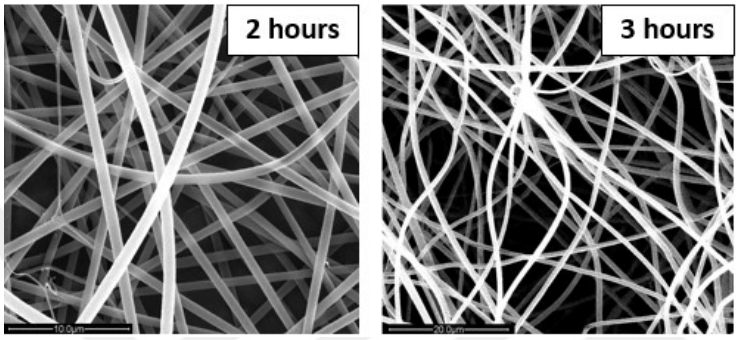

Figure 4.71: SEM images of PAN(core)- $AgNO_3$ (shell)(0.2 ml/h) nanofibers after 2 hours and 3 hours UV-irradiation.

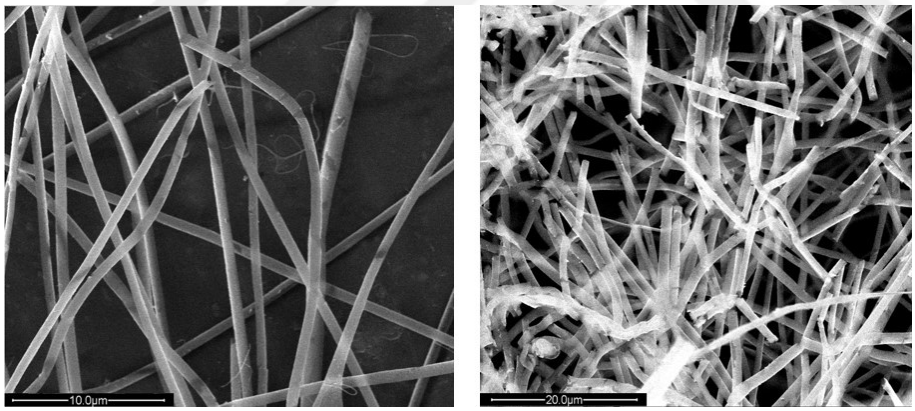

Figure 4.72 : SEM images of PAN(core)- $AgNO_3$ (shell)(0.2 ml/h) nanofibers after 5hours and 7 hours UV-irradiation.

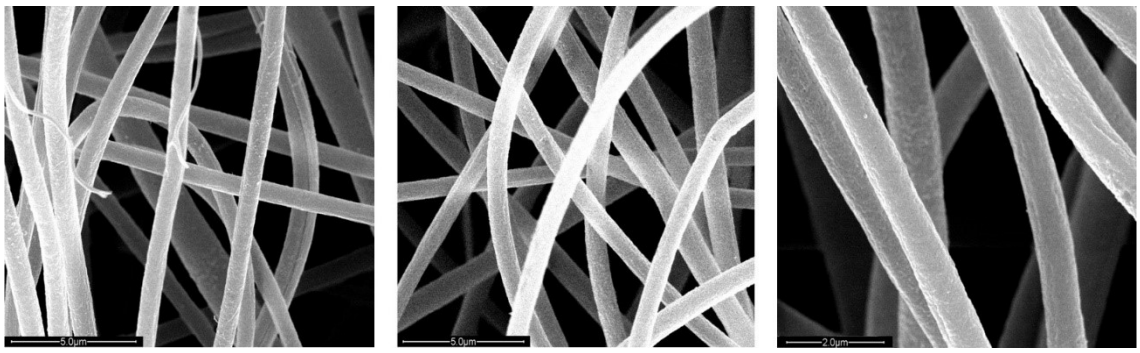

Figure 4.73 : SEM images of PAN (core) - $AgNO_3$ (shell) (0.2 ml/h) nanofibers after 3 hours UV-irradiation.

Related to the optimization results of both feed-rate of shell solution and UV-irrradition duration of PAN/Ag (core/shell) nanofibers, P(AN-co-IA)-PAN/Ag nanofibers were also produced via coaxial electrospinning. The same coaxial electrospinning set-up (Figure 3.5) was used. Feed rates were decided to be 1.0 ml/h and 0.2 ml/h for core and shell solutions, respectively. Figure 4.74 and Figure 4.75 show SEM images of the neat and after 3 hour UV-light treated P(AN-co-IA)-PAN (core)- $AgNO_3$ (shell)(0.2 ml/h) nanofibers, respectively.

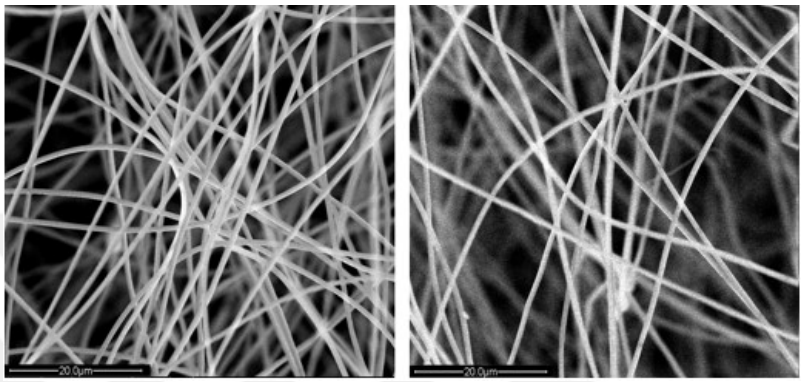

Figure 4.74 : SEM images of the neat P(AN-co-IA)-PAN (core)- $AgNO_3$ (shell)(0.2 ml/h) nanofibers.

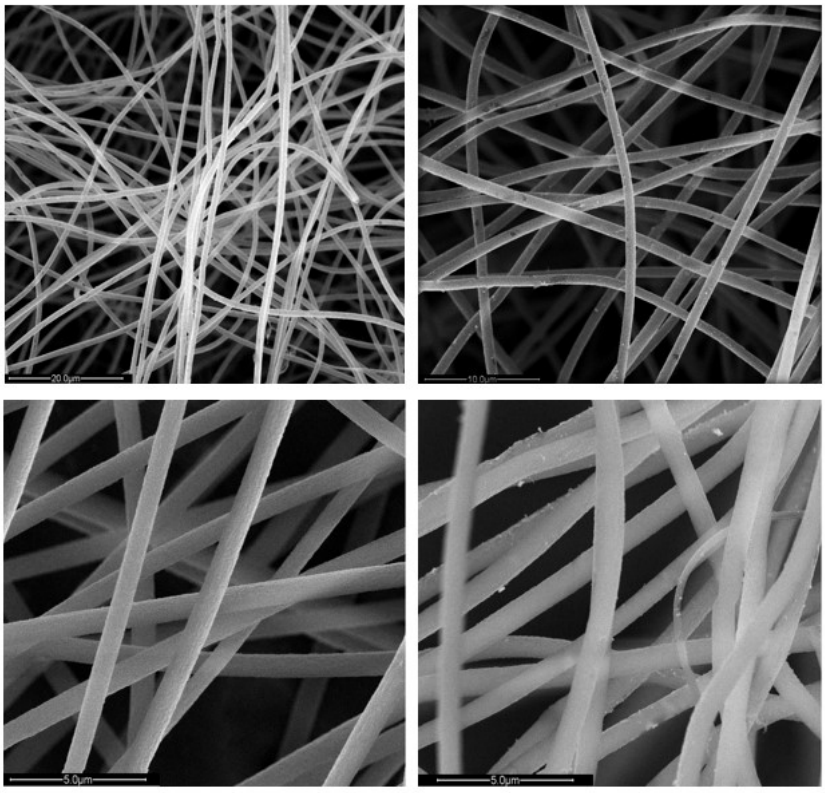

Figure 4.75 : SEM images of 3 hour UV-light treated P(AN-co-IA)-PAN (core)- AgNO3 (shell)(0.2 ml/h) nanofibers.

From Figure 4.74 and Figure 4.75, it was seen that UV-irradiation caused more porous structure as a result of reduction of $AgNO_3$ to AgNPs.

Average nanofiber diameters of the neat and UV-irradiated of PAN (core) - AgNO3 (shell) (0.2 ml/h) nanofibers and P (AN-co-IA)-PAN (core) - $AgNO_3$ (shell) (0.2 ml/h) nanofibers were calculated via Image J programme and are expressed in Table 4.8 and Figure 4.76.

Table 4.8: Average nanofiber diameters (nm) and their standard deviation of the neat and UV-irradiated of PAN (core) - $AgNO_3$ (shell) (0.2 ml/h) nanofibers and P (AN-co-IA)-PAN (core) - $AgNO_3$ (shell) (0.2 ml/h) nanofibers.

Nanofiber Samples	Nanofiber Diameter (nm)	Standard Deviation
PAN(core)-$AgNO_3$(shell)(0.2 ml/h) non-UV	712.11	68.295
P(AN-co-IA)-PAN (core)-$AgNO_3$(shell)(0.2 ml/h) non-UV	764.705	69.493
PAN(core)-$AgNO_3$(shell)(0.2 ml/h) 3 h-UV	919.272	184.733
P(AN-co-IA)-PAN(core)-$AgNO_3$(shell) (0.2 ml/h) 3 h-UV	800.607	72.621

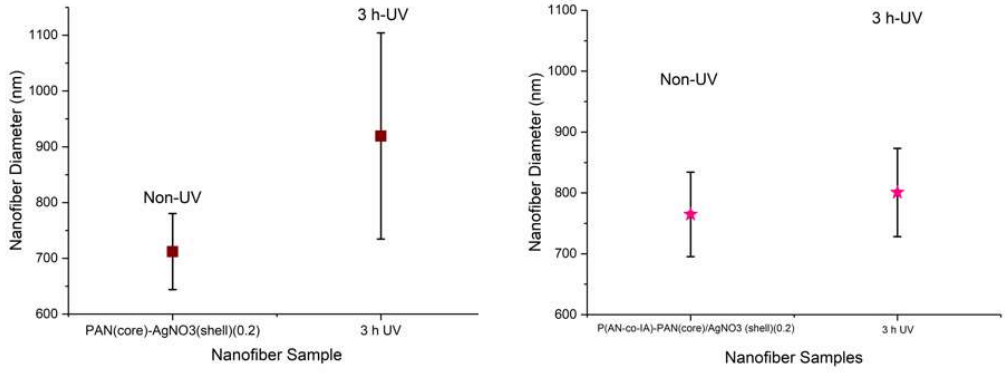

Figure 4.76 : Graphs of the average nanofiber diameters of PAN (core)-$AgNO_3$ (shell) (0.2 ml/h) nanofibers (non-UV and 3 hour-UV-treated) (left) and P (AN-co-IA)-PAN (core)- $AgNO_3$ (shell) (0.2 ml/h) nanofibers (non-UV and UV-3 hour-UV-treated) (right).

It was found out that UV-irradiation caused increase in nanofiber diameters because of mainly AgNPs formation, which covered the core polymer. The average nanofiber diameters of P (AN-co-IA)-based coaxial nanofibers were higher than PAN-based nanofibers.

Furthermore, EDS characterization was performed to verify the presence of silver and calculate the amount of it. Characterization was carried out only for the optimized 3 hour-UV light treated PAN(core)- $AgNO_3$ (shell)(0.2 ml/h) and P(AN-co-IA)-PAN (core)-Ag(shell)(0.2 ml/h) nanofibers. AgNPs amount in PAN (core) - $AgNO_3$ (shell) (0.2 ml/h) (after UV irradiation for 3 hours) was measured as 2.21 wt % and 0.56 at %, while it was 4.43 wt % and 1.15 at % in P (AN-co-IA)-PAN (core) - $AgNO_3$ (shell) (0.2 ml/h) (after UV irradiation for 3 hours).

4.5.2 UV-Visible spectroscopy

UV-visible spectroscopy characterizations were performed in the range of 200-800 nm by using nanofiber samples of the neat PAN, P (AN-co-IA) and non-UV and UV-irradiated PAN (core)-$AgNO_3$ (shell) (0.2 ml/h) and P (AN-co-IA)-PAN (core)-$AgNO_3$ (shell) (0.2 ml/h) nanofibers. Figure 4.77 depicts UV-Vis. spectroscopy results of neat PAN, PAN (core)-$AgNO_3$ (shell) (0.2 ml/h) and PAN (core)-$AgNO_3$ (shell) (0.2 ml/h)-3 h UV treated nanofibers.

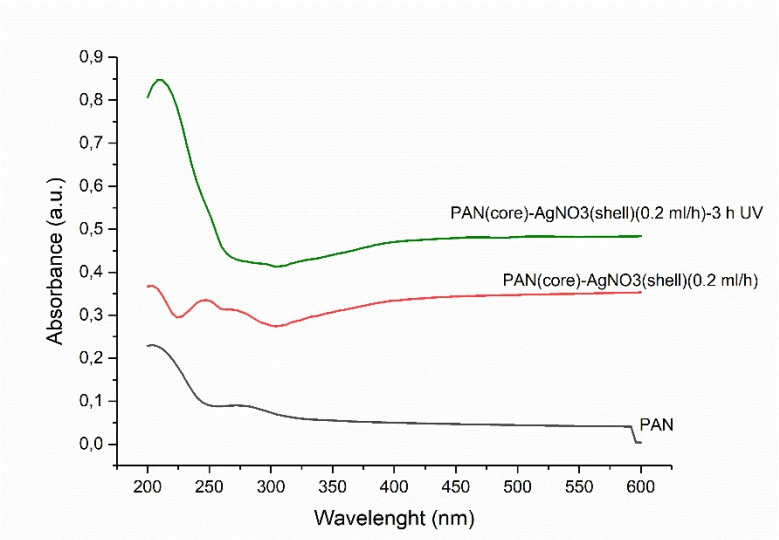

Figure 4.77 : UV-Vis. spectroscopy results of neat PAN, PAN (core)- $AgNO_3$ (shell) (0.2 ml/h) and PAN (core)- $AgNO_3$ (shell) (0.2 ml/h)-3 h UV treated nanofibers.

Figure 4.77 indicated that neat PAN nanofibers had an absorbance peak at 278 nm while PAN (core)-$AgNO_3$ (shell) (0.2 ml/h) nanofibers had two absorbance peaks at 246 and 273 nm. In case of UV-treatment, the observed peaks disappeared and only a wide absorbance was observed starting from 310 nm and having peak at 400 nm which exactly could be taken as a proof of Ag nanoparticle existence. Furthermore, the peak seen at 206 nm for both PAN and non-UV PAN (core)-$AgNO_3$ (shell) (0.2 ml/h) nanofibers shifted to 210 nm in case of UV-treatment, which also mentioned the effect of UV-treatment on chemical structure of PAN (core)-$AgNO_3$ (shell) (0.2 ml/h) nanofibers.

Figure 4.78 presents UV-Vis. spectroscopy of plain P (AN-co-IA) and non-UV and UV-treated P (AN-co-IA)-PAN (core)-$AgNO_3$ (shell) (0.2 ml/h) nanofibers, as well.

The plain P (AN-co-IA) nanofibers showed a characteristic absorbance peak at 272 nm but this peak shifted to 270 nm for non-UV P (AN-co-IA)-PAN (core)-$AgNO_3$ (shell) (0.2 ml/h) nanofibers and further shifted to 268 nm for UV-treated P (AN-co-IA)-PAN (core)-$AgNO_3$ (shell) (0.2 ml/h) nanofibers. As expected, AgNPs formation was proved by the absorbance curves observed for coaxial P (AN-co-IA)-PAN (core)-$AgNO_3$ (shell) (0.2 ml/h) and UV-irradiated P (AN-co-IA)-PAN (core)-$AgNO_3$ (shell) (0.2 ml/h) nanofibers with the absorbance curve, starting from 310 nm and having a maxima at 406 nm.

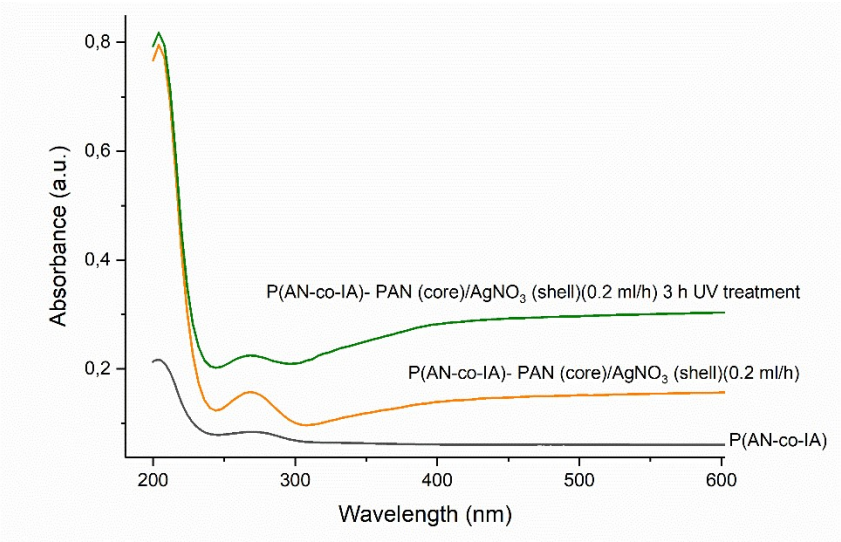

Figure 4.78 : UV-Vis. spectroscopy of neat P (AN-co-IA), P (AN-co-IA)-PAN (core)- $AgNO_3$ (shell) (0.2 ml/h) and P (AN-co-IA)-PAN (core)- $AgNO_3$ (shell) (0.2 ml/h)-3 h UV treated nanofibers.

4.5.3 FTIR-ATR spectroscopy

FTIR-ATR spectroscopy characterizations of the neat PAN, P (AN-co-IA) and non-UV and UV-irradiated PAN (core)-$AgNO_3$ (shell) (0.2 ml/h) and P (AN-co-IA)-PAN (core)- $AgNO_3$ (shell) (0.2 ml/h) nanofibers were performed in the range of 400 cm^{-1} and 4000 cm^{-1} with the signal resolution of 4 cm^{-1}. FTIR-ATR spectrum of PAN, PAN (core)-$AgNO_3$ (shell) (0.2 ml/h) and UV-implemented PAN (core)-$AgNO_3$ (shell) (0.2 ml/h) nanofibers are given in Figure 4.79.

Pure PAN nanofibers showed characteristic bands at 2244 cm^{-1}, 2930 cm^{-1}, 1453 cm^{-1}, and 1090 cm^{-1} corresponding to -CN stretching vibration, CH_2 stretching and bending vibration, and C–C stretching vibration [118]. The band at 1670 cm^{-1} was attributed to -C=N stretching vibration. The bands at 1330 cm^{-1} and 824 cm^{-1} were attributed to NO^{3-} ions. The weak band at 1040 cm^{-1} might be due to the synthesis of AgNPs via reducing Ag^{+} ions [243]. The weak broad band at 958 cm^{-1} might be assigned to N-O. It was observed that the characteristic peak of PAN nanofibers at 1670 cm^{-1} slightly decreased with the presence of AgNPs [248]. On formation of silver nanoparticles, the peak corresponding to the silver band at 782 cm^{-1} has broadened and shortened.

Additionally, FTIR-ATR spectrum of neat P (AN-co-IA), P (AN-co-IA)-PAN (core)-$AgNO_3$ (shell) (0.2 ml/h) and P (AN-co-IA)-PAN (core)-$AgNO_3$ (shell) (0.2 ml/h)-3 h UV treated nanofibers are demonstrated in Figure 4.80.

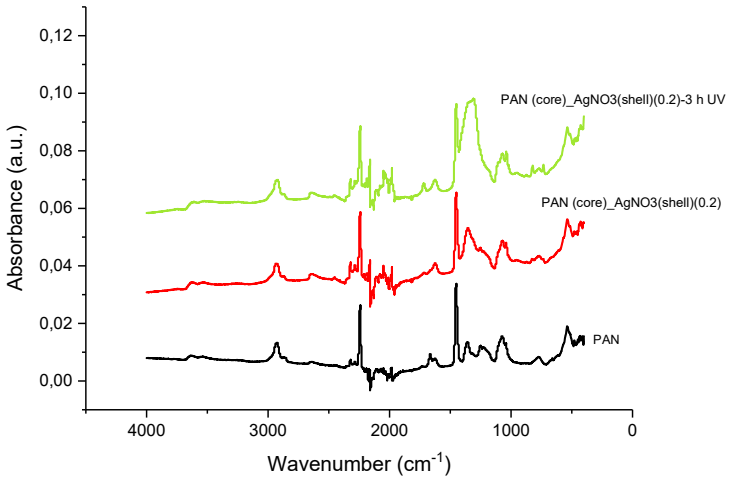

Figure 4.79 : FTIR-ATR spectrum of neat PAN, PAN (core)- $AgNO_3$ (shell) (0.2 ml/h) and PAN (core)- $AgNO_3$ (shell) (0.2 ml/h)-3 h UV treated nanofibers.

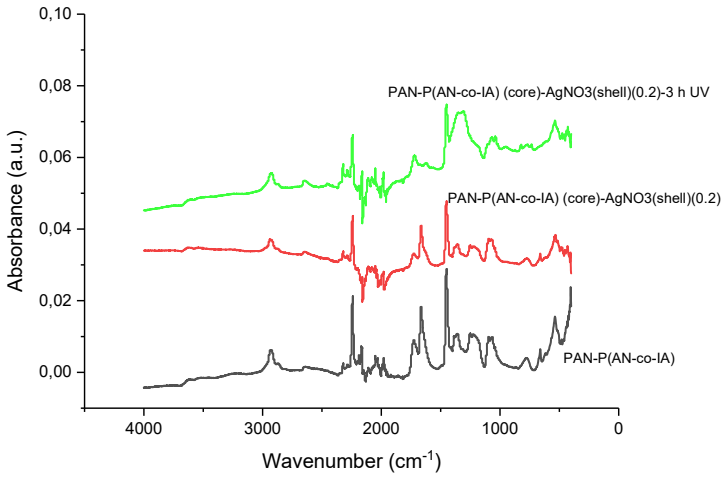

Figure 4.80 : FTIR-ATR spectroscopy results of neat P (AN-co-IA), P (AN-co-IA)-PAN (core)- $AgNO_3$ (shell) (0.2 ml/h) and P (AN-co-IA)-PAN (core)-$AgNO_3$ (shell) (0.2 ml/h)-3 h UV treated nanofibers.

The neat P (AN-co-IA) nanofibers showed a peak at 1730 cm^{-1} which was absent for PAN nanofibers, corresponding to the C=O group of itaconic acid. This band was slightly shifted to 1720 cm^{-1} for UV-treated P (AN-co-IA)-PAN (core)-$AgNO_3$ (shell) nanofibers, confirming the ionization of carboxyl groups of itaconic acid monomer and interaction of Ag^+ [249]. The bands at 1330 cm^{-1} and 824 cm^{-1} were attributed to NO^{3-} ions while the weak broad band at 956 cm^{-1} can be assigned to N-O [250]. It was observed that the characteristic peak of PAN nanofibers at wavelength of 1670 cm^{-1} decreased with the addition of Ag in PAN and weaks band at 1620 cm^{-1} and 1040 cm^{-1} appeared which might be due to the synthesis of AgNPs by reduction of Ag^+ ions [243, 248, 250]. On formation of silver nanoparticles, the band at 786 cm^{-1} corresponding to silver became broader and shorter.

4.5.4 DSC

DSC characterizations of non-UV and UV-treated PAN (core)-$AgNO_3$ (shell) (0.2 ml/h) and P (AN-co-IA)-PAN (core)-$AgNO_3$ (shell) (0.2 ml/h) nanofibers were performed between 0°C and 400°C at a heating rate of 10°C/min in the presence of N_2 atmosphere and DSC thermograms of PAN (core)-$AgNO_3$ (shell) (0.2 ml/h) and P (AN-co-IA)-PAN (core)-$AgNO_3$ (shell) (0.2 ml/h) nanofibers are presented in Figure 4.81 and Figure 4.82, respectively.

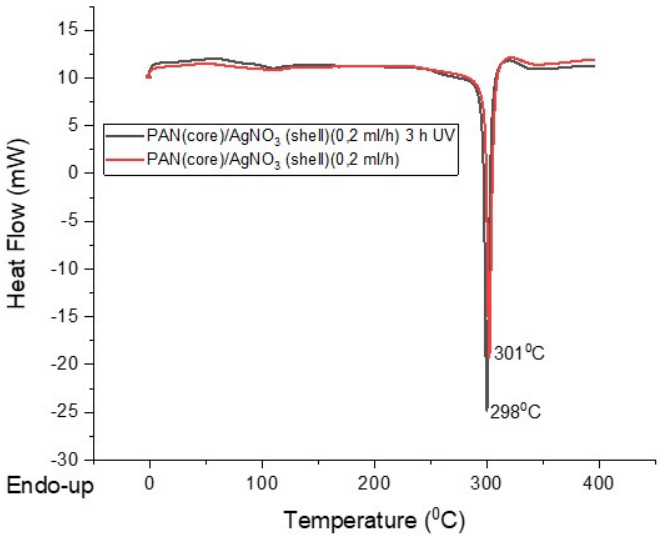

Figure 4.81 : DSC thermograms of non-UV treated and UV-treated PAN(core)/ AgNO3 (shell) nanofibers.

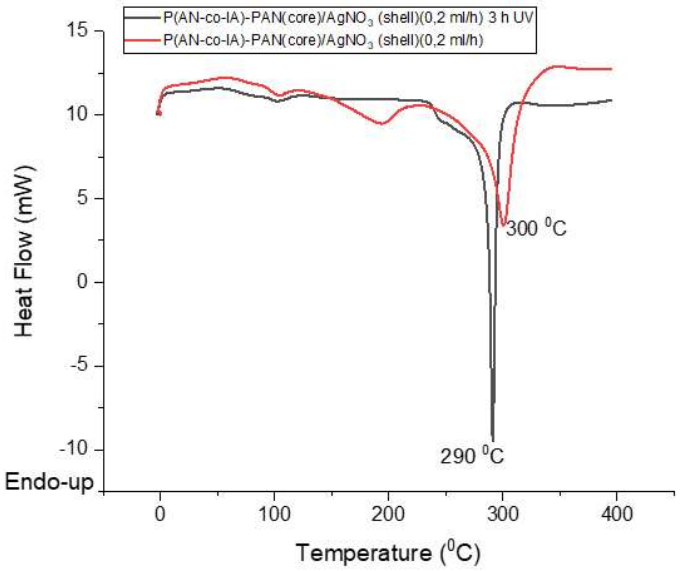

Figure 4.82 : DSC thermograms of non-UV treated and UV-treated P(AN-co-IA)-PAN (core)/ $AgNO_3$ (shell) nanofibers.

Based on Figure 4.81, it was observed that while T_c of PAN(core)/$AgNO_3$ (shell) (0.2 ml/h) nanofibers, which were not subjected to UV-irradiation, was 301 °C, while it was 298 °C for 3h-UV treated PAN(core)/$AgNO_3$ (shell) (0.2 ml/h) nanofibers. It was understood that UV-treatment caused to obtain AgNPs by the reduction of $AgNO_3$, which resulted in decrease in the T_c. Any other considerable difference between non-UV PAN(core)/$AgNO_3$ (shell) (0.2 ml/h) nanofibers and 3h-UV treated PAN(core)/$AgNO_3$ (shell) (0.2 ml/h) nanofibers were not observed. T_c was also 300 °C for non-UV P(AN-co-IA)-PAN(core)/$AgNO_3$ (shell) (0.2 ml/h) nanofibers. However, this value decreased to 290 °C in case of 3 h UV-treatment. Moreover, two

cyclization peaks were observed for non-UV P(AN-co-IA)-PAN(core)/$AgNO_3$ (shell) (0.2 ml/h) nanofibers that was due to the existence of P (AN-co-IA). But after reduction, one of the cyclization peaks disappeared, which meant that the chemical structure and hence the thermal features of the nanofibers was influenced by UV-irradiation.

4.6 Results of P (AN-co-IA)/PPy Nanocomposites

4.6.1 UV-Visible spectroscopy

UV-Vis. spectroscopy of in-situ polymerization of P (AN-co-IA) with Py and NMPy are demonstrated in Figure 4.83 and Figure 4.84, respectively. In Figure 4.83, it can be seen that in-situ polymerization of P (AN-co-IA)/PPy was investigated intervals of 30, 90, 150 and 180 min. Characteristic peaks were observed at approximately 195 nm and 215 nm. When absorbance values of the peak seen at 195 nm were examined in detail related to the polymerization time, it was observed that the absorbance value was decreased from 1.60 to 1.32 when the polymerization time increased from 30 min. to 180 min.

When in-situ polymerization of P (AN-co-IA)/PNMPy was investigated at 30, 90, 150 and 180 min. of polymerization duration, characteristic peaks were seen at 194 nm and 225 nm that can be observed in Figure 4.84. Absorbance values of the peak at 194 nm was 1.72 at 30 min of the polymerization increased to 2.2 and then decreased to 1.91 and 1.58 when the polymerization time reached to 90, 150 and 180 min., respectively.

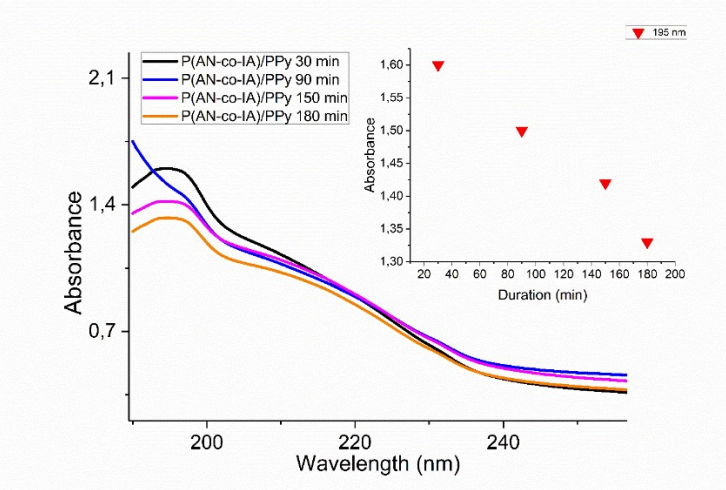

Figure 4.83 : UV-Vis spectroscopy of P (AN-co-IA)/PPy nanoparticles according to in situ polymerization time (minutes).

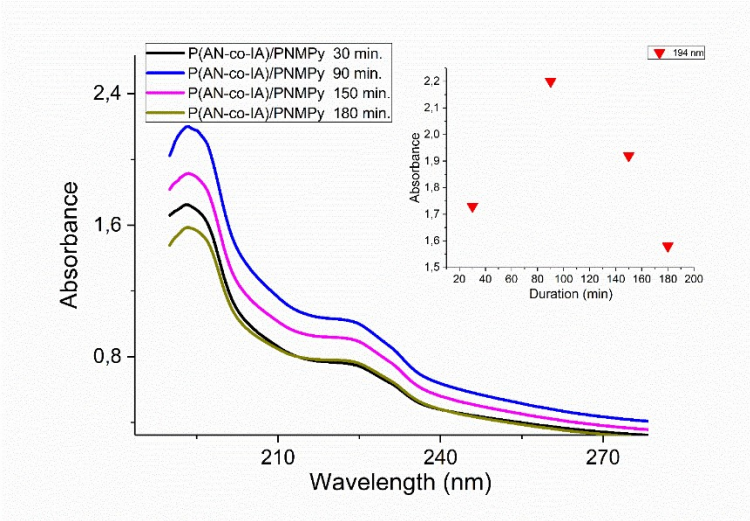

Figure 4.84 : UV-Vis spectroscopy of P (AN-co-IA)/PNMPy nanoparticles according to in situ polymerization time (minutes).

In Figure 4.85, UV-Vis. spectroscopy of produced nanoparticles containing PPy, PNMPy, PDMPy and PTIsPy compared with the matrix polymer nanoparticles at the end of the in-situ polymerization. It can be concluded from the figure that P(AN-co-IA) nanoparticles gave peak nearly at 222 nm and that peak shifted to 215 nm when PPy was polymerized onto P(AN-co-IA) and 225 nm in case of the PNMPy. Differently from the other produced nanoparticles, distinguishing peaks were observed at 428 and 470 nm for PTIsPy and PDMPy containing nanoparticles, respectively.

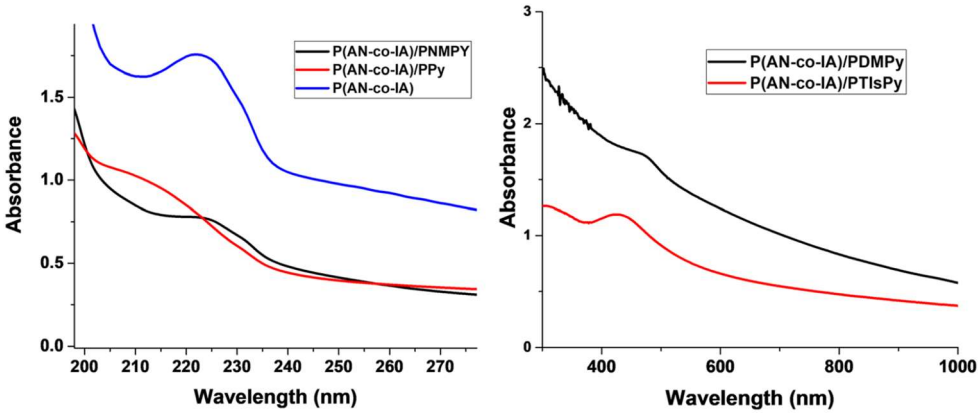

Figure 4.85 : Ultraviolet-visible (UV-Vis) spectroscopy of P (AN-co-IA), P (AN-co-IA)/PPy, P (AN-co-IA)/PNMPy, P (AN-co-IA)/PDMPy, and P (AN-co-IA)/PTIsPy nanoparticles at the end of in-situ polymerization.

Figure 4.86 shows UV-Vis. absorbance values of P (AN-co-IA) nanoparticles containing PPy, PNMPy, PTIsPy and PDMPy at 215 nm and 428 nm. It can be concluded from the Figure 4.86 that at 215 nm, the absorbance values of nanoparticles containing PPy and PNMPy are higher than PTIsPy and PDMPy whereas the absorbance values of nanoparticles containing PTIsPy and PDMPy are higher than PPy

and PNMPy at 428 nm, since the polymerization kinetics of conducting polymers vary, at 215 nm PPy and PNMPy containing nanoparticles gave higher absorbance values compared to the PTIsPy and PDMPy.

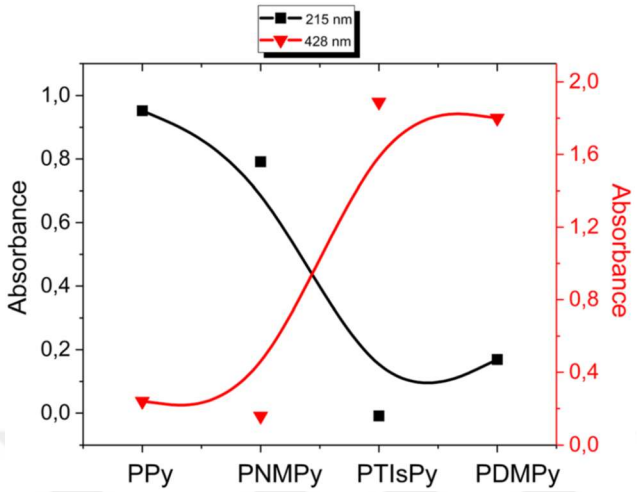

Figure 4.86 : Ultraviolet-visible (UV-Vis) absorbance values of produced nanoparticles.

4.6.2 FTIR-ATR spectroscopy

FTIR-ATR spectroscopic characterizations were performed from the powder form of the produced nanocomposites. Figure 4.87 shows FTIR-ATR spectroscopy results of P (AN-co-IA), P (AN-co-IA)/PPy, P (AN-co-IA)/PNMPy, P (AN-co-IA)/PDMPy and P (AN-co-IA)/PTIsPy nanocomposites. PAN shows its characteristic absorption peaks at 1453 cm^{-1} and 2244 cm^{-1}, corresponding to C≡N stretching and bending vibration of –CH, respectively [25, 30, 251]. 2933 cm^{-1} belongs to the aliphatic CH_2 stretching and 1733 cm^{-1} carbonyl stretching vibration of the carboxylic acid [14, 20, 25, 30, 251–253]. For nanocomposite including PPy, 1554 cm^{-1} corresponds to Py ring vibration (C-C stretching), 1455 cm^{-1} corresponds to C-N ring stretching vibration, 1209 cm^{-1} is attributed to C-H or C-N in plane deformation modes, 915 cm^{-1} relates to C-H out of plane vibration [20, 252, 254]. In the case of P (AN-co-IA)/PNMPy nanocomposite, related with C–C vibrations; bands at around 1447, 1380 and 1330 cm^{-1} and band stretching of carbonyl groups at 1700 cm^{-1} appeared in the polymer [253].

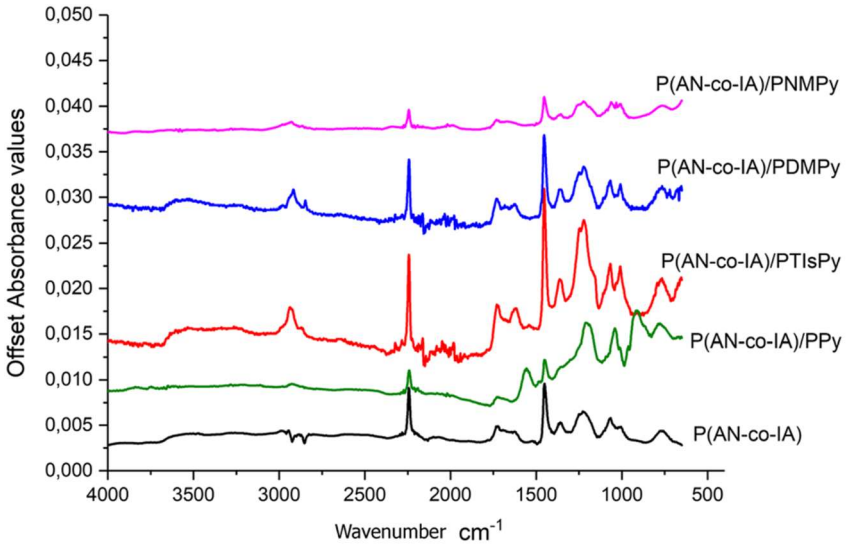

Figure 4.87 : FTIR-ATR spectroscopy of P (AN-co-IA), P (AN-co-IA)/PPy, P (AN-co-IA)/PNMPy, P (AN-co-IA)/PDMPy, P (AN-co-IA)/PTIsPy.

Moreover, Figure 4.88 represents the C-H/C≡N absorbance ratio according to FTIR-ATR results. All polymers consist of P (AN-co-IA) matrix thus, C≡N amount could be assumed as constant for all pyrrole derivatives. However, newly occurred peak (C-H) presented the alkyl effect and gave an approach to understand the relatively polymerization of Py derivatives. Increased C-H/C≡N ratio pointed out relative increase of the polymerization rate. In this case, polymerization speed for constant polymerization duration and conditions could be ordered as PPy>PNMPY> PTIsPy> PDMPy.

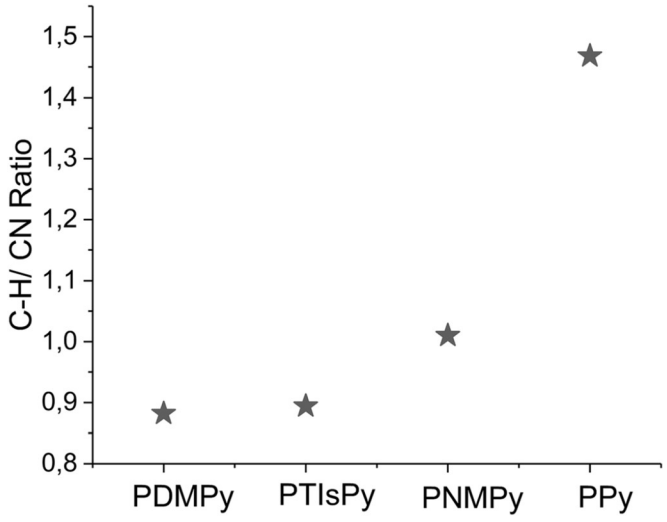

Figure 4.88 : C—H/CN triple bond absorbance ratio of nanoparticles containing PDMPy, PTIsPy, PNMPy, and PPy according to FTIR-ATR results.

4.6.3 Raman spectroscopy

Raman spectroscopy is a non-destructive characterization technique which provides information on chemical structure and molecular interactions of a material as a result of light scattering of vibrating molecules [255].

Figure 4.89 shows Raman spectrum of P(AN-co-IA)/PPy and P(AN-co-IA)/PNMPy. According to Raman spectroscopy results shown in Figure 4.89; peak at 1585 cm−1 comes from the C=C stretching vibrations in the ring [256, 257]. The band at around 1319 cm−1 -1355 cm−1 provided the information about polaron or on the C∼N+• vibrations of delocalized polaronic structures vibrations [256, 258] and band shifted from 1319 cm-1 to 1355 cm-1 for PNMPy containing nanoparticles. Intensity of the polaron bonds was higher for PPy containing powder due to higher affinity of the PPy than of the PNMPy.

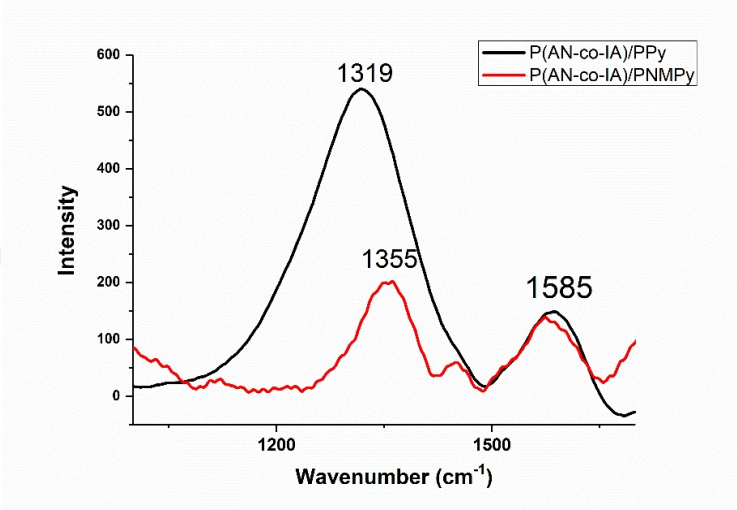

Figure 4.89 : Raman spectroscopy of P (AN-co-IA)/PPy and P (AN-co-IA)/ PNMPy.

4.6.4 AFM

Before AFM characterization of nanocomposite structures, their powder form was treated with DMF in order to obtain a solution concentration of 5 wt% for film casting. Then, prepared solutions were dripped to pure glass slides and spin-coating was applied for a minute using a spin-coater device. Finally, samples obtained by spin-coating were investigated in detail by AFM in order to observe the surface characteristics of the nanoparticles. Sizes of the nanoparticles were also evaluated by using Image J software. In Figure 4.90, image A showed well-distributed nanoparticles belonging to P (AN-co-IA). The size of the nanoparticles was approximately 130 nm.

When image B was examined, it could be clearly seen that the morphology changed due to the existence of PPy and surface roughness increased compared with image A. The size of the nanoparticles also increased to nearly 170 nm. Although there were some agglomerates on the film, it could be said that nanoparticles were distributed homogenously and took the shape which proved the existence of PPy. In a study conducted by Cetiner et al. [254] it was mentioned that the size of the grains was bigger in P (AN-co-VAc)/PPy than the polymer that did not contain PPy. AFM image of PPy containing nanoparticles also resembled AFM images achieved in that study. For image C, PNMPy containing nanoparticles, well-distributed nanoparticles could be seen, too. The nanoparticles had an eliptical shape and grain size was nearly 140 nm. However, surface roughness decreased for the film containing PNMPy. When nanoparticles containing polymers of PDMPy and PTIsPy were investigated, whose AFM images were given in Figure 10D and 10E, differently shaped and homogeneously distributed nanoparticles could be observed. The sizes of the nanoparticles were nearly 70 nm for PTIsPy containing ones and 52 nm for PDMPy containing ones. The surface of the nanoparticles was observed to be rough as in the previous nanoparticles containing PPy and PNMPy. When surface roughness was compared between the P (AN-co-IA) and nanoparticles containing monomers of conjugated polymers, it could be obviously seen that surface roughness of the nanoparticles consisting monomers of conjugated polymers were higher than the nanoparticles obtained from matrix polymer-P (AN-co-IA). It was also known that the characteristics of the conducting films mainly depended on the synthesis conditions and the method used to prepare them. Therefore, all these films containing monomers of conjugated polymer were consequences of the synthesis conditions. Although, there was not a clear explanation in the literature for the orientation of such nanoparticles in the film form, in our case, DMF did not dissolve the matrix polymer, P (AN-co-IA) completely, rather it helped nanoparticles to disperse well through the film. Polymers of PPy and PNMPy containing nanoparticles were also affected by this situation, and as a result, we could see the well-oriented nanoparticles.

Figure 4.91 demonstrates the relation of average nanoparticle sizes of produced nanocomposite structures. The sizes of the nanoparticles were measured by Image J software taking into account approximately 50 nanoparticles. It could be seen that nanoparticles containing PPy and PNMPy had larger nanoparticle diameters, whereas

nanoparticles containing PDMPy and PTIsPy had smaller nanoparticle diameters. Considering all nanoparticles, it could be concluded that average size of nanoparticles of PPy based nanocomposites of this study was between 50 and 170 nm and Figure 4.91 shows the size distribution of the different polymeric structures.

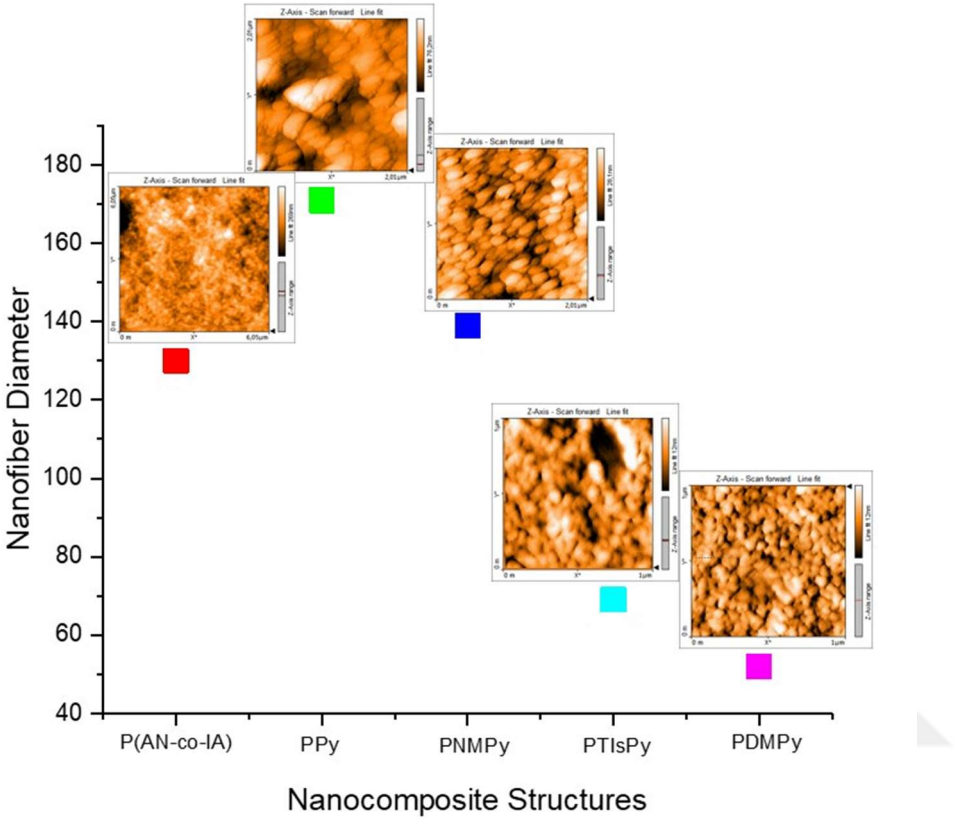

Figure 4.90 : Relation of the average nanoparticle sizes (nm) of P (AN-co-IA) and PPy, PNMPy, PTIsPy, and PDMPy containing nanocomposite structures.

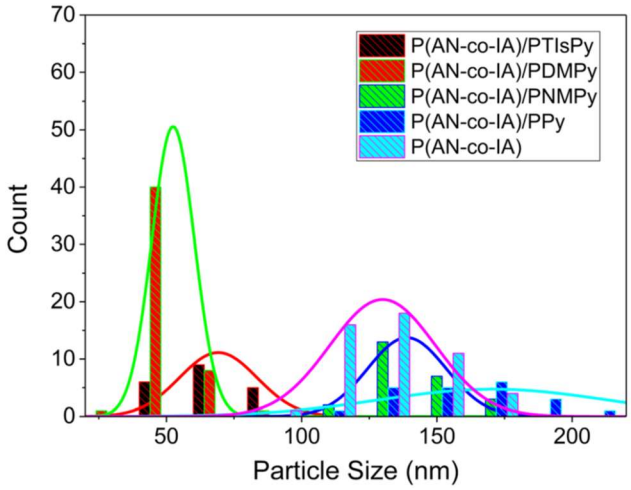

Figure 4.91 : Nanoparticle size distribution of synthesized polymers.

4.7 Results of Coaxial P (AN-co-IA)/AgPPy Nanofibers

4.7.1 Morphology of coaxial P (AN-co-IA)/AgPPy nanofibers (SEM-EDS)

Surface morphologies of PAN (core)/AgPPy (shell) (0.2 ml/h) and P (AN-co-IA)-PAN (core)/AgPPy (shell) (0.2 ml/h) nanofibers were analyzed by SEM and AgNPs existence was confirmed by EDS characterization. Figure 4.92 shows SEM images of PAN (core)/AgPPy (shell) (0.2 ml/h) nanofibers.

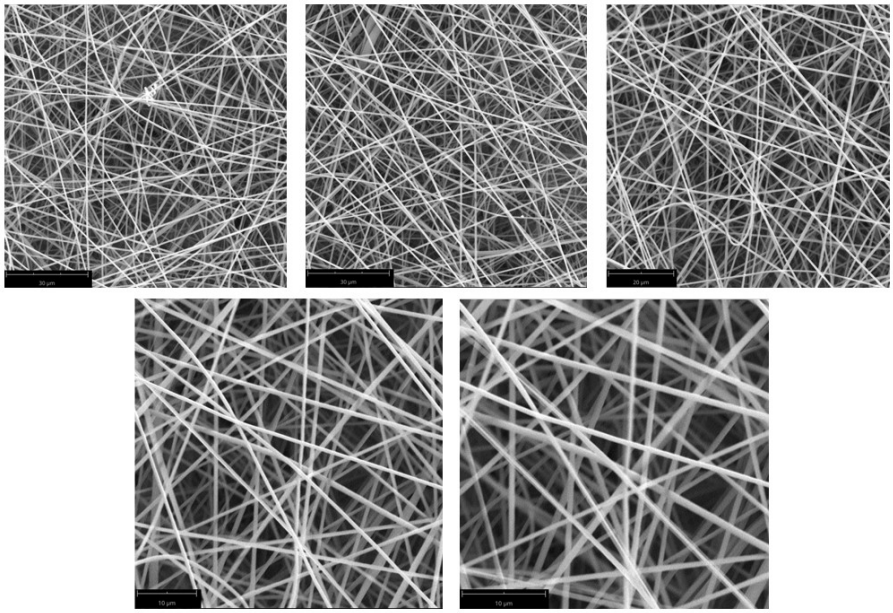

Figure 4.92 : SEM images of PAN (core)/AgPPy (shell) (0.2 ml/h) nanofibers.

As informed from Figure 4.92, the obtained PAN (core)/AgPPy (shell) (0.2 ml/h) nanofibers had bead-free and continuous morphology with an average nanofiber diameter of 515 ± 118 nm (Figure 4.93).

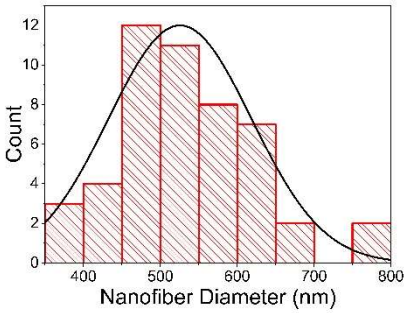

Figure 4.93 : Nanofiber diameter distribution graph of PAN (core)/AgPPy (shell) (0.2 ml/h) nanofibers.

SEM images of P (AN-co-IA)-PAN (core) /AgPPy (shell) (0.2 ml/h) nanofibers and their diameter distribution graph are demonstrated in Figure 4.94 and Figure 4.95 in order.

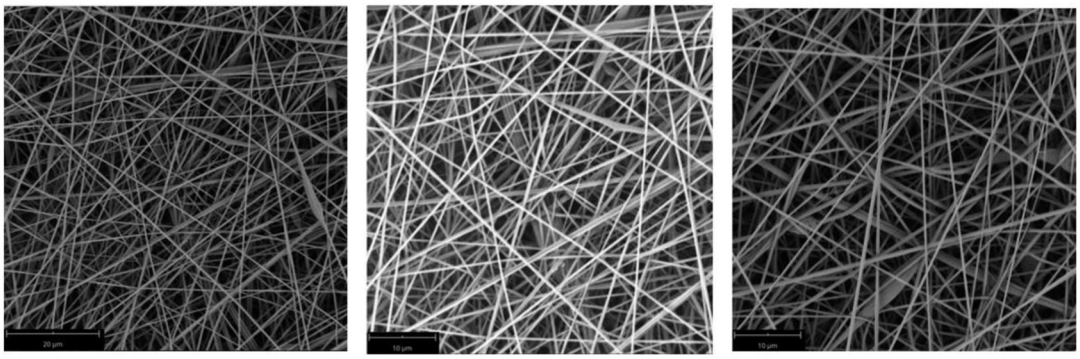

Figure 4.94 : SEM images of P (AN-co-IA)-PAN (core)/AgPPy (shell) nanofibers.

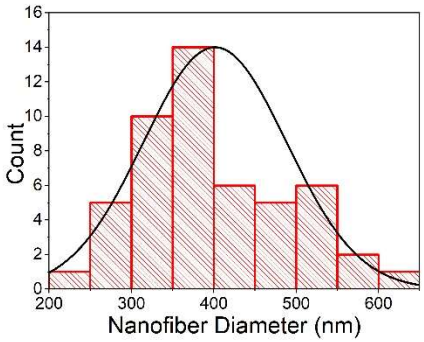

Figure 4.95 : Nanofiber diameter distribution graph of P (AN-co-IA) PAN (core)/AgPPy (shell) (0.2 ml/h) nanofibers.

As in the case of PAN (core)/AgPPy (shell) (0.2 ml/h) nanofibers, P (AN-co-IA)-PAN (core)/AgPPy (shell) (0.2 ml/h) nanofibers also had bead-free and continuous morphology. The average nanofiber diameters were calculated by the same protocol and mentioned as 401±86 nm. It was evaluated that P (AN-co-IA)-PAN (core)/AgPPy (shell) (0.2 ml/h) nanofibers had finer nanofiber diameters which may depend on the presence of IA.

Related to EDS characterization, existence of Ag in PAN (core)/AgPPy (shell) (0.2 ml/h) nanofibers was found to be 3.72 wt % and 0.54 at % while the values were 4.91 wt % and 0.63 at % for P (AN-co-IA)-PAN (core)/AgPPy (shell) (0.2 ml/h) nanofibers.

4.7.2 UV-Visible spectroscopy

UV-visible spectroscopy characterizations of neat PAN and P (AN-co-IA), PAN (core)/AgPPy (shell)(0.2 ml/h) and P (AN-co-IA)-PAN (core)/AgPPy (shell) (0.2 ml/h) nanofibers were performed in the range of 200-1100 nm the results for PAN based nanofibers are shown in Figure 4.96 and for P(AN-co-IA) based nanofibers, they are given in

.

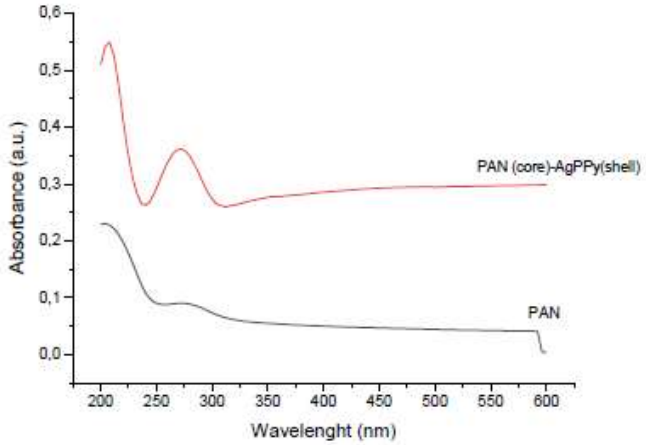

Figure 4.96 : UV-Visible spectroscopy of PAN and PAN (core)/AgPPy (shell) (0.2 ml/h) nanofibers.

It was observed from Figure 4.96 that the peak at 276 nm seen in PAN nanofibers shifted to 271 nm and became sharper in case of AgPPy inclusion. In addition, the broad peak between 310-600 nm confirmed the existence of Ag nanoparticles and informed that the size of the nanoparticles were distributed in a wide of range [258].

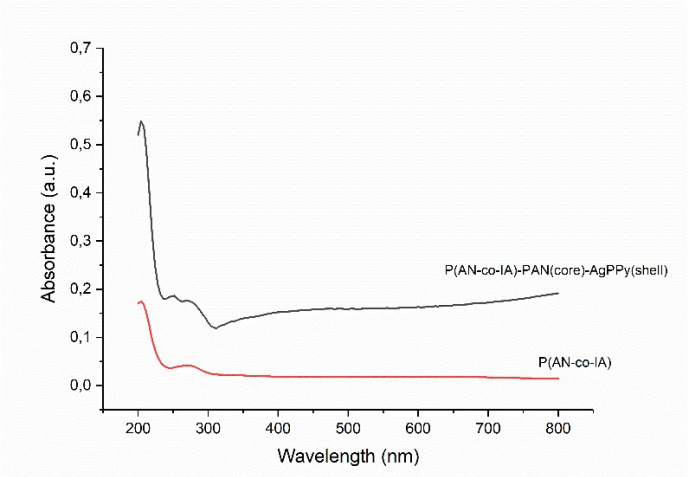

Figure 4.97 : UV-Vis. spectroscopy of P (AN-co-IA) and P (AN-co-IA)-PAN (core)-AgPPy (shell) (0.2 ml/h) nanofibers.

A peak at 272 nm was observed in P(AN-co-IA) nanofibers and shifted to 276 nm in case of AgPPy existence. In addition, a small new peak was detected at 249 nm in P (AN-co-IA)-PAN (core)-AgPPy (shell) (0.2 ml/h) nanofibers. As in

, the presence of Ag was proved by the absorbance curve which was between 311 nm and 600 nm with a maxima at 442 nm. The size of the AgNPs were also distributed in a wide range [259].

4.7.3 FTIR-ATR spectroscopy

FTIR-ATR spectroscopy characterizations were performed in the range of 400 cm^{-1} and 4000 cm^{-1} with the signal resolution of 4 cm^{-1}. FTIR-ATR spectroscopy of PAN, P (AN-co-IA), PAN (core)/AgPPy (shell) and P (AN-co-IA)-PAN (core)/AgPPy (shell) nanofibers are displayed in Figure 4.98.

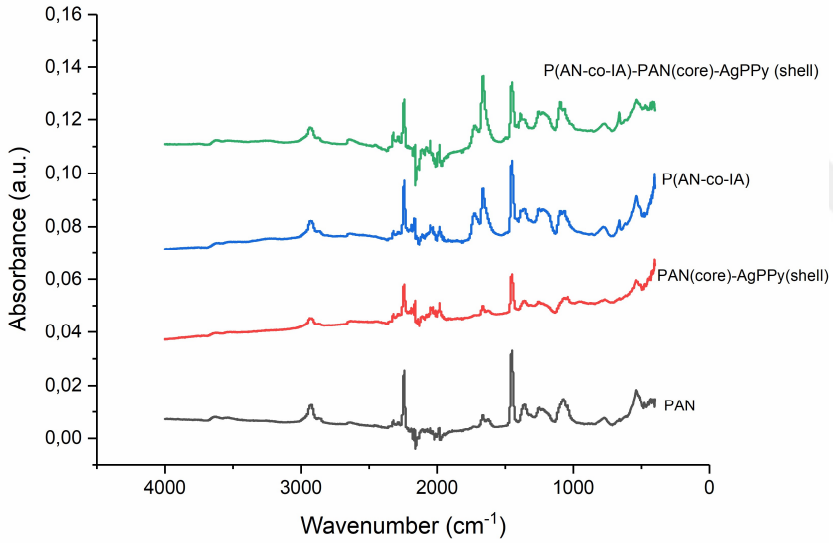

Figure 4.98 : FTIR-ATR spectroscopy of PAN, P (AN-co-IA), PAN (core)/AgPPy (shell) and P (AN-co-IA)-PAN (core)/AgPPy (shell) nanofibers.

Except reduction in absorbance values, no considerable change of peak positions was observed in the nanofibers. The band at 1242 cm^{-1} was assigned to the C-N plane bending and the peak at 1073 cm^{-1} was related to the C-H bending vibration. The specific symmetric and asymmetric stretching absorption bands of C=C, C-N, and aromatic C-H bonds were seen at 1659 cm^{-1}, 1451 cm^{-1} and 1067 cm^{-1}, in order [260]. Due to the presence of IA, an absorbance was seen at 1727 cm^{-1} [202] in P (AN-co-IA)-PAN (core)/AgPPy (shell) (0.2 ml/h) nanofibers. A shoulder was seen between

1947 cm^{-1} and 1789 cm^{-1} due to the presence of AgPPy. Since, that shoulder was not observed in PAN (core)/AgPPy (shell) nanofibers, it could be clearly said that it occured as a result of the interaction of IA and Ag.

4.7.4 DSC

DSC characterizations of PAN(core)/AgPPy (shell) (0.2 ml/h) and P (AN-co-IA)-PAN (core)/AgPPy (shell) (0.2 ml/h) nanofibes were conducted between 0°C and 400°C at a heating rate of 10°C/min in the presence of N_2 atmosphere. Figure 4.99 corresponds to DSC thermograms of PAN(core)/AgPPy(shell) (0.2 ml/h) and P(AN-co-IA)-PAN(core)/AgPPy (shell) (0.2 ml/h) nanofibers.

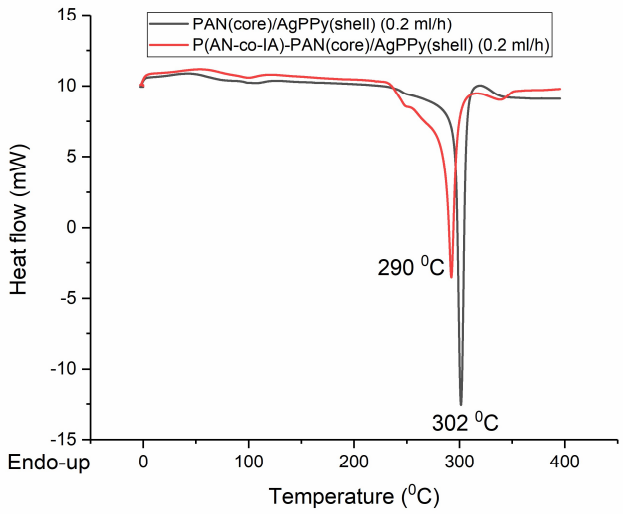

Figure 4.99 : DSC thermograms of PAN(core)/AgPPy (shell) (0.2 ml/h) and P(AN-co-IA)-PAN(core)/AgPPy (shell) (0.2 ml/h) nanofibers.

Figure 4.99 informed that T_c of P (AN-co-IA)-PAN(core)/AgPPy (shell) nanofibers decreased from 302 °C to 290 °C in case of P (AN-co-IA) existence. In case of IA existence in PAN structure, cyclization reactions initiates with an ionic mechanism rather than a radical mechanism and shows doublet exothermic peak with maximum points approximately at 180°C and 310 °C, respectively [30]. However, only a single and distinct peak was observed for P (AN-co-IA)-PAN (core)/AgPPy (shell) nanofibers. That could be explained by the presence of AgPPy.

5. CONCLUSIONS AND RECOMMENDATIONS

In the scope of this thesis, it was aimed to combine metal/metal oxide nanoparticles with novel polymers and obtain functional nanofibrous webs for mainly biological applications. As metal oxide nanoparticles, Fe_3O_4 and Al_2O_3 nanoparticles were utilized whereas as metal nanoparticle silver was preferred. P (AN-co-IA), PAN and P (3HB)/P (3HO-3HD) polymers were the host polymers combined with metal/metal oxide nanoparticles. Nanofiber mats from these functional materials were obtained via both conventional and coaxial electrospinning and detailed charaterizations of each study were performed. The major conclusions can be mentioned as follows:

- P (AN-co-IA), a novel polymer, was synthesized by emulsion polymerization without using any additional surfactant or stabilizer. It was tried to integrate Fe_3O_4 nanoparticles into P (AN-co-IA) polymer and then obtain P (AN-co-IA)/ Fe_3O_4 nanofibers. Optimization studies on finding the appropriate amount of Fe_3O_4 nanoparticles in polymer solutions was determined from the characterization results of PAN/ Fe_3O_4 nanofibers. 5 wt % Fe_3O_4 nanoparticles was identified as the optimum value for stable electrospinning process. Both PAN/ Fe_3O_4 and P (AN-co-IA)/ Fe_3O_4 nanofibers were continuous, smooth and bead-free with fine nanofiber diameters. The presence and effect of Fe_3O_4 nanoparticles were examined by EDS, UV-Visible and FTIR-ATR spectroscopy, and DSC. It was observed that the presence of Fe_3O_4 nanoparticles in P (AN-co-IA) nanofibers altered the thermal and spectroscopic features of the resultant nanofiber web.

- Al_2O_3 nanoparticles were also integrated into P (AN-co-IA) by using the same protocol of Fe_3O_4 studies. However, it was seen that more than 1 wt % of Al_2O_3 nanoparticle loading was not possible due to the beaded structure of the final nanofibers. To this end, in addition to conventional electrospinning, Al_2O_3 nanoparticles were incorporated into P (AN-co-IA) polymer via coaxial electrospinning as shell material by using two (0.2 ml/h and 0.5 ml/h) feed-rates. As expected, the spectroscopy of neat P (AN-co-IA) nanofibers changed

by the addition of Al_2O_3 nanoparticles. Most importantly, thermal decomposition of P(AN-co-IA) nanofibers was enhanced by Al_2O_3 nanoparticles. Moreover, when the nanoparticles were fed to the polymer structure as shell material, the improvements were higher.

- Besides, P (AN-co-IA) polymer, novel P (3HB) and P (3HO-3HD) polymers were also utilized in the thesis. Electrospinnability of P(3HO-3HD) was facilitated by blending with P(3HB). The solubility parameters both for P(3HB) and P(3HO-3HD) were examined and several parameters were evaluated for the eco-friendly electrospinning of P(3HO-3HD). Since, an improved coating method based on silver nanoparticles can be promising for reducing the toxicity while improving the antimicrobial activity, AgNPs were deposited onto P (3HB)/ P (3HO-3HD) nanofibers via dip-coating. Intense and uniform distibution of AgNPs on the nanofiber were achieved by this method. The presence and influence of AgNPs was certified by EDS, UV-Visible and FTIR-ATR spectroscopy, and DSC. Furthermore, immunomodulatory and indirect antimicrobial activity of both the plain and the silver-containing nanofibers were studied in vitro by using HaCaT cells, revealing ability to efficiently act in the wound process. In fact, the most important ILs were modulated in 24 h, and HBD-2 was upregulated with respect to the basal condition of HaCaT cells. Those findings were found to be very suitable in wound dressing applications.

- Beyond supplying AgNPs prepared, they were synthesized in-situ by the help of P (AN-co-IA) and DMF. 10 wt % and 20 wt % $AgNO_3$ (the weight percentage of $AgNO_3$ in the solution was calculated on the basis of P (AN-co-IA) weight) were added to the prepared P(AN-co-IA) solutions. Reduction of $AgNO_3$ to AgNPs was achieved by means of P(AN-co-IA), and DMF without using any additional reductant or process. For comparison, all the experiments were also conducted with PAN polymer. Color change of the solutions confirmed the formation of AgNPs as well as UV-visible spectroscopy, FTIR-ATR spectroscopy, and SEM-EDS analyses. It was observed that P(AN-co-IA) was much more effective on reduction process than PAN. In addition, electrical conductivity of the nanofibers increased dramatically from E^{-13} to E^{-4} related to the presence of silver nanoparticles. The last but not the least, incorporation

of AgNPs to the nanofiber membranes let bactericidal/fungicidal activities against S. aureus, E. coli, P. aeruginosa, and C. albicans for both PAN/Ag and P (AN-co-IA)/Ag nanofibers. The bactericidal/fungicidal activities started at 6–24 h and continued for up to 168 h. P (AN-co-IA)/Ag nanofibers showed satisfying antimicrobial results and can be regarded as good candidates for potential use in the biomedical and pharmaceutical applications.

- In addition to in-situ preparation of AgNPs, reduction of $AgNO_3$ to AgNPs was also achieved via UV-irradition. In this regard, P (AN-co-IA) based polymer solution was used as a core material and $AgNO_3$/DMF solution was fed as a shell material. After coaxial electrospinning, UV-irradiation was applied to the nanofibers for 3 hours (optimized duration) and AgNPs formation was proved via SEM-EDS, UV-Visible spectroscopy and FTIR-ATR spectroscopy. From SEM images, the presence of AgNPs could be seen obviously. That's why, P(AN-co-IA)/Ag nanofibers could be obtained via coaxial electrospinning for the first time with a different AgNPs synthesis method.
- On the other hand, pyrrole and pyrrole derivatives were aimed to utilize with AgNPs. To this end, firstly, pyrrole derivatives (NMPy, 1-(Triisopropylsilyl) pyrrole, and 2,5-dimethylpyrrole) together with pyrrole were polymerized on the polymer matrix (P(AN-co-IA)) via in situ polymerization. Polymerization stages were followed by UV-Vis spectroscopy. Using the absorbances of the UV-Vis and FTIR-ATR characterization results, reactivity of polymerization of pyrrole and pyrrole derivatives were determined as PPy >PNMPy>poly (1-(Triisopropylsilyl) pyrrole) > poly (2,5-dimethylpyrrole). As a additional characterization, Raman spectroscopy was performed to understand the suitability of the nanocomposites for carbon fiber production. Most importantly, this was first time of investigating the morphology of P (AN-co-IA)/PPys via specifically AFM rather than SEM. The nanoparticles containing PPy and PNMPy had larger nanoparticle diameters, whereas nanoparticles containing PDMPy and PTIsPy had smaller nanoparticle diameters. Although, the nanocomposites were seen as oriented nanoparticles in AFM, which was caused by DMF. It was understood that DMF did not dissolve the nanocomposites, rather it helped them to disperse in the solution.

- Since it was not possible to spin P (AN-co-IA), AgNPs and PPy together in a single step, AgPPy synthesis was conducted first. In order to generate AgPPy, $AgNO_3$ was used as a precursor and converted to AgNPs in the presence of Py. Except Py, PNMPy, poly (1-(Triisopropylsilyl) pyrrole) or poly (2,5-dimethylpyrrole) could not be synthesized with $AgNO_3$ since silver-mirror reaction occured. The produced AgPPy was combined with P (AN-co-IA) by the help of coaxial electrospinning. It was fed as a shell material to supply both biological properties and conductivity to the resultant nanofibers. Effect of AgPPy on the resultant nanofibers was determined by SEM-EDS, UV-Visible, FTIR-ATR spectroscopy and DSC characterizations.

  The abovementioned studies showed that AgNPs could be successfully synthesized from $AgNO_3$ by the help of produced P(AN-co-IA) copolymer and DMF in-situ. They could be also be deposited onto the nanofibers via dip-coating or could be introduced via coaxial electrospinning. At the end of all those three experimental procedures, novel and functional nanofibers could be achieved for mainly biological applications such as wound dressing and tissue engineering. Moreover, AgNPs could be combined with conducting polymers in order to alter the properties of the resultant nanofibers and prevent the difficulties on spinning of conducting polymers.

REFERENCES

[1] **Yanilmaz, M., Kalaoglu, F., Karakas, H., and Sarac, A.S.** (2012). Preparation and characterization of electrospun polyurethane-polypyrrole nanofibers and films. *Journal of Applied Polymer Science*, *125*, 4100–4108. doi: 10.1002/app.36386.

[2] **Pintér, E., Patakfalvi, R., Fülei, T., Gingl, Z., Dékány, I. and Visy, C.** (2005). Characterization of polypyrrole-silver nanocomposites prepared in the presence of different dopants. *Journal of Physical Chemistry B*, *109*, 17474. doi: 10.1021/jp0517652.

[3] **Kudryashov, M., Mashin, I., Tyurin, S., Chidichimo, G., and Filpo, G.** (2010). Metal-polymer composite films based on polyacrylonitrile and silver nanoparticles. Preparation and properties. *Journal of Surface Investigation. X-ray, Synchrotron and Neutron Techniques*, *4*(3), 437–441. doi: 10.1134/S1027451010030134.

[4] **Selvam, A.K., and Nallathambi, G.** (2015). Polyacrylonitrile/silver nanoparticle electrospun nanocomposite matrix for bacterial filtration. *Fibers and Polymers*, *16*(6), 1327–1335. doi: 10.1007/s12221-015-1327-8.

[5] **Bajpai, S.K., Chand, N., and Mahendra, M.** (2013). In situ formation of silver nanoparticles in poly(methacrylic acid) hydrogel for antibacterial applications. *Polymer Engineering and Science*, *53* (8) 1751–1759. doi: 10.1002/pen.23424.

[6] **Shi, Y., Li, Y., Zhang, J., Yu, Z., and Yang, D.** (2015). Electrospun polyacrylonitrile nanofibers loaded with silver nanoparticles by silver mirror reaction. *Materials Science and Engineering C*, *51*, 346–355. doi: 10.1016/j.msec.2015.03.010.

[7] **Huang, Z.M., Zhang, Y.Z., Kotaki, M., and Ramakrishna, S.** (2003). A review on polymer nanofibers by electrospinning and their applications in nanocomposites. *Composites Science and Technology*, *63*(15), 2223–2253. doi: 10.1016/S0266-3538(03)00178-7.

[8] **Bhardwaj, N., and Kundu, S.C.** (2010). Electrospinning: A fascinating fiber fabrication technique. *Biotechnology Advances*, *28*(3), 325–347. doi: 10.1016/j.biotechadv.2010.01.004.

[9] **Rahaman, M.S.A., Ismail, A.F., and Mustafa, A.** (2007). A review of heat treatment on polyacrylonitrile fiber. *Polymer Degradation and Stability*, *92*(8), 1421–1432. doi: 10.1016/j.polymdegradstab.2007.03.023.

[10] **Warner, S.B.** (1995). Fiber Science. *Prentice Hall, Englewood Cliffs, N.J.*

[11] **Nataraj, S.K., Yang, K.S., and Aminabhavi, T.M.** (2012). Polyacrylonitrile-based nanofibers - A state-of-the-art review. *Progress in Polymer*

Science (Oxford), *37*(3), 487–513. doi: 10.1016/j.progpolymsci.2011.07.001.

[12] **Sánchez-Soto, P.J., Avilés, M.A., Del Río, J.C., Ginés, J.M., Pascual, J., and Pérez-Rodríguez, J.L.** (2001). Thermal study of the effect of several solvents on polymerization of acrylonitrile and their subsequent pyrolysis. *Journal of Analytical and Applied Pyrolysis*, *58–59*, 155–172. doi: 10.1016/S0165-2370(00)00203-5.

[13] **Xia, Y., and Lu, Y.** (2010). Conductive polymers/polyacrylonitrile composite fibers: Fabrication and properties. *Polymer Composites*, *31*(2), 340–346. doi: 10.1002/pc.20811.

[14] **Wangxi, Z., Jie, L., and Gang, W.** (2003). Evolution of structure and properties of PAN precursors during their conversion to carbon fibers. *Carbon*, *41*(14), 2805–2812. doi: 10.1016/S0008-6223(03)00391-9.

[15] **Bai, Y.J., Wang, C.G., Lun, N., Wang, Y.X., Yu, M.J., and Zhu, B.** (2006). HRTEM microstructures of PAN precursor fibers. *Carbon*, *44*(9), 1773–1778. doi: 10.1016/j.carbon.2005.12.041.

[16] **Bajaj, P.** (1997). *Acrylic Fibers*, In: Gupta V., & Kothari VK, editors Manuf. Fiber Technol. *SPRINGER-SCIENCE+BUSINESS MEDIA, Delhi*; pp 406–456.

[17] **Cho, D.W., and Hong, S.C.** (2019). Synergistic effect of comonomers on the thermal oxidative stabilization of polyacrylonitrile copolymers for carbon materials. *Polymer Degradation and Stability*, *161*, 191–197. doi: 10.1016/j.polymdegradstab.2019.01.027.

[18] **Liu, H., Luo, Q., Zhang, S., Shi, L., Yang, J., Liu, R., …Xu, J.** (2018). New comonomer for polyacrylonitrile-based carbon fiber: Density functional theory study and experimental analysis. *Polymer*, *153*, 369–377. doi: 10.1016/j.polymer.2018.08.041.

[19] **Cai, J.Y., McDonnell, J., Brackley, C., O'Brien, L., Church, J.S., Millington, K., …Phair-Sorensen, N.** (2016). Polyacrylonitrile-based precursors and carbon fibers derived from advanced RAFT technology and conventional methods – The 1st comparative study. *Materials Today Communications*, *9*, 22–29. doi: 10.1016/j.mtcomm.2016.09.001.

[20] **Bhanu, V.A., Rangarajan, P., Wiles, K., Bortner, M., Sankarpandian, M., Godshall, D,. …McGrath, J.E.** (2002). Synthesis and characterization of acrylonitrile methyl acrylate statistical copolymers as melt processable carbon fiber precursors. *Polymer*, *43*(18), 4841–4850. doi: 10.1016/S0032-3861(02)00330-0.

[21] **Mohammady, S.Z., Elkholy, S.S., and Elsabee, M.Z.** (2007). Investigation of the relaxation behavior of novel terpolymers of acrylonitrile, methyl methacylate and indene. *Polymer International*, *56*, 7–13. doi: 10.1002/pi.2100.

[22] **Miller, G.C., Yu, J., Joseph, R.M., Choudhury, S.R., Mecham, S.J., Baird, D.G.,…Riffle, J.S.** (2017). Melt-spinnable polyacrylonitrile copolymer precursors for carbon fibers. *Polymer*, *126*, 87–95. doi: 10.1016/j.polymer.2017.08.023.

[23] **Cetiner, S., Sen, S., Arman, B., and Sarac, A.S.** (2013). Acrylonitrile/vinyl acetate copolymer nanofibers with different vinylacetate content. *Journal of Applied Polymer Science*, *127*(5), 3830–3838. doi: 10.1002/app.37690.

[24] **Rao, M.M., Liu, J.S., Li, W.S., Liang, Y., Liao, Y.H., and Zhao, L.Z.** (2009). Performance improvement of poly(acrylonitrile-vinyl acetate) by activation of poly(methyl methacrylate). *Journal of Power Sources*, *189*, 711–715. doi: 10.1016/j.jpowsour.2008.08.049.

[25] **Ismar, E., and Sarac, A.S.** (2016). Synthesis and characterization of poly (acrylonitrile-co-acrylic acid) as precursor of carbon nanofibers. *Polymers for Advanced Technologies*, *27*(10), 1383–1388. doi: 10.1002/pat.3807.

[26] **Yang, Y., Li, X., Shen, L., Wang, X., and Hsiao, B.S.** (2017). Ionic Cross-Linked Poly(acrylonitrile-co-acrylic acid)/Polyacrylonitrile Thin Film Nanofibrous Composite Membrane with High Ultrafiltration Performance. *Industrial and Engineering Chemistry Research*, *56*(11), 3077–3090. doi: 10.1021/acs.iecr.7b00244.

[27] **Willke, T., and Vorlop, K.D.** (2001). Biotechnological production of itaconic acid. *Applied Microbiology and Biotechnology*, *56*(3–4), 289–295. doi: 10.1007/s002530100685.

[28] **Nguyen-Thai, N.U., and Hong, S.C.** (2014). Controlled architectures of poly(acrylonitrile-co-itaconic acid) for efficient structural transformation into carbon materials. *Carbon*, *69*, 571–581. doi: 10.1016/j.carbon.2013.12.068.

[29] **Devasia, R., Reghunadhan Nair, C.P., Sivadasan, P., Katherine, B.K., and Ninan, K.N.** (2003). Cyclization reaction in poly(acrylonitrile/itaconic acid) copolymer: An isothermal differential scanning calorimetry kinetic study. *Journal of Applied Polymer Science*, *88*(4), 915–920. doi: 10.1002/app.11706.

[30] **Ouyang, Q., Cheng, L., Wang, H., and Li, K.** (2008). Mechanism and kinetics of the stabilization reactions of itaconic acid-modified polyacrylonitrile. *Polymer Degradation and Stability*, *93*(8), 1415–1421. doi: 10.1016/j.polymdegradstab.2008.05.021.

[31] **Yu, M., Wang, C., Zhao, Y., Zhang, M., and Wang, W.** (2010). Thermal properties of acrylonitrile/itaconic acid polymers in oxidative and nonoxidative atmospheres. *Journal of Applied Polymer Science*, *116*, 1207–1212. doi: 10.1002/app.31664.

[32] **Hao, J., Wei, H., Lu, C., and Liu, Y.** (2019). New aspects on the cyclization mechanisms of Poly(acrylonitrile-co-itaconic acid). *European Polymer Journal*, *121*(June), 109313. doi: 10.1016/j.eurpolymj.2019.109313.

[33] **Ismar, E., Micusik, M., Gergin, I., Omastova, M., and Sarac, A.S.** (2020). Thermal stabilization of poly(acrylonitrile-co-itaconic acid) nanofibers as carbon nanofiber precursor. *Polymer Degradation and Stability*, *175*. doi: 10.1016/j.polymdegradstab.2020.109142.

[34] **Fu, Z., Liu, B., Deng, Y., Ma, J., Cao, C., Wang, J., …Zhang, H.** (2016). The

suitable itaconic acid content in polyacrylonitrile copolymers used for PAN-based carbon fibers. *Journal of Applied Polymer Science*, *133*(38), 1–10. doi: 10.1002/app.43919.

[35] **Ghorpade, R. V., Lee, S., and Hong, S.C.** (2020). Effect of different itaconic acid contents of poly(acrylonitrile-co-itaconic acid)s on their carbonization behaviors at elevated temperatures. *Polymer Degradation and Stability*, *181*, 109373. doi: 10.1016/j.polymdegradstab.2020.109373.

[36] **Zhang, H., Quan, L., Gao, A., Tong, Y., and Shi, F.** (2020). Thermal Analysis and Crystal Structure of Poly(Acrylonitrile-Co-Itaconic Acid) Copolymers Synthesized in Water*12*(1), 221–235.

[37] **Devasia, R., Reghunadhan Nair, C.P., and Ninan, K.N.** (2002). Solvent and kinetic penultimate unit effects in the copolymerization of acrylonitrile with itaconic acid. *European Polymer Journal*, *38*(10), 2003–2010. doi: 10.1016/S0014-3057(02)00086-1.

[38] **Zhao, Y., Wang, C., Yu, M., Cui, C., Wang, Q., and Zhu, B.** (2009). Study on monomer reactivity ratios of acrylonitrile/itaconic acid in aqueous deposited copolymerization system initiated by ammonium persulfate. *Journal of Polymer Research*, *16*(4), 437–442. doi: 10.1007/s10965-008-9246-7.

[39] **Fu, Z., Liu, B., and Zhang, H.** (2017). Study on thermal oxidative stabilization reactions of poly(acrylonitrile-co-itaconic acid) copolymers synthesized at different polymerization stages. *Journal of Applied Polymer Science*, *134*(35), 45245. doi: 10.1002/app.45245.

[40] **Nida, N., Subri, S., Aziera, N., Nur, H., Faujan, H., Nurul, S., and Jamil, A.** (2019). Preparation Of Chemically Modified Poly (Acrylonitrile-Co-Itaconic Acid) Non-Woven Fibers. *Journal of Multidisciplinary Engineering Science and Technology, 6*(12), 121–125.

[41] **Abeykoon, N.C., Mahmood, S.F., Yang, D.J., and Ferraris, J.P.** (2019). Electrospun poly(acrylonitrile-co-itaconic acid) as a porous carbon precursor for high performance supercapacitor: Study of the porosity induced by in situ porogen activity of itaconic acid. *Nanotechnology*, *30*(43), 435401. doi: 10.1088/1361-6528/ab32c0.

[42] **Sanhueza, C., Acevedo, F., Rocha, S., Villegas, P., Seeger, M., and Navia, R.** (2019). Polyhydroxyalkanoates as biomaterial for electrospun scaffolds. *International Journal of Biological Macromolecules*, *124*, 102–110. doi: 10.1016/j.ijbiomac.2018.11.068.

[43] **Raza, Z.A., Abid, S., and Banat, I.M.** (2018). Polyhydroxyalkanoates: Characteristics, production, recent developments and applications. *International Biodeterioration and Biodegradation*, *126*(January 2017), 45–56. doi: 10.1016/j.ibiod.2017.10.001.

[44] **Brigham, C. J., and Sinskey, A. J.** (2012). Applications of Polyhydroxyalkanoates in the Medical Industry. *International Journal of Biotechnology for Wellness Industries*, *1*, 53–60. doi: 10.6000/1927-3037.2012.01.01.03.

[45] **Masood, F., Yasin, T., and Hameed, A.** (2015). Polyhydroxyalkanoates – What are the uses? Current challenges and perspectives. *Critical Reviews in Biotechnology*, *35*(4), 514–521. doi: 10.3109/07388551.2014.913548.

[46] **Li, W., Cicek, N., Levin, D.B., and Liu, S.** (2019). Enabling electrospinning of medium-chain length polyhydroxyalkanoates (PHAs) by blending with short-chain length PHAs. *International Journal of Polymeric Materials and Polymeric Biomaterials*, *68*(9), 499–509. doi: 10.1080/00914037.2018.1466136.

[47] **Vigneswari, S., Chai, J.M., Shantini, K., Bhubalan, K., and Amirul, A.A.** (2019). Designing novel interfaces via surface functionalization of short-chain-length polyhydroxyalkanoates. *Advances in Polymer Technology*, *2019*, 1–15. doi: 10.1155/2019/3831251.

[48] **Ali, I., and Jamil, N.** (2016). Polyhydroxyalkanoates: Current applications in the medical field. *Frontiers in Biology*, *11*(1), 19–27. doi: 10.1007/s11515-016-1389-z.

[49] **Kalia, V.C.** (2019). Biotechnological applications of polyhydroxyalkanoates. *Biotechnological Applications of Polyhydroxyalkanoates*, 1–420. doi: 10.1007/978-981-13-3759-8.

[50] **Ray, S., and Kalia, V.C.** (2017). Biomedical Applications of Polyhydroxyalkanoates. *Indian Journal of Microbiology*, *57*(3), 261–269. doi: 10.1007/s12088-017-0651-7.

[51] **Sudesh, K., Abe, H., and Doi, Y.** (2000). Synthesis, structure and properties of polyhydroxyalkanoates: Biological polyesters. *Progress in Polymer Science (Oxford)*, *25*(10), 1503–1555. doi: 10.1016/S0079-6700(00)00035-6.

[52] **O'Connor, S., Szwej, E., Nikodinovic-Runic, J., O'Connor, A., Byrne, A.T., Devocelle, M., … O'Connor, K.E.** (2013). The anti-cancer activity of a cationic anti-microbial peptide derived from monomers of polyhydroxyalkanoate. *Biomaterials*, *34*(11), 2710–2718. doi: 10.1016/j.biomaterials.2012.12.032.

[53] **Shishatskaya, E.I., Khlusov, I.A., and Volova, T.G.** (2006). A hybrid PHB-hydroxyapatite composite for biomedical application: Production, in vitro and in vivo investigation. *Journal of Biomaterials Science, Polymer Edition*, *17*(5), 481–498. doi: 10.1163/156856206776986242.

[54] **Li, X.T., Zhang, Y., and Chen, G.Q.** (2008). Nanofibrous polyhydroxyalkanoate matrices as cell growth supporting materials. *Biomaterials*, *29*(27), 3720–3728. doi: 10.1016/j.biomaterials.2008.06.004.

[55] **Xu, X.Y., Li, X.T., Peng, S.W., Xiao, J.F., Liu, C., Fang, G.,…Chen, G.Q.** (2010). The behaviour of neural stem cells on polyhydroxyalkanoate nanofiber scaffolds. *Biomaterials*, *31*, 3967–3975. doi: 10.1016/j.biomaterials.2010.01.132.

[56] **Lu, X., Wang, L., Yang, Z., and Lu, H.** (2013). Strategies of polyhydroxyalkanoates modification for the medical application in neural regeneration/nerve tissue engineering. *Advances in Bioscience and Biotechnology*, *04*(06), 731–740. doi: 10.4236/abb.2013.46097.

[57] **Sudesh, K., Lee, Y.-F., Sridewi, N., and Ramanathan, S.** (2016). The Influence of Electrospinning Parameters and Drug Loading on Polyhydroxyalkanoate (PHA) Nanofibers for Drug Delivery. *International Journal of Biotechnology for Wellness Industries*, *4*(4), 103–113. doi: 10.6000/1927-3037.2015.04.04.1.

[58] **Li, W., Cicek, N., Levin, D.B., Logsetty, S., and Liu, S.** (2020). Bacteria-triggered release of a potent biocide from core-shell polyhydroxyalkanoate (PHA)-based nanofibers for wound dressing applications. *Journal of Biomaterials Science, Polymer Edition*, *31*(3), 394–406. doi: 10.1080/09205063.2019.1693882.

[59] **Drew, C., Liu, X., Ziegler, D., Wang, X., Bruno, F.F., Whitten, J., …Kumar, J.** (2003). Metal oxide-coated polymer nanofibers. *Nano Letters*, *3*(2), 143–147. doi: 10.1021/nl025850m.

[60] **Arora, A.K., Jaswal, V.S., Singh, K., and Singh, R.** (2016). Applications of metal/mixed metal oxides as photocatalyst: A review. *Oriental Journal of Chemistry*, *32*(4), 2035–2042. doi: 10.13005/ojc/320430.

[61] **Zia, M., Phull, A.R., and Ali, J.S.** (2016). Challenges of Iron Oxide Nanoparticles. *Powder Technology*, *7*(6), 49–67.

[62] **Zhang, D., Karki, A.B., Rutman, D., Young, D.P., Wang, A., Cocke, D., …Guo, Z.** (2009). Electrospun polyacrylonitrile nanocomposite fibers reinforced with Fe_3O_4 nanoparticles: fabrication and property analysis. *Polymer*, *50*(17), 4189–4198. doi: 10.1016/j.polymer.2009.06.062.

[63] **Guo, J., Ye, X., Liu, W., Wu, Q., Shen, H., and Shu, K.** (2009). Preparation and characterization of poly(acrylonitrile-co-acrylic acid) nanofibrous composites with Fe_3O_4 magnetic nanoparticles. *Materials Letters*, *63*(15), 1326–1328. doi: 10.1016/j.matlet.2009.02.068.

[64] **Sabzroo, N., Bastami, T.R., Karimi, M., and Heidari, T.** (2019). Optimization of Electrospinning Conditions for Magnetic Poly (acrylonitrile- co-acrylic acid) Nanofibers*9*(2), 301–315. doi: 10.22052/JNS.2019.02.012.

[65] **Liu, Q., Zhong, L., Bin. Zhao, Q.B., Frear, C., and Zheng, Y.M.** (2015). Synthesis of Fe_3O_4/Polyacrylonitrile Composite Electrospun Nanofiber Mat for Effective Adsorption of Tetracycline. *ACS Applied Materials and Interfaces*, *7*(27), 14573–14583. doi: 10.1021/acsami.5b04598.

[66] **Tingting, H.E., Dawei, L.I., Fenglin, H., Qufu, W.E.I., and Xiaoling, W.** (1989). Electromagnetic properties of Hollow PAN / Fe_3O_4 composite nanofibers via Coaxial Electrospinning, *46*(51006046), 1–8.

[67] **Huang, F., Zhang, H., Shi, J., Chen, F., Cai, Y., and Wei, Q.** (2012). Preparation and characterization of polyaniline/ Fe_3O_4-polyacrylonitrile composite nanofibers. *International Journal of Materials Research*, *103*(11), 1390–1394. doi: 10.3139/146.110770.

[68] **Ourang, A., Pilehvar, S., Mortezaei, M., and Damircheli, R.** (2017). Effect of aluminum doped iron oxide nanoparticles on magnetic properties of the polyacrylonitrile nanofibers. *Journal of Polymer Engineering*, *37*(2), 135–141. doi: 10.1515/polyeng-2015-0303.

[69] **Ghapanvari, M., Madrakian, T., Afkhami, A., and Ghoorchian, A.** (2020). A modified carbon paste electrode based on Fe_3O @multi-walled carbon nanotubes@polyacrylonitrile nanofibers for determination of imatinib anticancer drug. *Journal of Applied Electrochemistry*, *50*(2), 281–294. doi: 10.1007/s10800-019-01388-x.

[70] **Hayes, K.L., Mui, J., Song, B., Sani, E.S., Eisenman, S.W., Sheffield, J.B., and Kim, B.** (2020). Effects, uptake, and translocation of aluminum oxide nanoparticles in lettuce: A comparison study to phytotoxic aluminum ions. *Science of the Total Environment*, *719*, 137393–137493. doi: 10.1016/j.scitotenv.2020.137393.

[71] **Azad, A.M.** (2006). Fabrication of transparent alumina (Al_2O_3) nanofibers by electrospinning. *Materials Science and Engineering A*, *435–436*, 468–473. doi: 10.1016/j.msea.2006.07.075.

[72] **Shehata, F., Fathy, A., Abdelhameed, M., and Moustafa, S.F.** (2009). Preparation and properties of Al_2O_3 nanoparticle reinforced copper matrix composites by in situ processing. *Materials and Design*, *30*(7), 2756–2762. doi: 10.1016/j.matdes.2008.10.005.

[73] **Peng, L., Xu, X., Lv, Z., Song, J., He, M., Wang, Q., …Li, Z.** (2012). Thermal and morphological study of Al_2O_3 nanofibers derived from boehmite precursor. *Journal of Thermal Analysis and Calorimetry*, *110*(2), 749–754. doi: 10.1007/s10973-011-1962-2.

[74] **Dadvar, S., Tavanai, H., and Morshed, M.** (2012). Effect of embedding MgO and Al_2O_3 nanoparticles in the precursor on the pore characteristics of PAN based activated carbon nanofibers. *Journal of Analytical and Applied Pyrolysis*, *98*, 98–105. doi: 10.1016/j.jaap.2012.08.001.

[75] **Broujeni, B.R., and Nilchi, A.** (2018). Preparation and characterization of polyacrylonitrile/aluminum oxide nanofiber adsorbent modified with 2-amino-3-methyl-1-hexanethiol for the adsorption of thorium (IV) ion from aqueous solution. *Journal of Environmental Engineering*, *144*(10), 04018099. doi: 10.1061/(asce)ee.1943-7870.0001446.

[76] **Ke, H., and Li, Y.** (2018). The effects of using aluminum oxide nanoparticles as heat transfer fillers on morphology and thermal performances of form-stable phase change fibrous membranes based on capric–palmitic–stearic acid ternary eutectic/polyacrylonitrile composite. *Materials*, *11*(9), 1785. doi: 10.3390/ma11091785.

[77] **Fu, W., Li, Z., Xu, W., Wang, Y., Sun, Y., and Dai, Y.** (2020). Exceptionally thermal-stable Al_2O_3/TiO_2 nanofibers by depressing surface-initiated grain growth as new supports for anti-sintering Pt nanoparticles. *Materials Today Nano*, *11*, 100088. doi: 10.1016/j.mtnano.2020.100088.

[78] **Sondi, I., and Salopek-Sondi, B.** (2004). Silver nanoparticles as antimicrobial agent: a case study on e. coli as a model for gram-negative bacteria. *Journal of Colloid and Interface Science*, *275* (1), 177-182. doi: 10.1016/j.jcis.2004.02.012.

[79] **Martínez-Castañón, G.A., Niño-Martínez, N., Martínez-Gutierrez, F., Martínez-Mendoza, J.R., and Ruiz, F.** (2008). Synthesis and

antibacterial activity of silver nanoparticles with different sizes. *Journal of Nanoparticle Research*, *10*, 1343-1348. doi: 10.1007/s11051-008-9428-6.

[80] **Guzman, M., Dille, J., and Godet, S.** (2012). Synthesis and antibacterial activity of silver nanoparticles against gram-positive and gram-negative bacteria. *Nanomedicine: Nanotechnology, Biology, and Medicine*, *8* (1), 37-45. doi: 10.1016/j.nano.2011.05.007.

[81] **Lara, H.H., Garza-Treviño, E.N., Ixtepan-Turrent, L., and Singh, D.K.,** (2011). Silver nanoparticles are broad-spectrum bactericidal and virucidal compounds. *Journal of Nanobiotechnology, 9*, 30. https://doi.org/10.1186/1477-3155-9-30

[82] **Lara, H.H., Ayala-Nuñez, N. V., Ixtepan-Turrent, L., and Rodriguez-Padilla, C.** (2010). Mode of antiviral action of silver nanoparticles against HIV-1. *Journal of Nanobiotechnology*, *8*(1), 1–10. doi: 10.1186/1477-3155-8-1.

[83] **Manea, F., Motoc, S., Pop, A., Remes, A., and Schoonman, J.** (2012). Silver-functionalized carbon nanofiber composite electrodes for ibuprofen detection. *Nanoscale Research Letters*, *7*, 331. doi: 10.1186/1556-276X-7-331.

[84] **Rodríguez-León, E., Iñiguez-Palomares, R., Navarro, R.E., Herrera-Urbina, R., Tánori, J., Iñiguez-Palomares, C., and Maldonado, A.** (2013). Synthesis of silver nanoparticles using reducing agents obtained from natural sources (Rumex hymenosepalus extracts). *Nanoscale Research Letters*, *8*, 318. doi: 10.1186/1556-276X-8-318.

[85] **Kim, K.J., Sung, W.S., Suh, B.K., Moon, S.K., Choi, J.S., Kim, J.G., and Lee, D.G.** (2009). Antifungal activity and mode of action of silver nano-particles on Candida albicans. *BioMetals*, *22*(2), 235–242. doi: 10.1007/s10534-008-9159-2.

[86] **Jo, Y.K., Kim, B.H., and Jung, G.** (2009). Antifungal activity of silver ions and nanoparticles on phytopathogenic fungi. *Plant Disease*, *93*(10), 1037–1043. doi: 10.1094/PDIS-93-10-1037.

[87] **Panáček, A., Kolář, M,. Večeřová, R., Prucek, R., Soukupová, J., Kryštof, V., …Kvítek, L.** (2009). Antifungal activity of silver nanoparticles against Candida spp. *Biomaterials*, *30*(31), 6333–6340. doi: 10.1016/j.biomaterials.2009.07.065.

[88] **Zhang, S., Tang, Y., and Vlahovic, B.** (2016). A Review on Preparation and Applications of Silver-Containing Nanofibers. *Nanoscale Research Letters*, *11*(1), 1–8. doi: 10.1186/s11671-016-1286-z.

[89] **Tolaymat, T.M., El Badawy, A.M., Genaidy, A., Scheckel, K.G., Luxton, T.P,. and Suidan, M.** (2010). An evidence-based environmental perspective of manufactured silver nanoparticle in syntheses and applications: A systematic review and critical appraisal of peer-reviewed scientific papers. *Science of the Total Environment*, *408*(5), 999–1006. doi: 10.1016/j.scitotenv.2009.11.003.

[90] **Creighton, J.A., Blatchford, C.G., and Albrecht, M.G.** (1979). Plasma

resonance enhancement of Raman scattering by pyridine adsorbed on silver or gold sol particles of size comparable to the excitation wavelength. *Journal of the Chemical Society, Faraday Transactions 2: Molecular and Chemical Physics*, *75*, 790-798. doi: 10.1039/F29797500790.

[91] **Sui, Z., Chen, X., Wang, L., Chai, Y., Yang, C., and Zhao, J.** (2005). An improved approach for synthesis of positively charged silver nanoparticles. *Chemistry Letters*, *34*(1), 100-101. doi: 10.1246/cl.2005.100.

[92] **Shi, Y., Lv, L., and Wang, H.** (2009). A facile approach to synthesize silver nanorods capped with sodium tripolyphosphate. *Materials Letters*, *63*(30), 2698-2700. doi: 10.1016/j.matlet.2009.09.046.

[93] **Horiuchi, Y., Shimada, M., Kamegawa, T., Mori, K., and Yamashita, H.** (2009). Size-controlled synthesis of silver nanoparticles on Ti-containing mesoporous silica thin film and photoluminescence enhancement of rhodamine 6G dyes by surface plasmon resonance. *Journal of Materials Chemistry*, *19*, 6745-6749. doi: 10.1039/b910474g.

[94] **Zielińska, A., Skwarek, E., Zaleska, A., Gazda, M., and Hupka, J.** (2009). Preparation of silver nanoparticles with controlled particle size. *Procedia Chemistry, 1*(2), 1560-1566. doi.org/10.1016/j.proche.2009.11.004

[95] **Henglein, A., and Giersig, M.** (1999). Formation of colloidal silver nanoparticles: capping action of citrate arnim henglein. *Journal of Physical Chemistry B*, *103* (44), 9533-9539. doi: 10.1021/jp9925334.

[96] **Pietrobon, B., and Kitaev, V.** (2008). Photochemical synthesis of monodisperse size-controlled silver decahedral nanoparticles and their remarkable optical properties. *Chemistry of Materials*, *20*(16), 5186-5190. doi: 10.1021/cm800926u.

[97] **Mayer, A.B.R., Hausner, S.H., and Mark, J.E.** (2000). Colloidal silver nanoparticles generated in the presence of protective cationic polyelectrolytes. *Polymer Journal*, *32*, 15-22. doi: 10.1295/polymj.32.15.

[98] **Yoosaf, K., Ipe, B.I., Suresh, C.H., and Thomas, K.G.** (2007). In situ synthesis of metal nanoparticles and selective naked-eye detection of lead ions from aqueous media. *Journal of Physical Chemistry C*, *111*(34), 12839–12847. doi: 10.1021/jp073923q.

[99] **Chou, K., and Lai, Y.S.** (2004). Effect of polyvinyl pyrrolidone molecular weights on the formation of nanosized silver colloids. *Materials Chemistry and Physics*, *83*(1), 82-88. doi: 10.1016/j.matchemphys.2003.09.026.

[100] **Chou, K. Sen., Lu, Y.C., and Lee, H.H.** (2005). Effect of alkaline ion on the mechanism and kinetics of chemical reduction of silver. *Materials Chemistry and Physics*, *94* (2-3), 429-433. doi: 10.1016/j.matchemphys.2005.05.029.

[101] **Durán, N., Cuevas, R. ,Cordi, L., Rubilar, O., and Diez, M.C.** (2014). Biogenic silver nanoparticles associated with silver chloride nanoparticles (Ag@AgCl) produced by laccase from Trametes versicolor. *SpringerPlus*, *3*, 645. doi: 10.1186/2193-1801-3-645.

[102] **Naik, R.R., Stringer, S.J., Agarwal, G., Jones, S.E., and Stone, M.O.** (2002). Biomimetic synthesis and patterning of silver nanoparticles. *Nature Materials*,*1*, 169-172. doi: 10.1038/nmat758.

[103] **Wang, H., Qiao, X., Chen, J., Wang, X., and Ding, S.** (2005). Mechanisms of PVP in the preparation of silver nanoparticles. *Materials Chemistry and Physics*, *94*(2-3), 449-453. doi.org/10.1016/j.matchemphys.2005.05.005

[104] **Chaudhary, A., Gupta, A., Mathur, R.B., and Dhakate, S.R.** (2014). Effective antimicrobial filter from electrospun polyacrylonitrile-silver composite nanofibers membrane for conducive environment. *Advanced Materials Letters*, *5*(10), 562–568. doi: 10.5185/amlett.2014.572.

[105] **Masood, N., Ahmed, R., Tariq, M., Ahmed, Z., Masoud, M.S., Ali, I., …Hasan, A.** (2019). Silver nanoparticle impregnated chitosan-PEG hydrogel enhances wound healing in diabetes induced rabbits. *International Journal of Pharmaceutics*, *559*, 23-36. doi: 10.1016/j.ijpharm.2019.01.019.

[106] **Zhang, Z., Zhang, L., Wang, S., Chen, W., and Lei, Y.** (2001). A convenient route to polyacrylonitrile/silver nanoparticle composite by simultaneous polymerization-reduction approach. *Polymer*, *42*(19), 8315–8318. doi: 10.1016/S0032-3861(01)00285-3.

[107] **Wang, J.Z., Chen, Q.W., Zhou, J.P., Lei, Y.X., and Menke, N.** (2019). Two-step hydrothermal fabrication of Na0.23TiO2 nanofibers and enhanced photocatalysis after loaded with gold or silver determined by surface potentials. *International Journal of Energy Research*, *43*(9), 4062-4073. doi: 10.1002/er.4466.

[108] **Yao, Y., Shen, L., Wei, A., Wang, T., and Chen, S.** (2019). Facile synthesis, microstructure, photo-catalytic activity, and anti-bacterial property of the novel Ag@gelatin–silica hybrid nanofiber membranes. *Journal of Sol-Gel Science and Technology*, *89*, 651-662. doi: 10.1007/s10971-018-04914-z.

[109] **Wang, Y., Yang, Q., Shan, G., Wang, C., Du, J., Wang, S., …Wei, Y.** (2005). Preparation of silver nanoparticles dispersed in polyacrylonitrile nanofiber film spun by electrospinning. *Materials Letters*, *59*(24–25), 3046–3049. doi: 10.1016/j.matlet.2005.05.016.

[110] **Selvam, A.K., and Nallathambi, G.** (2015). Polyacrylonitrile/silver nanoparticle electrospun nanocomposite matrix for bacterial filtration. *Fibers and Polymers*, *16*(6), 1327–1335. doi: 10.1007/s12221-015-1327-8.

[111] **Bortolassi, A.C.C., Nagarajan, S., de Araújo Lima, B., Guerra, V.G., Aguiar, M.L., Huon, V.,…Bechelany, M.** (2019). Efficient nanoparticles removal and bactericidal action of electrospun nanofibers membranes for air filtration. *Materials Science and Engineering C*,

102(April), 718–729. doi: 10.1016/j.msec.2019.04.094.

[112] **Ren, S., Dong, L., Zhang, X., Lei, T., Ehrenhauser, F., Song, K.,…Wu, Q.** (2017). Electrospun nanofibers made of silver nanoparticles, cellulose nanocrystals, and polyacrylonitrile as substrates for surface-enhanced raman scattering. *Materials*, *10*(68), 1–12. doi: 10.3390/ma10010068.

[113] **Wang, S., Bai, J., Li, C., and Zhang, J.** (2012). Functionalization of electrospun β-cyclodextrin/polyacrylonitrile (PAN) with silver nanoparticles: Broad-spectrum antibacterial property. *Applied Surface Science*, *261*, 499–503. doi: 10.1016/j.apsusc.2012.08.044.

[114] **Karbownik, I., Rac, O., Fiedot, M., Suchorska-Woźniak, P., and Teterycz, H.** (2015). In situ preparation of silver-polyacrylonitrile nanocomposite fibres. *European Polymer Journal*, *69*, 385–395. doi: 10.1016/j.eurpolymj.2015.06.024.

[115] **Siyanbola, T.O., Gurunathan, T., Akinsola, A.F., Adekoya, J.A., Akinsiku, A.A., Aladesuyi, O.,…Nayak, S.K.** (2016). Antibacterial and morphological studies of electrospun silver-impregnated polyacrylonitrile nanofibre. *Oriental Journal of Chemistry*, *32*(1), 159–164. doi: 10.13005/ojc/320116.

[116] **Huang, T.M., Pang, F., Hsieh, I.F., and Cakmak, M.** (2016). Control of radial structural gradient in PAN/silver nanofibers using solvent vapor treatment. *Synthetic Metals*, *221*, 309–318. doi: 10.1016/j.synthmet.2016.09.009.

[117] **Sichani, G.N., Morshed, M., Amirnasr, M., and Abedi, D.** (2010). In situ preparation, electrospinning, and characterization of polyacrylonitrile nanofibers containing silver nanoparticles. *Journal of Applied Polymer Science*, *116*(2), 1021–1029. doi: 10.1002/app.31436.

[118] **Phan, D.N., Dorjjugder, N., Saito, Y., Taguchi, G., Ullah, A., Kharaghani, D., and Kim, I.S.** (2020). The synthesis of silver-nanoparticle-anchored electrospun polyacrylonitrile nanofibers and a comparison with as-spun silver/polyacrylonitrile nanocomposite membranes upon antibacterial activity. *Polymer Bulletin*, *77*(8), 4197–4212. doi: 10.1007/s00289-019-02969-8.

[119] **Kudryashov, M.A., Mashin, A.I., Tyurin, A.S., Chidichimo, G., and De Filpo, G.** (2010). Metal-polymer composite films based on polyacrylonitrile and silver nanoparticles. preparation and properties. *Journal of Surface Investigation*, *4*(3), 437–441. doi: 10.1134/S1027451010030134.

[120] **Tyurin, A., de Filpo, G., Cupelli, D., Nicoletta, F.P., Mashin, A., and Chidichimo, G.** (2010). Particle size tuning in silver-polyacrylonitrile nanocomposites. *Express Polymer Letters*, *4*(2), 71–78. doi: 10.3144/expresspolymlett.2010.12.

[121] **Mahapatra, A., Garg, N.,, Nayak, B.P. Mishra, B.G., and Hota, G.** (2012). Studies on the synthesis of electrospun PAN-Ag composite nanofibers for antibacterial application. *Journal of Applied Polymer Science*, *124*, 1178–1185. doi: 10.1002/app.35076.

[122] **Zhang, G., Xiao, Y., Yin, Q., Yan, J., Zang, C., and Zhang, H.** (2021). In Situ Synthesis of Silver Nanoparticles on Amino-Grafted Polyacrylonitrile Fiber and Its Antibacterial Activity. *Nanoscale Research Letters*, *16*(36), 1–9. doi: 10.1186/s11671-021-03496-0.

[123] **Shirakawa, H., Louis, E.J., MacDiarmid, A.G., Chiang, C.K., and Heeger, A.J.** (1977). Synthesis of electrically conducting organic polymers: Halogen derivatives of polyacetylene, (CH)x. *Journal of the Chemical Society, Chemical Communications*, *16*, 578-580. doi: 10.1039/C39770000578.

[124] **Svirskis, D., Travas-Sejdic, J.,, Rodgers, A. and Garg, S.** (2010). Electrochemically controlled drug delivery based on intrinsically conducting polymers. *Journal of Controlled Release*, *146*(1), 6-15. doi.org/10.1016/j.jconrel.2010.03.023

[125] **Baskan, H., Ismar, E., Karakas, H., and Sarac, A.S.** (2020). Nanocomposite structures of polypyrrole derivatives and poly (acrylonitrile-co-itaconic acid) produced by in situ polymerization as carbon nanofiber precursor. *Polymers for Advanced Technologies*, *31*(3), 536-543. doi: 10.1002/pat.4794.

[126] **Kincal, D., Kumar, A., Child, A.D., and Reynolds, J.R.** (1998). Conductivity switching in polypyrrole-coated textile fabrics as gas sensors. *Synthetic Metals*, *92*(1), 53-56. doi: 10.1016/s0379-6779(98)80022-2.

[127] **Kemp, N.T., Flanagan, G.U., Kaiser, A.B., Trodahl, H.J., Chapman, B., Partridge, A.C., and Buckley, R.G.** (1999). Temperature-dependent conductivity of conducting polymers exposed to gases. *Synthetic Metals*, *101* (1-3), 434-435. doi: 10.1016/S0379-6779(98)01118-7.

[128] **Campbell, T.E., Hodgson, A.J., and Wallace, G.G.** (1999). Incorporation of Erythrocytes into Polypyrrole to Form the Basis of a Biosensor to Screen for Rhesus (D) Blood Groups and Rhesus (D) Antibodies. *Electroanalysis*, *11*(4), 215-222. doi: 10.1002/(sici)1521-4109(199904).

[129] **Vidal, J.C., García, E., and Castillo, J.R.** (1999). In situ preparation of a cholesterol biosensor: entrapment of cholesterol oxidase in an overoxidized polypyrrole film electrodeposited in a flow system. Determination of total cholesterol in serum. *Analytica Chimica Acta*, *385*(1-3), 213-222.

[130] **Smela, E.** (1999). Microfabrication of PPy microactuators and other conjugated polymer devices. *Journal of Micromechanics and Microengineering*, *9* (1). doi: 10.1088/0960-1317/9/1/001.

[131] **Skotheim, T.A., and Reynolds, J.R.** (2007). Handbook of Conducting Polymers: Conjugated Polymers Processing and Applications.

[132] **Wang, L.X., Li, X.G., and Yang, Y.L.** (2001). Preparation, properties and applications of polypyrroles. *Reactive and Functional Polymers*, *47*(2), 125-139. doi: 10.1016/S1381-5148(00)00079-1.

[133] **Kim, W., Lee, J.S., Shin, D.H., and Jang, J.** (2018). Platinum nanoparticles immobilized on polypyrrole nanofibers for non-enzyme oxalic acid

sensor. *Journal of Materials Chemistry B*, *6*, 1272–1278. doi: 10.1039/c7tb00629b.

[134] **Kumar, D., and Sharma, R.C.** (1998). Advances in conductive polymers. *European Polymer Journal*, *34*(8), 1053-1060. doi: 10.1016/S0014-3057(97)00204-8.

[135] **Cetiner, S., Karakas, H., Ciobanu, R., Olariu, M., Kaya, N.U., Unsal, C., …Sarac, A.S.** (2010). Polymerization of pyrrole derivatives on polyacrylonitrile matrix, FTIR-ATR and dielectric spectroscopic characterization of composite thin films. *Synthetic Metals*, *160*(11–12), 1189-1196. doi: 10.1016/j.synthmet.2010.03.007.

[136] **Ilicheva, N.S., Kitaeva, N.K., Duflot, V.R., and Kabanova, V.I.** (2012). Synthesis and Properties of Electroconductive Polymeric Composite Material Based on Polypyrrole. *ISRN Polymer Science*, 2012, doi: 10.5402/2012/320316.

[137] **Balci, N., Toppare, L., and Bayramli, E.** (1995). Conducting polymer composites of pyrrole with polyacrylic acid and epoxy matrices. *Composites*, *26*(3), 229-231.doi: 10.1016/0010-4361(95)91387-K.

[138] **Saraç, A.S., Ustamehmetoğlu, B., Mustafaev, M.I., Erbil, C., and Uzelli, G.** (1995). Oxidative polymerization of pyrrole in polymer matrix. *Journal of Polymer Science Part A: Polymer Chemistry*, *33*, 1581–1587. doi: 10.1002/pola.1995.080331004.

[139] **Ruckenstein, E., and Yang, S.** (1993). Processable conductive polypyrrole/poly(alkyl methacrylate) composites prepared by an emulsion pathway. *Polymer*, *34* (22), 4655-4660. doi: 10.1016/0032-3861(93)90698-A.

[140] **Yang, S., and Ruckenstein, E.** (1993). Preparation and mechanical properties of electrically conductive polypyrrole-poly(ethylene-co-vinyl acetate) composites. *Synthetic Metals*, *60*(3), 249-254.doi: 10.1016/0379-6779(93)91287-C.

[141] **Li, X., Hao, X., Yu, H., and Na, H.** (2008). Fabrication of Polyacrylonitrile/polypyrrole (PAN/Ppy) composite nanofibres and nanospheres with core-shell structures by electrospinning. *Materials Letters*, *62*, 1155–1158. doi: 10.1016/j.matlet.2007.08.003.

[142] **Cetiner, S., Kalaoglu, F., Karakas, H., and Sarac, A.S.** (2010). Electrospun nanofibers of polypyrrole-poly(acrylonitrile-co-vinyl acetate). *Textile Research Journal*, *80*(17), 1784–1792. doi: 10.1177/0040517510365953.

[143] **Sarac, A.S., Cetiner, S., Karakas, H., and Kalaoglu, F.** Morphology and electrical properties of intrinsically conducting polymer composites. *Society of Plastics Engineers*, 1–3.

[144] **Arman, B., and Sarac, A.S.** (2014). In Situ Preparation of Core Shell-Polypyrrole /Poly (Acrylonitrile-Co-Vinyl Acetate) Nanoparticles and Their Nanofibers. *Soft Nanoscience Letters*, *04*(02), 42–49. doi: 10.4236/snl.2014.42006.

[145] **Ince Yardimci, A., Baskan, O., Yilmaz, S., Mese, G., Ozcivici, E., and**

Selamet, Y. (2019). Osteogenic differentiation of mesenchymal stem cells on random and aligned PAN/PPy nanofibrous scaffolds. *Journal of Biomaterials Applications*, *34*(5), 640–650. doi: 10.1177/0885328219865068.

[146] **Matysiak, W., Tański, T., Smok, W., Gołombek, K., and Schab-Balcerzak, E.** (2020). Effect of conductive polymers on the optical properties of electrospun polyacrylonitryle nanofibers filled by polypyrrole, polythiophene and polyaniline. *Applied Surface Science*, *509*(October 2019), 145068. doi: 10.1016/j.apsusc.2019.145068.

[147] **Ramanathan, K., Bangar, M.A., Yun, M., Chen, W., Mulchandani, A. and Myung, N. V.** (2007). In situ fabrication of single poly(methyl pyrrole) nanowire. *Electroanalysis*, *19*(7-8), 793-797. doi: 10.1002/elan.200603773.

[148] **Tüken, T., Tansuğ, G., Yazici, B., and Erbil, M.** (2007). Poly(N-methyl pyrrole) and its copolymer with pyrrole for mild steel protection. *Surface and Coatings Technology*, *202*(1), 146-154. doi: 10.1016/j.surfcoat.2007.05.022.

[149] **Sarac, A.S., Sezgin, S., Ates, M., Turhan, C.M., Parlak, E.A., and Irfanoglu, B.** (2008). Electrochemical impedance spectroscopy of poly(N-methyl pyrrole) on carbon fiber microelectrodes and morphology. *Progress in Organic Coatings*, *62*(3), 331-335. doi: 10.1016/j.porgcoat.2008.01.016.

[150] **Cetiner, S., Olariu, M., Ciobanu, R., Karakas, H., Kalaoglu, F., and Sarac, A.S.** (2010). Polypyrrole/polyacrylonitrile composite films: Dielectric, spectrophotometric and morphologic characterization. *Fibers and Polymers*, *11*(6), 843-850. doi: 10.1007/s12221-010-0843-9.

[151] **Ursache, S.** (2013). Dielectric Properties and Electromagnetic Behaviour ofPan/Nmpy Conductive Composites. *International Journal of Information and Electronics Engineering*, *3*(4), 413-428. doi: 10.7763/ijiee.2013.v3.350.

[152] **Ozkazanc, H., Menkuer, M., Gundogdu, O., and Ozkazanc, E.** (2020). Multifunctional poly(N-methylpyrrole)/nano-oxide composites: Optoelectronic, charge transport and antibacterial properties. *Polymer*, *189*(January), 122188. doi: 10.1016/j.polymer.2020.122188.

[153] **Patil, V.M.. Sinha, R.. Masand, N.. and Jain, J.** (2009). Synthesis and anticonvulsant activities of small n-substituted 2, 5-dimethyl pyrrole and bipyrrole. *Digest Journal of Nanomaterials and Biostructures*, *4*(3), 471–477.

[154] **Chirico, R.D., and Kazakov, A.F.** (2018). Thermodynamic properties of pyrrole, 1-methylpyrrole, 2,4-dimethylpyrrole, and 2,5-dimethylpyrrole: Experimental and computational results. *Journal of Chemical Thermodynamics*, *116*, 213–229. doi: 10.1016/j.jct.2017.09.005.

[155] **Chern, C.S.** (2006). Emulsion polymerization mechanisms and kinetics. *Progress in Polymer Science (Oxford)*, *31*(5), 443–486. doi: 10.1016/j.progpolymsci.2006.02.001.

[156] **Yamak, H.B.** (2013). Emulsion Polymerization: Effects of Polymerization Variables on the Properties of Vinyl Acetate Based Emulsion Polymers. *Polymer Science*, 35-72.

[157] **Odian, G.** (2004). *Emulsion Polymerization*. Principles of Polymers, pp 350–371.

[158] **Bovey, F.A., Kolthoff, I.M., Medalla, A.I., and Meehan, E.J.** (1955). *Emulsion Polymerization*. Interscience, New York-London.

[159] **Eliseeva, V.I., Ivanchev, S.S., Kuchanov, S.I., and Lebedev, A.V.** (1981). *Emulsion Polymerization and Its Applications in Industry*. Plenum Publishing Corporation, New York.

[160] **Blackley, D.C.** (1975). *Emulsion Polymerization.* Applied Science, London.

[161] **Yildirim Erbil, H.** (2000). *Vinyl acetate emulsion polymerization and copolymerization with acrylic monomers.* CRC Press.

[162] **S.El-Aasser, M.** (1990). *Emulsion Polymerization.* An Introduction to Polymer Colloids. Springer, Dordrecht; pp 1–34.

[163] **Guyot, A., Tauer, K., Asua, J.M., Van Es, S., Gambier, C., Hellgren, A.C., …Sjoberg, F.M.** (1999). Reactive surfactants in heterophase polymerization. *Acta Polymerica*, *50*, 57–66. doi: 10.1002/(SICI)1521-4044(19990201).

[164] **Lovell, P.A., and Schork, F.J.** (2020). Fundamentals of emulsion polymerization. *Biomacromolecules*, *21*(11), 4396–4441. doi: 10.1021/acs.biomac.0c00769.

[165] **Grafe, T., and Graham, K.** (2003). Polymeric nanofibers and nanofiber webs: a new class of nonwovens. *International Nonwovens Journal*, 51–55, doi: 10.1177/1558925003os-1200113.

[166] **Ramakrishna, S., Fujihara, K., Teo, W.E., Lim, T.C., and Ma, Z.** (2005). *An introduction to electrospinning and nanofibers*. Singapore, World Scientific.

[167] **Fang, J. Wang, X. and Li, T.** (2011). *Functional Applications of Electrospun Nanofibers*. Nanofibers - Production, Properties and Functional Applications, pp 288–326.

[168] **Beachley, V., and Wen, X.** (2009). Effect of electrospinning parameters on the nanofiber diameter and length. *Materials Science and Engineering C*, *29*(3), 663–668. doi: 10.1016/j.msec.2008.10.037.

[169] **Ramakrishna, S., Fujihara, K., Teo, W.E., Yong, T., Ma, Z., and Ramaseshan, R.** (2006). Electrospun nanofibers: Solving global issues. *Materials Today*, *9*(3), 40–50. doi: 10.1016/S1369-7021(06)71389-X.

[170] **Frenot, A., and Chronakis, I.S.** (2003). Polymer nanofibers assembled by electrospinning. *Current Opinion in Colloid and Interface Science*, *8*, 64–75. doi: 10.1016/S1359-0294(03)00004-9.

[171] **Pham, Q.P., Sharma, U., and Mikos, A.G.** (2006). Electrospinning of polymeric nanofibers for tissue engineering applications: A review. *Tissue Engineering*, *12*(5), 1197–1211. doi: 10.1089/ten.2006.12.1197.

[172] **Hu, X., Liu, S., Zhou, G., Huang, Y., Xie, Z., and Jing, X.** (2014). Electrospinning of polymeric nanofibers for drug delivery applications. *Journal of Controlled Release*, *185*, 12–21. doi: 10.1016/j.jconrel.2014.04.018.

[173] **Bajakova, J., Chaloupek, J., Lukaš, D., and Lacarin, M.** (2011). Drawing"- The production of individual nanofibers by experimental method. *NANOCON 2011* - Brno, Czech Republic, 21-23 September.

[174] **Karakas, H.** (2014). *Electrospinning of Nanofibers and Their Applications*. MDT 'Electrospinning'.

[175] **Eatemadi, A., Daraee, H., Zarghami, N., Yar, H.M., and Akbarzadeh, A.** (2016). Nanofiber: Synthesis and biomedical applications. *Artificial Cells, Nanomedicine and Biotechnology*, *44*, 111–121. doi: 10.3109/21691401.2014.922568.

[176] **Hamzeh, S., Miraftab, M., and Yoosefinejad, A.** (2014). Study of electrospun nanofibre formation process and their electrostatic analysis. *Journal of Industrial Textiles*, *44*(1), 147–158. doi: 10.1177/1528083713480379.

[177] **Doshi, J., and Reneker, D.H.** (1995). Electrospinning process and applications of electrospun fibers. *Journal of Electrostatics*, *35*(2–3), 151–160. doi: 10.1016/0304-3886(95)00041-8.

[178] **Wang, H.-S. Fu, G.-D. and Li, X.-S.** (2008). Functional Polymeric Nanofibers from Electrospinning. *Recent Patents on Nanotechnology*, *3*(1),: 21–31, doi: 10.2174/187221009787003285.

[179] **Deitzel, J.M., Kleinmeyer, J.D., Hirvonen, J.K., and Beck Tan, N.C.** (2001). Controlled deposition of electrospun poly(ethylene oxide) fibers. *Polymer*, *42*(19), 8163–8170. doi: 10.1016/S0032-3861(01)00336-6.

[180] **Reneker, D.H., Yarin, A.L., Zussman, E., and Xu, H.** (2007). Electrospinning of Nanofibers from Polymer Solutions and Melts. *Advances in Applied Mechanics*, *41*, 43–195. 345–346, doi: 10.1016/S0065-2156(07)41002-X.

[181] **Deitzel, J.M., Kleinmeyer, J., Harris, D., and Beck Tan, N.C.** (2001). The effect of processing variables on the morphology of electrospun nanofibers and textiles. *Polymer*, *42*, 261–272. doi: 10.1016/S0032-3861(00)00250-0.

[182] **Sukigara, S., Gandhi, M., Ayutsede, J., Micklus, M., and Ko, F.** (2003). Regeneration of Bombyx mori silk by electrospinning - Part 1: Processing parameters and geometric properties. *Polymer*, *44*(19), 5721–5727. doi: 10.1016/S0032-3861(03)00532-9.

[183] **Koski, A., Yim, K., and Shivkumar, S.** (2004). Effect of molecular weight on fibrous PVA produced by electrospinning. *Materials Letters*, *58*(3–4), 493–497. doi: 10.1016/S0167-577X(03)00532-9.

[184] **Weber, J., Singhai, R., Zekri, S., and Kumar, A.** (2008). One-dimensional nanostructures: Fabrication, characterisation and applications. *International Materials Reviews*, *53*(4), 235–255. doi: 10.1179/174328008X348183.

[185] **Zong, X., Kim, K., Fang, D., Ran, S., Hsiao, B.S., and Chu, B.** (2002).

Structure and process relationship of electrospun bioabsorbable nanofiber membranes. *Polymer*, *43*(16), 4403–4412. doi: 10.1016/S0032-3861(02)00275-6.

[186] **Yang, Q., Zhenyu, L.I., Hong, Y., Zhao, Y., Qiu, S., Wang, C.E., and Wei, Y.** (2004). Influence of solvents on the formation of ultrathin uniform poly(vinyl pyrrolidone) nanofibers with electrospinning. *Journal of Polymer Science, Part B: Polymer Physics*, *42*(20), 3721–3726. doi: 10.1002/polb.20222.

[187] **Li, Z. and Wang, C.** (2013). *One-Dimensional nanostructures*.

[188] **Reneker, D.H., and Chun, I.** (1996). Nanometre diameter fibres of polymer, produced by electrospinning. *Nanotechnology*, *7*(3), 216–223. doi: 10.1088/0957-4484/7/3/009.

[189] **Zhang, C., Yuan, X., Wu, L., Han, Y., and Sheng, J.** (2005). Study on morphology of electrospun poly(vinyl alcohol) mats. *European Polymer Journal*, *41*(3), 423–432. doi: 10.1016/j.eurpolymj.2004.10.027.

[190] **Demir, M.M., Yilgor, I., Yilgor, E., and Erman, B.** (2002). Electrospinning of polyurethane fibers. *Polymer*, *43*(11), 3303–3309. doi: 10.1016/S0032-3861(02)00136-2.

[191] **Zhang, S., Shim, W.S., and Kim, J.** (2009). Design of ultra-fine nonwovens via electrospinning of Nylon 6: Spinning parameters and filtration efficiency. *Materials and Design*, *30*(9), 3659–3666. doi: 10.1016/j.matdes.2009.02.017.

[192] **De Vrieze, S., Van Camp, T., Nelvig, A., Hagström, B., Westbroek, P., and De Clerck, K.** (2009). The effect of temperature and humidity on electrospinning. *Journal of Materials Science*, *44*(5), 1357–1362. doi: 10.1007/s10853-008-3010-6.

[193] **Moghe, A.K., and Gupta, B.S.** (2008). Co - axial electrospinning for nanofiber structures : preparation and applications. *Polymer Reviews*, *48*,: 353–377, doi: 10.1080/15583720802022257.

[194] **Garg, K., Bowlin, G.L., Garg, K., and Bowlin, G.L.** (2014). Electrospinning jets and nanofibrous structures. *Biomicrofluids*, *5* (2011),: 013403, doi: 10.1063/1.3567097.

[195] **Cui, W., Zhou, Y., and Chang, J.** (2010). Electrospun nanofibrous materials for tissue engineering and drug delivery. *Science and Technology of Advanced Materials*, *11*(1). doi: 10.1088/1468-6996/11/1/014108.

[196] **Yu, D.G., White, K., Yang, J.H., Wang, X., Qian, W. ,and Li, Y.** (2012). PVP nanofibers prepared using co-axial electrospinning with salt solution as sheath fluid. *Materials Letters*, *67*(1), 78–80. doi: 10.1016/j.matlet.2011.09.035.

[197] **Fallahiarezoudar, E., Ahmadipourroudposht, M., Yusof, N.M., and Idris, A.** (2015). Fabrication (ferrofluid/polyvinyl alcohol) magnetic nanofibers via co-axial electrospinning. *Journal of Dispersion Science and Technology*, *36*(1), 28–31. doi: 10.1080/01932691.2014.888005.

[198] **Komur, B., Bayrak, F., Ekren, N., Eroglu, M.S., Oktar, F.N., Sinirlioglu,**

Z.A.,…Gunduz, O. (2017). Starch/PCL composite nanofibers by co-axial electrospinning technique for biomedical applications. *BioMedical Engineering Online*, *16*(1), 1–13. doi: 10.1186/s12938-017-0334-y.

[199] **Mao, Z., Li, J., Huang, W., Jiang, H., Zimba, B.L., Chen, L.,… Wu, Q.** (2018). Preparation of poly(lactic acid)/graphene oxide nanofiber membranes with different structures by electrospinning for drug delivery. *RSC Advances*, *8*(30), 16619–16625. doi: 10.1039/c8ra01565a.

[200] **Kaewsaenee, J., Duriyasart, F., and Pavarajarn, V.** (2020). Fabrication of flexible titania/polyacrylonitrile co-axial nanofibers via electrospinning. *Journal of Asian Ceramic Societies*, *8*(1), 203–210. doi: 10.1080/21870764.2020.1723196.

[201] **Baykara, T., and Taylan, G.** (2021). Coaxial electrospinning of PVA/Nigella seed oil nanofibers: Processing and morphological characterization. *Materials Science and Engineering B: Solid-State Materials for Advanced Technology*, *265*, 115012. doi: 10.1016/j.mseb.2020.115012.

[202] **Baskan, H., Unsal, C., Karakas, H. and Sarac, A.S.** (2017). Poly(acrylonitrile-co-itaconic acid)-poly(3,4-ethylenedioxythiophene) and poly(3-methoxythiophene) nanoparticles and nanofibres. *Bulletin of Materials Science*, *40*(5), 957–969. doi: 10.1007/s12034-017-1438-5.

[203] **Mogomotsi, R.N., Akinola, S.S., Emeka, E.E., and Fayemi, O.E.** (2020). Cyclic voltammetry, photocatalytic and antimicrobial comparative studies of fabrication Fe_3O_4 and Fe_3O_4/PAN nanofibers. *Materials Research Express*, *7*(5), 055001. doi: 10.1088/2053-1591/ab8ba1.

[204] **Chen, S., Chi, M., Zhu, Y., Gao, M., Wang, C., and Lu, X.** (2018). A Facile synthesis of superparamagnetic Fe_3O_4 nanofibers with superior peroxidase-like catalytic activity for sensitive colorimetric detection of L-cysteine. *Applied Surface Science*, *440*, 237–244. doi: 10.1016/j.apsusc.2018.01.152.

[205] **Tan, S.T., Wendorff, J.H., Pietzonka, C., Jia, Z.H., and Wang, G.Q.** (2005). Biocompatible and biodegradable polymer nanofibers displaying superparamagnetic properties. *ChemPhysChem*, *6*(8), 1461–1465. doi: 10.1002/cphc.200500167.

[206] **Takai, Z.I., Mustafa, M.K., and Asman, S.** (2018). Preparation of high performance conductive polyaniline magnetite (PANI/ Fe_3O_4) nanocomposites by sol-gel method. *Asian Journal of Chemistry*, *30*(12), 2625–2630. doi: 10.14233/ajchem.2018.21473.

[207] **Munteanu, D., Ion, R.-M., and Cocina, G.-C.** (2010). Synthesis and characterization of magnetic nanoparticles embedded in polyacrylonitrile nanofibers. *Advanced Topics in Optoelectronics, Microelectronics, and Nanotechnologies V*, *7821*(December 2010), 78210J. doi: 10.1117/12.883788.

[208] **Ding, D., Yan, X., Zhang, X., He, Q., Qiu, B., Jiang, D.,…Wei, S.** (2015). Preparation and enhanced properties of Fe_3O_4 nanoparticles reinforced

polyimide nanocomposites. *Superlattices and Microstructures*, *85*, 305–320. doi: 10.1016/j.spmi.2015.03.008.

[209] **Mahdieh, A., Mahdavian, A.R., and Salehi-Mobarakeh, H.** (2017). Chemical modification of magnetite nanoparticles and preparation of acrylic-base magnetic nanocomposite particles via miniemulsion polymerization. *Journal of Magnetism and Magnetic Materials*, *426*(August 2016), 230–238. doi: 10.1016/j.jmmm.2016.11.091.

[210] **Peng, C., Zhang, J., Xiong, Z., Zhao, B., and Liu, P.** (2015). Fabrication of porous hollow γ-Al_2O_3 nanofibers by facile electrospinning and its application for water remediation. *Microporous and Mesoporous Materials*, *215*, 133–142. doi: 10.1016/j.micromeso.2015.05.026.

[211] **Maaza, L., Djafri, F., Belmokhtar, A., and Benyoucef, A.** (2021). Evaluation of the influence of Al_2O_3 nanoparticles on the thermal stability and optical and electrochemical properties of PANI-derived matrix reinforced conducting polymer composites. *Journal of Physics and Chemistry of Solids*, *152*, 109970. doi: 10.1016/j.jpcs.2021.109970.

[212] **Mudra, E., Streckova, M., Pavlinak, D., Medvecka, V., Kovacik, D., Kovalcikova, A.,…Duzsa, J.** (2017). Development of Al_2O_3 electrospun fibers prepared by conventional sintering method or plasma assisted surface calcination. *Applied Surface Science*, *415*, 90–98. doi: 10.1016/j.apsusc.2016.11.162.

[213] **Rai, R., Keshavarz, T., Roether, J.A., Boccaccini, A.R., and Roy, I.** (2011). Medium chain length polyhydroxyalkanoates, promising new biomedical materials for the future. *Materials Science and Engineering R: Reports*, *72*(3), 29–47. doi: 10.1016/j.mser.2010.11.002.

[214] **Jacquel, N., Lo, C.W., Wu, H.S., Wei, Y.H., and Wang, S.S.** (2007). Solubility of polyhydroxyalkanoates by experiment and thermodynamic correlations. *AIChE Journal*, *53*(10), 2704–2714. doi: 10.1002/aic.11274.

[215] **Gumel, A.M., Annuar, M.S.M., Ishak, K.A., and Ahmad, N.** (2014). Carbon nanofibers-poly-3-hydroxyalkanoates nanocomposite: Ultrasound-assisted dispersion and thermostructural properties. *Journal of Nanomaterials*, *2014*, 1–10. doi: 10.1155/2014/264206.

[216] **Phukon, P., Saikia, J.P., and Konwar, B.K.** (2011). Enhancing the stability of colloidal silver nanoparticles using polyhydroxyalkanoates (PHA) from Bacillus circulans (MTCC 8167) isolated from crude oil contaminated soil. *Colloids and Surfaces B: Biointerfaces*, *86*, 314–318. doi: 10.1016/j.colsurfb.2011.04.014.

[217] **Castro-Mayorga, J.L., Martínez-Abad, A., Fabra, M.J., Olivera, C., Reis, M., and Lagarón, J.M.** (2014). Stabilization of antimicrobial silver nanoparticles by a polyhydroxyalkanoate obtained from mixed bacterial culture. *International Journal of Biological Macromolecules*, *71*, 103–110. doi: 10.1016/j.ijbiomac.2014.06.059.

[218] **Nobbs, J.H.** (1985). Kubelka—Munk Theory and the Prediction of Reflectance. *Review of Progress in Coloration and Related Topics*, doi: 10.1111/j.1478-4408.1985.tb03737.x.

[219] **Martínez-Sanz, M., Villano, M., Oliveira, C., Albuquerque, M.G.E., Majone, M., Reis, M.,…Lagaron, J.M.** (2014). Characterization of polyhydroxyalkanoates synthesized from microbial mixed cultures and of their nanobiocomposites with bacterial cellulose nanowhiskers. *New Biotechnology*, *31*(4), 364–376. doi: 10.1016/j.nbt.2013.06.003.

[220] **Sato, H., Padermshoke, A., Nakamura, M., Murakami, R., Hirose, F., Senda, K.,…Ozaki, Y.** (2005). Infrared spectroscopy and x-ray diffraction studies on the structure and thermal behavior of biodegradable polyhydroxyalkanoates. *Macromolecular Symposia, 220* (1), 123–138.

[221] **Dai, Y., Lambert, L., Yuan, Z., and Keller, J.** (2008). Characterisation of polyhydroxyalkanoate copolymers with controllable four-monomer composition. *Journal of Biotechnology*, *134*, 137–145. doi: 10.1016/j.jbiotec.2008.01.013.

[222] **Castro-Mayorga, J.L., Fabra, M.J., and Lagaron, J.M.** (2016). Stabilized nanosilver based antimicrobial poly(3-hydroxybutyrate-co-3-hydroxyvalerate) nanocomposites of interest in active food packaging. *Innovative Food Science and Emerging Technologies*, *33*, 524–533. doi: 10.1016/j.ifset.2015.10.019.

[223] **Martínez-Sanz, M., Lopez-Rubio, A., Villano, M., Oliveira, C.S.S., Majone, M., Reis, M., and Lagarón, J.M.** (2016). Production of bacterial nanobiocomposites of polyhydroxyalkanoates derived from waste and bacterial nanocellulose by the electrospinning enabling melt compounding method. Journal of Applied Polymer Science, 133(2), 42486.

[224] **Laycock, B., Arcos-Hernandez, M. V., Langford, A., Pratt, S., Werker, A., Halley, P.J., and Lant, P.A.** (2014). Crystallisation and fractionation of selected polyhydroxyalkanoates produced from mixed cultures. *New Biotechnology*, *31*(4), 345–356. doi: 10.1016/j.nbt.2013.05.005.

[225] **Ten, E., Turtle, J., Bahr, D., Jiang, L., and Wolcott, M.** (2010). Thermal and mechanical properties of poly(3-hydroxybutyrate-co-3-hydroxyvalerate)/cellulose nanowhiskers composites. *Polymer*, *51*(12), 2652–2660. doi: 10.1016/j.polymer.2010.04.007.

[226] **Arcos-Hernández, M. V., Laycock, B., Donose, B.C., Pratt, S., Halley, P. Al-Luaibi, S.,…Lant, P.A.** (2013). Physicochemical and mechanical properties of mixed culture polyhydroxyalkanoate (PHBV). *European Polymer Journal*, *49*(4), 904–913. doi: 10.1016/j.eurpolymj.2012.10.025.

[227] **Esposito, E., and Cuzzocrea, S.** (2009). TNF-alpha as a therapeutic target in ınflammatory diseases, ıschemia- reperfusion ınjury and trauma. *Current Medicinal Chemistry*, *16*(24), 3152–3167. doi: 10.2174/092986709788803024.

[228] **Rujitanaroj, P.O., Pimpha, N., and Supaphol, P.** (2010). Preparation, characterization, and antibacterial properties of electrospun polyacrylonitrile fibrous membranes containing silver nanoparticles. *Journal of Applied Polymer Science*, *116*(4), 1967–1976. doi:

10.1002/app.31498.

[229] **Pastoriza-Santos, I., and Liz-Marzán, L.M.** (2000). Reduction of silver nanoparticles in DMF. Formation of monolayers and stable colloids*. *Pure Appl. Chem*, *72*(1–2), 83–90. doi: 10.1351/pac200072010083.

[230] **Tomić, S.L., Mićić, M.M., Dłokić, D., Vasiljević-Radović, D.G., Filipović, J.M., and Suljovrujić, E.H.** (2009). Preparation of silver(I) complexes with itaconic acid-based hydrogels for biomedical application. *Materials and Manufacturing Processes*, *24*(10–11), 1197–1201. doi: 10.1080/10426910903022247.

[231] **Eid, M., and Araby, E.** (2013). Bactericidal effect of poly(acrylamide/itaconic acid)-silver nanoparticles synthesized by gamma irradiation against pseudomonas aeruginosa. *Applied Biochemistry and Biotechnology*, *171*(2), 469–487. doi: 10.1007/s12010-013-0357-1.

[232] **Bal, A., Çepni, F.E., Çakir, Ö., Acar, I., and Güçlü, G.** (2015). Synthesis and Characterization of Copolymeric and Terpolymeric Hydrogel-Silver Nanocomposites Based on Acrylic Acid , Acrylamide and Itaconic Acid : Investigation of Their Antibacterial Activity Against Gram-Negative Bacteria. *Brazilian Journal of Chemical Engineering* , *32*(02), 509–518.

[233] **Ucar, N., Demirsoy, N., Onen, A., Karacan, I., Kizildag, N., Eren, O., …Ustamehmetoglu, B.** (2015). The effect of reduction methods and stabilizer (PVP) on the properties of polyacrylonitrile (PAN) composite nanofibers in the presence of nanosilver. *Journal of Materials Science*, *50*(4), 1855–1864. doi: 10.1007/s10853-014-8748-4.

[234] **Thompson, C.J., Chase, G.G., Yarin, A.L., and Reneker, D.H.** (2007). Effects of parameters on nanofiber diameter determined from electrospinning model. *Polymer*, *48*(23), 6913–6922. doi: 10.1016/j.polymer.2007.09.017.

[235] URL-1 < *https://www.sciencedirect.com/topics/engineering/probe-point*> date retrieved 16.03.2021.

[236] **Hasegawa, S., Shiraki, I., Tanikawa, T., Petersen, C.L., Hansen, T.M., Boggild, P., and Grey, F.** (2002). Direct measurement of surface-state conductance by microscopic four-point probe method. *Journal of Physics Condensed Matter*, *14*(35), 8379–8392. doi: 10.1088/0953-8984/14/35/309.

[237] **Qavamnia, S.S., and Nasouri, K.** (2015). Conductive polyacrylonitrile/polyaniline nanofibers prepared by electrospinning process. *Polymer Science - Series A*, *57*(3), 343–349. doi: 10.1134/S0965545X1503013X.

[238] **Almuhamed, S., Khenoussi, N., Schacher, L., Adolphe, D., and Balard, H.** (2012). Measuring of electrical properties of MWNT-reinforced PAN nanocomposites. *Journal of Nanomaterials*, *2012*(January 2014). doi: 10.1155/2012/750698.

[239] **CLSI.** (2015). M02-A12 Performance Standards for Antimicrobial Disk.

[240] **Bajpai, S.K., Jyotishi, P., and Bajpai, M.** (2016). Synthesis of nanosilver

loaded chitosan/poly(acrylamide-co-itaconic acid) based inter-polyelectrolyte complex films for antimicrobial applications. *Carbohydrate Polymers*, *154*, 223–230. doi: 10.1016/j.carbpol.2016.08.044.

[241] (2012). Methods for Dilution Antimicrobial Susceptibility Tests for Bacteria That Grow Aerobically ; Approved Standard — Ninth Edition.

[242] **CLSI.** (2007). Clinical and Laboratory Standards Institute.

[243] **Kharaghani, D., Kee Jo, Y., Khan, M.Q., Jeong, Y., Cha, H.J., and Kim, I.S.** (2018). Electrospun antibacterial polyacrylonitrile nanofiber membranes functionalized with silver nanoparticles by a facile wetting method. *European Polymer Journal*, *108*, 69–75. doi: 10.1016/j.eurpolymj.2018.08.021.

[244] **Shalaby, T., Hamad, H., Ibrahim, E., Mahmoud, O., and Al-Oufy, A.** (2018). Electrospun nanofibers hybrid composites membranes for highly efficient antibacterial activity. *Ecotoxicology and Environmental Safety*, *162*(April), 354–364. doi: 10.1016/j.ecoenv.2018.07.016.

[245] **Birajdar, M.S., Cho, H., Seo, Y., Choi, J., and Park, H.** (2018). Surface conjugation of poly (dimethyl siloxane) with itaconic acid-based materials for antibacterial effects. *Applied Surface Science*, *437*, 245–256. doi: 10.1016/j.apsusc.2017.12.125.

[246] (1999). M26-A: Methods for Determining Bactericidal Activity of Antimicrobial Agents; Approved Guideline (September),.

[247] **Yu, D.G., Zhou, J., Chatterton, N.P., Li, Y., Huang, J., and Wang, X.** (2012). Polyacrylonitrile nanofibers coated with silver nanoparticles using a modified coaxial electrospinning process. *International Journal of Nanomedicine*, *7*, 5725–5732. doi: 10.2147/IJN.S37455.

[248] **Ullah, S., Hashmi, M., Kharaghani, D., Khan, M.Q., Saito, Y., Yamamoto, T.,…Kim, I.S.** (2019). Antibacterial properties of in situ and surface functionalized impregnation of silver sulfadiazine in polyacrylonitrile nanofiber mats. *International Journal of Nanomedicine*, *14*, 2693–2703. doi: 10.2147/IJN.S197665.

[249] **Baskan, H., Esentürk, I., Dösler, S., Sarac, A.S., and Karakas, H.** (2019). Electrospun nanofibers of poly (acrylonitrile-co-itaconic acid)/silver and polyacrylonitrile/silver: In situ preparation, characterization, and antimicrobial activity. *Journal of Industrial Textiles*, doi: 10.1177/1528083719868170.

[250] **Zhang, L., Luo, J., Menkhaus, T.J., Varadaraju, H., Sun, Y., and Fong, H.** (2011). Antimicrobial nano-fibrous membranes developed from electrospun polyacrylonitrile nanofibers. *Journal of Membrane Science*, *369*(1–2), 499–505. doi: 10.1016/j.memsci.2010.12.032.

[251] **Ismar, E., and Sarac, A.S.** (2018). Oxidation of polyacrylonitrile nanofiber webs as a precursor for carbon nanofiber: aligned and non-aligned nanofibers. *Polymer Bulletin*, *75*(2), 485–499. doi: 10.1007/s00289-017-2043-x.

[252] **Chougule, M.A., Pawar, S.G., Godse, P.R., Mulik, R.N., Sen, S., and Patil,**

V.B. (2011). Synthesis and Characterization of Polypyrrole (PPy) Thin Films. *Soft Nanoscience Letters*, *1*, 6–10. doi: 10.4236/snl.2011.11002.

[253] **Vernitskaya, T. V., and Efimov, O.N.** (1997). Polypyrrole: A conducting polymer (synthesis, properties, and applications). *Uspekhi Khimii*, *66*(5), 443–457. doi: 10.1070/rc1997v066n05abeh000261.

[254] **Cetiner, S., Kalaoglu, F., Karakas, H., and Sarac, A.S.** (2011). Dielectric, FTIR spectroscopic and atomic force microscopic studies on polypyrrole-poly(acrylonitrile-co-vinyl acetate) composites. *Polymer Composites*, *32*(4), 546–557. doi: 10.1002/pc.21075.

[255] **Mulvaney, S.P. and Keating, C.D.** (2000). Raman Spectroscopy. Analytical Chemistry, *72*(12), 145–158.

[256] **Trchová, M., Morávková, Z., Bláha, M., and Stejskal, J.** (2014). Raman spectroscopy of polyaniline and oligoaniline thin films. *Electrochimica Acta*, *122*, 28–38. doi: 10.1016/j.electacta.2013.10.133.

[257] **Lu, X., Zhang, W., Wang, C., Wen, T.C., and Wei, Y.** (2011). One-dimensional conducting polymer nanocomposites: Synthesis, properties and applications. *Progress in Polymer Science (Oxford)*, *36*(5), 671–712. doi: 10.1016/j.progpolymsci.2010.07.010.

[258] **Bernard, M.C., and Hugot-Le Goff, A.** (1997). Raman spectroscopy for the study of polyaniline. *Synthetic Metals*, *85*(1–3), 1145–1146. doi: 10.1016/s0379-6779(97)80187-7.

[259] **Wang, S., and Shi, G.** (2007). Uniform silver/polypyrrole core-shell nanoparticles synthesized by hydrothermal reaction. *Materials Chemistry and Physics*, *102*(2–3), 255–259. doi: 10.1016/j.matchemphys.2006.12.014.

[260] **El-Sayed, N.S., Moussa, M.A., Kamel, S., and Turky, G.** (2019). Development of electrical conducting nanocomposite based on carboxymethyl cellulose hydrogel/silver nanoparticles@polypyrrole. *Synthetic Metals*, *250*(February), 104–114. doi: 10.1016/j.synthmet.2019.03.010.

CURRICULUM VITAE

Name Surname **:** Havva Başkan

Place and Date of Birth **:**

EDUCATION **:**

- **B.Sc.** **:** 2012, Istanbul Technical University, Textile Technologies and Design Faculty, Textile Engineering Department
- **M.Sc.** **:** 2015, Istanbul Technical University, Textile Technologies and Design Faculty, Textile Engineering Department

PROFESSIONAL EXPERIENCE AND REWARDS:

- 2013-2021, Research Assistant at Textile Technologies and Design Faculty in Istanbul Techical University
- 2016 Second Prize Winner of Medical Textiles and Medical Devices (VIII. R&D Project Brokage Event, Bursa, Turkey)
- Scholarship from TUBITAK 2211-A (1649B031500306) (2015-2019)
- Scholarship from TUBITAK 2214-A (1059B141800375) (2019-2020)
- Visiting researcher at University of Manchester between 17.06.2016-17.09.2016 for the EU project 'ETexWeld' (EU Grant Agreement Number: 644268)

PUBLICATIONS, PRESENTATIONS AND PATENTS ON THE THESIS:

- **Baskan, H.,** Esenturk, I., Dösler, S., Sarac, A.S., Karakas, H. 2019. Electrospun nanofibers of poly (acrylonitrile-co-itaconic-acid)/silver and polyacrylonitrile/silver: In situ preparation, characterization, and antimicrobial activity, *Journal of Industrial Textiles*, DOI: 10.1177/1528083719868170.
- **Baskan, H.,** Ismar, E., Karakas, H , Sarac, A.S. 2020. Nanocomposite structures of poly-pyrrole derivatives and poly(acrylonitrile-co-itaconic acid) produced by in-situ polymerization as carbon nanofiber precursor, *Polymers for Advanced Technologies*, 31(3), 536-543.

- **Baskan, H.,** Karakas, H , Sarac, A.S. 2017. The Suitable $AgNO_3$ Amount for P(AN-co-IA)/Ag Nanocomposite, *ITMC 2017*, 16.10.2017-18.10.2017, Ghent, Belgium.

- **Baskan, H.**, Karakas, H. and Sarac, A.S. 2018. Production and Characterization of Electrospun P(AN-co-IA)/Ag Nanofibers, *ANNIC 2018*, 22.10.2018-24.10.2018, Berlin, Germany.
- **Başkan, H.**, Kalaoğlu-Altan, Ö.İ., De Clerck, K. ve Karakaş, H. 2020. Poli(Akrilonitril-ko-İtakonik Asit)/Gümüş Nanopartikül Nanoliflerinin Koaksiyel Elektroeğirme Yöntemi ile Eldesi, *İTÜ Ulusal Tekstil Kongresi ve II.Ar-Ge Günü, Akademi Sanayi Buluşması*, 11.11.2020-12.11.2020, Istanbul, Turkey.

OTHER PUBLICATIONS, PRESENTATIONS AND PATENTS:

Patent

- Sarac, A.S., Baskan, H., Karakas, H. Method of forming a composite nanoparticle for nanofibers from a poly-(acrylonitrile-co-itaconic acid) poly 3-methoxythipohene (P (AN-co-IA)-PMOT) nano composite solution. US Patent, 10781277.

Articles

- **Baskan, H.**, Unsal, C., Karakas, H., and Sarac, A.S. 2017. Poly(acrylonitrile-co-itaconic acid)–poly(3,4-ethylenedioxythiophene) and poly(3-methoxythiophene) nanoparticles and nanofibres. *Bulletin of Materials Science*, 40 (5): 957-969.
- Suadiye-Can, D., **Baskan, H.**, Gumrukcu, S., and Sarac, A.S. 2019. A novel carbon nanofiber precursor: Poly(acrylonitrile-co-vinylacetate-itaconic acid) terpolymer. *Journal of Nanoscience and Nanotechnology*, 19 (7):3844-3853.

- Arat, R., **Baskan, H.**, Ozcan, G., and Altay, P. 2020. Hydrophobic silica-aerogel integrated polyacrylonitrile nanofibers. *Journal of Industrial Textiles*, DOI: 10.1177/1528083720939670
- **Baskan, H**., Tufan-Acikgoz, H., Atakan, R., Eryuruk, S.H., Akalin, N., Kose, H., Li, Y., Kursun-Bahadır, S. and Kalaoglu, F. 2017. Running Functional Sport Vest and Short for e-Textile Applications. *IOP Conf. Series: Materials Science and Engineering*, 254. doi:10.1088/1757-899X/254/7/072004

- Atakan, R., Tufan-Acikgoz, H., **Baskan, H.**, Eryuruk, S.H., Akalin, N., Kose, H., Li, Y., Kursun-Bahadır, S. and Kalaoglu, F. 2017. Design of an Electronic Chest Band. *IOP Conf. Series: Materials Science and Engineering*, 254. doi:10.1088/1757-899X/254/7/072002

- **Baskan, H.**, Isık, B., Erarslan, E., Ejder, P., Sezer, S. and Karakas, H. 2018. Design and Production of Tailored Rear Trunk Covering for Acoustic Applications. *IOP Conf. Series: Materials Science and Engineering*, 460, 012037. doi:10.1088/1757-899X/460/1/012037

Presentations

- Armagan, O.G., **Baskan, H.**, Kayaoglu-Karaguzel, B. and Karakas, H. 2013. Durability of Leather Effect on Plasma Pre-Treated and Polyurethane Coated Denim Fabric. *International Istanbul Textile Congress 2013*, 30.05.2013-31.05.2013, Istanbul, Turkey.

- Karakas, H., De Clerk, K., Sarac, A.S. and **Baskan, H**. 2013. Electrospinning of Nanofibers for Functional Textile Applications. *International R&D Project Market Innovative and Functional Textiles*, 01.06.2013, Istanbul, Turkey.

- **Baskan, H.**, Karakas, H. and Sarac, A.S. 2013. The Effect of Electrospinning Parameters on PCL(Polycaprolactone) Electrospun Nanofiber Mats. *Polymar 2013*, 03.11.2013-07.11.2013, Barcelona, Spain.

- **Baskan, H.**, Karakas, H. and Sarac, A.S. 2015. Electrospun Nanofibers of PAN-Poly(Acrylonitrile-co-Itaconic Acid)/ Poly(3-Methoxythiophene) Blend. *NART 2015*, 31.08.2015-02.09.2015, Liberec, Czechia.

- **Baskan, H.**, Karakas, H. and Sarac, A.S. 2015. Spectroscopic and Morphologic Study of Poly (Acrylonitrile-co-Itaconic Acid)/Poly (3,4 Ethylenedioxythiophene) Nanoparticles. *5th International Istanbul Textile Congress 2015*, 11.09.2015-12.09.2015, Istanbul, Turkey.

- **Baskan, H.**, Ismar, E., Karakas, H. and Sarac, A.S. 2015. Nanoparticles and Nanofibers of Poly (Acrylonitrile-co-Itaconic Acid) with Pyrrole Derivatives and Their Characterization. *5th International Istanbul Textile Congress 2015*, 11.09.2015-12.09.2015, Istanbul, Turkey.

- **Baskan, H.**, Karakas, H. and Sarac, A.S. 2015. The Effect of Pyrrole Amount on the Diameter of Poly (Acrylonitrile-co-Itaconic Acid)/ Polypyrrole Nanofibers. *Fiber Society 2015*, 28.10.2015-30.10.2015, Raleigh, USA.

- **Baskan, H.**, Karakas, H. and Sarac, A.S. 2015. Electrochemical Impedance Study of Poly (Acrylonitrile-co-Itaconic Acid) / PEDOT Nanofibers. *Fiber Society 2015*, 28.10.2015-30.10.2015, Raleigh, USA.

- **Baskan, H.**, Karakas, H. and Sarac, A.S. 2016. Production and Characterization of Conducting Nanofibers for Gas Sensing Applications. *VIII. International R&D Brokage Event*, 12.05.2016-13.05.2016, Bursa, Turkey.

- **Baskan, H.**, Karakas, H. and Sarac, A.S. 2017. A New Route for Fabrication Smart Military Clothing with Antibacterial and Electromagnetic Interference Shielding Properties. *IX. International R&D Brokage Event*, 27.04.2017-28.04.2017, Bursa, Turkey.

- **Baskan, H.**, Karakas, H. and Sarac, A.S. 2017. Biological Applications of Polyurethane Nanofibers, *IITAS 2017*, 26.10.2017-28.10.2017, İzmir, Turkey.

- **Baskan, H.**, Acikgoz-Tufan, H. and Karakas, H. 2018. Electrospun Cosmetic Skin Mask for Acne Therapy, *X. International R&D Brokage Event*, 08.03.2018-09.03.2018, Bursa, Turkey.

- **Baskan, H.**, Karakas, H. and Sarac, A.S. 2018. Otomotiv Endüstrisi için Anti-Statik Özelliğe Sahip Nonwoven Taban Halısı, *KTÜ TTO 2018 Düşünden Gerçeğine Proje Pazarı*, 06.06.2018-08.06.2018, Trabzon, Turkey.

- **Baskan, H.**, Karakas, H., Sarac, A.S. and Chatzimanolis, M. 2018. Conducting Polymer Thin Films and Nanofibers as Humidity Sensor, *AUTEX 2018*, 20.06.2018-22.06.2018, Istanbul, Turkey.

- **Başkan, H.**, Şensu, B., Van De Voorde, B., De Vos, L., Van Vlierberghe, S., De Clerck, K. Ve Karakaş, H. 2020. Kardiyovasküler Hastalıkların Tedavisi için Polialkilen Tereftalat (PAT) Nanoliflerinin Üretimi*, İTÜ Ulusal Tekstil Kongresi ve II.Ar-Ge Günü, Akademi Sanayi Buluşması*, 11.11.2020-12.11.2020, Istanbul, Turkey.